Development and Application of Soft Computing Techniques in Power System Optimization

Thesis submitted
by

Abhik Hazra

Doctor of Philosophy (Engineering)

Department of Power Engineering,
Faculty Council of Engineering and Technology
Jadavpur University
Kolkata, India

Year: 2018

JADAVPUR UNIVERSITY

KOLKATA – 700032, INDIA

INDEX NO.: – 187/13/E

1. Title of the thesis:

Development and Application of Soft Computing Techniques in Power System Optimization

2. Name, Designation & Institution of the Supervisor/s:

Prof. Dr. Mousumi Basu, Professor, Department of Power Engineering, Jadavpur University, Kolkata

Prof. Dr. Amitava Gupta, Professor, Department of Power Engineering, Jadavpur University, Kolkata

3. List of Publications:

Peer reviewed Journals:

[1] Hazra, Abhik, Saborni Das, and Mousumi Basu. "An efficient fault diagnosis method for PV systems following string current." Journal of Cleaner Production 154 (2017): 220-232.

[2] Das, Saborni, Abhik Hazra, and Mousumi Basu. "Metaheuristic optimization based fault diagnosis strategy for solar photovoltaic systems under non-uniform irradiance." Renewable Energy 118 (2018): 452-467.

[3] Hazra, A., and M. Basu. "Economic analysis to implement distributed generation system in a rail-way rake maintenance depot." Renewable Energy 78 (2015): 157-164.

[4] Hazra, Abhik, Saborni Das, and Mousumi Basu. "Heat Transfer Search Algorithm for Non-convex Economic Dispatch Problems." Journal of The Institution of Engineers (India): Series B (2018): 1-8.

[5] De, Shankha Suvra, Abhik Hazra, and Mousumi Basu. "Artificial immune system for multi-area economic dispatch." International Journal of Emerging Electric Power Systems 14.6 (2013): 581-590.

[6] Ganguly. D., A. Hazra, S. Das, and M. Basu. "Improved real coded genetic algorithm based short-term hydrothermal generation planning." *International Journal of Hybrid Intelligence,* Inderscience. [Accepted for publication: in production]

[7] Hazra. A., S. Das, and M. Basu. "Improved real coded genetic algorithm based short-term hydrothermal generation planning." *International Journal of Hybrid Intelligence,* Inderscience. [Under review]
[8] Hazra. A., D Bose, M. Basu and A. Gupta. " Economic Operational Control of A Solar Power Aided Nano-Grid." *IEEE Transactions on Power Delivery* . [(Under review)]
[9] Hazra. A., S. Das, and M. Basu. "Robust multi-area economic environmental dispatch of wind power integrated system considering area-wise uncertainty." *Expert Systems With Applications,* Elsevier[(Under review)]

4. List of Patent(s):

[1] *"Module level real-time open and short circuit fault detection scheme for solar photovoltaic system under non-uniform irradiance''* A. Hazra, S. Das & M. Basu. CBR No. 21507, Patent app. No. 201731036279. [Under examination]

5. List of Presentation in National/International Conferences:

[1] Hazra, Abhik, Saborni Das, Ashish Laddha, and Mousumi Basu. "Optimized power operational planning through DISGEN in a railway rake up keeping depot." IEEE International Transportation Electrification Conference India (ITECINDIA), 2017 IEEE. IEEE, 2017.

[2] Laddha, Ashish, Abhik Hazra, Saborni Das, and Mousumi Basu. "Implementation of Social Spider Optimization for Optimized Hydel-Thermic Operational Delineation." *2017 IEEE PES Asia-Pacific Power and Energy Engineering Conference (APPEEC)*. IEEE, 2017.

[3] Ganguly, D., Das, S., Hazra, A., Basu, M., & Laddha, A. "Optimalized hydel-thermic operative planning using IRECGA." In Research in Computational Intelligence and Communication Networks (ICRCICN), 2017 Third International Conference on (pp. 68-73). IEEE. (2017, November).

[4] Hazra, Abhik, Saborni Das, Pallav Kumar Sarkar, Ashish Laddha, and Mousumi Basu. "Optimal allocation and sizing of multiple DG and capacitor banks considering load variations using water cycle algorithm." 2017 4th International Conference on Power, Control & Embedded Systems (ICPCES), 2017 IEEE. IEEE, 2017.

[5] Laddha Ashish, Abhik Hazra and Mousumi Basu. "Power production strategies from renewable energy resources in a hospital campus considering economic aspect." 2016 IEEE 7th Power India International Conference (PIICON), 2016 IEEE. IEEE, 2016.

[6] Laddha, Ashish, Abhik Hazra, and Mousumi Basu. "Optimal operation of distributed renewable energy resources based micro-grid by using Social Spider Optimization." Power, Communication and Information Technology Conference (PCITC), 2015 IEEE. IEEE, 2015.

[7] Das, Saborni, Abhik Hazra, Ashish Laddha, and Mousumi Basu. "Optimized Hydel-thermic Operative Outlining Using Grey-Wolf Optimizing Technique." *2017 IEEE International Conference on Power, Control, Signals and Instrumentation Engineering (ICPCSI)*. IEEE, 2017. [Presented: in production for publication in IEEE explore]

[8] Hazra, Abhik, Ashish Laddha, Saborni Das and Mousumi Basu. and Mousumi Basu. "Nonconvex Economic Dispatch Problem for Wind Integrated Large Power Network Using HTS Algorithm." National Conference on Recent Trends in Custom Power supply,2018. [Published in proceedings]

CERTIFICATE FROM THE SUPERVISORS

This is to certify that the thesis entitled "Development and Application of Soft Computing Techniques in Power System Optimization" submitted by Shri ***Abhik Hazra****, who got his name registered on the* ***10th of June, 2013*** *for the award of the Ph.D. (Engg.) degree of Jadavpur University is absolutely based upon his own work under the supervision of* ***Prof. Dr. Mousumi Basu, Jadavpur University*** *and* ***Prof. Dr. Amitava Gupta, Jadavpur University*** *and that neither his thesis nor any part of the thesis has been submitted for any degree/diploma or any other academic award anywhere before.*

_____ _____

Signature of supervisor and date with Office seal

Signature of supervisor and date with Office seal

Dedicated to

my parents

and

grand-parents

Acknowledgement

I take this opportunity to express my sincere appreciation for my supervisors, Prof. Dr. Mousumi Basu and Prof. Dr. Amitava Gupta for their patience and encouragement during the whole period of my PhD. During the work, they continuously provided me with enthusiasm, vision and wisdom. The guidance received from him cannot be acknowledged with few words. Their unconditional love, moral support and lucid illustrations of the technical matters have made my PhD journey memorable.

I am extremely thankful to all the members of the respected Doctoral Committee for the valuable internal reviews they provided regarding the work which was pivotal in giving a perfect blend to the thesis.

I am also grateful to the Head of the Power Engineering Department for providing the necessary departmental laboratory and library facilities during my course of work. I would like to extend my heartfelt gratitude to all faculty and non-teaching staffs of this department for their helpful attitude and constant encouragement.

The entire work of this dissertation has been supported and funded by the Basic Scientific Research (BSR) scheme of University Grant Commission (UGC), Govt. of India and I acknowledge the support that was provided by them.

I want to thank my family members and all my beloved lab mates Saborni Das, Ashish Laddha, Debayan Bose and all other seniors and juniors who have helped me through this journey. The best part of having such people in my lab has been that they have always made me feel insecure with their outstanding research capabilities and thus I was compelled to push myself further so that I could achieve my goal.

I especially would thank my friends Santanika Saha, Ritabrata Saha and Shanakha Suvra De for the indomitable love and support that they have provided me throughout the tenure of my PhD.

Finally I would like to thank God and the role of millions of countrymen who do not have much to eat or wear and who could have been fed and clothed with the money used for supporting my research and many others like mine.

Abhik Hazra

Jadavpur University

Preface

This dissertation is the final documentation of my doctoral study at the Department of Power Engineering, Jadavpur University. This dissertation is guided by my thesis advisors Prof. Dr. Mousumi Basu and Prof. Dr. Amitava Gupta of the Department of Power Engineering, Jadavpur University and no part of the thesis belong to any other dissertation. This dissertation consists of five broad chapters which are mentioned as below:

Chapter 1 *introduces the basic definition of Power System Optimization followed by its classification, comprehensive brief outlining of the research work presented in the thesis. Literatures those motivate these works have also been addressed in this chapter.*

Chapter 2 *addresses the mathematical modeling and formulation of different power system optimization problems.*

Chapter 3 *deals with the solution procedures of those mathematical optimization problems as formulated in the previous chapter.*

Chapter 4 *addresses the obtained results from the experimentations along with discussions regarding those results.*

Chapter 5 *Conclusions of the dissertation and future scope of research are summarized in this chapter.*

Abhik Hazra

Jadavpur University

Abstract

This thesis is oriented toward optimization of power systems by application and development of soft computing techniques. Two most primary considerable aspects, when performing these tasks, are economic aspect and environmental aspect. In most of the cases, these two aspects are mutually contradictory from the view point of mathematical optimization problems.

The scope of technological advancement for power system optimization lies essentially in the domains of optimal power generation planning, optimal power operation planning and power system restructuring in optimal ways. The power system optimization problems have been proposed here to be categorized in two segments, namely, Large-scale power system optimization problems and Micro-scale power system optimization problems.

In class of Large-scale power system optimization problems, several studies have been done in this thesis about optimal strategies and operation planning for economic dispatch and economic-environmental dispatch of single area and multi area large power systems, Wind power integrated multi area economic-environmental dispatch and short term hourly basis hydro-thermal generation scheduling of different power systems considering several technical constraints. Mathematical modeling in form of objective functions and constraints have been formulated. A novel energy policy that encourages proper estimation and maximization of wind energy generation has been proposed. Applicability of different heuristic and meta-heuristic optimization algorithms like, Heat Transfer Search, Artificial Immune system, Multi Objective Differential Evolution, Non-dominated Sorting Genetic Algorithm II, Improved Real Coded Genetic Algorithm etc. for different cases have been studied. Comparative studies of the obtained solutions by different techniques have also been done.

In class of Micro-scale power system optimization problems, several studies have been done in this thesis on optimal placement and sizing of Distributed generation systems in power distribution networks. Transmission loss minimization along with voltage profile maintenance and have been focused. Studies with variation of load have been done. Optimal integration and operation of distributed renewable energy recourses focusing on economic aspect have been studied for several realistic cases with different demand profile like a whole township, a typical railway rake maintenance depot and a typical hospital campus. In those cases, economic power operation increasing the share of renewable energy recourses have been proposed. Active distribution systems have been thoroughly designed forming

mocro-grid and nano-grids. Comprehensive electrical modeling and then mathematical modeling have been done to optimally design these type of micro/nano scale power networks. Optimum economic power operation for a PV aided battery storage connected nano-grid for a typical hospital campus have been proposed. Robust tracking controllers for automatic power operation have been designed in this thesis. Focusing on the fault analysis aspect; faults of photovoltaic system, which takes a large share in renewable energy sector, have been considered for studying. Detailed mathematical model of photovoltaic string along with other accessories like maximum power point tracking converter etc, have been constructed. A novel optimization technique based fault detection scheme with methodology has been proposed in this thesis, that can proficiently detect and locate open and short circuit faults of modules in a photovoltaic string. Different optimizers like, Water Cycle Algorithm, Social Spider Optimization, Gravitational Search Algorithm, Improved Real Coded Genetic Algorithm Grey Wolf Optimization etc. have been applied to these mathematically formulated optimization problems.

List of Figures

List of Tables

Table of Contents

Chapter 2

Problem formulation

Chapter 3

Solution techniques

Chapter 4

Results and discussion

Chapter 5

Conclusion & Future-scope

Chapter 1

Introduction

==========

Optimization is an everywhere-needed technique in progressive human civilization. Optimization has been applied, though in very crude way, since the very beginning of our society to make things as perfect or effective as possible or to find the trade off among many possible options. In modern science this optimization techniques has been given different complex mathematical forms. In late 1940's, George Dantzig firstly used mathematical optimization technique for United States air force application. It can be easily realized that, the more we know about something, the more we see where optimization can be applied. For mathematical optimization, one or more objective functions need to be formed. The goal of the mathematical optimization techniques is to find values of the variables that minimize or maximize the objective function while satisfying the constraints. These mathematical techniques have to be robust, providing Good performance for a wide class of problems. Those have to be efficient, not having too much computational load. At the same time those have to be accurate in identifying errors.

This thesis is oriented toward optimization of power systems by application and development of soft computing techniques. A civilization cannot be expected without consumption of energy. Energy demand is continuously increasing with the development of our society. Electricity, being a compact and efficient form of energy, is a prime mover of modern civilization. To manage electricity, power systems with different social, economic, environmental and technological strategies have been formed. Power system optimization has been considered as a crucial socio techno-economical challenge since the very beginning.

Power system optimization can be done through some technological advancement. Two most primary considerable aspects, when performing these tasks, are economic aspect and environmental aspect. The technologies should be economically faceable and simultaneously

environment friendly. In most of the cases, these two aspects are mutually contradictory from the view point of mathematical optimization problems.

The scope of technological advancement for power system optimization lies mainly in the domains of optimal power generation planning, optimal power operation planning and power system restructuring in optimal ways. The power system optimization problems have proposed here to be categorized in two segments, namely, Large-scale power system optimization problems and Micro-scale power system optimization problems.

In class of Large-scale power system optimization problems, several studies have been done about optimal strategies and operation planning for economic dispatch and economic-environmental dispatch of single area and multi area large power systems, Wind power integrated multi area economic-environmental dispatch and short term hourly basis hydro-thermal generation scheduling of different power systems considering several technical constraints. Mathematical modeling in form of objective functions and constraints have been formulated. A novel energy policy that encourages proper estimation and maximization of wind energy generation has been proposed. Applicability of different heuristic and meta-heuristic optimization algorithms for different cases have been studied. Comparative studies of the obtained solutions by different techniques have also been done.

In class of Micro-scale power system optimization problems, several studies have been done on optimal placement and sizing of Distributed generation systems in power distribution networks. Transmission loss minimization along with voltage profile maintenance and have been focused. Studies with variation of load have been done. Optimal integration and operation of distributed renewable energy recourses focusing on economic aspect have been studied for several realistic cases with different demand profile like a whole township (where overall power demand prominently varies with the weather), a typical railway rake maintenance depot (contains very unique load profile) and a typical hospital campus. In those cases, economic power operation increasing the share of renewable energy recourses have been proposed. To fulfill these purposes, active distribution systems have been thoroughly designed forming mocro-grid and even nano-grids.

Two important optimization aspects of active distributed systems for being triumphant, are smooth automatic controlled operations by designing optimal controllers of power electronic devises, and power network reliability by fault analysis of renewable power sources. Focusing on the control prospect; comprehensive electrical modeling and then mathematical modeling have been done to optimally design these type of micro/nano scale power networks. Optimum economic power operation for a PV aided battery storage

connected nano-grid for a typical hospital campus have been proposed. Robust tracking controllers for automatic power operation have been designed. Focusing on the fault analysis aspect; faults of photovoltaic system, which takes a large share in renewable energy sector, have been considered for studying. Detailed mathematical model of photovoltaic string along with other accessories like maximum power point tracking converter etc, have been constructed. A novel optimization technique based fault detection scheme with methodology has been proposed that can proficiently detect and locate open and short circuit faults of modules in a photovoltaic string.

The outlining of the power system optimization problems, which have been developed to solve by application of soft computing techniques throughout this thesis, has been depicted in Figure 1.1.

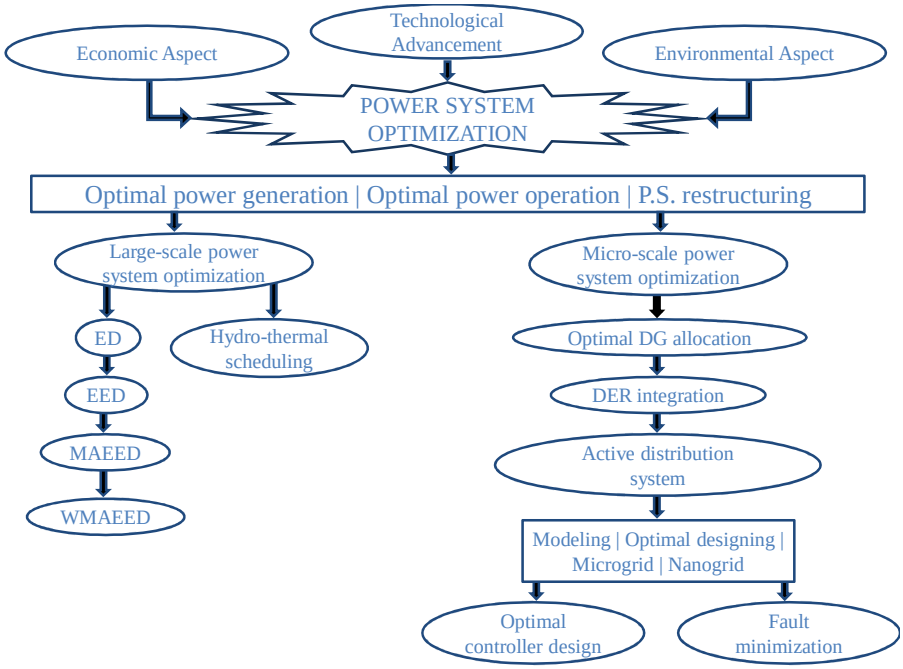

Figure 1.1. Outlining of power system optimization.

1.1 Large-scale power system optimization

1.1.1. Economic dispatch problems

Economic Dispatch (ED) is a crucial maneuver for power production through all online generators with least possible cost fulfilling a assortment of technical constraints. The valve-point effect [1] has been modeled mathematically by summing up the sinusoidal function and quadratic function. Shaft bearing shuddering, caused by the opening of steam entrance valve or machine burden, creates prohibited operating situation in a few sections of generation

region of a generator, commonly known as prohibited operating zone [2]. The lowest cost is attained in case of circumven this operating zone.

The traditional practice cannot solve these type of ED problems. Dynamic programming can solve these problems but it undergoes to the dimensionality quandary and restricted optimality. Meta-heuristic algorithms substantiate the potential for solving these class of ED problems. Improved tabu search (ITS) [3], genetic algorithm (GA) [1, 2, 4] evolutionary strategy optimization (ESO) [5], evolutionary programming (EA) [6, 7], particle swarm optimization (PSO) [8–12], biogeography-based optimization (BBO) [13], continuous quick group search optimizer (CQGSO) [14], differential evolution (DE) [15, 16], Distributed auction optimization algorithm (DAOA) [17], cuckoo search algorithm with interactive learning (CSAIL) [18] etc. have been on hand to solve complicated ED problems. Though these methods cannot always realize the global optima, they often achieve close up to the global optima.

Heat Transfer Search (HTS) algorithm, based on the proclamation of thermodynamics and heat transfer, emulates the thermal balance activities of any system. The penetrating route of HTS ponders over three stages, specifically ‘conduction phase’, ‘convection phase’ and ‘radiation phase’ [19].

In this thesis, the suggested HTS algorithm has been engaged to work out three complex economic dispatch problems. Test results obtained from HTS algorithm have been adjudicatored against to that other evolutionary techniques solving economic dispatch problems present in literature. It has been noted that the proposed Heat Transfer Search algorithm produces superior solution.

1.1.2. Multi area economic dispatch problems

Economic dispatch (ED) allots the load demand amongst the dedicated generators most economically while fulfilling the operational constraints in a single area. Usually, the generators are alienated into a number of generation areas interrelated by tie lines. Multi-area economic dispatch (MAED) is an expansion of ED. MAED settles on the generation level and exchange power among areas such that overall fuel cost in all areas is minimized while fulfilling technical constraints relsated to power balance, generating limits and tie line competence [20].

The ED problem is often resolved without taking into account for transmission constraints. Nevertheless, some researchers have taken transmission ability constraints into

consideration. Shoults et al. [21] solved ED problem considering power import and export constraints between areas. This work endows with a entire formulation of multi-area generation forecast, and a structure for multi-area studies. Romano et al. [22] opened the Dantzig–Wolfe decomposition rule to the constrained ED of multi-area systems. Doty and McEntire [23] resolved a MAED problem by using spatial dynamic programming and the outcome obtained was overall most favorable. Linear programming to transmission constrained delivery cost examination was proposed in Ref. [24]. MAED with area control error was solved Helmick et al. [25]. Heuristic multi-area unit commitment with ED was proposed by Ouyang et al. [26]. Wang and Shahidehpour [27] proposed a decomposition based approach for resolving multi-area generation setting up with tie line constraints using specialist systems. Network flow models to resolve the MAED with transmission constraints have been projected by Streiffert [28]. Calculation of short range margin cost-based prices for MAED problems has been presented by Wernerus and Soder [29], solving MAED problem via Newton–Raphson's method. Yalcinoz and Short [30] solved MAED problems by means of Hopfield neural network approach. Jayabarathi et al. [31] resolved MAED problems considering tie line flow constraints involving evolutionary programming. The direct search scheme for solving ED problem considering transmission line capacity constraints was offered in ref. [32].

Artificial immune system (AIS) [33-38] has appeared in the 1990s as a new area in computational intelligence. AIS is stirred by immunology and principles of immunity observed in life. It is now attention of lots of researchers and has been productively used in power system optimization problems [39-40].

In this thesis, AIS algorithm is developed for solving the MAED problem. The proposed come up to the clonal selection attitude and gears adaptive cloning, manic mutation, aging operator and contest selection.

The projected AIS algorithm has been emploied to solve MAED problem. Here, three types of MAED problems have been chosen. These are (A) multi-area economic dispatch with quadratic cost function prohibited operating zones and transmission losses, (B) multi-area economic dispatch with valve point loading and (C) multi-area economic dispatch with valve point loading multiple fuel sources and transmission losses.

The projected AIS technique has been authenticated by emploing it to three diverse test systems. The solution wise performance of the proposed AIS algorithm has been weighted against differential evolution (DE), evolutionary programming (EP) and real-coded genetic algorithm (RCGA).

1.1.3. Multi area economic environmental dispatch problems

The power production through fossil fuels emits Sulfur oxides, Carbon oxides, Nitrogen oxides and many others into the atmosphere. These emissions influence humans as well as other living beings in our planet. Other effects include vegetation damage, acid rain, less visible clarity, global warming etc. The environmental safety issue as well as the clean air act amendments, 1990 have bounded the amount of the emissions by a power generating station [41]. Therefore, a trade-off is required between generating electricity at the minimum possible cost with maintaining the emission level to the minimum.

Various techniques have been suggested for minimizing the emission level [42]. Some of these include post combustion cleaning device usage, using the fuels with less emission content, changing old fuel burner devices with new cleaner devices, power dispatching keeping in view emission limits etc. Choices other than the final one need investment in the form of new devices use and/or changes in the already installed devices involving significant monetary requirements. Therefore, they may be convenient for long duration aspect. Due to the aforementioned reason, the final choice seems to be convenient for practical implementation point of view.

Goals related to pricing and level of emission, seem to be contradictory. Both are required to be taken into consideration at the same time to determine feasible and optimal power dispatch. Various optimizing methods [43-53] are available in the literature related to the economic environmental power dispatch strategy. These problems deal with a single area power network and their related engineering constraints.

Large realistic power networks are spread over multiple areas connected to each other with tie lines. Several researches [21-32] have been conducted to deal with the power production strategies considering only economic aspect for multi area power systems.

Multi area economic environmental dispatch strategy (MAEED) is an extended version of the multi area economic dispatch problem. It gives an information about the level of power production as well as power exchange between areas in a manner such that total cost of fuel and pollution level in each of the area remain optimized simultaneously keeping various constraints such as equality between generated power and load demand, generation range and capacity consideration of tie line into consideration.

In recent time, the formulation of various multi objective evolutionary algorithms (MOEA) [54-57] took place. Aforementioned techniques are based on population, and various pareto-optimal results are obtained by running them just once. Strength pareto

evolutionary algorithm II (SPEA II) and multi objective differential evolution (MODE) have been used for solving the economic environmental power dispatch problems effectively for single area power networks. The presented work on this thesis emphasizes on the use of the MODE for the MAEED problem which has been formulated in the form of a nonlinear constrained multiple objective optimization task. For demonstrating the suggested technique's competence, a four area test system has been considered. A comparison has been made between the results achieved by the MODE and that of SPEA II.

1.1.4. Wind integrated multi area economic environmental dispatch problems

The MAEED settles on the generation levels and power transactions among areas such that cumulative generation cost and emission level get minimized in each of the areas maintaining power balance boundings, production limits boundings, boundings related to prohibited operating zones (POZ) and tie-line capacity boundings. The solution approaches for the MAEED available in the literature are based on different metaheuristic optimization algorithms and mathematical solvers. An analytical model possessing dependency on the multi objective particle swarm optimization with regional exploring has been developed for solving the MAEED task [58, 59]. Other multiple objective approaches such as improved differential evolution along with fuzzy selection, universal best artificial bee colony algorithmic technique with chaotic optimization have been suggested for solving the MAEED task [60, 61].

Hybridization of gradient search method with improved Jaya algorithm has been accomplished for a practical MAEED problem [62]. A Pareto-based teaching–learning optimization algorithm has been also proposed [63]. Since, the majority of the power systems are still generating power from fossil fuels, which are unsustainable, costly and are the major sources of atmospheric pollution, the modern power systems are gradually restructured with the strategic integration of renewable energy resources in conventional power systems. Amongst these, wind energy is gaining the most acceptances for meeting the rising energy demand at low cost without any harmful emissions [64], which significantly influence EED problems of power systems integrated with wind energy. But considering the scenario of large wind power producing units (WUs), randomness, low inertia characteristics and huge forecasting errors corresponding to wind speed and the produced wind power upset the

stability as well as security of the overall power system. Hence, intermittent wind power needs policies and dispatch tactics to uphold economy with reliability and security.

Different stochastic search methods and solvers such as, strength pareto evolutionary algorithm (SPEA) and simulated annealing-like particle swarm optimization equipped with specially encoded/ decoded chromosome's string [65-67], chaotic quantum genetic algorithm [68], harmony search algorithm [69] and GAMS BARON [70] solver have been used for some EED studies incorporating wind energy without the consideration of stochasticity in available wind power.

Several other EED, employing different stochastic programming, have included some modifications to conventional EED models to deal with intermittent wind integrated power system. Uncertainty constraints [71] and frequency stability constraint [72] have been incorporated in some EED problems to transact with the wind power indefiniteness. The entropy concept has been introduced in [73] to balance the uncertainty issue regarding wind power. Deterministic uncertainty set [74] and polyhedral uncertainty set [75] have been modelled to describe the volatile wind generation. Learning automata [76] has been used as a multi-objective optimizer where its strategies are modified according to the learning experience about current information of wind speed.

In latest EED studies, the Weibull probability distribution function (WPDF) [77] has been considered as the best fitting probability distribution model for forecasting the empirical wind speed distribution [78]. With the assortment of WPDF, different meta-heuristic methods such as, pareto based modified teaching-learning algorithm [79], artificial bee colony algorithm guided by Gbest [80], gravitational search algorithm [81], bacterial colony chemotaxis [82], decomposition based evolutionary algorithm [83], particle swarm optimization [84], honey bee mating optimization [85] and nondominated sorting genetic algorithm II (NSGA II) [86] have been considered to solve the EED with special consideration to uncertainty due to wind integration.

It is evident from the literature that, so far researches have concentrated on the impacts of WUs in either the single area single objective economic or environmental dispatch or bi-objective EED. In case of wide spread multi-area power system network, uncertainty of wind power availability notably differs for different areas. Moreover, for enhanced motivation of wind power operators to inject more power to the grid with maximum possible certainty, proper area-wise penalty cost formulation is needed. In this scenario, considering the inevitability of wind power integrated multi-area power system operation in modern power

system restructuring process, optimal wind integrated EED planning for large scale multi-area power system is a relevant research interest.

This thesis develops a novel model of multi-area bi-objective economic environmental dispatch of wind power integrated system (WMAEED), which would potentially optimize the schedules of the committed conventional and WUs with the tie-line power flow limitations while simultaneously reduce the operating cost and environmental emission levels considering several area-wise uncertainties of available wind power, special penalty costs for over and under estimation of committed WUs, dynamicity of the online generating units with operational and physical network constraints.

For resolving the multiple-objective optimization tasks, two usual paths can be followed. One merges all the objectives into a distinct amalgamated function by assigning adaptive weights to each objective through optimizers according to the prior knowledge. Moreover, the optimal result renders no knowledge about the compromise among objectives. The other way employs suitable multiple-objective algorithm which generates “Pareto front” solutions [87].

This WMAEED model formulation has been incorporated in the form of a bounded nonlinear multiple-objective optimization task. To validate the proposed approaches, a four area wind integrated test power system is considered in this work. Well recognized algorithms like nondominated sorting genetic algorithm II (NSGA II) [57] along with strength pareto evolutionary algorithm II (SPEA II) [88] have been employed here to generate Pareto fronts [89] of suitable compromised solutions for the proposed WMAEED model. The obtained results from the numerical experimentations confirm that the wind integration to conventionally sourced multi-area power system reduces the overall generation cost as well as emission level with the proposed dispatch modeling considering area-wise uncertainty and introducing area-wise penalty costs.

1.1.5. Hydro-thermal scheduling problems

Hydro electricity, being a cleaner production methodology, is becoming significant in our energy based society. Practice of hydro-electric energy generation may effectively reduce the environmental degradation caused by conventional thermal, diesel or nuclear power plants. On the basis of operating cost, hydro-electricity is truly convenient whereas thermal power generation is very expensive. Optimal operation coordinating hydro and thermal generation is a relevant engineering problem in the current energy scenario. Hydro and thermal plants can

give the optimal solution from cost perspective but it is very difficult to co-ordinate with each other. It is a big challenge for the researchers in the field of economic power system operations. Hence, the requirement is cost optimization through proficient operation planning. The operation planning is classified as small, intermediate and large horizon generation scheduling. Small horizon operation scheduling is for one day to one week, intermediate scheduling is for one week to one year and large horizon is for one year to several years.

Amongst these, short-term hydrothermal generation scheduling (SHTGS) problems are widely trending the now a days. Hydro-thermal generation constraints may comprise of generation-load power balance, upper and lower limits on reservoir capacity, water discharge rate, water spillage rate, hydraulic continuity restriction and operating capacity limits of different hydro and thermal units. The optimal scheduling of hydrothermal power system is usually more complex than that for all thermal systems. It is a complex multi-dimensional optimization problem with a non-linear highly constrained objective function. The aim of SHTGS is to determine the optimal amount of the water release for the hydro and thermal generation in the system to meet the load demands over a scheduled horizon of one day. Different mathematical optimization algorithms have been implemented for the solution of SHTGS problems. Those are gradient search [90, 91], mathematical decomposition [92-94], dynamic programming [95-98], and mixed integer type programming [99,100].

But, these methods have difficulties in handling various constraints and also take more time to solve. Hence, these methods are not suitable to address such types of problems. Dynamic programming has been frequently used. However, this method has difficulties in computational overburden for its large dimensionality when applied in a practical power system. Various stochastic search algorithms have been found in literature for hydro-thermal scheduling (HTS).Simulated annealing (SA) has been used in to find the global optimal solution [101] by Wong et al. But, appropriate setting of the relevant control parameter of the SA based algorithm is a difficult task and the speed of the algorithm is quite slow when applied to practical sized power system. Evolutionary programming (EP) is one of the oldest meta-heuristic optimization technique used to solve many optimization problems [102]. Yang et al. [103] and Hota et al. [104] projected EP to solve the HTS problem using Gaussian mutation. But it is useful in solving simple problems with fewer constraints.

Afterward, evolutionary programming and an improved fast EP technique were planned by Sinha et al. [102] for HTS. Later, Werner et al. [105] applied evolutionary approach to solve SHTGS problems of hydrothermal systems. A fuzzy based evolutionary programming

technique was reported for the economic HTS problem [106].Genetic algorithm (GA) is an evolutionary method [107, 108], and proposed by Orero et al. to solve HTS problem [109]. Kumar et al. offered GA to solve the HTS problem with optimal power flow [110]. Gjorgiev et al. planed an efficient multi-objective based GA for solving HTS [111]. A short-term HTS based differential evolution (DE) algorithm was introduced by Mandal et al. [112]. But, it is very difficult to correctly choose the control parameters of differential evolution. The faster convergence of DE results in a highest probability toward a local optimal solution. Parameters of DE generally are steady throughout the entire search process but it is difficult to properly set control parameters.

Particle swarm optimization (PSO), an another robust optimization technique, can produce stable convergence characteristics than most of the other stochastic methods [113-115]. An improved PSO (IPSO) based HTS to solve a multi-reservoir cascaded hydro-electric system having restricted discharge zones and a thermal unit with valve point loading have been introduced [116]. The simulation results showed its superiority over other techniques. Yu et al. used PSO to solve SHTGS problem with an equivalent thermal unit having smooth cost functions [117]. Modified adaptive PSO based HTS was introduced by Amjady et al. [118]. Mahor et al. presented self-adaptive inertia weight based PSO method to find the optimal generation planning for cascaded hydroelectric system [119].

Clonal selection algorithmic technique has been used in a practical sized power system related HTS problems [120].

Rao et al. developed teaching learning based optimization (TLBO) technique for HTS related power system optimization problem [121,122].

Tabu search algorithm technique based HTS for hydrothermal plant was first introduced by Bai et al. [123]. Huang et al. first initiated ant colony optimization (ACO) technique to solve HTS problems [124]. Adaptive artificial bee colony algorithm was first introduced by Liao et al. to solve long time dispatch of cascaded hydropower systems and also compared its efficiency with other available techniques [125]. Neural network technique can be used to solve HTS problems. But, the neural network-based approach suffers from large computational problem. The GA is one of the most promising EP having its origin corresponding to the human inbred chromosome operation. The GA is inspired from the Darwinian evolution theory “the survival of the fittest”. It engenders the universal or close to the universal optimized results corresponding to a minimizing optimization task. For this, it creates a number of communities during iterative run. The GA has some advantages such as

simple algorithm, able to handle different sorts of functional representations of problems and its robustness [126].

In this concise, improved real coded genetic algorithmic technique (IRCGA) has been implemented to increase the convergence speed and solution quality. The IRCGA has been used to plan a short-spell, hourly basis optimized operative scheduling for the considered hydrothermal network. Restricted operating sections have been taken into consideration for hydro producer. Different test solutions of the IRCGA have been compared with acquired by other EPs. It has been noticed that the implemented IRCGA gives superior results. The test results for short term hydro-thermal scheduling are compared with other methods available in literature, such as Real coded Genetic algorithm (RCGA) [127-128], Improved first evolutionary programming (IFEP), Genetic Algorithm (GA), Modified differential evolution (MDE), Improved particle swarm optimization (IPSO) and Teaching learning based optimization technique (TLBO). Numerical results show that the projected Improved real coded Genetic algorithm (IRCGA) based algorithm can provide quality solutions.

1.2. Micro-scale power system optimization

1.2.1. Optimal DG allocation

Coal and oil based traditional centralized methods have been applied for power generation, from very early age. In these schemes, the generated power is transmitted over extended distances with huge transmission systems which involves massive amount of transmission losses. Besides, fossil fuels originates loads of environmental vulnerability. On these grounds, DG is gaining magnitude in haste. In case of DG, the power is generated in the vicinity of the load centers. Nonconventional energy resources such as solar photovoltaic system, biomass, fuel cell, wind power etc. are being involved to generate power. By that ground, DGs may be tagged as reliable, flexible and atmosphere gracious system with enhanced power quality [129-130]. Considering the transmission losses, DG is more energy efficient than traditional centralized power generating schemes [130]. It initiates diversification in energy resources with a reduction of speculation risks [131]. DG can also make power available to those distant areas, small localities where traditional fossil fuel fired methods of power generation are unable to convey power.

DGs may be clusterred according to the amount of generated power by them. DGs, which can generate up to 5 kW, are known as micro DGs. From 5 kW to 5 MW, are small DGs.

From 5 MW to 50 MW, are medium DGs. From 50 MW to 300 MW, are classified as large DGs [132]. DGs may also be classified according to the mode they transact with real and reactive power [133]. The DGs, which convey just real power, are of Type 1. DGs which carry in cooperation real and reactive power are of Type 2 while the DGs which deliver real power but take up reactive power come up to the Type 3. DG allocation and sizing have elevated considerable notice in modern times. Most of the recommended schemes are analytical or meta-heuristic or heuristic in nature. Determination of optimal allocation and sizing of DG using loss compassion factor technique was used in [134]. Similarly, methods have also been developed invilvong exact loss equation for manifold DG unit assignment in order to attain greater loss reduction [135]. Other methods, based on novel power stability index [136] and power loss factors [137], have also been employed for DG assignment. Other methods, which have been used for DG placement are bee colony algorithm [138], a GA induced algorithm [139], improved PSO and Monte Carlo replication [140], modified teaching learning optimization algorithm [141]. These works have been done for optimal assignment and sizing of DG, lessening of power losses, and voltage profile as well as reliability upgrading. In order to reduce system losses addressing uncertainties, a probabilistic technique based scheme was anticipated in [142].

Usually, a DG is positioned to bring in real power into the system but reactive power is significant as well to uphold the voltage at the requisite point. Alteration of reactive power results in voltage level shifts that affects the voltage stability. Therefore, reactive power reparation is essential. The traditional practice facing this issue is to place capacitor banks. In previous era, synchronous condensers were employed for power factor enhancement. In recent situations, static VAR compensator is placed extensively for regulation of voltage, power factor and the system stability. Novel Global Harmony Search algorithm (NGHSA) has been proposed for optimal allotment of VAR compensators in a power system [143], which have also been used for reactive power management [144]. A combined scheme of modal analysis, simulated annealing and Tabu search was used in [142] for optimal placement of VAR compensator.

All the above research work to DG or VAR compensator placement has been employed separately in power systems. In this thesis, a method of optimal placement and sizing of both DG and VAR compensator has been proposed. In this optimization problem, multiple DGs, those inject active power in the system at different buses and along with capacitor banks, which inject reactive power at different system buses, have been projected to be put in in the powr network. This technique is implemented in a standard IEEE 33 bus radial distribution

system using water cycle algorithm (WCA), a newly developed optimizer, based on the flow of water from rain drop to water stream to river to sea finally [145].

1.2.2. Optimal power operation integrating distributed renewable energy resources

With the growing consciousness about the necessity of economic power production measuring the concern of environmental security, most of conventional energy resources in centralized power delivery schemes are trailing popularity. Whereas, a recently mounting technology of dispersed generation explicitly decentralized generation or distributed generation is approaching the front. Distributed Energy Resources (DER) are singing a crucial role to check the environmental effluence through employment of non-conventional and renewable energy sources such as fuel cells, wind power, solar modules, biomass gasifier units etc. Many researches related to the design and operations of DERs are being done [131, 146-150]. Potentialities of implementing micro-grid with the DERs are also discussed someplace [151-153]. Special treatments are also being paid to the economics of Hybrid Distributed Energy Resources [154].

Optimal integration and operation of distributed renewable energy recourses (DER) spotlighting on economic aspect have been analyzed for several realistic cases with different demand profiles.

1.2.2.1. Optimal power operation planning in a township

Currently, fossil fuel ablaze power generation is mostly used. In this scheme, generation of power is done far away from localities and nearby the places where fuel is readily obtainable. By executing this, the transportation expenses stay least and localities are also free from effluence. After production, power is transmitted to different places with the help of transmission lines. With the incessantly growing energy demand, additional power generation is obligatory. Fossil fuel fired power generation has arrived at that level, where additional generation should be controlled due to limited accessibility of these fuels and environmental alarm. Thus, various other methodologies for power generation should be involved. Distributed generation is a superior idea concerning this. In it, the power generation takes place near the consumers with the help of traditional energy resources or nonconventional energy resources like solar photovoltaic system, fuel cells, biomass gasifier units etc [155]. It has many advantages over fossil fuel fired power generation. It offers environmental benefits,

better energy efficiency, energy independence, fuel diversification and engage less investment risks [131]. DG can fulfill the power necessities of those distant areas and petite localities, where power has not attained yet by conventional power generation. DERs are established to be more reliable power provider and have compact transmission systems [130]. A amalgamation of DERs provides more flexibility and reliability to accomplish requisite power demand and named as hybrid DER. Micro-grid is a excellent notion to alleviate the intricacies of traditional centralized power generation schemes. Micro-grid may be constructed involving DERs. A lot of technical studies has been done on hybrid DER but not much work associated to its economic analysis. In this thesis, development of micro-grid by involving hybrid DER has been studied, consumer loads, transformers, circuit breakers, cables and controllers. Five types of consumers, like market, campus quarters, hospital, bank and post office and hostel have been considered in Kharagpur Township of West Bengal, India. Two types of seasonal load variation have been considered for the economic scrutiny of hybrid DERs [154]. At this place, it is pragmatic that the day by day solar irrradiance are consistent. So, solar energy can be a practical energy resource here. Biomass is also easily accessible here and can produce sufficient power. FC is free from losses due to mechanical to electrical alteration process. However, wind power has not been found dependable at this place. In this thesis, economic analysis of hybrid DERs has been made by using a newly developed social spider optimization (SSO) algorithm [156]. This algorithm endowed with better solutions as compared to other evolutionary or swarm algorithms [157, 158].

1.2.2.2. Optimal power operation planning in a rail-way rake maintenance depot

Previous part was about the study of optimal power operation for a whole township. There delineated demand dissimilarity depends on the seasons throughout the year. Though in the case of some distinctive industries, where power stipulation do not have seasonal craving, detailed optimal power operation studies and economic analysis in this low scale level is indispensable. In this thesis, such an industry, like a rail-way rake maintenance depot has been taken as a realistic case.

A Rail Ways rake maintaining depot, where electrical and mechanical maintenance of Traction Rolling Stocks are performed, namely “Sonarpur TRS/EMU Railways Car-shed, E.Rly” was established in the year 1979. It is situated in Sonarpur, the south sub-urban of Kolkata City. Total premises area of this car-shed is about 68550 m^2, where total covered space is 8850 m^2 and area of open space is about 59700 m^2. This depot has an average

electrical consumption of about 50 KVA with a maximum demand contract of 200KVA. This power is drawn from Sonarpur 33/11 KV Substation of West Bengal State Electricity Distribution Company Ltd (WBSEDCL).

In this thesis, a proposal is initiated to implement distributed energy or decentralized energy generation system in the aforesaid site of Eastern Railways. This car-shed is in the run of 24X7 hours by 3 shifts per day. The load profile of 24 hours is inspected and it is noted that the load arrangement is very taut and highly optimal (considering all constraints regarding their routine working schedule) with average load of 50 KVA , maximum demand of 120 KVA and with connected load of 400 KVA. They uphold their power factor 0.98 to 1 introducing capacitor bank in their sub-station. In this situayion, optimal power operation planning is to be done extenuating the hourly demand.

Solar and wind impending of this region was taken from West Bengal Renewable Development Agency **(**WBREDA) and as per the reports wind power generation is not apposite there but its solar potential is considerable to generate power. Large amount of spare area is available In the premises to set up renewable power generators like biomass gasifier units, fuel cells, etc. Considering this scenario, only solar power system (SPS), biomass gasifier unit (BMGU) and phosphoric acid fuel cell (PAFC) are projected as DERs here along with a battery energy storage system (BESS).

Beside the environmental reimbursement, the main objective for introducing distributed generation here is to lessen the electricity invoice charged by WBSEDCL to Eastern Rail Ways and if possible to earn back some money feeding spare power to the grid, so that this proposal becomes pretty to the consumer ie. the Rail Ways company.

To fulfill the objective, optimal power operation planning and the optimal capacity of the afforsaid renewable power generators are projected. A comparative study is also done for three set of generators. ie. Case I, II & III.

Case I. Biomass gasifier unit (BMGU) and solar power system (SPS), along with a battery energy storage system (BESS).

Case II. Phosphoric acid fuel cell (PAFC) and solar power system (SPS), along with a battery energy storage system (BESS).

Case III. Biomass gasifier unit (BMGU), phosphoric acid fuel cell (PAFC) and solar power system (SPS), along with a battery energy storage system (BESS).

Here Gravitational Search Algorithm (GSA) is chosen to optimize this highly constrained problem. Gravitational Search Algorithm is a strong heuristic search algorithm. It is based on the law of gravity and mass interactions [159]. Though GSA is not very common to solve

such optimization problems, it has success solving a variety of optimization problems in other field like symmetric traveling salesman problem [160], flow shop scheduling problem [161], DNA sequence design problem [162] etc. Considering these, GSA is chosen to solve this optimization problem. To ensure the reliability of the performance of GSA for this optimization problem, the problem is also resolved by well recognized Particle Swarm Optimization (PSO) technique.

1.2.3. Optimal power controller design of active distribution network

On the contrariety of cleaner energy productions, these distributed renewable energy recourses are appearing with several challenges in forming optimally reliable, efficient, smooth and economic power supply arrangements.

The energy produced by the renewable energy systems has been increased due to improvement in technology and awareness among the people, around the world. Although, these alternate energy systems still have various drawbacks, such as over dependency on environmental conditions, which varies from place to place and hence can lead to designing flaws. The system, thus developed for a particular application, may be found to be oversized or undersized. This makes the problem difficult to solve as the fluctuating source may not be able to supply the demand at some critical conditions [163]. These situations have led us to a significant increase in the number of scientific publications on the field of renewable energy sector over the last few decades [164].

In India, a large portion of population lives in rural and remote areas which are far away from grid supply and a heavy cost is involved in extending the grid. Therefore, such areas can be electrified in a decentralized mode by renewable energy plants such as small hydro, biomass, solar, wind, etc. and their combination in an integrated manner. Apart from electrification of individual household by renewable energy, the integrated renewable energy system (IRES) and the hybrid energy system (HES) [165] can also be developed. HES or IRES requires the knowledge of parameters like existing technologies, available government policies, customer requirements and resource limitations [166]. Incorporation of recent energy solutions are required for energy delivery betterment, assurance of seamless power supply and handiness along with monetarily favorable operation [167].

A regulating network is required to estimate the needed active and reactive power which can be obtained through each power producer while assuring the required voltage as well as

frequency values. Each power producer along with its own regulator is desired in order to attain optimized power operation by utilizing the available informative details of the corresponding instant. On addressing these purposes, various planning, schematics and methodologies are available in the resent literature.

Most of the time, classification of the regulating network involves centralized, decentralized and hybrid type model and a multiple layered approach towards regulation [165]. The impact of solar photovoltaic system can also be mitigated by a proper regulation network incorporation support in attaining grid favorable operation [168]. A two stage model predictive control strategy has been proposed for an economic diesel-pv-battery integrated operation in [163]. Load prediction and energy storage sizing methodologies have been proposed for a university campus in [166]. A MILP model for micro-grid energy management has been proposed in [169]. Optimal sizing and operation of a standalone islanded micro-grid have been studied [170]. Study on experimentations on real-time energy management of a islanded micro-grid are also present in [171] and micro-grid power scheduling considering multi period islanding constraints has been treated in [172] and many others.

Out of numerous inexhaustible energy production schemes [163-172], a combination of solar photovoltaic system along with battery storage is mostly used and is the subject of interest of this part of the thesis.

In this context, considering the emphasized research activities on operation and management of PV integrated dispersed power generation system, the presented work is motivated to propose a comprehensive economic operational strategy and control scheme of battery energy storage connected solar power aided nano-grid, formed in a typical urban hospital campus.

In this work, the considered practical system to validate the proposed scheme is the power supply system of a typical medium scale hospital situated in Kolkata, India. Its premises contain main building, oncology building and daycare building. Major healthcare and auxiliary facilities of the hospital are spread around an area about 4879.78 square m. The power requirement is brought to fruition through connection from Calcutta Electric Supply Corporation (CESC).

This problem has been mathematically formulated as a cost minimization optimization problem finding the optimized power operation. An improved real coded genetic algorithm (IMRCGA) is employed for achieving economic power dispatch through solar photovoltaic network and battery energy storage accumulating network constituting a nano-grid. The

obtained results have been compared with well established real coded genetic algorithm (RLCGA). The electrical model of this nano-grid has been presented mathematically along with designed controllers which suit to perform as per the optimum solution obtained by the proposed methodology. The transient behavior of the closed loop system for a realistic change of reference due to ambient disturbances has been studied by real-time Hardware-in-Loop simulations using the real-time platform Opal RT OP4500 and MATLAB real-time Windows target.

1.2.4. Optimization based fault detection scheme in photovoltaic system

With the speedy exhaustion of fossil fuels, the global energy scenario is altering drastically by tactical replacement with renewable energy resources throughout the past few decades. Amongst these, solar photovoltaics (PV) is going to have the uppermost yield increment of roughly 230 times of its existing assembly and will share 16% of total electrical energy production by the year 2050 [173, 174]. This vast growth in PV industry can be ascribed to various environmental, economic, technical and social factors and their sustaining policies [175, 176].

Huge PV plants, with hundreds of megawatts generation capability, are constructed over thousands acres of plant vicinity. Such massive PV plants are outfitted with hefty number of PV modules, balance of system components and protection devices like power fuses, ground fault detection interrupter, over current protection devices etc. [177-181]. PV modules are typically connected in series-parallel amalgamation to get optimum current and voltage ratings [182]. Any unanticipated module failures, even in any single module, can lead to great fault current and severely degrade the capitulative performance of the plant. Furthermore, the protection devices are often unable to clear the faults under non-uniform irradiation state and during "night-to-day" shifting mode [183]. Though fault possibility of PV modules is relatively less, but different module associated system faults, mainly, open circuit (OC) and short circuit (SC) faults arise recurrently, causing major deterioration of output electrical parameters and overall system efficiency [184].

So, in this situation, it is an unavoidable need to detect these kinds of faults fast and efficiently. There are several recent significant studies on fault diagnosis of PV system for identification of different faults including SC and OC faults. Most of these fault detection procedures are implemented online and have adopted different fault detection techniques

based on threshold estimation, fuzzy logic, domain transformation, classification methods like artificial neural networks, state estimation and hybridization among these techniques [185, 186].

Thermo-graphic inspection using thermal imaging cameras or infrared radiation sensors, mainly mounted on unmanned aerial vehicles, are popular methodologies to trace hotspot caused by SC, OC, mismatch or other faults [187-189]. These actions cannot discriminate among the dissimilar faults. A threshold-based method, executed by comparing current and voltage indicators with their threshold values, has been engaged to recognize the occurrence of faults in a PV sub-string, but failed to classify and locate the OC, SC or bypassed PV module [190]. Graph-Based Semi-supervised machine learning and Fractional-Order Color Relation Classifier have also been studied for OC and SC faults [182]. Artificial neural network and probabilistic neural network based OC and SC fault detection and classification have been reported in the literature [191, 192]. The concept of wireless self-powered sensor monitoring has also been introduced [193]. There are some studies of PV string electrical parameters based OC and SC fault diagnosis, where string output power and voltage window were created. These are probabilistic methodologies and have used probabilistic factors based on string output power or voltage along with module irradiation data and temperature captured using sensors [194, 195]. These methods can detect the number of faulty modules, but still cannot locate the faulty modules in the string. Furthermore, these methods have not considered the occurrence of both OC and SC faults together in PV string.

From the above brief literature review, it can be noted that, the so far proposed techniques for OC and SC fault diagnosis in PV system have some intricacies to wholly diagnose OC and SC faults along with the locations of faulty modules in PV string. Interestingly, direct application of heuristic optimization approaches in the case of PV system fault diagnosis is rare in the literature. Though, some partial uses of optimization techniques, like optimal placement of voltage sensors using optimizer and optimization of BP neural network for SC and OC fault diagnosis have been noted in the literature [196].

Hence, motivation of this work is to apply metaheuristic optimization based soft computing technique to develop an efficient PV fault diagnosis methodology that is able to quantify, locate and identify open circuited and short circuited modules in a PV system. The fundamental concept of this proposed fault diagnosis methodology exploits the fact that for a large PV system, experiencing heterogeneous irradiance and temperature distribution throughout the string, the resultant string current is explicit for a particular fault combination and specific locations of the faulty modules in that string. This very phenomenon has been

utilized in this work to formulate fitness function. There exist so many probable combinations of faulty modules in a PV string. From this huge search space, the proposed technique makes use of metaheuristic optimizer to seek out the exact combination of faulty modules and their respective locations, which may cause the string current same as monitored from the PV string at the particular irradiance and temperature conditions prevailing at that instant.

There are some potential key challenges in the case of PV fault diagnosis. In running condition, the PV system is supposed to be operated at maximum power point (MPP). Under non-uniform irradiation or partial shading condition and during faults in a PV string yield nonlinear electrical characteristics, thereby upset overall output power. Modified Perturb & Observe (P&O) MPPT controller is widely used to track the maximum generated power in order to increase output efficiency and make up environmental fluctuations [197]. Again, PV string output current varies with environmental conditions and fault types. Many times, healthy PV systems act like faulty under non-uniform irradiation with few highly shaded PV modules. Distinguishing among these conditions and faults is also a challenge.

The proposed scheme has been tested in a 100W PV system in a laboratory environment. To carry out the experiment, Matlab simulation model imitating the existing setup has been constructed and random situations, which represent different possible fault combinations, have been created at the existing PV setup. The generated current of PV string, operating at maximum power point (MPP), is obtained from the MPPT controller and converter. The simulated and measured string currents are fed to an in-house developed Matlab program of the proposed fault diagnosis algorithm employing metaheuristic optimizer.

Selection of optimizer is a vital issue. The considered optimization problem in this work is associated with an online fault detection scheme of PV system. Mathematically, it is a multidimensional, nonlinear constrained system. So, it is desirable that the optimizer, involved in this scheme, has less computational complexity and rapid convergence with proficiency to find global optima.

Recently, Mirjalili et al. have introduced a simple and robust meta-heuristic algorithm known as Grey Wolf Optimization (GWO), which is inspired by social leadership of grey wolves that attack preys for hunting drive in nature. GWO considers problems as black boxes. Hence, it can be easily applied to varieties of problems in unknown environments without much change in the algorithm. Besides, it involves fewer operators and parameters of adjustment in comparison with other heuristic methodologies. GWO has efficient exploration and exploitation scheme with better transmission mechanism and information sharing capability. It provides a more stochastic and diverse searches in the solution space. During

the process of optimization, there is no need to compute the gradient of the objective function and thus the derivative of search spaces, which lessen the computational complexity. GWO has excellent local optima avoidance capability compared to other conventional optimization techniques. All these properties of GWO make it highly suitable to solve highly nonlinear, multivariable, multi-constrained optimization problems with rapid convergence. It is evident in literature that GWO shows adeptness in various engineering problems [198]. Moreover, different type of classical well recognized optimization techniques like, Genetic Algorithm (GA) [199] and Tabu Search (TS) Algorithm [200], have also been used in this study as optimizers to evaluate the flexibility of the proposed fault diagnosis algorithm. Results and comparative studies of the proposed PV system fault diagnosis methodology, using these aforesaid optimization techniques, have been provided in the work for the purpose of validation and performance assessment.

This page is left blank intentionally

Chapter 2

Problem formulation

==========

The various power system optimization problems stated in the previous chapter of the thesis, requisite objective functions and expressions of different constraints have to be constructed to mathematically formulate these problems. Problem formulation of these various power system optimization problems are stated in this chapters as follows.

2.1. Economic dispatch problems

The endeavor of the economic dispatch (ED) problem is to minimize the fuel cost of a power producing station at the same time fulfilling a variety of constraints. The ED problem takes to mean valve-point effect, excluded workable zone and multiple fuels in concurrence with the load demand, transmission loss and working capacity limits.

2.1.1. Economic dispatch with prohibited operating zones

The ED problem can be stated as:

$$MinC_{ED}\left(P_g\right) = Min \sum_{i=1}^{N_g} F_i\left(P_{gi}\right) = \sum_{i=1}^{N_g} a_i + b_i P_{gi} + c_i P_{gi}^2 \tag{2.1}$$

Where, a_i, b_i and c_i are the cost coefficients of the i^{th} generator, P_{gi} is the power output of the i^{th} generator and N_g is the total number of generators.

2.1.2. Constraints

2.1.2.1. Load balance constraint

$$\sum_{i=1}^{N_g} P_{gi} - P_D - P_L = 0 \tag{2.2}$$

The transmission loss P_L can be stated as:

$$P_L = \sum_{l=1}^{N_g}\sum_{i=1}^{N_g} P_{gl} B_{li} P_{gi} + \sum_{i=1}^{N_g} B_{0i} P_{gi} + B_{00} \tag{2.3}$$

Where P_D is load demand and B_{li}, B_{0i} and B_{00} are the B -coefficients.

2.1.2.2.Generating capacity limit constraints

The generator power output must be within its minimum and maximum limits such that,

$$P_{gi}^{\min} \le P_{gi} \le P_{gi}^{\max}, \quad i = 1,2,...,N_g \tag{2.4}$$

Where, $P_{gi}^{\min}$ is the minimum limit and $P_{gi}^{\min}$ is the maximum limit of the i^{th} generator.

2.1.2.3. Prohibited operating zone

The workable region of a generator with precluded workable county can be stated as:

$$\begin{aligned} &P_{gi}^{\min} \le P_{gi} \le P_{gi,1}^{l} \\ &P_{gi,r-1}^{u} \le P_{gi} \le P_{gi,r}^{l}, \quad r = 2,3,...,n_i \\ &P_{gi,,r_i}^{u} \le P_{gi} \le P_{gi}^{\max}, \quad i = 1,2,...,N_g \end{aligned} \tag{2.5}$$

Where, r indicates the number of disallowed workable county of the i the generator. $P_{gi,r-1}^{u}$ is the maximum limit of $(r-1)^{th}$ disallowed feasible county and $P_{gi,r}^{l}$ is the minimum limit of r^{th} disallowed feasible county. Total number of disallowed feasible county of i^{th} generator is n_i.

2.1.3. Economic dispatch with valve-point effect

The ED problem subject to constraints endowed with the equations (2.2) and (2.4) can be stated as:

$$MinC_{ED}(P_g) = Min \sum_{i=1}^{N_g} F_i(P_{gi}) = \sum_{i=1}^{N_g} a_i + b_i P_{gi} + c_i P_{gi}^2 + \left| d_i \times \sin\{e_i \times (P_{gi}^{\min} - P_{gi})\} \right| \tag{2.6}$$

Where, d_i and e_i are the cost coefficients of i^{th} generator due to valve-point effect.

2.1.4. Economic dispatch with valve-point effect and multiple fuels

The generator is usually offered with multiple fuels [4], characterized by a number of piecewise quadratic functions allowing for the valve-point effect. The cost function of i^{th} generator with N_F fuel types can be stated as:

$$F_i(P_{gi}) = \alpha_{ir} + \beta_{ir} P_{gi} + \gamma_{ir} P_{gi}^2 + \left| \eta_{ir} \times \sin\{\delta_{ir} \times (P_{gir}^{min} - P_{gi})\} \right| \quad (2.7)$$

If $P_{gir}^{min} \le P_{gi} \le P_{gir}^{max}$ for fuel type r and $r = 1,2,..., N_F$

Where, P_{gir}^{min} and P_{gir}^{max} are the minimum and maximum power limits of the ith generator for r^{th} fuel type respectively. α_{ir}, β_{ir}, γ_{ir}, η_{ir} and δ_{ir} are the cost coefficients of the i^{th} generator for fuel type r.

The objective function subject to constraints endowed with the equations (2.2) and (2.4) can be stated as:

$$MinC_{ED}(P_g) = Min \sum_{i=1}^{N_g} F_i(P_{gi}) \quad (2.8)$$

2.2. Multi area economic dispatch problems

The aim of Multi area economic dispatch (MAED) problems is to minimize the total production cost of supplying loads to all areas while fulfilling power balance constraints, generating limits constraints and tie line capacity constraints. Three different types of MAED problems have been accounted.

2.2.1. MAED with prohibited operating zone and line loss consideration

The objective function F_t , total cost of dedicated generators of all areas, of MAED problem may be presented as

$$F_t = \sum_{i=1}^{N} \sum_{j=1}^{M_i} F_{ij}(P_{ij}) = a_{ij} + b_{ij} P_{ij} + c_{ij} P_{ij}^2 \quad (2.9)$$

where $F_{ij}(P_{ij})$ is the cost function of j^{th} generator in area i and typically expressed as a quadratic polynomial; a_{ij}, b_{ij} and c_{ij} are the cost coefficients of j^{th} generator in area i; N is the number of areas, M_i is the number of dedicated generators in area i; Pij is the real power

output of jth generator in area *i*. The MAED problem minimizes F_t subject to the following constraints.

2.2.1.1. Real power balance constraint

$$P_{iM_i} = P_{Di} + P_{Li} + \sum_{k,k\neq i} T_{ik} - \sum_{j=1}^{M_i-1} P_{ij} \tag{2.10}$$

The transmission loss PLi of area i may be articulated by using B-coefficients as

$$P_{Li} = \sum_{l=1}^{M_i}\sum_{j=1}^{M_i} P_{ij} B_{ilj} P_{il} + \sum_{j=1}^{M_i} B_{0ij} P_{ij} + B_{00i} \tag{2.11}$$

Where PD_i is real power demand of area *i*; T_{ik} is the tie line real power transfer from area *i* to area *k*. T_{ik} is positive when power flows from area *i* to area *k* and T_{ik} is negative when power flows from area *k* to area *i*.

2.2.1.2. Tie line capacity constraints

The tie line real power transfer T_{ik} from area *i* to area *k* should not exceed the tie line transfer capacity for security concern.

$$-T_{ik}^{max} \leq T_{ik} \leq T_{ik}^{max} \tag{2.12}$$

where T_{ik}^{max} is the power flow limit from area *i* to area *k* and $-T_{ik}^{max}$ is the power flow limit from area *k* to area *i*.

2.2.1.3 Real power generation capacity constraints

The real power generated by each generator should be within its lower limit P_{il}^{min} and upper limit P_{il}^{max}, so that

$$P_{il}^{min} \leq P_{ij} \leq P_{il}^{max};\ i \in N\ and\ j \in M_i \tag{2.13}$$

2.2.1.4 Prohibited operating zone

The prohibited operating zones are the range of power output of a generator where the operation originates unwanted vibration of the turbine shaft bearing due to opening or closing of the steam valve. This undue vibration might cause damage to the shaft and bearings. In general, operation is evaded in these regions. The practicable operating zones of unit can be illustrated as follows:

$$
\begin{aligned}
P_{ij}^{\min} \le P_{ij} \le P_{ij,1}^{l} \\
P_{ij,m-1}^{u} \le P_{ij} \le P_{ij,m}^{l} ; m = 2,3,...,n_{ij} \\
... \\
P_{ij,n_{ij}}^{u} \le P_{ij} \le P_{Gij}^{\max}
\end{aligned}
\tag{2.14}
$$

Where m stands for the number of prohibited operating zones of *j* the generator in area *i*. $P_{ij,m-1}^{u}$ is the upper limit of *(m-1)*th prohibited operating zone of *j* the generator in area *i*. $P_{ij,m}^{l}$ is the lower limit of m^{th} prohibited operating zone of *j* the generator in area *i*. Total number of prohibited operating zone of *j* the generator in area *i* is n_{ij}.

2.2.2. MAED with valve point loading

The generator cost function is acquired from data points taken during “heat run” tests, when input and output data are calculated as the unit is slowly varied through its working region. Wire drawing effects, occurring as each steam entrance valve in a turbine starts to open, generate a rippling effect on the unit curve. To model the effect of valve-points, a recurring rectified sinusoid contribution is added to the quadratic function [201]. The fuel cost function accounting valve-point loadings of the generator is given as

$$
F_t = \sum_{i=1}^{N} \sum_{j=1}^{M_i} F_{ij}\left(P_{ij}\right) = a_{ij} + b_{ij} P_{ij} + c_{ij} P_{ij}^2 + \left| d_{ij} \times \sin\left\{ e_{ij} \times \left(P_{ij}^{\min} - P_{ij} \right) \right\} \right| \tag{2.15}
$$

where d_{ij} and e_{ij} are cost coefficients of i^{th} generator in area *i* due to valve-point effect. The aim of MAED with VPL is to minimize F_t subject to the constraints given in eqn. (2.10), (2.12) and (2.13). Here transmission loss (PL) is not accounted.

2.2.3. MAED with valve point loading multiple fuel and transmission loss

Since generators are sensibly supplied with multi-fuel sources [202], each generator should be embodied with several piecewise quadratic functions superimposed sine terms reflecting the effect of fuel-type changes and the generator must identify the most economical fuel to burn. The fuel cost function of the i^{th} generator with *NF* fuel types considering valve-point loading is articulated as

$$
F_{ij}\left(P_{ij}\right) = a_{ijm} + b_{ijm} P_{ijm} + c_{ijm} P_{ij}^2 + \left| d_{ijm} \times \sin\left\{ e_{ijm} \times \left(P_{ijm}^{\min} - P_{ij} \right) \right\} \right| \tag{2.16}
$$

if $P_{ijm}^{min} \leq P_{ij} \leq P_{ijm}^{max}$ for fuel type m and m =1, 2, . . . , NF;

The objective function F_t is given by

$$F_t = \sum_{i=1}^{N} \sum_{j=1}^{M_i} F_{ij}\left(P_{ij}\right) \tag{2.17}$$

The objective function Ft is to be minimized subject to the constraints given in eqns. (2.10), (2.12) and (2.13).

2.2.4. Determination of generation level of slack generator

M_i Committed generators in area i deliver their power output subject to the power balance constraint (2.10), tie line capacity constraints (2.12) and the respective generation capacity constraints (2.13). Assuming the power loading of first (M_i-1) generators are known, the power level of the M_i^{th} generator (i.e. the slack generator) is given by

$$P_{iM_i} = P_{Di} + P_{Li} + \sum_{k,k\neq i} T_{ik} - \sum_{j=1}^{M_i-1} P_{ij} \tag{2.18}$$

The transmission loss P_{Li} is a function of all generator outputs including the slack generator and it is given by

$$P_{Li} = \sum_{l=1}^{M_i}\sum_{j=1}^{M_i} P_{ij} B_{ilj} P_{il} + 2P_{iM_i}\left(\sum_{j=1}^{M_i-1} B_{iM_i j} P_{ij}\right) + B_{iM_iM_i} P_{iM_i}^2 + \sum_{j=1}^{M_i-1} B_{0ij} P_{ij} + B_{0iM_i} P_{iM_i} + B_{00i} \tag{2.19}$$

Expanding and rearranging, eq. (2.18) becomes

$$B_{iM_iM_i} P_{iM_i}^2 + \left(2\sum_{j=1}^{M_i-1} B_{iM_i j} + B_{0iM_i} - 1\right) P_{iM_i} + \left(P_{Di} + \sum_{k,k\neq i} T_{ik} + \sum_{l=1}^{M_i}\sum_{j=1}^{M_i} P_{ij} B_{ilj} P_{il} + \sum_{j=1}^{M_i-1} B_{0ij} P_{ij} + B_{0iM_i} P_{iM_i} + B_{00i}\right) = 0 \tag{2.20}$$

The loading of the slack generator (i.e. M_i^{th}) can then be found by solving eq. (2.20) using standard algebraic method

2.3. Multi area economic environmental dispatch problems

Required objective, corresponding to the Multi area economic environmental dispatch (MAEED) problems, is the optimization of total cost as well as the level of emission at the same time related to the supplied load demands corresponding to each of the area along with fulfilling the criteria corresponding to aforementioned constraints. The goals along with the

constraints, which have to be considered while formulating the MAEEDS problem, are as mentioned below.

2.3.1. Cost calculation

The function, corresponding to fuel cost for each of fossil source generator while taking into consideration the effect of valve point [203], can be expressed in the form of addition of a second order polynomial and a sinusoid type function. The expression of fuel cost related to committed generators considering all areas is given below in (2.21).

$$f_1 = \sum_{g=1}^{NA} \sum_{h=1}^{NC_g} f_{1gh}(p_{gh}) \tag{2.21}$$

$$f_{1gh}(p_{gh}) = a_{gh} + b_{gh}p_{gh} + c_{gh}p_{gh}^2 + \left| d_{gh} \times \sin\{e_{gh} \times (p_{gh}^{\min} - p_{gh})\} \right| \tag{2.22}$$

Here, $f_{1gh}(p_{gh})$ in (2.22) represents the cost function matched up to the h^{th} power generating unit located in area g. $a_{gh}, b_{gh}, c_{gh}, d_{gh}$, and e_{gh} represent cost coefficients corresponding to the aforementioned unit. NA specifies areas under consideration (total), NC_g representing the total dedicated generating units located at area g. p_{gh} represents the power generated by the aforementioned unit.

2.3.2.Emission calculation

The modeling corresponding to various pollutants like Sulfur oxides, Carbon dioxide as well as Nitrogen oxides emitted from fossil resources based power production can be made individually. In order to make a comparison among these, the total emission is represented in the form of summation of a second order polynomial along with an exponential function [204]. The version of entire emission corresponding to committed generators of all areas can be done as per (2.23).

$$f_{1'} = \sum_{g=1}^{NA} \sum_{h=1}^{NC_g} f_{1'gh}(p_{gh}) \tag{2.23}$$

$$f_{1'gh}(p_{gh}) = \alpha_{gh} + \beta_{gh}p_{gh} + \gamma_{gh}p_{gh}^2 + \eta_{gh}\exp(\delta_{gh}p_{gh}) \tag{2.24}$$

Here, $f_{1'gh}(p_{gh})$ in (2.24) represents emission function of h^{th} generating unit located at area g. α_{gh}, β_{gh}, γ_{gh}, η_{gh}, and δ_{gh} indicate the coefficients of emission for abovementioned generating unit.

2.3.3 Constraints

2.3.3.1. Power balance

$$\sum_{h=1}^{NC_g} p_{gh} = p_{D_g} + p_{L_g} + \sum_{o,o\neq 1} T_{go} \quad \forall g \in NA \tag{2.25}$$

Where, p_{D_g} represents an power demand corresponding to the g in (2.25). T_{go} corresponds to tie line power flow from the g to o . It remains positive for the period of power exchange between the g to the o while becomes negative corresponding to the course of power exchange from the o to the g .

2.3.3.2. Tie-line capability

As stated above, the T_{go} possesses limits for exchanging the power in order to consider security issue as mentioned in (2.26).

$$-T_{go}^{\max} \leq T_{go} \leq T_{go}^{\max} \tag{2.26}$$

Where $T_{go}^{\max}$ represents the limit corresponding to power exchange from the g to the o . Similarly, - $T_{go}^{\max}$ indicates the limit when power exchanges from the o to the g .

2.3.3.3. Power generating capacity

The power generation through each of the generators should remains between $p_{go}^{\min}$, the lower limit and $p_{go}^{\max}$, the upper limit as per (2.27).

$$p_{go}^{\min} \leq p_{go} \leq p_{go}^{\max} \quad \forall g \in NA, h \in NC_g \tag{2.27}$$

2.4. Windn integrated multi area economic environmental dispatch problems

To formulate dynamic WMAEED problem for a multi-area wind power integrated network, the main components considered are conventional TUs and WUs. Here, it is considered that WUs' operators can also take part in dispatching and exchanging operation among different power network areas in the electricity market. However, the utility operators

should obey appropriate margin for each tie-line power flow during operational planning. The optimal scheduling with WUs, dispersed in different power system areas, is of utmost important to optimally monitor, operate, control and plan power networks to deal with the indefiniteness and area-wise variability of dynamic wind speed distribution. The wind turbine output is predicted by taking into consideration the zone wise weather forecasting.

Since the input power to the wind turbine is uncertain, the outcome from the generator is also uncertain which can be modelled using different probability distribution function (PDF). To deal with the dynamic behaviour of online generation and load demand, ramp rate limits for TUs and Weibull Probability Density Function (WPDF) of wind are considered [77,205].Hence, the dynamic WMAEED problem is a nonlinear dual-objective optimization task restricted to several complex equality and inequality constraints associated with TUs, WUs and tie-lines. First objective is associated with economic dispatch which assesses the total power production price by maintaining all the power network boundings.

Another function is about environmental dispatch which estimates the net emission across all the areas. The objectives and boundings as mentioned below are taken into consideration to formulate dynamic WMAEED problem.

2.4.1 Generation cost

The operational cost of a thermal-wind system comprises the fuel cost for fossil fuel fired plants along with the cost of WUs. The total generation price formulates in accordance to (2.28).

$$F_C = \sum_{i=1}^{M} \left\{ \sum_{j=1}^{N_{Gi}} f_{Gij}\left(P_{Gij}\right) + \sum_{k=1}^{N_{Wi}} f_{Wik}\left(P_{Wik}\right) \right\} \tag{2.28}$$

Where, N_{Gi} and N_{Wi} are the number of TUs and WUs in i^{th} area of a power system having M number of areas. The beginning term in (2.28) represents the total fuel cost function corresponding to committed fossil fuel fired TUs of all areas by considering the effect of valve-point as in (2.29).

$$f_{Gij}\left(P_{Gij}\right) = a_{Gij} + b_{Gij}P_{Gij} + c_{Gij}P_{Gij}^2 + \left| d_{Gij} \times \sin\left\{ e_{Gij} \times \left(P_{Gij}^{\min} - P_{Gij} \right) \right\} \right| \tag{2.29}$$

Where, P_{Gij} indicates the scheduled power dispatch through the j^{th} TU in i^{th} area. a_{Gij}, b_{Gij}, c_{Gij}, d_{Gij} and e_{Gij} represent the fuel cost coefficients belonging to j^{th} TU in i^{th} area. The second term in (2.28), the cost of wind power, comprises of three functions, a direct cost (f_{Dik}), an under estimation penalty cost (f_{Pik}) for not utilizing all the available wind power and a reserve cost (f_{Rki}) because of over estimation corresponding to wind power when wind power availability lacks to the scheduled wind power. So the wind power cost of k^{th} WU can be calculated as (2.30) [206].

$$f_{Wik}(P_{Wik}) = \left\{ f_{Dik}(P_{Dik}) + f_{Pik}\left(W_{Available,ik} - P_{Wik}\right) + f_{Rik}\left(P_{Wik} - W_{Available,ik}\right) \right\} \tag{2.30}$$

Where, P_{Wik} indicates the scheduled power dispatch through the k^{th} WU in i^{th} area and $W_{Available,ik}$ is the available wind power of the same WU at the scheduled time. Direct cost for scheduled wind generation is linear cost function (2.31) where d_{Wik} is the direct cost coefficient.

$$f_{Dik}\left(P_{Wik}\right) = d_{Wik} \times \left(P_{Wik}\right) \tag{2.31}$$

The under estimation penalty cost, where p_{Wik} is the penalty cost coefficient, can be expressed as (2.32).

$$f_{Pik}\left(W_{Available,ik} - P_{Wik}\right) = P_{Wik} \times \int_{P_{Wik}}^{W_{Rated,ik}} \left(w_{ik} - P_{Wik}\right) f_{Wik}\left(w_{ik}\right) dw_{ik} \tag{2.32}$$

Where, $W_{Rated,ik}$ represents the rated power produced through the k^{th} WU in i^{th} area. $f_{Wik}\left(w_{ik}\right)$ is Weibull Probability Density Function (WPDF) of wind power for k^{th} WU in i^{th} area. The overestimation cost or reserve cost, where r_{Wik} denotes the reserve cost coefficient, can be represented in accordance to (2.33).

$$f_{Rik}\left(P_{Wik}-W_{Available,ik}\right)=r_{Wik}\times\int_{0}^{P_{Wik}}\left(P_{Wik}-w_{ik}\right)f_{Wik}\left(w_{ik}\right)dw_{ik} \tag{2.33}$$

2.4.2 Emission level

To model the emission level of atmospheric pollutants from fossil fuel fired generators, a summation involving a quadratic and an exponential function is utilized. The WUs are emission free. Hence, the total emission level of committed fossil fuel fired generators of all areas can be represented in accordance to (2.34).

$$F_{E}=\sum_{i=1}^{M}\left\{\sum_{j=1}^{N_{Gi}}\alpha_{Gij}+\beta_{Gij}P_{Gij}+\gamma_{Gij}P_{Gij}^{2}+\eta_{Gij}\exp(\delta_{Gij}P_{Gij})\right\} \tag{2.34}$$

Where, α_{Gij}, β_{Gij}, γ_{Gij}, η_{Gij} and δ_{Gij} denote the emission coefficients corresponding to j^{th} fossil fuel fired TU in i^{th} area.

2.4.3. Constraints

2.4.3.1. Real power production constraint

The real power production through each of the generators should remain between pre-specified lower and upper limiting values.

$$P_{Gij}^{\min}\le P_{Gij}\le P_{Gij}^{\max},\quad i\in\{1,...,M\}\ \&\ j\in\{1,...,N_{Gi}\} \tag{2.35}$$

$$P_{Wik}^{\min}\le P_{Wik}\le P_{Wik}^{\max},\quad i\in\{1,...,M\}\ \&\ k\in\{1,...,N_{Wi}\} \tag{2.36}$$

2.4.3.2 POZ constraint

$$P_{Gij}\in\begin{cases}P_{Gij}^{\min}\le P_{Gij}\le P_{Gij,1}^{lower}\\ P_{Gij,k-1}^{upper}\le P_{Gij}\le P_{Gij,k}^{lower}\\ \quad\ldots\\ P_{Gij,Z}^{upper}\le P_{Gij}\le P_{Gij}^{\max}\end{cases}\quad i\in\{1,...,M\},\ j\in\{1,...,N_{Gi}\}\ \&\ k\in\{1,...,N_{Wi}\}$$

(2.37)

Due to some limitations, a TU may have some POZs in between lower limit and upper limit of generation during operation, where it is unable to generate any power [207]. In (2.37), Z represents the total number of prohibited zones for j^{th} TU in i^{th} area. $P^{lower}_{Gij,k}$ and $P^{upper}_{Gij,k}$ are the lower and upper limits of the k^{th} prohibited zones for j^{th} TU in i^{th} area.

2.4.3.3. Real time demand-production balance constraint

$$\sum_{j=1}^{N_{Gi}} P_{Gij} + \sum_{k=1}^{N_{Wi}} P_{Wik} = P_{Di} + P_{Li} \tag{2.38}$$

Where, P_{Di} and P_{Li} indicate the real power demand and transmission losses corresponding to area i respectively.

2.4.3.4. Spinning reserve constraint

In order to achieve stable and reliable power system operation under the wind power indefiniteness and the load demand fluctuations, a certain amount of spinning reserve requirement should be maintained. This constrains WMAEED as (2.39) and (2.40).

$$\sum_{i=1}^{M} \left\{ \sum_{j=1}^{N_{Gi}} \left(P^{\max}_{Gij} - P_{Gij} \right) + \sum_{k=1}^{N_{Wi}} \left(P^{\max}_{Wik} - P_{Wik} \right) \right\} \geq \in_1 P^{up}_{Demand,i} \tag{2.39}$$

$$\sum_{i=1}^{M} \left\{ \sum_{j=1}^{N_{Gi}} \left(P_{Gij} - P^{\min}_{Gij} \right) + \sum_{k=1}^{N_{Wi}} \left(P_{Wik} - P^{\min}_{Wik} \right) \right\} \geq \in_2 P^{down}_{Demand,i} \tag{2.40}$$

Where, $P^{up}_{Demand,i}$ and $P^{down}_{Demand,i}$ are the demand when the upward spinning reserve and the downward spinning reserve are needed in i^{th} area.

2.4.3.5. Tie line capacity constraint

The real power transmission T_{il} from area i to area l through tie lines should not go beyond the tie line transfer capacity limits due to security consideration.

$$-T_{il}^{\max} \le T_{il} \le T_{il}^{\max},\ i,l \in \{1,...,M\} \tag{2.41}$$

Where, $T_{il}^{\max}$ indicates the power flow limiting value from area i to area l while $-T_{il}^{\max}$ denotes the power flow limiting value from area l to area i.

2.4.3.6. Wind power uncertainty constraint

The WPDF of wind speed v_{ik} for k^{th} WU in i^{th} area can be formulated as a two-parameter WPDF (2.42).

$$f_{Vik}(v) = \left(\frac{\theta_{ik}}{\lambda_{ik}}\right)\left(\frac{v_{ik}}{\lambda_{ik}}\right)^{\theta_{ik}-1} \exp\left[-\left(\frac{v_{ik}}{\lambda_{ik}}\right)^{\theta_{ik}}\right] \tag{2.42}$$

Where, θ_{ik} and λ_{ik} are the shape and scale factor for the WPDF of wind speed for k^{th} WU in i^{th} area respectively. The cumulative density function of wind speed v_{ik} for k^{th} WU in i^{th} area can be summed up as (2.43).

$$c_{Vik}(v_{ik}) = 1 - \exp\left[-\left(\frac{v_{ik}}{\lambda_{ik}}\right)^{\theta_{ik}}\right] \tag{2.43}$$

Wind power of k^{th} WU in i^{th} area at any instant is restricted to a limit set by the cut-in speed ($v_{Cut-in,ik}$) and cut-out speed ($v_{Cut-out,ik}$) of the same WU as (2.44).

$$w_{ik} = \begin{cases} 0 & \forall \quad v_{ik} < v_{Cut-in,ik} \ and \quad v_{ik} > v_{Cut-out,ik} \\ W_{Rated,ik}\left(\dfrac{v_{ik} - v_{Cut-in,ik}}{v_{ik} - v_{Cut-out,ik}}\right) & \forall \quad v_{Cut-in,ik} \le v_{ik} \le v_{Rated,ik} \\ W_{Rated,ik} & \forall \quad v_{Rated,ik} \le v_{ik} \le v_{Cut-out,ik} \end{cases} \tag{2.44}$$

Where, $v_{Rated,ik}$ denotes the rated speed of k^{th} WU in i^{th} area. Thus, in the discrete region, the probability of the wind power of k^{th} WU in i^{th} area being zero is given by (2.45).

$$pr_{ik}\left\{w_{ik}=0\right\}=c_{Vik}\left(v_{Cut-in,ik}\right)+\left(1-c_{Vik}\left(v_{Cut-out,ik}\right)\right)=1-\exp\left[-\left(\frac{v_{Cut-in,ik}}{\lambda_{ik}}\right)^{\theta_{ik}}\right]+\exp\left[-\left(\frac{v_{Cut-out,ik}}{\lambda_{ik}}\right)^{\theta_{ik}}\right] \quad (2.45)$$

The probability of the wind power of k^{th} WU in i^{th} area being rated is given by (2.46).

$$pr_{ik}\left\{w_{ik}=W_{Rated,ik}\right\}=c_{Vik}\left(v_{Cut-out,ik}\right)+\left(1-c_{Vik}\left(v_{Rated,ik}\right)\right)$$
$$=\exp\left[-\left(\frac{v_{Rated,ik}}{\lambda_{ik}}\right)^{\theta_{ik}}\right]-\exp\left[-\left(\frac{v_{Cut-out,ik}}{\lambda_{ik}}\right)^{\theta_{ik}}\right] \quad (2.46)$$

In the continuous region, the WPDF of wind power for k^{th} WU in i^{th} area is expressed as (2.47).

$$f_{Wik}\left(w_{ik}\right)=\frac{\theta_{ik}h_{ik}v_{Cut-in,ik}}{W_{Rated,ik}\lambda_{ik}}\left[\frac{\left(1+\frac{h_{ik}w_{ik}v_{Cut-in,ik}}{W_{Rated,ik}}\right)}{\lambda_{ik}}\right]^{\theta_{ik}-1}\times\exp\left\{-\left[\frac{\left(1+\frac{h_{ik}w_{ik}v_{Cut-in,ik}}{W_{Rated,ik}}\right)^{\theta_{ik}}}{\lambda_{ik}}\right]\right\} \quad (2.47)$$

Where, $h_{ik}=\left(\frac{v_{Rated,ik}}{v_{Cut-in,ik}}\right)-1$

2.5. Hydro-thermal scheduling problems

The cost of hydropower plants is negligible compared to thermal power plants, so the hydro-thermal scheduling problem is designed to minimize the total thermal production cost making maximum possible use of the available hydro-resource considering different constraints.

2.5.1. Objective task

The main objective of short-term hydrothermal scheduling is to provide maximum use of available hydro resources to minimize the thermal cost over a scheduling period TI. The cost equation of thermal power can be expressed in accordance to (2.48).

$$F_c=\sum_{ti=1}^{TI}\sum_{s=1}^{N_{th}}\left[a_s+b_sP_{s,ti}+c_sP_{s,ti}^2+\left|d_s\times\sin\left\{e_s\times(P_s^{mn}-P_{s,ti})\right\}\right|\right] \quad (2.48)$$

Here F_c is the total generation cost of thermal system. a_s, b_s and c_s in (2.49) represent cost curve coefficients for thermal producer s. d_s and e_s indicate the valve point coefficients of s unit. P_s^{mn} and $P_{s,t}$ indicate minimum and total amount of thermal power production through s^{th} unit respectively at ti^{th} time index. N_{th} and TI indicate total number of thermal power producers and time indices sequentially.

2.5.2. Power balance constraint

The total power generated by the hydro and thermal units per hour must be equal to total load demand and power transmission loss. It can be mathematically expressed in accordance to (2.49).

$$\sum_{s=1}^{N_{th}} P_{s,ti} + \sum_{h=1}^{N_{hy}} P_{h,ti} - P_{D,ti} - P_{L,ti} = 0, \forall ti \in TI \tag{2.49}$$

N_{hy} represents total number of hydro power producers. $P_{D,ti}$ and $P_{L,ti}$ are total power demand and power losses respectively during transmission within a specified period. The hydro power generation $P_{h,ti}$ as a function of storage capacity and discharge rate is in accordance to (2.50).

$$P_{h,ti} = PC_{1h}SV_{h,ti}^2 + PC_{2h}WDR_{h,ti}^2 + PC_{3h}SV_{h,ti}WDR_{h,ti} + PC_{4h}SV_{h,ti} + PC_{5h}WDR_{h,ti} + PC_{6h,} \quad \forall h \in N_{hy} \,\&\, ti \in TI \tag{2.50}$$

Here, $P_{h,ti}$ indicates power production through the h^{th} hydro unit at ti^{th} time index. $WDR_{h,ti}$ represents water discharge rate at ti^{th} time index. $SV_{h,ti}$ represents tank storing capability. PC_{1h}, PC_{2h}, PC_{3h}, PC_{4h}, PC_{5h} and PC_{6h} represent power production coefficients corresponding to the h^{th} hydro unit. Total power transmission loss depends on loss coefficient and can be expressed in accordance to (2.51). B_{sh}, B_{0s}, and B_{00} represent the power transmission loss coefficients.

$$P_{L,ti} = \sum_{s=1}^{N_{th}+N_{hy}} \sum_{h=1}^{N_{th}+N_{hy}} P_{s,ti} B_{sh} P_{h,ti} + \sum_{s=1}^{N_{th}+N_{hy}} B_{0s} P_{s,ti} + B_{00} \tag{2.51}$$

2.5.3. Ramp rate limiting values constraint

Thermal power generation cannot be increase or decrease suddenly. The power generation $P_{s,ti}$ in a definite time span should not be enhanced by a certain amount RU_s to

that of the last interval $P_{s,(ti-1)}$. RU_s is known as ramping up limiting value. Similarly, power generation should not be curtailed to that of the last interval by a definite amount RD_s known as ramping down limiting value. Boundaries relating these limiting values can be expressed by equation (2.52) and (2.53).

$$P_{s,ti} - P_{s,(ti-1)} \le RU_s, \forall s \in N_{th} \,\&\, ti \in TI \tag{2.52}$$

$$P_{s,(ti-1)} - P_{s,ti} \le RD_s, \forall s \in N_{th} \,\&\, ti \in TI \tag{2.53}$$

2.5.4. Reservoir flow balance constraint

The reservoir water flow balance equation relates the current water storage volume to previous interval storage volume, inflow rate, discharge rate and spillage. Here, water transportation delay between reservoirs is also considered because of some upstream units exist exactly above the h^{th} unit. This can be mathematically expressed as,

$$SV_{h,(ti+1)} = SV_{h,ti} + IF_{h,ti} - WDR_{h,ti} - SP_{h,ti} + \sum_{m=1}^{US_h} \left(WDR_{drm(ti-WTD_{mh})} + SP_{drm(ti-WTD_{mh})} \right), \forall h \in N_{hy} \,\&\, ti \in TI \tag{2.54}$$

Here, $SV_{h,ti}$ denotes spillage of tank of h^{th} hydro unit at ti^{th} time index. $IF_{h,ti}$ represents inflow rate for the same tank. US_h indicates total upstream units exactly above the h^{th} unit and WTD_{mh} represents water transporting delay from tank m to the h.

2.5.5. Power generation constraint

Hydro and thermal power cannot be produce at will. Production limiting values corresponding to the hydro as well as thermal producers can be expressed by equation (2.55) and (2.56) sequentially.

$$P_h^{mn} \le P_{h,ti} \le P_h^{mx}, \forall h \in N_{hy} \,\&\, ti = TI \tag{2.55}$$

$$P_s^{mn} \le P_{s,ti} \le P_s^{mx}, \forall s \in N_{th} \,\&\, ti \in TI \tag{2.56}$$

Here, P_h^{mn} and P_h^{mx} are respectively the minimum and maximum value of power production by the h^{th} hydro unit. The P_s^{mn} and P_s^{mx} represents the minimum and maximum value of thermal power production respectively.

2.5.6. Water discharge rate constraint

Water discharge rate is limited by lower bound, upper bound and further within minimum and maximum range. Considering total restricted operating sections (RSO_h) corresponding to the h^{th} hydro producer is expressed in accordance to (2.57).

$$WDR_h \in \begin{cases} WDR_h^{mn} \le WDR_h \le WDR_{h,p-1}^{lwr} \\ WDR_{h,p-1}^{upr} \le WDR_h \le WDR_{h,p}^{lwr}, \forall \quad p = 2,3,4,5,....., RSO_h \\ WDR_{h,p}^{upr} \le WDR_h \le WDR_h^{mx} \end{cases} \tag{2.57}$$

RSO_h represents total restricted operating sections. $WDR_{h,p}^{lwr}$ and $WDR_{h,p}^{upr}$ represent lower bound and upper bound on the to the restricted operating section p for the h^{th} producer sequentially, and p is the restricted operating section index.

2.5.7. Reservoir storage capacity and hydro discharge constraints

2.5.7.1. Reservoir storage capacity constraint

The operating volume of reservoir storage must lie between its minimum and maximum capacity limits.

$$SV_h^{mn} \le SV_{h,ti} \le SV_h^{mx}, \forall h \in N_{hy} \,\&\, ti \in TI \tag{2.58}$$

2.5.7.2. Hydro discharge constraint

The physical limitation of water discharge of turbines in m^3 must lie within its minimum and maximum operating limits as (2.59).

$$WDR_h^{mn} \le WDR_{h,ti} \le WDR_h^{mx}, \forall h \in N_{hy} \,\&\, ti \in TI \tag{2.59}$$

Thermal plants emit pollutants like oxides of sulfur, carbon and nitrogen which cause environmental damage. Nowadays economic and environmental objectives are becoming one of the most important optimization problems in power system. The harmful emission produced by steam power plants must be considered in power system operation. The aim of hydrothermal scheduling in this paper is to determine the optimal water discharge rates of hydropower plants and power generation of thermals plants that can simultaneously minimize both of environmental pollution and fuel costs in the whole scheduling period.

2.6. Optimal DG allocation problem

For the formulation of DG assignment in the power system, the load system must be analyzed using load flow analysis. Load flow analysis can be branch based or node based. The current injection or bus voltage is taken as variable for node based methods while branch currents or power for branch based methods. The basic load flow equations are given as below:

$$P_i = \sum_{j=1}^{n} V_i V_j Y_{ij} \cos(\theta_i - \theta_j - \alpha_{ij}) \tag{2.60}$$

$$Q_i = \sum_{j=1}^{n} V_i V_j Y_{ij} \sin(\theta_i - \theta_j - \alpha_{ij}) \tag{2.61}$$

Where, V_i, V_j are the voltages at i^{th} and j^{th} buses, respectively, P_i is the active power injection at the i^{th} bus, Q_i is the reactive power injection at the i^{th} bus, n is the number of buses, θ_i and θ_j are voltage phase angles at i^{th} and j^{th} buses respectively.

Fig. 2.1 depicts a single line diagram (SLD) of IEEE 33 bus test system.

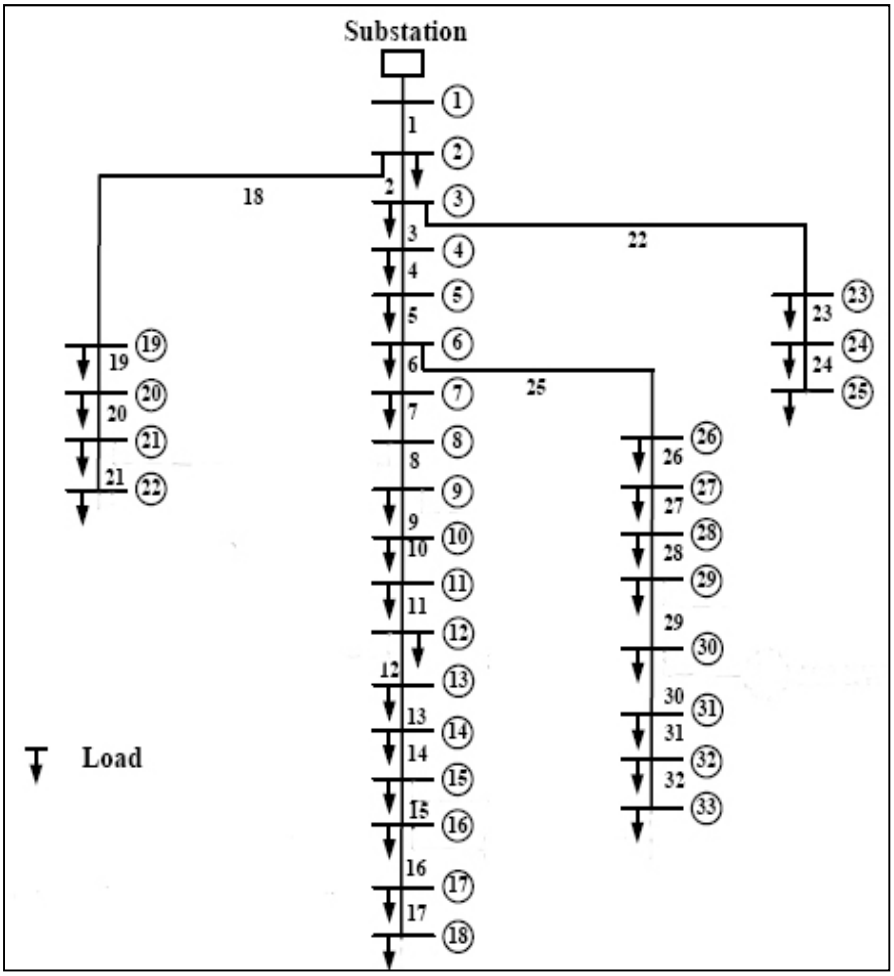

Figure 2.1. IEEE 33 bus radial distribution system

Techniques like Gauss-Seidel method, Newton-Raphson method, Fast decoupled method have been used for load flow analysis. In this thesis, load flow is analyzed using forward backward sweep method [139].

It has virtues of low memory, high computational efficiency, high convergence capability, simple structure, unbalanced system applicability. For this method, there are two steps: backward sweep (BWS) and forward sweep (FWS). In BWS, voltage and current are calculated using KVL and KCL. Whereas, in FWS, the downstream voltage is calculated starting from the source node. To begin with, we take the rated voltage at the end node and KCL is applied to determine the current flowing from node using the equation:

$$I_{(i,i+1)} = I_{i+1} + \sum CurrentEmanating \tag{2.62}$$

This current is computed with the voltage at the i^{th} node using the equation:

$$V_{(i+1)} = V_i + I_{(i,i+1)} * Z_{(i,i+1)} \tag{2.63}$$

This process is unremitting till the junction node is reached and the voltage hence computed is stored. Continuing in this alike fashion with a further node end of the system we compute till the reference node is reached. Comparing the calculated voltage with the specified source voltage, if the disparity is lesser than specified criteria we stop otherwise we move on to the FWS.

The node voltage in the forward direction is calculated using the following equation

$$V_{(i+1)} = V_i - I_{(i,i+1)} * Z_{(i,i+1)} \tag{2.64}$$

This updated bus voltage as calculated in FWS is used for calculation in BWS. After node voltage and line currents are calculated using BWS/FWS algorithm, the losses are calculated. The objective of this work is to minimize power losses. The real power losses are calculated as given below [140].

$$P_L = \sum_{i=1}^{N_b} \sum_{j=1}^{N_b} \left[a_{ij} \left(P_i P_j + Q_i Q_j \right) + b_{ij} (Q_i P_j - P_i Q_j) \right] \tag{2.65}$$

Where,

$$a_{ij} = \frac{R_{ij}}{V_i V_j} \cos(\delta_i - \delta_j) \tag{2.66}$$

$$b_{ij} = \frac{R_{ij}}{V_i V_j} \sin(\delta_i - \delta_j) \tag{2.67}$$

Load models are of constant power, constant current, and constant impedance type. In this work, the system is supposed to be under diverse loading conditions, so the constant power

load model is chosen. DG can be mainly classified into three types based on how it transacts with the real and reactive power [141]. Type 1 DG injects only active power, Type 2 injects both real and reactive power and Type 3 injects active power but consumes reactive power from the system. Here, in this case, Type 2 DG is selected for analysis.

The reduction in power losses due to optimal placement of DG and also its optimal size has been premeditated in this work. Due to the introduction of DG, the nature of voltage profile under varying load conditions is observed. The load is varied linearly from 50% to 150% of the tangible value. Here, the bus number as well as the size of DG has been set up using WCA. The amalgamation of bus number and DG size, for which the power losses are the minimum, has been considered as the optimum.

2.7. Optimal power operation planning in a township

In this work, two cases of hybrid DER for the economical analysis of micro-grid have been considered which are as follows:

Case 1. SPS and BMGU with BESS and

Case 2. SPS and PAFC with BESS.

Studied systems for different hybrid DERs used in this article are shown below in Fig. 2.2 and Fig. 2.3.

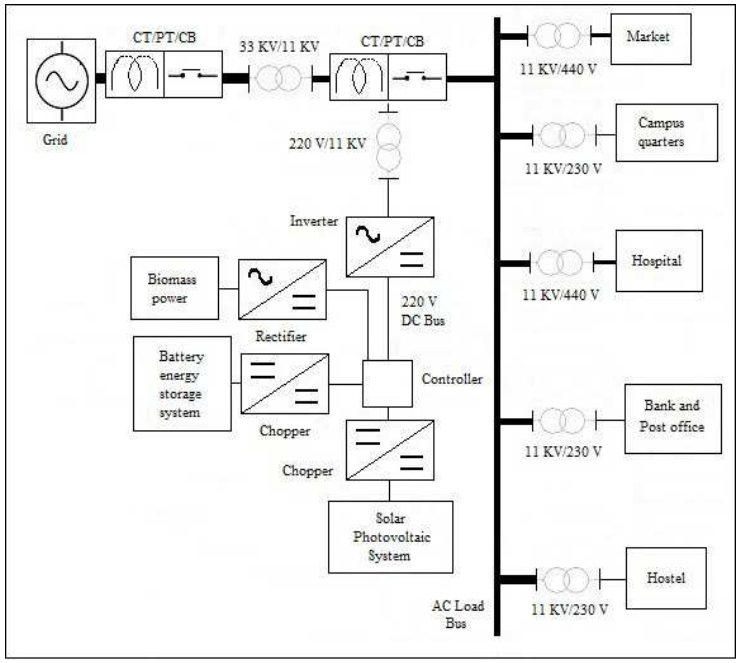

Figure. 2.2 Studied system for case 1 of hybrid DER

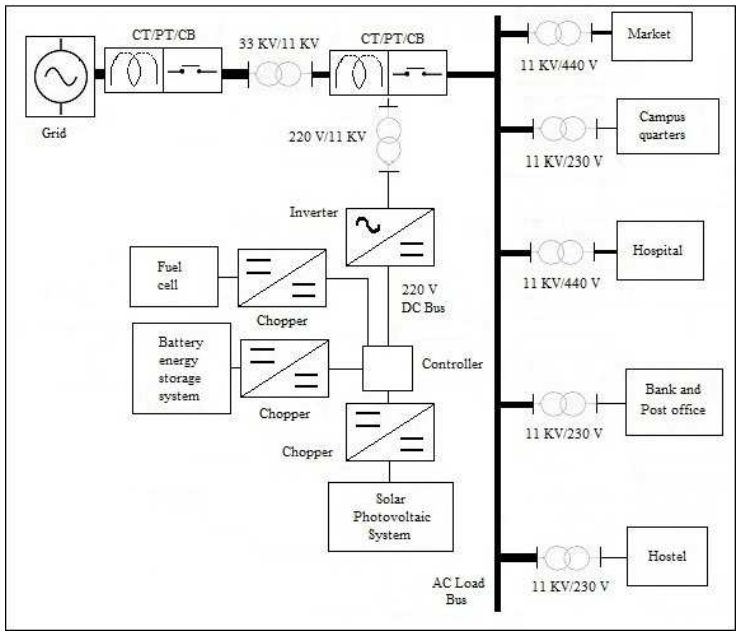

Figure. 2.3. Studied system for case 2 of hybrid DER

Phosphoric Acid Fuel Cell (PAFC) has been found to be the best among all types of FC. PAFCs have low chemical and thermal emissions, more reliability, siting and fuel flexibility, less upholding requirement, ultimate part load performance and towering efficiency [154]. Although, biomass gasification process is less efficient than biomass combustion, but it has been found more environment friendly. Lead acid battery has been found to be the best among all types of battery. Purchasing and selling of power with the utility is required according to the difference in generated power and load demand [154]. If the generated power from all the sources is less than required load demand then, power has to be purchased from utility. On the other hand, if the generated power from all the sources is more than the required load demand then, this excess power is sold to the utility.

2.7.1. Objective function

The objective function is to determine equated annual cost of the micro-grid for each case of hybrid DER and is given by:

$$R = R_O + R_I + R_M + R_U \tag{2.68}$$

Where, R_O, R_I, R_M and R_U are operating cost, initial cost, micro-grid cost and utility cost respectively. Operating cost for case 1 is given by:

$$R_O^{bios} = \sum_{cons=1}^{n} \sum_{ss=1}^{m} Nod_s \times \left[\sum_{\substack{hr=t_1 \\ hr \neq t_8 : t_{16}}}^{t_{24}} P_{BM}(ss,hr,cons) O_{BM} + \sum_{hr=t_1}^{t_{24}} P_{BT}(ss,hr,cons) O_{BT} + \sum_{hr=t_8}^{t_{16}} P_{SO}(ss,hr,cons) O_{SO} \right] \tag{2.69}$$

Where, P_{BM} , $P_{BT}$and P_{SO} are the power generated from BMGU, BESS and SPS respectively. O_{BM} , O_{BT} and O_{SO} are the operating cost of BMGU, BESS and SPS respectively.

The operating cost for case 2 is:

$$R_O^{fcs} = \sum_{cons=1}^{n} \sum_{ss=1}^{m} Nod_s \times \left[\sum_{\substack{hr=t_1 \\ hr \neq t_8 : t_{16}}}^{t_{24}} P_{FC}(ss,hr,cons) O_{FC} + \sum_{hr=t_1}^{t_{24}} P_{BT}(ss,hr,cons) O_{BT} + \sum_{hr=t_8}^{t_{16}} P_{SO}(ss,hr,cons) O_{SO} \right] \quad (2.70)$$

Where, P_{FC} , $P_{BT}$and P_{SO} are the power generated from PAFC , BESS and SPS respectively. O_{FC} , O_{BT} and O_{SO} are the operating cost of PAFC, BESS and SPS respectively.

Equation (2.70) explain the total operating cost of first hybrid DER. The first term on right hand side describes the operating cost of BMGU as the product of power generated by it and the cost involved with it. The second and third terms describe the operating cost of BESS and SPS respectively. Equation (2.71) describes the total operating cost of second hybrid DER. The operating cost of SPS is zero. The number of days per season, consumer, season and hour in (2.70) and (2.71) are represented by Nod_s , cons, ss and hr respectively.

The BMGU produces power P_{BM} in kW and after multiplying it by operating cost O_{BM} in Rs/kWh, we get the operating cost of BMGU in Rs/hr for a particular hour. After summing the P_{BM} O_{BM} over twenty four hours, we get the operating cost of one day. When it is multiplied by number of days in a season (243 days in summer and 122 days in winter), the operating cost of a season is obtained. On summing the costs of both the season, the annual operating cost of the BMGU is obtained. This process is repetitive with diverse DERs to obtain their yearly operating cost.

Initial cost for case 1 is given by:

$$R_I^{bios} = \sum_{cons=1}^{n} [\alpha\ ic_{BM}(\text{cons}) + \beta\ ic_{BT}(\text{cons}) + I_{BM}\ ic_{BM} + I_{BT}\, ic_{BT} + ic_{SO}\ ] \quad (2.71)$$

The initial cost for case 2 is:

$$R_I^{fcs} = \sum_{cons=1}^{n} [\gamma\ ic_{FC}(\text{cons}) + \beta\ ic_{BT}(\text{cons}) + I_{FC}\, ic_{FC} + I_{BT}\, ic_{BT} + ic_{SO}\ ] \quad (2.72)$$

Where, ic_{BM} , ic_{BT} , ic_{SO} and ic_{FC} are the initial cost of BMGU, BESS, SPS and PAFC respectively. To resolve the total annual depreciation expenses, the initial costs have to be multiplied by depreciation factors α, β and γ respectively. I_{BM} , I_{BT}, and I_{FC} are the allowed interest rate of return on the initial investments for BMGU, BESS and PAFC respectively by the funding agency. α, β and γ can be found by the following equation:

$$\alpha, \beta, \gamma = \mathrm{dr} \times \frac{dr^{(Lft_{BM,BT,FC}-1)}}{(1+dr)^{Lft_{BM,BT,FC}}-1} \quad (2.73)$$

Where, Lft_{BM}, Lft_{BT}, Lft_{FC} and dr are the lifetime of BMGU, BESS, PAFC and rate of depreciation respectively. The micro-grid cost is evaluated using the following equation:

$$R_M = \delta\, ic_{sw} + \eta\, ic_{tfm} + \lambda\, ic_{cbl} + \sigma\, ic_{cont} + I_{sw}\, ic_{sw} + I_{tfm}\, ic_{tfm} + I_{cbl}\, ic_{cbl} + I_{cont}\, ic_{cont} \quad (2.74)$$

Where, ic_{sw}, ic_{tfm}, ic_{cbl} and ic_{cont} are the initial cost of switching equipment, transformer, cable and controller respectively. δ, η, λ and σ are the depreciation factor of switching equipment, transformer, cable and controller respectively. I_{sw}, I_{tfm}, I_{cbl} and I_{cont} are the allowed interest rate of return on the initial investments for switching equipment, transformer, cable and controller respectively.

The utility cost is given as follows:

$$R_U = \sum_{cons=1}^{n} \sum_{ss=1}^{m} Nod_s \times \sum_{hr=t_1}^{t_{24}} \{ e_P\, P_P(\mathrm{ss, hr, cons}) - e_{sell}\, P_{sell}(\mathrm{ss, hr, cons})\} + 12\, e_B \{\max[P_P(\mathrm{cons})]\} \quad (2.75)$$

Where, e_P, e_{sell} and e_B are cost of purchasing power (Rs/kWh), cost of selling power (Rs/kWh) and base charge of electricity (Rs/kW/month) respectively.

2.7.2. Constraints

To optimize the equated annual cost of (2.68), optimal operation of hybrid DERs is the main functional constraint.

$$\sum_{cons=1}^{n} D_E(\mathrm{ss, hr, cons}) = P_{BM}(\mathrm{ss, hr, cons}) + P_{BT}(\mathrm{ss, hr, cons}) + P_{SO}(\mathrm{ss, hr, cons}) + P_{FC}(\mathrm{ss, hr, cons}) + P_P(\mathrm{ss, hr, cons}) - P_{sell}(\mathrm{ss, hr, cons}) \quad (2.76)$$

Where, D_E represents power demand of consumers of micro-grid at a particular hour of a day in a season in kW.

Besides above, there are some other constraints for cost optimization:

$$0 \le P_{BM}(\mathrm{hr, cons}) \le IC_{BM}(\mathrm{hr, cons}) \quad (2.77)$$

$$0 \le P_{SO}(\mathrm{hr, cons}) \le IC_{SO}(\mathrm{hr, cons}) \quad (2.78)$$

$$0 \le P_{FC}(\mathrm{hr, cons}) \le IC_{FC}(\mathrm{hr, cons}) \quad (2.79)$$

$$-IC_{BT}(\text{hr, cons}) \leq P_{BT}(\text{hr, cons}) \leq IC_{BT}(\text{hr, cons}) \quad (2.80)$$

$$P_{BM},\ P_{SO},\ P_{FC},\ IC_{BM},\ IC_{SO},\ IC_{FC} \geq 0 \quad (2.81)$$

Equation (2.77), (2.78) and (2.79) determine the lower and upper limit of power generation by BMGU, SPS and PAFC respectively. Relation (2.80) determines the lower and upper limit of power generation by BESS. The negative sign in lower limit indicates the charging of battery. On any day, the total sum of power generated by BESS should be zero. But practically, battery does not discharge completely due to its efficiency. Hence, the total sum of generated power by BESS has very small deviation from zero value. Relation (2.81) determines that P_{BM}, P_{SO}, P_{FC}, IC_{BM}, IC_{SO} and IC_{FC} should have values greater than or equal to zero.

2.8. Optimal power operation planning in a rail-way rake maintenance depot

A railway rake up keeping depot, to perform electrical as well as mechanical up keeping of Traction Rolling Stock (TRS), named, Sonarpur TRS/Electrical Multiple Unit railway car-shed, Eastern Railways of India, came into the existence in the 1979. It is located at Sonarpur, the south sub-urban of Kolkata, India. Its total premising area is approximately 68,550 square meters. Out of this, current utilizing space is 8850 square meters.

Mean value of the electrical energy usage for the aforesaid depot is approximately 50 KVA including a maximum demand agreement of 200 KVA. The required power is supplied by the Sonarpur 33/11 KV substation, WEBSEDCL. Analyzed results of the load power requirement profile (corresponding to each day) tell that load scheduling is very critical as well as highly optimized (including each of the constraints with respect to their normal operating schedule) with 50 KVA mean load, 120 KVA peak power requirement along with 400 KVA connected load. They maintain their power factor 0.98 to 1 placing capacitor bank in their sub-station. So optimal power operation planning is to be done mitigating the hourly demand.

Solar and wind potential of this area was taken from West Bengal Renewable Development Agency **(**WBREDA) and as per the reports wind power generation is not suitable there but its solar potential is fair enough to generate power. In the premises large

amount of spare area is available to set up renewable power generators like biomass gasifier units, fuel cells, etc. Considering this scenario, only solar power system (SPS), biomass gasifier unit (BMGU) and phosphoric acid fuel cell (PAFC) are proposed as DERs here along with a battery energy storage system (BESS).

Beside the environmental benefits, the main objective for introducing distributed generation here is to minimize the electricity bill charged by WBSEDCL to Eastern Rail Ways and if possible to earn back some money feeding surplus power to the grid, so that this proposal becomes attractive to the consumer ie. the Rail Ways company.

To fulfill the objective, optimal power operation planning and the optimal capacity of the above mentioned renewable power generators are proposed. A comparative study is also done for three set of generators. ie. Case I, II & III.

Case I. Biomass gasifier unit (BMGU) and solar power system (SPS), along with a battery energy storage system (BESS).

Case II. Phosphoric acid fuel cell (PAFC) and solar power system (SPS), along with a battery energy storage system (BESS).

Case III. Biomass gasifier unit (BMGU), phosphoric acid fuel cell (PAFC) and solar power system (SPS), along with a battery energy storage system (BESS).

Fig. 2.4 depicts the satellite image of the depot campus, captured from Google maps online application [208]. Fig. 2.5 shows a representation relating necessary controllers, power contactors, converters, relay panels, circuit breakers, diesel generator set etc.

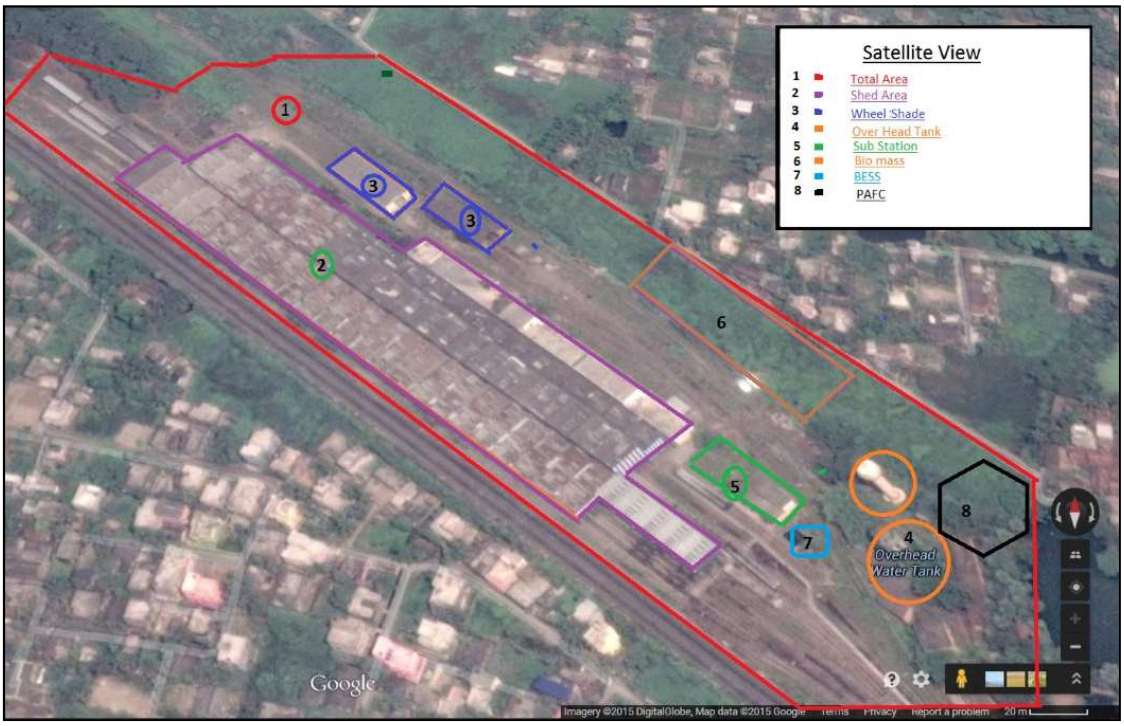

Figure 2.4. Satellite view of the railway rake up-keeping depot.

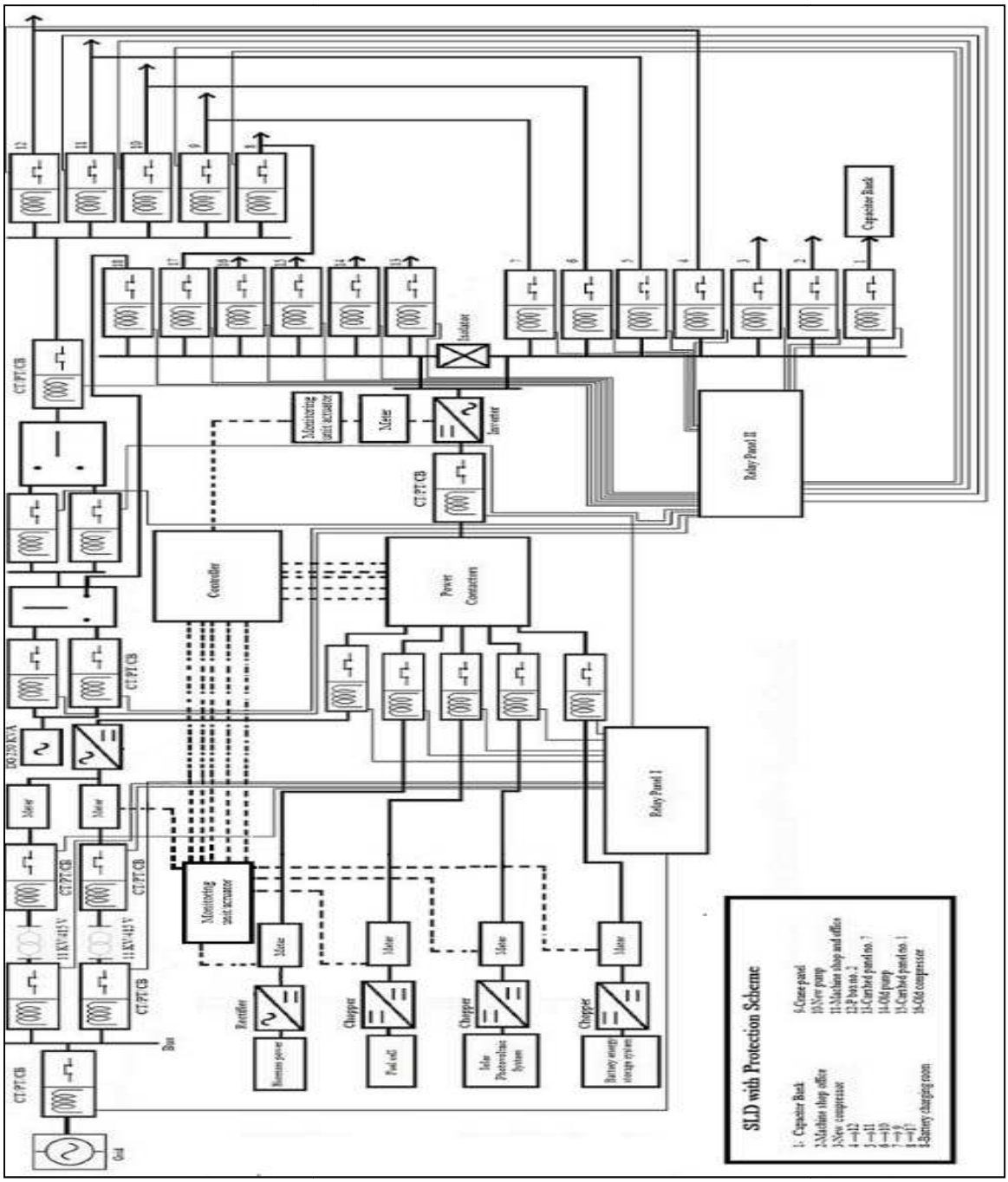

Figure 2.5. Single line diagram of the proposed protection system.

The cost evolution for this distributed generation system, three set of generators are considered as mentioned above. The test cases have been chosen in anticipation of the scenario that as per our present technology, BMGU has low installation cost and operating cost but power density is less. Whereas, PAFC has high installation and operating cost, but it

has high power density.ie. less space is required to install a high capacity power plant comparative to other DERs.

Among various type of fuel cells, PAFC, with high efficiency, low chemical and thermal emissions, fuel flexibility, reliability, low maintenance, excellent part-load performance, is considered as most advanced in the range of 50 KW to 1000 KW [209,210]. Presently it is proved that, in micro-power systems, Solar power system (SPS) performs good with economic merit to mitigate nearby loads [211,212]. As per the scenario of Indian context, BMGUs are also playing a vital role in the area of decentralized energy generation systems [213-217]. Among existing batteries, VRLA (valve regulated lead acid) shows most technological maturity in respect of efficiency, initial cost etc [215].

2.8.1. Objective Functions

Here the objective function is total annual cost of this distributed generation system which is given by

$$R = R_O + R_I + R_M + R_U \tag{2.82}$$

where R_O , R_I , R_M , R_U are operating cost, initial cost, micro-grid cost, and utility cost, respectively.

Here the objective is to minimize the total annual cost ***R,*** with optimal power operation and to find the optimum installed capacity of various DERs. It is considered that, the control variables, P_{bm}, P_{fc}, P_{bt}, P_{so} are the vectors which represent the hourly basis power generation of a day in KW and IC_{bm}, IC_{fc}, IC_{bt}, IC_{so} are the installed capacities of Biomass, fuel cell, battery energy storage system and solar power system respectively.

Operating cost varies for different type of DERs. O_{bm}, O_{fc}, O_{bt}, O_{so} are the operating costs per KW of BMGU, PAFC, BESS, SPS respectively. That implies,

For Case I

$$R_O = 365.\sum_{hr=1}^{24} P_{bm}.O_{bm} + P_{bt}.O_{bt} + P_{so}.O_{so} \tag{2.83}$$

For Case II

$$R_O = 365.\sum_{hr=1}^{24} P_{fc}.O_{fc} + P_{bt}.O_{bt} + P_{so}.O_{so} \tag{2.84}$$

For Case III

$$R_O = 365.\sum_{hr=1}^{24} P_{fc}.O_{fc} + P_{bm}.O_{bm} + P_{bt}.O_{bt} + P_{so}.O_{so} \tag{2.85}$$

Different DERs have different initial costs. Let I be the market rate of interest, $IC_{bm, fc, bt, so}$ and $C_{bm, fc, bt, so}$ are the optimal installed capacities and installation costs per KW capacity of BMGU, PAFC, BESS, SPS respectively. The $IC_{bm, fc, bt, so}$ are calculated as

$$IC_{bm, fc, bt, so} = max \mid P_{bm, fc, bt, so} \mid \quad (2.86)$$

So the equated annual cost for installations considering depreciation,

for Case I

$$R_I = (f_{bm} + I).IC_{bm} . C_{bm} + (f_{bt} + I).IC_bt . C_{bt} + (f_{so} + I).IC_{so} . C_{so} \quad (2.87)$$

for Case II

$$R_I = (f_{fc} + I).IC_{fc} . C_{fc} + (f_{bt} + I).IC_bt . C_{bt} + (f_{so} + I).IC_{so} . C_{so} \quad (2.88)$$

for Case III

$$R_I = (f_{bm} + I).IC_{bm} . C_{bm} + (f_{fc} + I).IC_{fc} . C_{fc} + (f_{bt} + I).IC_bt . C_{bt} + (f_{so} + I).IC_{so} . C_{so} \quad (2.89)$$

Where $f_{bm, fc, bt, so}$ are factors associated with sinking fund depreciation value, which are given below.

$$f_{bm, fc, bt, so} = dr. \frac{(1+dr)^{(Lft_{bm, fc, bt, so} - 1)}}{(1+dr)^{Lft_{bm, fc, bt, so}} - 1} \quad (2.90)$$

Here, $Lft_{sw, tfm, cbl, ctrl}$ are the estimated life times of these various DER power plants, with ***dr*** as the rate of depreciation.

The micro-grid installation cost (including depreciation and interest on the invested money for these installations) can be expressed as

$$R_M = (f_{sw} + I).C_{sw} + (f_{tfm} + I).C_{tfm} + (f_{cbl} + I).C_{cbl} + (f_{ctrl} + I).C_{ctrl} \quad (2.91)$$

Where $C_{sw, tfm, cbl, ctrl}$ are the costs of optimum installed capacities of switch gears (including CTs, PTs, LAs), transformers (1100 / 415 V), cable and controller (including panel) respectively. Here, the subjected site for implementing distributed generation is not very large. Transformers (1100 / 415 V) are needed here as the interface between the grid and the micro-grid. As the DERs will be existed near the loads, the local network is proposed of 415V. $f_{sw, tfm, cbl, ctrl}$ are the factors associated with sinking fund depreciation value, and are expressed as

$$f_{sw, tfm, cbl, ctrl} = dr. \frac{(1+dr)^{(Lft_{sw, tfm, cbl, ctrl} - 1)}}{(1+dr)^{Lft_{sw, tfm, cbl, ctrl}} - 1} \quad (2.92)$$

Here, $Lft_{sw, tfm, cbl, ctrl}$ are the estimated life times of these various equipments and dr is the depreciation rate.

The utility cost R_U includes the cost related for the purchasing of electricity from the grid and the selling of electricity to the grid.

$R_U = 365.\sum_{hr=1}^{24}(E_p . P_p - E_{sl} . P_{sl}) + 12.E_b.max (P_p)$ (2.93)

Here the first part, ie. $E_p . P_p$, implies the cost to purchase electricity from the grid, with E_p being the rate of energy (which varies as normal, peak or off load time) and *Pp* amount of purchased energy per hour. The last term signifies base price of electricity charged by the utility on the basis of maximum demand contract, which charged by the electricity board in every month. The middle term, ie. $E_{sl} . P_{sl}$ indicates the income of the consumer feeding or selling the surplus power to the grid. Here P_{sl} is the amount of energy fed to the grid per hour and E_{sl} is considered as selling price per unit amount of energy generated from DERs. It is enquired in 'Vidyut Bhavan', the Head Office of WBSEDCL, that there is no prominent scheme at which rate they can buy energy from any distributed generation system, but they have individual tariff for energy generated from different renewable energy generators which is fixed throughout every hours of the day. So the possible tariff to sale power to the grid is proposed here as

$$E_{sl} = \frac{S_{bm}.\sum_{hr} P_{bm} + S_{fc}.\sum_{hr} P_{fc} + S_{so}.\sum_{hr} P_{so}}{\sum_{hr} P_{bm} + \sum_{hr} P_{fc} + \sum_{hr} P_{so}} \quad (2.94)$$

where $S_{bm, fc, so}$ are the individual tariffs as regulated by the utility body.

2.8.2. Constraints

There are several constraints to solve this optimization problem. The primary constraint for the optimal power operation is to meet the power demand (*Pd*) of the consumer for all instances. This can be formulated as

$| P_d^i |=P_{bm}^i + P_{fc}^i + P_{so}^i + P_{bt}^i + |P_p^i|- |P_{sl}^i|$, *(for i = 1… to ... 24)* (2.95)

$P_{fc}^i = 0$, *(for i = 1… to ... 24, Case I)* (2.96)

$P_{bm}^i = 0$, *(for i = 1… to ... 24, Case II)* (2.97)

Also, there are some auxiliary constraints in this optimization procedure. Let $M_{bm, fc, bt, so}$ are the maximum installable capacities of different DERs. Then

$0 \le P_{bm}^i \le M_{bm}$, $\forall i$ (2.98)

$0 \le P_{fc}^i \le M_{fc}$, $\forall i$ (2.99)

$0 \le P_{bt}^i \le M_{bt}$, $\forall i$ (2.100)

Battery energy storage system has certain storage efficiency. Let η_{bt} be the efficiency of the BESS. Considering that positive power indicates power delivered by BESS**,**

$$\sum_{hr} P_{bt} = -(1-\eta_{bt}) \times \max|P_{bt}| \quad (2.101)$$

Solar power system can produce electricity neither in night and evening hours nor at uniformed rate throughout the day time. If *SOP* be the hourly basis solar potential to generate electrical power, then

$$0 \leq P_{so}^{\,i} \leq SOP^{i}, \quad \forall\, i \tag{2.102}$$

Thereafter, a crucial constraint for this particular case, is associated with the size of Transformer. Transformers have high costs and are nonlinearly related with their capacities. Besides, there are only some standard sizes of transformers available in market. Here, as mentioned earlier, the consumer has a maximum consumption of 120KVA and has connected load of 400 KVA. However they have installed 2 transformers (11000 / 415 V) with total capacity of 700 KVA. So, in case of excess production of power by the DERs, when the maximum amount of fed power is below 700 KW, no extra transformer is needed to be installed. But when it exceeds 700 KW, cost of transformer will be added. These facts are indicated as,

$$C_{tfm} = 0, \ (\text{for } Max\,|P_{sl}| \leq 700) \tag{2.103}$$

$$C_{tfm} = Tr_{100}, \ (\text{for } 700 \leq Max\,|P_{sl}| \leq 800) \tag{2.104}$$

$$C_{tfm} = Tr_{315}, \ (\text{for } 800 \leq Max\,|P_{sl}| \leq 1000) \tag{2.105}$$

$$C_{tfm} = Tr_{700}, \ (\text{for } 1000 \leq Max\,|P_{sl}| \leq 1400) \tag{2.106}$$

where $Tr_{100,\ 315,\ 700}$ are the costs of transformers of capacities 100, 315, 700 KVA respectively.

2.9. Optimal power controller design of active distribution network

Taking environmental and technical floors into consideration, solar photovoltaic network (PV system) and valve regulated Lead Acid battery bank as battery energy storage system (BES system)) have been considered here to form a nano power network.

2.9.1. Objective Function

In this context, the objective is to minimize the net annual operating price R_{anu} along with optimized power operation of the installable renewable power producers. The P_{batt} and P_{phv} represent the control vectors indicating a quarter hour basis daily power generation by the BES and PV system sequentially. This power generation takes place in accordance with the load power requirement data of similar time horizon. The C_{batt} and C_{phv} represent the installed

capacities of the battery energy accumulating media and solar photovoltaic network in a sequential manner.

An overall annum term operating price (R_{anu}) can be represented as

$$R_{anu} = R_{gen} + R_{utl} \tag{2.107}$$

where, the first term on the right side of the equation (R_{gen}) represents the power production price and can be expressed as

$$R_{gen} = 365\sum_{t=1}^{96} P_{batt}(t) r_{batt} + P_{phv}(t) r_{phv} \tag{2.108}$$

where $P_{batt}(t)$ and $P_{phv}(t)$ indicate the quarter hourly power supplied by the battery energy storage system and the solar photovoltaic network sequentially at t^{th} time duration. The terms r_{batt} and r_{phv} represent the equivalent prices of the aforesaid producers corresponding to per kWh energy in the same sequence.

The utility price, R_{utl} is the transaction cost associated with electricity buying and selling with the grid and can be expressed as

$$R_{utl} = \left\{ 365\sum_{t=1}^{96} E_{bu}(t) r_{bu}(t) - E_{sl}(t) r_{sl}(t) \right\} + 12 r_{mnl} \max\left(E_{bu}(t) \right) \tag{2.109}$$

where, $E_{bu}(t)$ and $E_{sl}(t)$ indicate the amount of energy bought and vended respectively and the terms $r_{bu}(t)$ and $r_{sl}(t)$ represent corresponding tariff rates. The term r_{mnl} indicates the utility grid contractual, thirty days basis minimal price in relation to the maximum consumable energy at the demand side.

The surplus energy to the grid can be supplied at a price determined by using the individual tariff plan for inexhaustible energy resources involved in this objective task. Hence, by utilizing the combined tariff plan, the vending price of the surplus energy is can be expressed as

$$r_{sl,srp} = \frac{V_{phv} \sum_{hr} P_{phv}}{\sum_{hr} P_{phv}} \tag{2.110}$$

where, V_{phv} indicates the individual basis vending price of the solar photovoltaic network. This price is regulated by the utility body.

2.9.2. Constraints

Imposition of the following constraints has been considered for the chosen optimization task. At the outset, the total power demand (P_{dem}) of the hospital premise should be computed at every time instance as

$$\left|P_{dem}(t)\right| = P_{batt}(t) + P_{phv}(t) + \left|P_{bu}(t)\right| - \left|P_{sl}(t)\right|, \quad \forall t \tag{2.111}$$

The producers cannot produce power beyond the installed capacities of the renewable energy resources and battery energy storage system considered in the power network. Solar photovoltaic networks possess complete dependence on the irradiance level throughout the day. A limitation on this power production is observed during different durations of the day. This happens in accordance to the irradiance level for each duration and thus,

$$0 \le \left|P_{batt}(t)\right| \le C_{batt}, \quad \forall t \tag{2.112}$$

$$0 \le P_{phv}(t) \le SO_p(t), \quad \forall t \tag{2.113}$$

where, $SO_p(t)$ shows time based paramount electricity generation by the installed solar photovoltaic network. Considering e_{batt} as the battery bank storing efficiency, energy lost in the battery energy accumulating media is deducted from the total power calculation. It has been assumed that power supplied by the battery energy accumulating media is positive (in terms of sign) and can be expressed as

$$\sum_{hr} P_{batt} = -\left(1 - e_{batt}\right) \times \max\left|P_{batt}\right| \tag{2.114}$$

2.9.3. System modeling

Figure 2.6 represents the single line block diagram schematic of the electrical power system in the hospital campus.

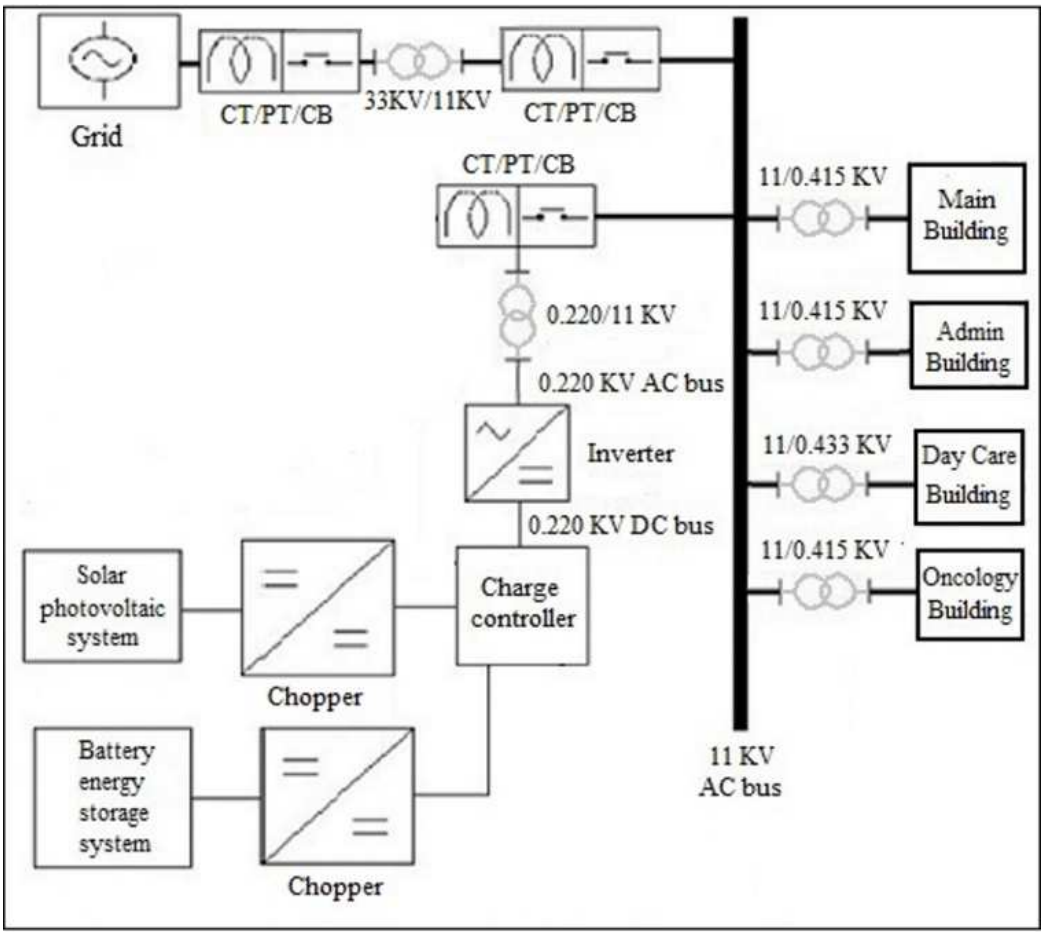

Figure. 2.6 Schematic of the electrical power network in the hospital

The PV system is connected through a non-controlled grid connected inverter. In this scheme the PV system and inverter are modeled by their Norton equivalents linearizing the PV characteristics around the maximum power point. Figure 2.7 represents the electrical model of the PV inverter system.

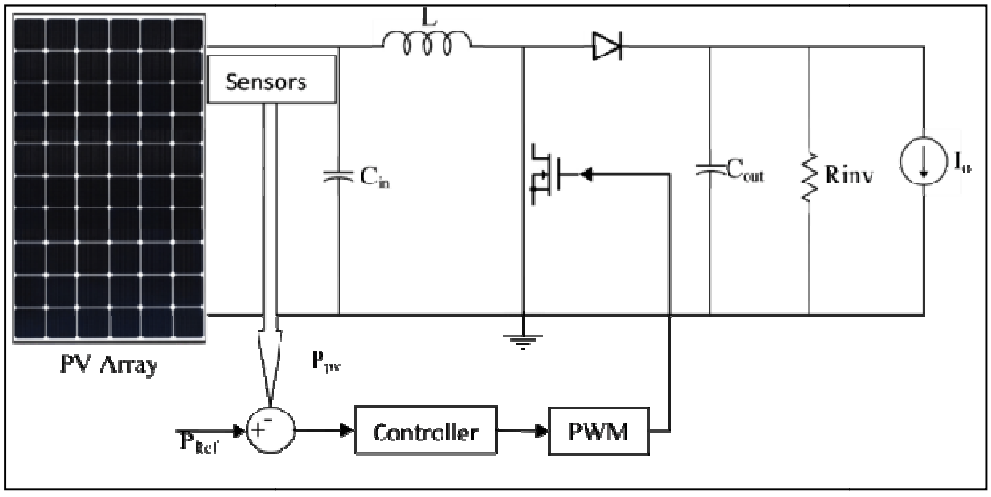

Figure. 2.7. Electrical model of the PV inverter system.

This system can be mathematically modeled in state-variable representation applying the average modeling technique as below [218].

$$\dot{\boldsymbol{X}} = \boldsymbol{AX} + \boldsymbol{BU} \tag{2.115}$$

$$\boldsymbol{Y} = \boldsymbol{CX} + \boldsymbol{DU} \tag{2.116}$$

$$\boldsymbol{X} = [i_L \; v_{Cin} \; v_{Cout}]^T \tag{2.117}$$

$$\boldsymbol{U} = \left[d \; I_{pv} \; I_O\right]^T \tag{2.118}$$

$$\boldsymbol{Y} = [v_{Cin}] \tag{2.119}$$

where

$$\boldsymbol{A} = \begin{bmatrix} 0 & \frac{1}{L} & -\frac{(1-d)}{L} \\ -\frac{1}{C_{in}} & -\frac{1}{C_{in} \cdot R_{MPP}} & 0 \\ \frac{(1-d)}{C_{out}} & 0 & -\frac{1}{C_{out} \cdot R_{inv}} \end{bmatrix} \tag{2.120}$$

$$\boldsymbol{B} = \begin{bmatrix} \frac{v_{Cout}}{L} & 0 & 0 \\ 0 & \frac{1}{C_{in}} & 0 \\ \frac{-i_L}{C_{out}} & 0 & -\frac{1}{C_{out}} \end{bmatrix} \tag{2.121}$$

$$\boldsymbol{C} = [0 \; 1 \; 0] \tag{2.122}$$

$$\boldsymbol{D} = [0 \; 0 \; 0] \tag{2.123}$$

In the above referred equations, i_L is the current through the inductor L. The v_{Cin} and v_{Cout} are the voltages across the input and output capacitors C_{in} and C_{out} respectively. The required duty is represented by d. Other inputs to the system, I_{pv} and I_o are the equivalent current of PV array and the inverter respectively. R_{MPP} is the equivalent resistance of the PV array at maximum power point.

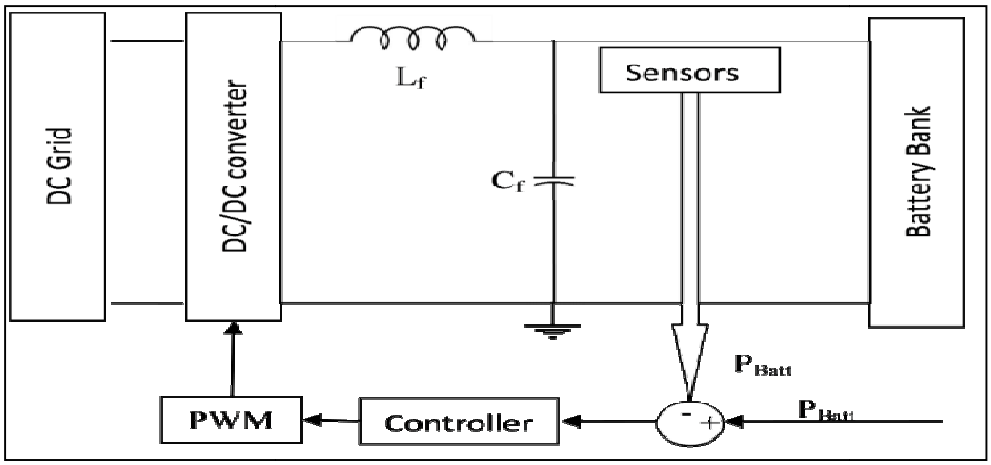

Figure 2.8. Electrical model of the BESS.

The electrical model of battery energy storage system (BESS) has been represented by Fig. 2.8. The charging/discharging current of the battery energy storage system is modeled

$$I_{Batt} = \frac{V_{Batt} - V_{DC}}{r_{Batt}} \tag{2.124}$$

where I_{Batt} is the charging/discharging current, V_{Batt} and r_{Batt} are the internal battery potential and resistance respectively. V_{DC} is the battery bank terminal voltage. Mathematically this BESS can be modeled as

$$\begin{bmatrix} \dot{V_{DC}} \\ \dot{I_{Lf}} \end{bmatrix} = \begin{bmatrix} -1/RC_f & 1/C_f \\ -1/L_f & 0 \end{bmatrix} \begin{bmatrix} V_{DC} \\ I_{Lf} \end{bmatrix} + \begin{bmatrix} 0 \\ 1/L_f \end{bmatrix} [d.V_{Grid}] \tag{2.125}$$

$$V_{DC} = \begin{bmatrix} 0 & 1/C_f \end{bmatrix} \begin{bmatrix} V_{DC} \\ I_{Lf} \end{bmatrix} \tag{2.126}$$

Where R is the equivalent resistance of the battery at equilibrium, C_f and L_f are the filter capacitance and inductance, d is the required duty of the DC-DC converter and V_{Grid} is the DC bus voltage.

The comprehensive schematic of the nano-grid is depicted as Figure 2.9

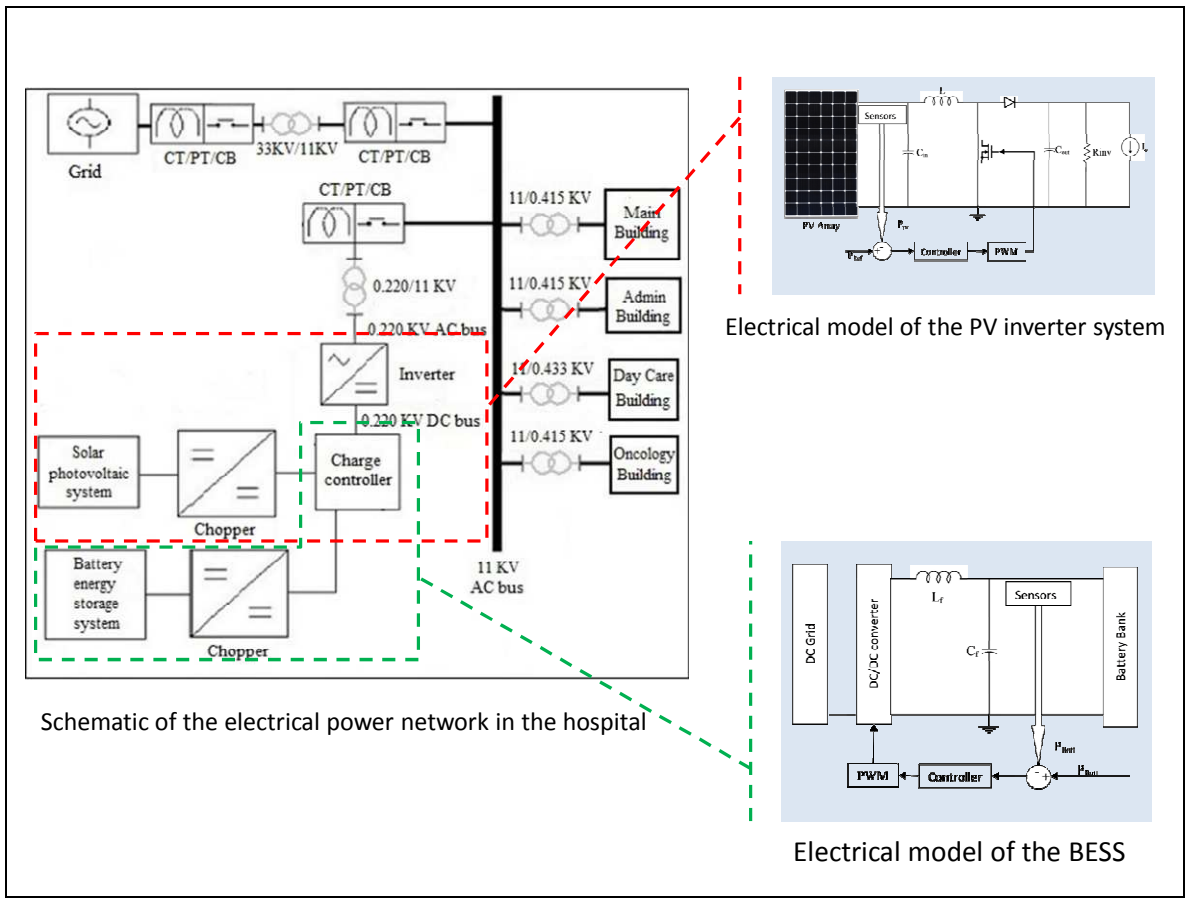

Figure 2.9. Comprehensive schematic of the nano-grid.

2.10. Optimization based fault detection scheme in photovoltaic system

2.10.1. PV system characteristics

Fig. 1 represents a single diode photovoltaic cell equivalent circuitry that contains a photo current source, a diode, a series (R_s) and a shunt (R_{sh}) resistors.

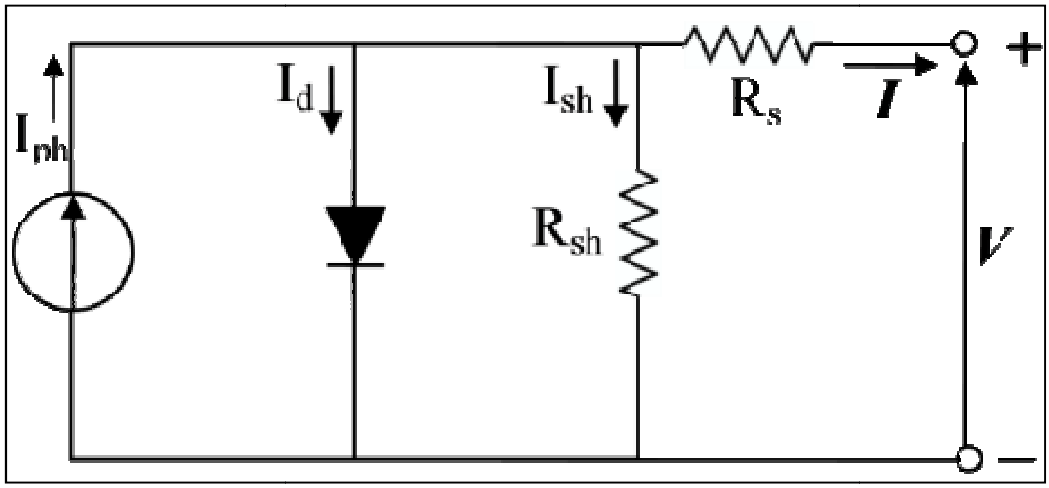

Figure 2.10 Equivalent Circuit of PV Cell.

This single diode cell model entails the following current-voltage (*I-V*) relationship as in (2.127) [219].

$$I = I_{ph} - I_o\left[\exp\left\{\frac{q\left(V + I.R_s\right)}{n.k.T}\right\} - 1\right] - \frac{V + I.R_s}{R_{sh}} \tag{2.127}$$

Where, I_{ph} is the generated photocurrent, I_o denotes the diode saturation current, n is the diode ideality factor, *q* represents the elementary charge, k is the Boltzmann constant and T is cell temperature. I and V are current and voltage output respectively.

In a PV module, these solar cells are connected in series and parallel combination. Thus, the *I-V* relationship of a module can be formulated as in (2.128) [219].

$$I = N_p.I_{ph} - N_p.I_o\left[\exp\left\{\frac{q\left(V/N_s + I.R_s/N_p\right)}{n.k.T}\right\} - 1\right] - \frac{N_p.V/N_s + I.R_s}{R_{sh}} \tag{2.128}$$

Where, N_s is the number of PV cell connected in series in a module and N_p is the number of

PV cell connected in parallel in a module.

2.10.2. Effect of non-uniform irradiance

It is very probable that solar irradiance be nonuniform throughout the panels in PV string. This causes dissimilar quantity of power production in PV units and also changes the operating temperature of the PV modules, which remarkably affects the PV current hence the power generation.

To harvest the maximum possible amount of energy from the PV system, various MPPT processes have been used, most commonly, regulating the operating voltage. Modified Perturb & Observe (P&O) is a readily used algorithm, which achieves great success tracking the voltage at the maximum power point [197]. It instantaneously calculates the operating duty of the DC-DC power converter connected to the PV string which controls the operating voltage in real time. The operating PV string voltage at MPP (V_{str}^{MPP}) is given by (2.129).

$$V_{str}^{MPP} = d.\Sigma_{j=1}^{m} V_{oc}^{j} \tag{2.129}$$

Where, d is the duty of DC-DC power converter, m is number of PV modules connected in series in a string, in the PV string and V_{oc}^{j} is the open circuit voltage of the j^{th} module.

2.10.3. Formulation of OC and SC faults in PV string

To introduce heuristic search technique as a tool for fault diagnosis in PV system, a fault related system parameter based objective function is required. So, it is intended to develop a fitness function that helps to locate open and short circuited modules in a PV string.

For each PV module three possible fault situations are considered: no fault, OC fault and SC fault. These fault conditions can be realized, as depicted in Fig. 2.11, by opened and closed positions of imaginary switches as SWO1-SWOm (switches to cause open circuit faults) and SWS1-SWSm (switches to cause short circuit faults). These SWOs and SWSs are connected with each module in series and shunt respectively. Here SWOs are normally closed and SWSs are normally open. An OC fault in the i^{th} module is realized by open SWOi and a SC fault in the i^{th} module is realized by closed SWSi of the corresponding PV module.

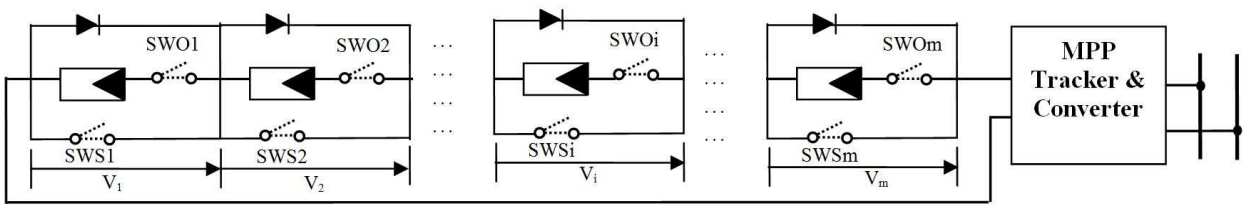

Figure 2.11 Connection Scheme of PV string.

As each module in a string experiences different solar irradiation and module temperature, operating voltages of each module are different. But, being connected in series, current through the modules (string current) is same. The operating voltage of individual module can be obtained from (2.128) with the information of module irradiance, temperature and string current obtained from respective sensors. In case of OC fault in a module, the voltage across the module terminals is negative of forward biased voltage of reverse bypass diode. During module SC fault, the voltage across that module will be zero. Voltage available at the string terminal is the summation of the voltages across each module. It is supposed that, whenever the PV string is faulty or healthy, the MPP tracker, connected across the string, is on its job to continuously control the operating voltage of the PV string for the sake of harvesting maximum power from the string. The string voltage at MPP can be realized by (2.129). Again, the string current at MPP depends on all of these module voltages. Hence, for different fault combinations, the string current varies. This property is mathematically exploited here to create the fitness function. Numerical expression of string output current at MPP (I_{str}^{MPP}) is derived based on the above narrated fault diagnosis concept.

During normal operation (no fault), the string output current at MPP can be represented as (2.130).

$$I_{str}^{MPP} = \left(\frac{1}{R}\right) \cdot \sum_{i=1}^{m} V_i^{MPP}(T_i, G_i) \tag{2.130}$$

Where, R is the equivalent load resistance, i denotes the position of the modules in the string, m is the total number of modules connected in series in the string, T_i is the temperature of module at i^{th} position, G_i is the solar irradiance on module at i^{th} position, $V_i^{MPP}(T_i, G_i)$ is the voltage output of module at i^{th} position for T_i and G_i when the whole string is operating at MPP.

The imaginary switches (SWOs and SWSs), as presented in Fig. 2, have been considered to introduce open and short circuit faults in the equation of string current. Here, in this problem, *SWO* and *SWS* are the decision vectors with dimension *m*, where m is the total number of modules connected in series in the string. The elements of the vectors *SWO* and *SWS* are bound to be 0 or 1. The value of SWO_i as 0, indicates an open SWO associated with the i^{th} module, which implies the i^{th} module to be open circuited. Otherwise, the value of that

SWO_i being 1, it implies no open circuited fault in that i^{th} module. In the same way, the value of SWS_i as 1 indicates closed SWS associated with the i^{th} module, which implies the i^{th} module to be short circuited. Otherwise the value of that SWS_i being 0, it implies no short circuited fault in that module.

In occurrence of only open circuit faults, the open circuited modules are detached. At that time, the string current will flow through the normally connected modules and the bypass diodes connected across the respective open circuited modules. The current through those bypass diodes causes some power loss in the form of voltage drops across those bypass diodes. Thus, the string output current equation at MPP can be expressed as (2.131).

$$I_{str}^{MPP} = \frac{1}{R} \cdot \left[\sum_{i=1}^{m} \left\{ SWO_i \times V_i^{MPP}\left(T_i, G_i\right) - V_{BD} \times \left(1 - SWO_i\right) \right\} \right] \tag{2.131}$$

Where, $SWO = \{SWO_1, ..., SWO_i, ..., SWO_m\}$ and V_{BD} is the voltage drop at bypass diode in conduction state.

For example, if 4^{th}, 6^{th} and 9^{th} modules of the string, consisting of 10 numbers of modules, are open circuited, then, $m = 10$ and $SWO = \{1,1,1,0,1,0,1,1,0,1\}$. Thus, SWO indicates the locations of OC faults in the string.

Again, in case of only short circuited conditions of modules in the string, the voltage across short circuited modules will become zero. So, the string output current can be formulated as (2.132).

$$I_{str}^{MPP} = \frac{1}{R} \cdot \left[\sum_{i=1}^{m} \left\{ \left(1 - SWS_i\right) \times V_i^{MPP}\left(T_i, G_i\right) \right\} \right] \tag{2.132}$$

Where, $SWS = \{SWS_1, ..., SWS_i, ..., SWS_m\}$.

For example, if 2^{th}, 5^{th}, 6^{th} and 8^{th} modules of the string, consisting of 10 numbers of modules, are short circuited, then, $m = 10$ and $SWS = \{0,1,0,0,1,1,0,1,0,0\}$. In this manner, SWS indicates the locations of SC faults.

Now, to realize both OC and SC faults together, possible numerical combinations (Cb1-Cb4) of SWO_i and SWS_i are tabulated in Table 2.1. In case of Cb1, it indicates normal operation, i.e., no fault in that module. At that situation, the bypass diode across that module is operating at reverse biased condition. In case of Cb2, indicating an OC fault, the bypass diode is in forward biased operation causing a voltage drop of V_{BD} in the string. Again, in case of both Cb3 and Cb4, the value of SWS_i is 1. In these situations, whatever is the value of SWO_i (0 or 1); the effects of both these switching combinations to the string are same as

short circuited operation of that module. In these cases, the terminal voltage across the bypass diode is zero.

Table 2.1

Realization of faults by switching combinations.

Combination	SWO_i	SWS_i	Associated operating condition of the i^{th} module	Terminal voltage across the i^{th} Module	Voltage across the bypass diode shunted to the i^{th} Module
Cb1	1	0	No fault	$V_i^{MPP}(T_i, G_i)$	$-V_i^{MPP}(T_i, G_i)$
Cb2	0	0	Open	$-V_{BD}$	V_{BD}
Cb3	1	1	Short	0	0
Cb4	0	1	Short	0	0

Considering these combinations and their effects on the string electrical parameters, (2.131) and (2.132) are combined to form a generalised equation (2.133) for I_{str}^{MPP}, where both OC and SC faults are considered in the string.

$$I_{str}^{MPP} = \frac{1}{R} \cdot \left[\sum_{i=1}^{m} \left\{ SWO_i \times (1 - SWS_i) \times V_i^{MPP}(T_i, G_i) - V_{BD} \times (1 - SWO_i) \times (1 - SWS_i) \right\} \right] \quad (2.133)$$

So, the actual faults can be detected by following the actual current measured at the string operating at MPP and comparing the same with the calculated string current (I_{sim}^{MPP}), which is equal to (I_{str}^{MPP}), as given by (133). Hence, the objective function can be modelled as the absolute difference between measured string current (I_{meas}^{MPP}) and calculated string current (I_{sim}^{MPP}), operating at MPP. Thus, the fitness function, $FIT(SWO, SWS)$ for PV string is formulated as a minimization problem (2.134).

$$FIT(SWO, SWS) = abs\left| I_{meas}^{MPP} - I_{sim}^{MPP} \right| \quad (2.134)$$

Where, $SWO = \{SWO_1, ..., SWO_i, ..., SWO_m\}$.

$SWS = \{SWS_1, ..., SWS_i, ..., SWS_m\}$.

I_{meas}^{MPP}= Measured faulty string current at MPP.

I_{sim}^{MPP} = Calculated faulty string current at MPP.

The global minima of the fitness function (2.134) is zero (i.e., when I_{sim}^{MPP} and I_{meas}^{MPP} are the same). And the decision variables, that give the optimum solution, indicate the fault combination (location of OC faults and location of SC faults, individually), that has actually occurred in the string.

2.10.4. Optimality condition

There may be many suboptimal solutions, solved by different optimizer for different fault combinations, those are close to zero. Suboptimal solutions may fail to indicate the actual fault combination. As simulated irradiation and temperature distribution throughout the modules are taken same as existed in the operating physical PV string, the difference in value of I_{sim}^{MPP} and I_{meas}^{MPP} is supposed to be caused by the dissimilarity of simulated fault combination from the actually occurred faults in the string. But, on the other hand, the optimal solution of the fitness function may not be exactly zero, but close to zero, due to various accuracy limitations of various sensors and measuring and recording devices. Hence, to guarantee the truthfulness of the solution, obtained by minimization of the fitness function (2.134), necessary optimality condition has been set.

To set the optimality condition, the minimum difference of the effect on a PV string, due to the actual fault combination and some other combination of faults, has to be identified. It is interesting to note that, the minimum possible difference of total string power output between any two combinations of faults is either the power loss in a single bypass diode at any particular string current or the difference in power generation between those two modules whose irradiance values are the closest in that string, whichever is smaller for a particular faulty (or healthy) string.

Thus, the optimality condition has to be set initially during the fault diagnosis procedure every time. Here, the optimality condition is: the difference, between actual power output (P_{actual}) of the physical PV string and the simulated power output ($P_{simulated}$) of the simulated model for the fault combination provided by the optimizer, must be less than a small number ε.

So, the optimality condition can be mathematically expressed as, $\left|P_{simulated} - P_{actual}\right| < \varepsilon$

Where, the value of ε is determined as follows using simulated PV model:

---

calculate P_{BD}

---

calculate ΔP_{module}

if $P_{BD} < \Delta P_{module}$

$\varepsilon = P_{BD}$

else

$\varepsilon = \Delta P_{module}$

Where, P_{BD}, the power loss in a single bypass diode carrying the measured string current (I_{meas}^{MPP}), is obtained as (2.135).

$$P_{BD} = V_{BD} \times I_{meas}^{MPP} \tag{2.135}$$

And ΔP_{module}, the difference in power generation between those two modules whose irradiance values and thus the generated power are closest in that string, may be obtained as (2.136).

$$\Delta P_{module} = \min\{\Delta V_{module}\} \times I_{meas}^{MPP} \tag{2.136}$$

Where, ΔV_{module} can be obtained by the following steps.

```
{
for i=1 to m
   {
   for j=1 to m
      {
      if i≠j
        {
        ΔV_module(i.j) = V_i^MPP(T_i, G_i) − V_j^MPP(T_j, G_j)
        }
      }
   }
}
```

2.10.5. Fault diagnosis scheme using optimizer

The proposed fault diagnosis scheme is represented as in Fig. 2.12. It shows the different blocks of the diagnosis process. The acquired physical data from the PV string are fed to the soft computing based diagnosis platform through a computer interface to carry out the search of the actual fault combination. Optimization technique is employed here to minimize the fitness function (2.134), so that, the actual fault combination can be identified.

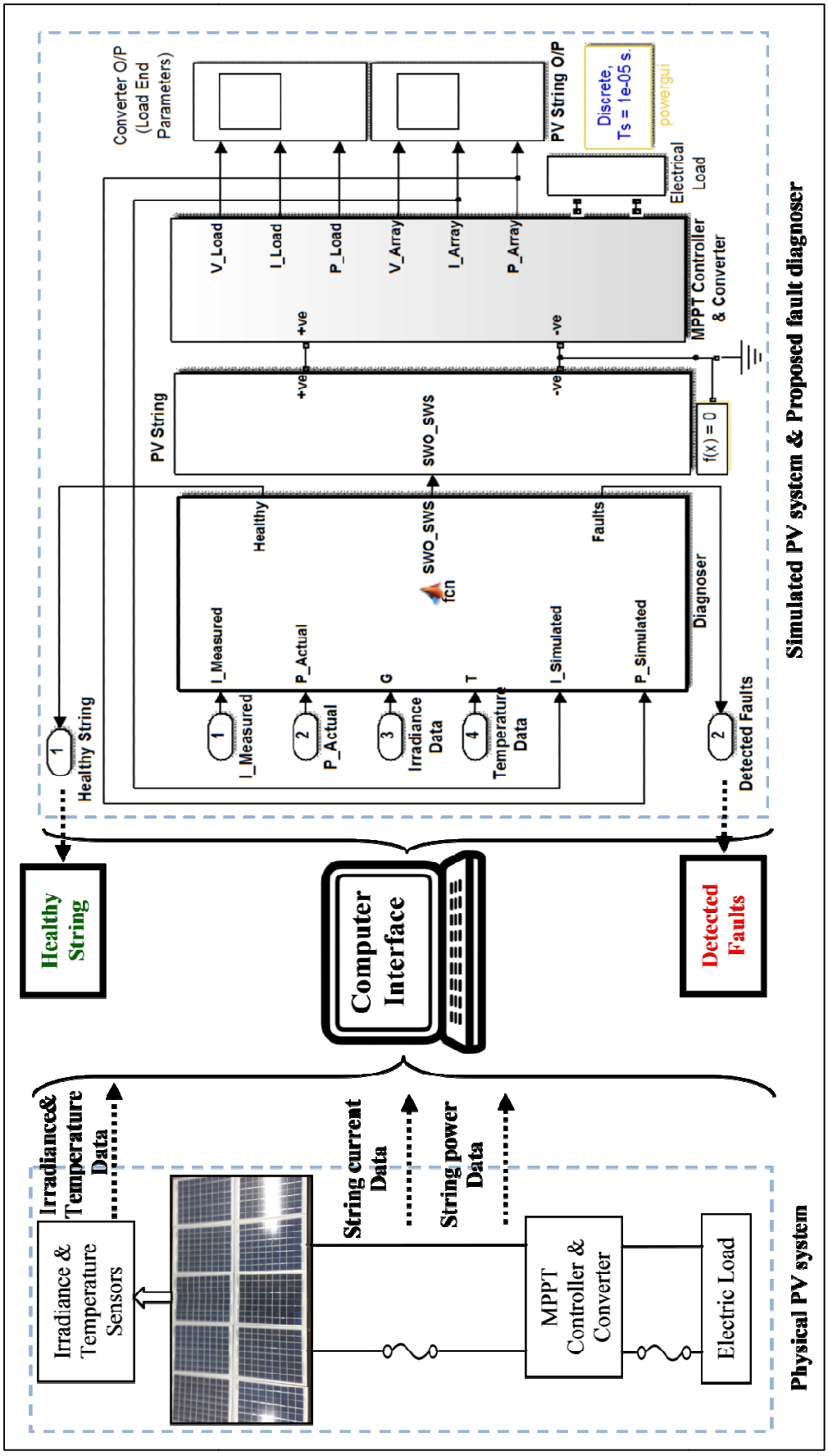

Figure 2.12. Block Diagram of the proposed fault diagnosis scheme.

All the physically measured data obtained from the respective sensors are exported to the diagnosis platform via computer interface. The data fed by the computer interface have been computed by the computing machine equipped with simulation software. A simulation model, replicating the physical PV string, is constructed. This simulated PV string is used to carry out the intermediate function evaluations as required by the optimizer block in Fig. 2.12. After computation by the optimizer, for the generated solution (i.e., the detected fault combination), the optimality condition is checked. If the solution satisfies the optimality condition, the detected fault is displayed. The logical flow chart of this fault diagnosis scheme is depicted in Fig. 2.13.

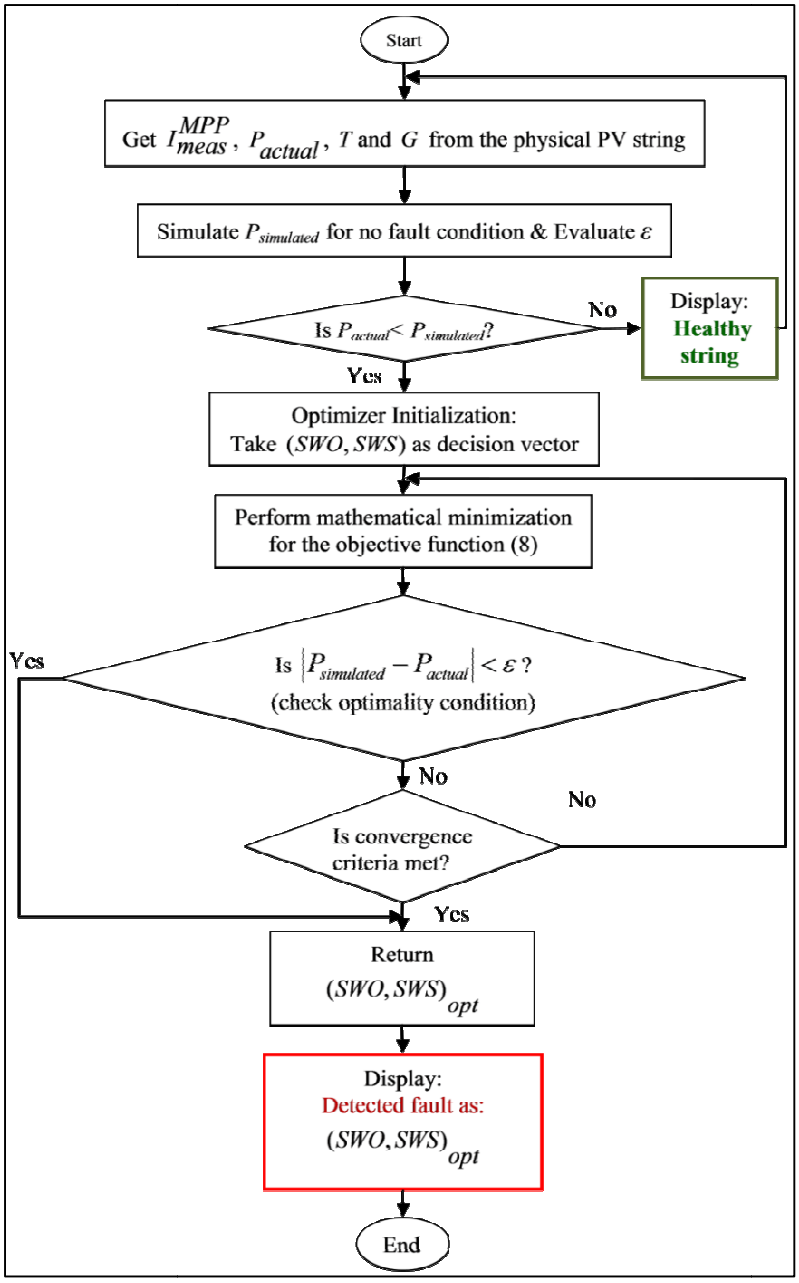

Figure 2.13. Computational flowchart of the fault diagnosis methodology.

This page is left blank intentionally

Chapter 3

Solution techniques

==========

3.1. Mathematical optimization

A procedure to obtain the best possible solution(s) under given situations is named as optimization. Considering the design, maintenance, and construction of an engineering system, various technical and managerial decisions are needed at different stages. The ultimate aim of each of these decisions includes either to maximize the required advantage or to minimize the effort count [220]. For mathematical optimization, one or more objective functions need to be formed. The goal of the mathematical optimization techniques is to find values of the variables that minimize or maximize the objective function while satisfying the constraints.

3.1.1. Expressional stating

An optimization goal can be stated as,

determine X in (), resulting in minimized or maximized values of $F(X)$.

$W:\{W_1,W_2,...,W_n\}=F(X),$ (3.1)

Here, W is known as objective(s) and

$X:\{x_1, x_2,....,x_m\}$ is decision vector.

This is subjected to satisfy the equality and inequality constraints as in (3.2) and (3.3).

$H_j(X) = 0\,, \qquad j = 1,2,...,h$ (3.2)

$G_i(X) \le 0, \qquad i = 1,2,...,g$ (3.3)

3.1.2. Solution methodologies for power system optimization problems

An elevated interest in algorithms encouraged by the aptness of natural phenomena is seen throughout the last few decades [221-227]. A lot of studies seeking to find optimal solution are being done [223,228,229]. Some algorithms perform better to solve some particular problems than others. A number of effective optimization algorithms are available in the literature.

In the previous chapter of this thesis, various power system optimization problems have been formulated constructing the objective functions and according constraints. All of the problems stated here are in the form of minimization problems. Different available heuristic and meta-heuristic optimization algorithms have been applied to solve the power system optimization problems stated here in this thesis. These optimization algorithms and their application methodologies have been discussed in the following sections.

3.2. Heat transfer search algorithm for economic dispatch problems

In Heat transfer search (HTS) algorithm, the population is considered as a group of molecules that participate in a heat transfer attaining different temperature echelons [19]. Here variables correspond to different molecule temperature. The molecular energy level denotes the value of the fitness function. The HTS begins with a random initial population of pop, and every solution has a N_g numbers of decision variables. The values are updated with each iteration. The selection procedure here adopted is the greedy selection technique which allows the modernized solution in HTS, if it provides better solution. The worst solution is replaced by the best. The whole search process is conducted as in three equally probable phases which are determined by a parameter ϕ. The phase wise solution algorithm for ED problem applying HTS are as below.

3.2.1.Conduction Phase

In conduction phase, the system seeks to reach thermal equilibrium by heat transfer following conduction process. During this phase where $iter \le iter_{\max} / f_{cd}$ $\{ f_{cd} : \text{conduction\_factor} \}$, the solutions are modeled as follows:

$$Pg_{j,i}^{iter+1} = Pg_{k,i}^{iter} + cd_1 \text{; for } C_{ED}\left(Pg_j\right) > C_{ED}\left(Pg_k\right) \quad (3.4)$$

$$Pg_{k,i}^{iter+1} = Pg_{j,i}^{iter} + cd_2 \text{; for } C_{ED}\left(Pg_k\right) > C_{ED}\left(Pg_j\right) \quad (3.5)$$

Where, *iter* is the current iteration, $j = 1,..., pop$, $k \in (1,...., pop)$, $j \neq k$ and k^{th} generation is randomly selected from the population, $i \in (1,..., N_g)$. cd_1 and cd_2 are the respective conduction steps stated as follows:

$$cd_1 = -\phi^2 Pg_{k,i}^{iter} \quad (3.6)$$

$$cd_2 = -\phi^2 Pg_{j,i}^{iter} \quad (3.7)$$

Here, ϕ^2 is matched up to the conductance from the Fourier's law equation and $Pg_{k,i}$ and $Pg_{j,i}$ are matched up to the temperature gradients.

In the next part where, $iter \geq iter_{\max} / f_{cd}$, the solution are brought up to date as:

$$Pg_{j,i}^{iter+1} = Pg_{k,i}^{iter} + cd_3 \text{; for } C_{ED}\left(Pg_j\right) > C_{ED}\left(Pg_k\right) \quad (3.8)$$

$$Pg_{k,i}^{iter+1} = Pg_{j,i}^{iter} + cd_4 \text{; for } C_{ED}\left(Pg_k\right) > C_{ED}\left(Pg_j\right) \quad (3.9)$$

Where, cd_3 and cd_4 are the steps of conduction phase stated as follows:

$$cd_3 = -r_i Pg_{k,i}^{iter} \quad (3.10)$$

$$cd_4 = -r_i Pg_{j,i}^{iter} \quad (3.11)$$

Where, r_i symbolizes the conductance in the Fourier's equation. Temperature gradient of the same Fourier's equation is represented by $Pg_{k,i}$ and by $Pg_{j,i}$.

3.2.2. Convection Phase

In this phase, the system attempts to reach thermal equilibrium by heat transfer following convection process. The surrounding is considered as the best generation. At iteration $iter < iter_{\max} / f_{co}$ { f_{co} : convection _factor }, Pg_t is the surrounding temperature, Pg_{mt} is the mean system temperature. When the system acquire higher energy than that of the surrounding i.e. $C_{ED}\left(Pg_t\right) < C_{ED}\left(Pg_{mt}\right)$, the solution can be modeled as follows:

$$Pg_{j,i}^{iter+1} = Pg_{j,i}^{iter} + co \tag{3.12}$$

Where, $j = 1,..., pop$, $i = 1,...,N_g$. The decision vectors are updated in the conduction phase. co is the convection step expressed as follows:

$$co = \phi\left(Pg_t - Pg_{mt} \times tf\right) \tag{3.13}$$

Where, ϕ becomes equal to the convection element of the Newton's law of cooling and Pg_t and Pg_{mt} the surrounding temperature and the mean system temperature respectively. The system temperature constantly changes with the heat transfer process. The surrounding becomes the heat source or heat sink, so its temperature remains constant. To consider this effect, temperature change factor (tf) is initiated. Thus, based on tf , the mean system temperature can be varied. The value of tf is determined as follows:

$$tf = abs\left(\phi - r_i\right); \text{ for } iter \le iter_{\max} / f_{co} \tag{3.14}$$

$$tf = round\left(1 + r_i\right); \text{ for } iter \ge iter_{\max} / f_{co} \tag{3.15}$$

Where, r_i varies in the range [0, 1]. Initially the tf changes between 0 and 1 at random. The value of tf becomes either 1 or 2. Different values of tf are required to ensure balanced exploration and exploitation. The value of f_{co} is assigned 10 for the convection phase.

3.2.3. Radiation Phase

The heat transfer following radiation process is the cause here for system thermal equilibrium. Here, the system and the surrounding are interacted with each other within the system to achieve thermal balance. Initially in the radiation phase, where $iter \le iter_{\max} / f_{rd}$ { f_{rd} : radiation_ factor }, the solution is updated (i.e. energy lessening of the system) as follows:

$$Pg_{j,i}^{iter+1} = Pg_{j,i}^{iter} + rd_1; \text{ if } C_{ED}\left(Pg_j\right) > C_{ED}\left(Pg_k\right) \tag{3.16}$$

$$Pg_{j,i}^{iter+1} = Pg_{j,i}^{iter} + rd_2; \text{ if } C_{ED}\left(Pg_k\right) > C_{ED}\left(Pg_j\right) \tag{3.17}$$

Where, $j = 1,....., pop$, $k \in (1,....., pop)$, $j \ne k$ and k^{th} solution is a randomly selected from the population, $i \in (1,..., N_g)$. All design variables of the solution is brought up to date during each iteration of the radiation phase. rd_1 and rd_2 are the radiation steps stated as follows:

$$rd_1 = \phi\left(Pg_{k,i}^{iter} - Pg_{j,i}^{iter}\right) \tag{3.18}$$

$$rd_2 = \phi\left(P_{g\,j,i}^{\,iter} - P_{g\,k,i}^{\,iter}\right) \tag{3.19}$$

Where, ϕ matches up to the radiation element of the Stefan-Boltzmann law and $P_{g\,k}$ and $P_{g\,j}$ matches up to the temperatures of system and the surrounding respectively.

Where, $iter \geq iter_{\max} / f_{rd}$, the solution is brought up to date as follows:

$$P_{g\,j,i}^{\,iter+1} = P_{g\,j,i}^{\,iter} + rd_3 \text{; if } C_{ED}\left(P_{g\,j}\right) > C_{ED}\left(P_{g\,k}\right) \tag{3.20}$$

$$P_{g\,j,i}^{\,iter+1} = P_{g\,j,i}^{\,iter} + rd_4 \text{; if } C_{ED}\left(P_{g\,k}\right) > C_{ED}\left(P_{g\,j}\right) \tag{3.21}$$

Where, rd_3 and rd_4 are the radiation steps stated as follows:

$$rd_3 = r_i\left(P_{g\,k,i}^{\,old} - P_{g\,j,i}^{\,old}\right) \tag{3.22}$$

$$rd_4 = r_i\left(P_{g\,j,i}^{\,old} - P_{g\,k,i}^{\,old}\right) \tag{3.23}$$

Where, r_i :[0, 1] and f_{rd} : radiation_ factor , which finds out the exploration and exploitation propensity in this phase. The value of f_{rd} has the value of 2.

Fig 3.1. portrays the flow chart of heat transfer search algorithm.

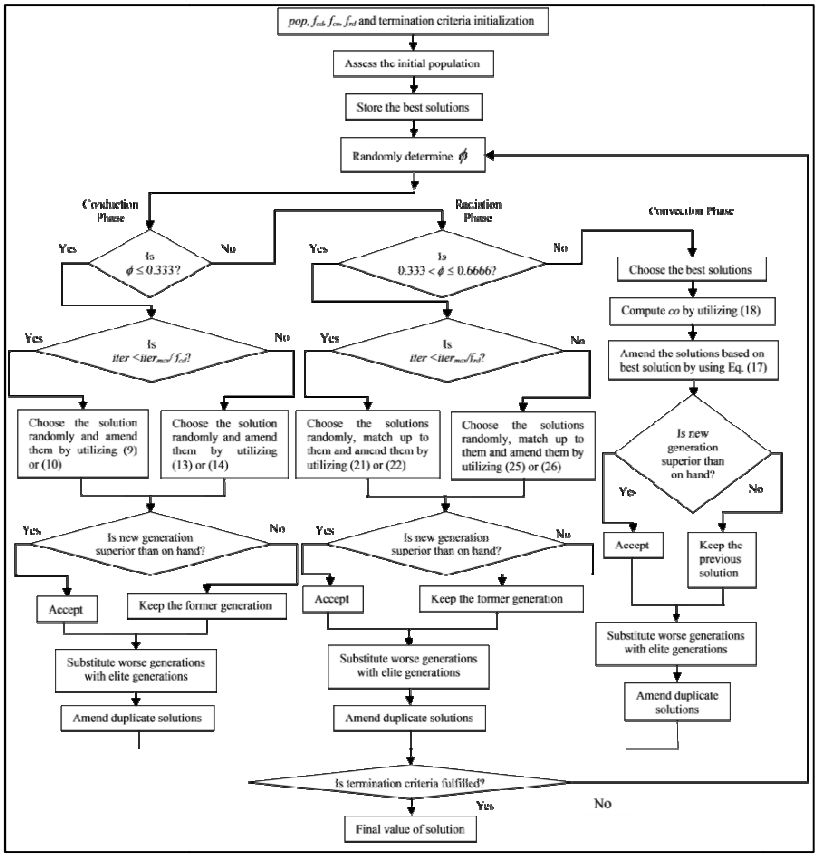

Figure 3.1 Computational flowchart of the HTS algorithm.

3.3. Artificial immune system (AIS) for MAED problems

3.3.1. Immune system

The immune system of vertebrates including human is self-possessed of cells, molecules and organs in the body which protect the body against infectious diseases caused by foreign pathogens such as viruses, bacteria, and so forth. To perform these roles, the immune system has to be capable to differentiate between the body's own cells as the self cells and foreign pathogens as the non-self cells or antigens. After distinguishing between self and non-self cells, the immune system has to perform an immune response in order to get rid of non-self cell or antigen. Antigens are further classified in order to activate the suitable defense method and at the same time, the immune system also developed a memory to enable more competent responses in case of further infection by the similar antigen.

Clonal selection theory explains how the immune system Fights against an antigen. It establishes the idea that only those cells which be familiar with the antigen are selected to proliferate. The selected cells are subjectedto an affinity maturation process which improves their attraction to the selected antigens.

Clonal selection operates both on B-lymphocytes or B cells produced by the bone marrow and T-lymphocytes or T cells shaped by the thymus. When the body is exposed to an antigen, B cells would respond to secrete specific antibodies to the particular antigen. Thereafter, a second signal from the T-helper cells, a subclass of T cells, would then stimulate the B cell to proliferate and mature into terminal (non-dividing) antibody secreting cells called plasma cells. In proliferation, clones are generated in order to achieve the state of plasma cells as they are the mainly active secretors of the antibodies at a larger rate than rate of antibody discharge by the B cells. The propagation rate is directly comparative to the affinity level, i.e. higher the resemblance level of B cells more clones is generated. Clones are mutated at a rate inversely proportional to the antigen affinity, i.e. clones of higher affinity are subjected to less mutation compared to those which exhibit lower affinity. This process of selection and muta-tion of B cells is known as affinity maturation.

T cells do not exude antibodies but play a middle role in the parameter of the B-cell response and are the most excellent in cell-mediated immune reaction. Lymphocytes, in addition to proliferating into plasma cells, can distinguish into long-lived B memory cells.

These memory cells circulate through the blood, lymph and tissues, so that when exposed to a second antigenic stimulus, they commence to differentiate into plasma cells capable of producing high affinity antibody, prese-lected for the specific antigen that had stimulated the primary response.

3.3.2. Artificial immune system

Artificial immune system (AIS) mimics these biological principles of clone generation, proliferation and maturation. The main steps of AIS based on clonal selection principle are activation of antibodies, prolif-eration and differentiation on the encounter of cells with antigens, maturation by carrying out affinity maturation process, eliminating old antibodies to maintain the diversity of antibodies and to avoid pre-mature convergence, selection of those antibodies whose affinities with the antigen are greater.

In order to emulate AIS in optimization, the antibo-dies and affinity are taken as the feasible solutions andthe objective function, respectively. Real number is used to represent the attributes of the antibodies.

Initially, a population of random solutions is gen-erated which represent a pool of antibodies. These antibodies undergo proliferation and maturation. The proliferation of antibodies is realized by cloning each member of the initial pool depending on their affinity. In minimization problem, a pool member with lesser objective value is measured to have higher affinity. The propagation rate is directly proportional to the affinity of the antibodies. The maturation process is carried through hyper-mutation which is inversely pro-portional to the antigenic affinity of the antibodies. The next step is the application of the aging operator. This aging operator eliminates old antibodies in order to maintain the diversity of the population and to avoid the premature convergence. In this operator, an anti-body is allowed to remain in the population for at most τB production. After this period, it is assumed that this antibody corresponds to local optima and must be abolished from the current population, no matter what its affinity may be. During the cloning expansion, a clone inherits the age of its parent and is assigned an age equal to zero when it is successfully hyper-mutated, i.e. when hyper-mutation improves its resemblance. Figure 1 demonstrates the flowchart of artificial immune system algorithm

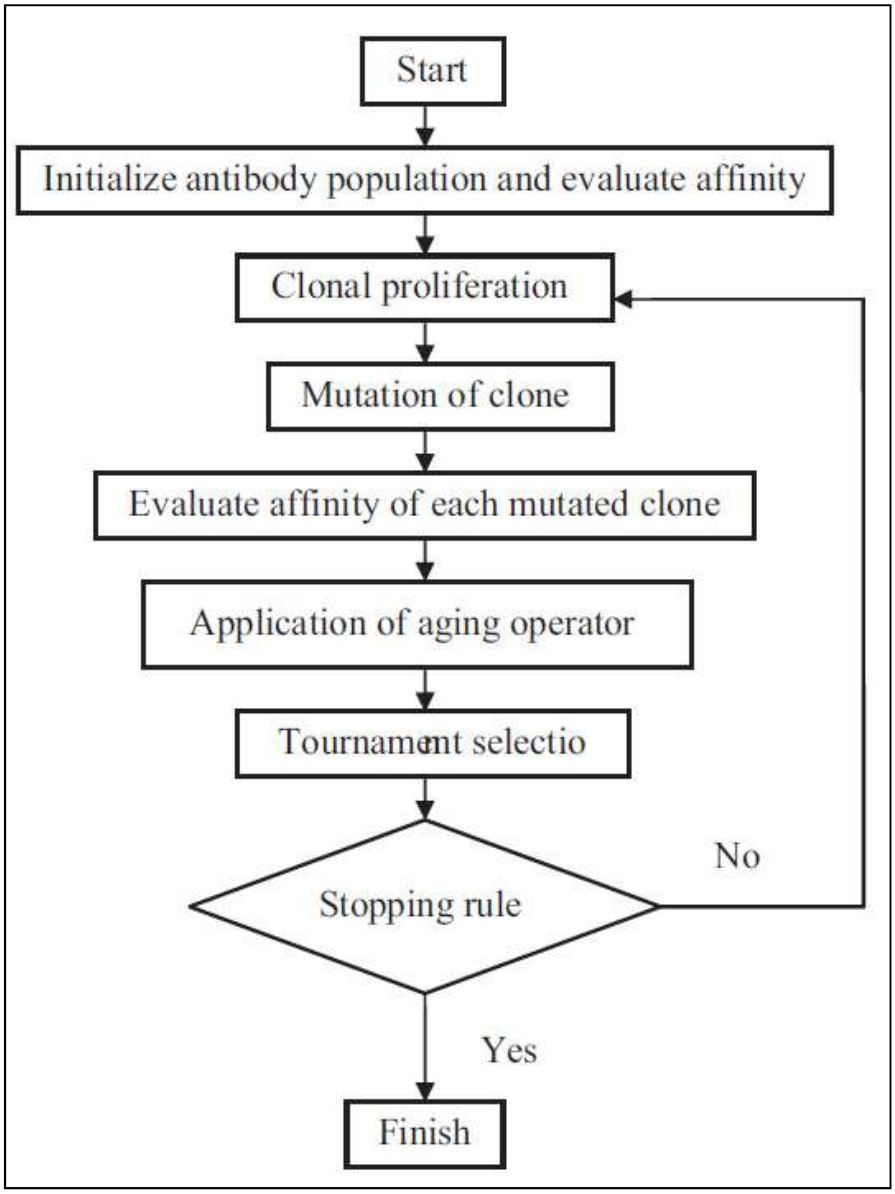

Figure 3.2 Computational flowchart of the AIS algorithm.

3.3.3. Implementation of AIS algorithm

In this section, an algorithm based on artificial immune system for solving MAED problem is described below.

Step 1. Let

$$P_n = [(P_{11}, P_{12}, \ldots P_{1M_1}), \ldots, (P_{i1}, P_{i2}, \ldots P_{iM_i}), \ldots, (P_{N1}, P_{N2}, \ldots P_{NM_1}), (T_{12}, T_{13}, \ldots T_{1N}), (T_{23}, T_{24}, \ldots T_{2N}), \ldots, (T_{(N-1)N})]' \quad (3.24)$$

be the nth antibody of a population to be evolved and n = 1, 2, ..., N_P. The elements of p_n are real power outputs of the committed generators of all areas and tie line real power flows. The

real power output of the j^{th} generator in area i is determined by setting $P_{ij} \sim U\left(P_{ij}^{\min}, P_{ij}^{\max}\right)$, where $i = 1, 2, ..., N$ and $j = 1, 2, ..., M_i$. Tie line real power flow is determined by setting $T_{ik} \sim U\left(-T_{ik}^{\max}, T_{ik}^{\max}\right)$. $U_{a,b}$ denotes a uniform random variable ranging over [a,b]. Each antibody should satisfy the constraints given by eqns. (2.10), (2.12), (2.13) and (2.14). [ref. chapter 2, sec. 2.2]

Step 2. As MAED is a minimization problem, the affinity is the inverse of the objective function and it is given by the following equation.

$$Affinity = \frac{1}{F_t} \tag{3.25}$$

Step 3. The antibodies are cloned directly proportional to their affinities.

Step 4. The clones undergo maturation process through hyper-mutation mechanism and are given by the following equation

$$P_{mij}^{/} = P_{nij} + mul_G \times \frac{F_{tn}}{F_{t\min}} \times N(0,1) \times \left(p_{ij}^{\max} - p_{ij}^{\min}\right);\ n \in N_P,\ m \in N_c,\ i \in N,\ j \in M_i \tag{3.26}$$

$$T_{mik}^{/} = T_{nik} + mul_T \times \frac{F_{tn}}{F_{t\min}} \times N(0,1) \times \left(T_{ik}^{\max} - \left(-T_{ik}^{\max}\right)\right);\ n \in N_P,\ m \in N_c,\ i \in N,\ k \in N,\ i \neq k \tag{3.27}$$

where F_{tmin} is the minimum value of F_t among the N_P solutions, mul_G and mul_T are scaling factors of real power generation and tie line power transfer respectively, F_{tn} is the value of the function associated with p_n and N(0,1) represents a Gaussian random variable with mean 0 and standard deviation 1. The term $\frac{F_{tn}}{F_{t\min}}$ makes the mutation more intensive in antibodies with a high production cost and smooth in antibodies with low production cost. Each mutated clone must satisfy the constraints given by eqns. (2.10), (2.12), (2.13) and (2.14). [ref. chapter 2, sec. 2.2]

Step 5. The affinities of the mutated clones are evaluated.

Step 6. Aging operator eliminates those individuals which have more than τ_B generations from the current population. When an individual is $\tau_B + 1$ old it is erased from the current population, no matter what its fitness value may be.

Step 7. Tournament selection is done to select a new population of the same size as the initial from the antibodies and mutated clones which are remained after application of aging

operator. Each of the antibodies and mutated clones which are remained after the application of aging operator undergoes a series of N_t tournaments with randomly selected opponents. The score for each population after a stochastic competition is given by

$$S_{p_n} = \sum_{l=1}^{N_t} S_l$$

$$S_l = 1 \text{ if } F_{tp_n} \prec F_{tp_r}$$

$$= 0 \text{ otherwise} \qquad (3.28)$$

The competitor p_r is selected at random from among the antibodies and mutated clones. After competing the antibodies and mutated clones are ranked in descending order of the score obtained in eq. (3.28). The first N_P population is selected for the next generation.

Step 8. If the maximum number of generations is reached, output the optimal solution, i.e. the highest affinity value obtained so far and terminates the proposed algorithm. Otherwise, go back to **Step 3**.

3.4. Multi objective differential evolution (MODE) algorithm for MAEED problems

3.4.1. Principle of Multi-objective Optimization

Most of the practical problems involve concurrent optimization of numerous objective functions with non-commensurable, competing and conflicting objectives causing a rise to a set of optimal solutions, namely pareto-optimal solutions, instead of one optimal solution. No solution can be measured as better than any other in consideration of all objective functions together.

Mathematically, a multi-objective optimization problem several equality and inequality constraints can be expressed as below.

$$\text{Minimize } f_i(x) \quad i = 1,\ldots, N_{obj} \qquad (3.29)$$

$$\text{Subject to } \begin{cases} g_k(x) = 0 & k = 1,\ldots,\mathrm{K} \\ h_l(x) \le 0 & l = 1,\ldots,L \end{cases} \qquad (3.30)$$

where f_i is the i^{th} objective function, x is a decision vector.

3.4.2. Multi-objective Differential Evolution

Differential Evolution (DE) is a fast, simple and robust optimizer in continuous domain [230-232]. It adapts the search during the evolutionary process. In the early stage of evolution, the perturbations of the intermediate solutions are large since parent populations are far away from each other in the search space. At the matured stage of the evolutionary process, the population converges to a tiny area and the perturbations of the probable solutions adaptively become diminutive. Uniquely, in DE, the fittest of an offspring competes one-to-one with that of corresponding parent. This one-to-one competition cause earlier convergence. In multi-objective differential evolution (MODE), a pareto-based approach is introduced to employ the assortment of the best individuals.

3.4.3. Application of MODE in the problem

Initially, a randomly generated population of size N_P are used to evaluate objective functions. i.e. (2.21) and (2.23). Here population indicates different amount of power generation of thermal units. Subjected to the all constraints (2.25), (2.26) and (2.27). [ref. chapter 2, sec. 2.3]

At a specified iteration, non-domination based sorting and ranking of the population is performed. Non-dominated sorting procedure is described below.

Non-dominated sorting: To acquire solutions of the fast non-dominated front in a population of size N_P, each solution can be matched up to every other solution in the population to unearth if it is dominated. At this step, all individuals in the first non-dominated front are generated. In order to unearth the individuals in the next non-dominated front, the solutions of the first front are marked down for the time being and each solution of the residual population can be matched up to every other solution of the residual population to unearth if it is dominated. Thus all individuals in the second non-dominated front are generated. This is right for generating third and higher levels of non-domination.

After that, DE operations are carried out over the individuals. After iteration and evaluation of trial vectors of size N_P, these are combined with the parent vectors to form a population of size $2N_P$. Then, the ranking of the combined population and the crowding distance calculation are carried out.

Crowded distance estimation procedure: To acquire an estimation of the density of solutions contiguous a particular solution in the population, the average distance of two points on either side of this point along each of the objectives is computed. This quantity provides as an estimation of the perimeter of the cuboid structured by the nearest neighbors as the vertices. This is called crowding distance. The crowding-distance computation necessitates categorization of the population according to each objective function value in ascending order of magnitude. Thereafter, for each objective function, the boundary populations (populations with smallest and largest function values) are given very high distance value so that boundary points are always chosen. All other intermediate populations are given a distance value equal to the absolute normalized difference in the function values of two adjacent populations. This computation is kept on with other objective functions. The crowding-distance value is computed as the sum of individual distance values matching to each objective. Each objective function is normalized before computing the crowding distance.

Crowded-comparison operator: The crowded-comparison operator conducts the assortment procedure at a variety of stages of the algorithm toward a uniformly spread-out pareto-optimal front. Every individual i in the population has two features:

a) nondomination rank (i_{rank})

b) crowding distance $(i_{dis\,tance})$

$i \prec j$ if $i_{rank} < j_{rank}$ or $((i_{rank} = j_{rank})$ and $(i_{dis\,tance} > j_{dis\,tance}))$

Between two populations with differing non-domination ranks, the population with the lower (better) rank is favored. If both populations belong to the same front, then the population with larger crowding distance is favored.

Thus, top N_P individuals are selected based on its ranking and crowding distance. These individuals are the new parent vectors for the subsequent iteration.

Figure 3.3 portrays the flowchart of multi-objective differential evolution.

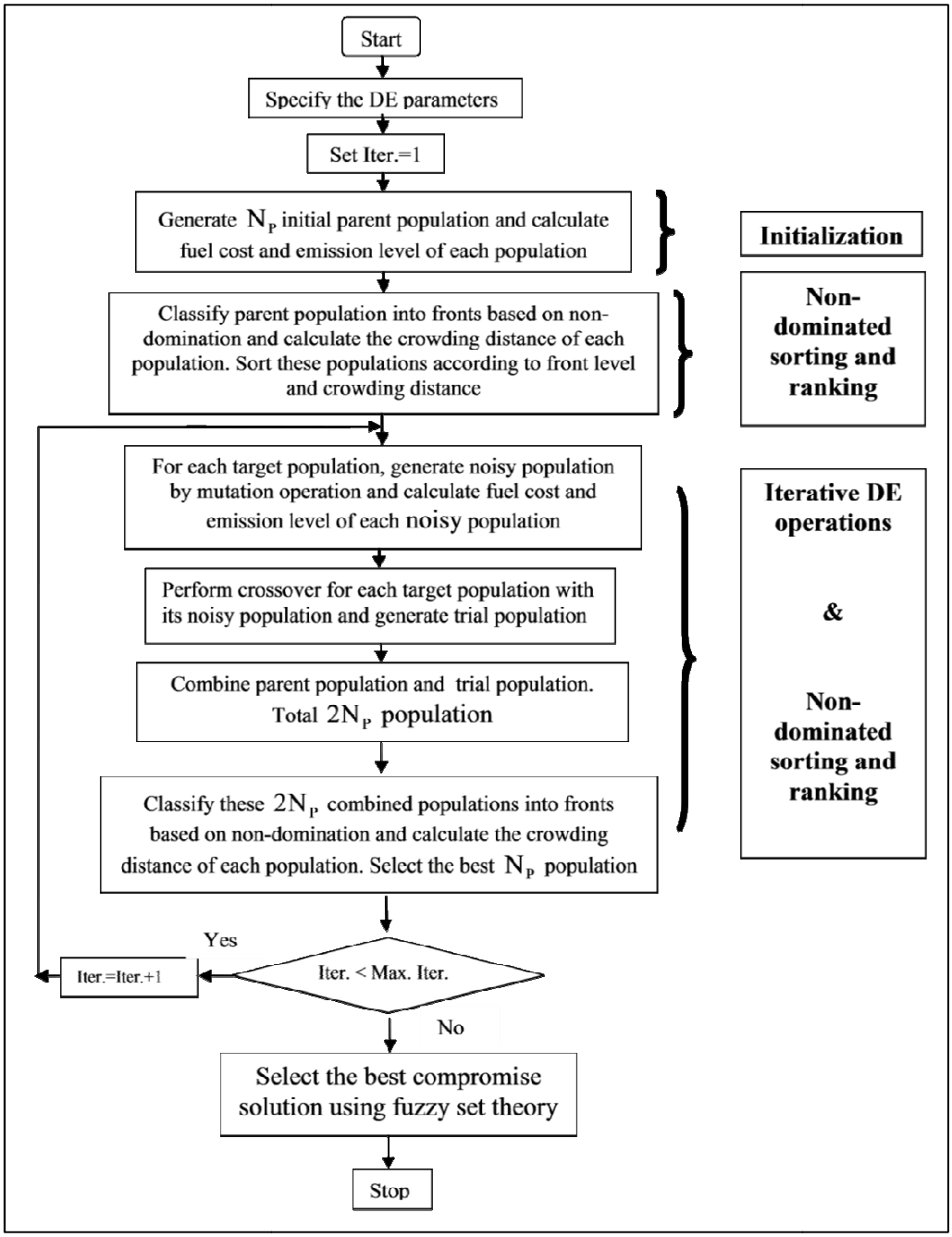

Figure 3.3. Flowchart of Multi-objective Differential Evolution

3.5. Non-dominated sorting genetic algorithm II (NSGA II) for WMAEED problems

To deal with a multiple objective and constrained incorporating optimizing task like the WMAEED, NSGA II has been taken for implementation. Selection of dominating solution has been determined here by fuzzy selection. The NDSGA II can be explained using the following calculation steps.

3.5.1. Dominance determination by fuzzy selection

Let, f_i is the i^{th} objective function, x is a decision vector that represents a solution, and N_{obj} is the number of objectives. Decision vector x_1 dominates decision vector x_2, if both the following conditions (3.31) and (3.32) are attained.

a. Sufficient condition: The decision vector x_1 is better than x_2 for all the objectives.

$$\forall\ i \in \{1,...,N_{obj}\},\ f_i(x_1) \leq f_i(x_2) \tag{3.31}$$

b. Necessary condition: The decision vector x_1 is strictly better than decision vector x_2 in at least one of the objective functions.

$$\exists\ i \in \{1,...,N_{obj}\},\ f_i(x_1) < f_i(x_2) \tag{3.32}$$

The optimum compromised solution gets preference among pareto-optimal solutions in agreement with the decision maker's fuzzy in nature precondition. So, in order to describe membership functions, decision maker's experiences and instinctive knowledge is used. The linear membership function ($\mu_i(x_j)$) for objective functions is as expressed in (3.33).

$$\mu_i(x_j) = \begin{cases} 1, & \text{if, } f_i(x_j) \leq f_i^{\min}(x_j) \\ \dfrac{f_i^{\max}(x_j) - f_i(x_j)}{f_i^{\max}(x_j) - f_i^{\min}(x_j)}, & \text{if, } f_i^{\min}(x_j) < f_i(x_j) < f_i^{\max}(x_j) \\ 1, & \text{if, } f_i(x_j) \geq f_i^{\max}(x_j) \end{cases} \tag{3.33}$$

where, pareto optimal solution set is $X = \{x_1, x_2, ..., x_k\}$, $x_i \in X$ and $i = 1,2,...,k$. $f_i^{\min}(x_j)$ and $f_i^{\max}(x_j)$ represents to the minima and the maxima of the i^{th} objective function with j^{th} pareto optimal solution respectively.

3.5.2. Calculation steps of NSGA II application

Step 1. Initialization: At the beginning, an arbitrary parent population (P_{Gij} , P_{Wik}) with N_1 members is generated [ref. chapter 2, sec. 2.4]. This N_1 number of (P_{Gij} , P_{Wik}) variables are referred hereafter as PA_{POP} .

Step 2. Fast nondominated PA_{POP} sorting: The sorting takes place in accordance with the non domination. Different ranks correspondent of their level of nondominance / front numbers (best level by '1', corresponds to the subsequent best level by '2',and so on)are credited to each of the populations.

Step 3. Selection by tournament: Two of the individuals are selected in an arbitrary manner. A comparison is made between their front numbers as well as for crowding separation and superior one gets selected. After this, it is ready for the mating pool.

Step 4. Crossover and successive mutation: In this work, simulated binary crossover (SIBNCO), and polynomial type mutation [127] have been considered. A child population CH_{POP} with same members as that of PA_{POP} is generated.

Step 5. Merging: The aforementioned PA_{POP} and CH_{POP} are merged to form a resultant population $RES_{POP} = PA_{POP} \cup CH_{POP}$ with twice the members of both PA_{POP} as well as CH_{POP} i.e. $2N_1$.

Step 6. Fast nondominance based RES_{POP} sorting: The RES_{POP} gets sorted in accordance with nondominance. Due to the involvement of each of the members of the PA_{POP} as well as the CH_{POP} , elitism is assured. After that, the populations corresponding to the best nondominated set ND_{B1} include best populations from the RES_{POP} by emphasizing more on these than any other population in the RES_{POP} . With the assumption that the size of the ND_{B1} is lesser than the N_1, each of the members corresponding to the ND_{B1} gets selected in order to generate a new community. Other members corresponding to it get selected from succeeding fronts based on the nondominance according to ranking assigned to them.

Hence, the succeeding selection is made for solutions from the ND_{B2} grouping which is further succeeded by population members from the ND_{B3} grouping and the process continues. The process continues till the selection of all the possible groupings. The grouping ND_{Bl} represents the selection of final one based on nondominance. Normally, the number of solutions including all the aforementioned groupings ND_{B1}, ND_{B2},…, ND_{Bl} remains larger than N_1. For having absolutely N_1 solutions, population members from the final ND_{Bl} front are sorted with the $(\prec)$ operator in the decreasing order. Best population members get selected for filling of each of the population spots.

A new population $PA_{POP'}$ with N_1 members forms. Now, the tournament selection, crossover as well as mutation take place with the newly formed $PA_{POP'}$. Then, a new child population $CH_{POP'}$ is formed with N_1 members.

Step 7. Terminating criterion: The procedure terminates after execution of definite generations. Now, the terminating criterion is evaluated. In case, the criterion fulfils, the control shifts to the **Step 8** otherwise $PA_{POP'}$ gets copied to PA_{POP}. After copying, the similar procedure is repeated from **Step 3**.

Step 8. Final selection: The first solution that is the population member corresponding to the first front gets selected.

Step 9. Termination: The procedure gets terminated.

An expressional explanation related to the NSGA II has been mentioned next.

$RES_{POP} = PA_{POP} \cup CH_{POP}$ (Merging of the PA_{POP} and the CH_{POP})

- F_S denotes fast nondominance based sorting(RES_{POP}).

$F_S = (ND_{B1}, ND_{B2}, ..., ND_{Bl})$

Where ND_{Bi} denotes a nondominance based front corresponding to the RES_{POP}.

$PA_{POP'} = \phi$, &

$p = 1$

Until $|PA_{POP}| + |FN_p| \leq N_1$ (i.e. the PA_{POP} fills)

- **Assigning of** p_{dist} $\left(FN_p\right)$**:**

$PA_{POP'} = PA_{POP'} \cup FN_p$ (Inclusion of p^{th} nondominance based front in the PA_{POP})

$p = p + 1$ (Checking of the succeeding front in order to include)

- **Sorting** $\left(FN_p, \prec\right)$**:**

$\prec$ is utilized for sorting in a decreasing order.

$PA_{POP'} = PA_{POP'} \cup FN_p\left[1 : \left(N_1 - \left|PA_{POP'}\right|\right)\right]$

Selecting the starting $\left(N_1 - \left|PA_{POP'}\right|\right)$ elements corresponding to FN_p

$CH_{POP'}$ = Generation of child population corresponding to the $PA_{POP'}$

3.6. Improved real coded genetic algorithm (IRCGA) for short term hydro-thermal scheduling

The Genetic Algorithm (GA) is pioneered by John Holland [126]. A random initial population is created corresponding to candidate results. The ability to attain the universal or close to the universal optimized results corresponding to each new community is assessed by its fitness value. After getting selected for propagation, parents produce offspring through the crossover and mutation procedures. The generated individuals during propagation operate in differential regions of the exploring freedom. Tasks involving continuous exploration of large space are dealt with real coded genetic algorithm (RCGA) because of the difficulties corresponding to the binary form presentation [127-128]. Simulated binary crossover (SBC) along with the multinomial mutation has been adopted in this concise.

To implement IRCGA, personal basis matching challenge has been incorporated in RCGA for boosting convergence speed as well as solution quality.

Here, a child copes with the matching parent on individual basis. Initialization, selection of parent community, crossover, mutation, and selection between parent and offspring are the five levels of IRCGA. The fittest offspring competes on one-to-one basis with the corresponding parent to boost the convergence speed and solution quality, which is different from the other evolutionary algorithms. This powerful optimization technique is analogous to the natural selection process in genetics. It has the capability to converge to a global optimum with the maximum probability with relatively less computational time.

3.6.1. Population initialization

In this optimization problem, the decision vector is P_s , the thermal power generation amount, and there is a dependent vector P_h {in eqn. (2.49)}, the hydro-electric power generation amount. The objective function (F_c) is calculated according to (48) [ref. chapter 2, sec. 2.5]. This decision variable $P_{s,ti}$ is indicated hereafter as (p_{qr}).

The initial population (p_{qr}^0) corresponding to control variables gets selected arbitrarily from a uniform grouping of these variables ranging over the corresponding upper and lower limiting values. Population size is chosen as a function of the string span. This can be expressed in accordance to (3.34).

$$p_{qr}^0 \approx UNF(p_r^{mn}, p_r^{mx}), \forall q \in N_{pq}, r \in n_{dv} \tag{3.34}$$

Here, p_{qr}^0 is the initial population corresponding to r^{th} variable of the q^{th} community. UNF(p_r^{mn} , p_r^{mx}) is an random variable ranging over(p_r^{mn} , p_r^{mx}) in an uniform manner. p_r^{mn} and p_r^{mx} represents the minimum and the maximum limiting values corresponding to the r^{th} variable respectively. N_{pq} is population size. n_{dy} represents total number of decision variables corresponding to an individual.

3.6.2. Parent population selection

The selection method of GA is the process to determine the number of copies of each individual parent that can take part in the reproduction or mating pool. There are different processes to implement the selection method. Those are roulette wheel selection [108], tournament selection [233] and stochastic remainder selection [234]. The binary tournament selection method is utilized for choosing parents for mating pool. Two chromosomes are selected randomly from the population. The chromosome with lower objective function, f_i i.e. the winner one is set aside in the mating pool. This process is repetitive till the pool gets filled by the chromosomes.

3.6.3. Simulated binary crossover (SBC)

The main responsibility of crossover operator is to search for the global optimum. This operator basically combines the substructures of two parent chromosomes to produce new offspring, with a selected probability. SBC operator has been discussed in the following part of the concise.

a. Selection of an arbitrary number ar between [0,1].

b. Computation of a parameter γ with the help of a multinomial type probability allocation as in (3.35).

$$\gamma = (ar.\sigma)^{1/(\eta_v+1)} \quad \text{in case} \quad ar \le 1/\sigma$$
$$= (1/(2 - ar.\sigma))^{1/(\eta_v+1)}, \text{otherwise} \tag{3.35}$$

$$\sigma = 2 - \frac{1}{B^{(\eta_v+1)}} \tag{3.36}$$

$$B = 1 + \frac{2}{(p_{q2} - p_{q1})} mn\left[(p_{q1} - p_q^{mn}), (p_q^{mx} - p_{q2})\right] \tag{3.37}$$

Here, μ_v represents allocation index corresponding to the SBC. Any positive value can be assigned to it. Generation of a descendant community depends on the value assigned to the η_v. The generated offspring would be very far or at closed quarters from the parent people corresponding to a smaller or larger value of the η_v. The calculation of intermediary communities takes place in accordance to (3.38) as well as (3.39).

$$p_{qp1} = 2^{-1}\left[(p_{q1} + p_{q2}) - \gamma(\left|p_{q2} - p_{q1}\right|)\right] \tag{3.38}$$

$$p_{qp2} = 2^{-1}\left[(p_{q1} + p_{q2}) + \gamma(\left|p_{q2} - p_{q1}\right|)\right] \tag{3.39}$$

3.6.4. Multinomial mutation operation

The multinomial probability distribution is utilized to produce an offspring nearby the parent population by using an operator corresponding to the mutation. This can be stated as next.

a. Selection of an arbitrary number *ar′ between* [0, 1].

b. Calculation of parameter α as (3.40).

$$\alpha = \left[2.ar' + (1 - 2.ar').(1 - \phi)^{(\eta_m+1)}\right]^{\frac{1}{(\eta_m+1)}} - 1, \text{ in case } ar' \le 2^{-1}$$
$$= 1 - \left[2.(1 - ar') + 2.(ar' - 2^{-1}).(1 - \phi)^{(\eta_m+1)}\right]^{\frac{1}{(\eta_m+1)}}, \text{ otherwise} \tag{3.40}$$

$$\text{Where, } \phi = \frac{mn\left[(p_{qp} - p_q^{mn}).(p_q^{mx} - p_{qp})\right]}{(p_q^{mx} - p_q^{mn})} \tag{3.41}$$

Parameter η_m is in equation (3.44) represents the allocation index corresponding to the mutation. Any positive value can be considered.

c. Empirical expressions associated with the mutated offspring can be expressed as (3.42) and (3.43) respectively.

$$p'_{q1} = p_{qp1} + \alpha.(p_q^{mx} - p_q^{mn}) \tag{3.42}$$

$$p'_{q2} = p_{qp2} + \alpha.(p_q^{mx} - p_q^{mn}) \tag{3.43}$$

The perturbation can be altered by varying the η_m and pr_{mt} with iterations as equation (3.44) and (3.45).

$$\eta_m = \eta_{m,mn} + iter \tag{3.44}$$

$$pr_{mt} = \frac{1}{\eta_{ch}} + \frac{iter}{iter_{mx}}(1 - \frac{1}{\eta_{ch}}) \tag{3.45}$$

Where, $\eta_{m,mn}$ represents the lowest value which is equivalent to the η_m. pr_{mt} and n_{ch} indicate the mutation stochastic value and total selection variables respectively. The objective function (F_c) in eqn. (2.49) is treated here as f_i. The f_i corresponding to each offspring is computed.

3.6.5. Selection between a parent and an offspring

The value of f_i of each parent $p_{qr}$is compared with that of matching offspring p_{qr}'. The population that has lower f_i between $p_{qr}$and matching p_{qr}' gets selected in order to operate in the following iteration as in equation (3.46).

$p_{qr} = p'_{qr}$, in case $f(p'_{qr}) \leq f(p_{qr})$

$= p_{qr}$, otherwise (3.46)

An IRCGA typically searches for the optimal solution by maximizing or minimizing a given fitness function. Therefore an estimation function which evaluates the quality of the problem solution must be provided. This procedure is replicated till the maximum iteration is reached. The algorithmic flow of IRCGA is depicted in Fig. 3.4.

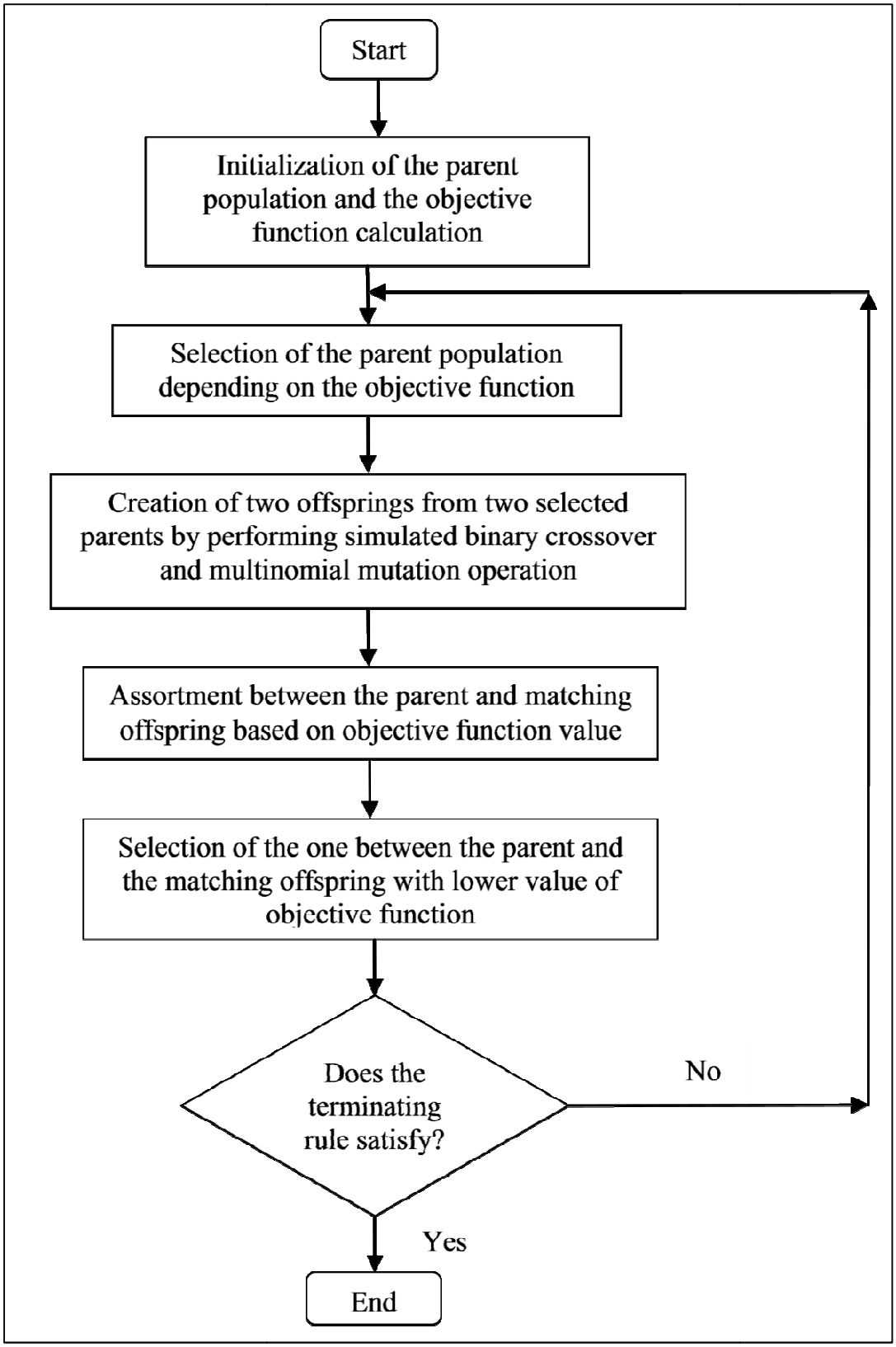

Figure 3.4. Flowchart of the improved real coded genetic algorithm.

3.7. Water cycle algorithm (WCA) for optimal DG allocation problem

3.7.1. Water cycle algorithm

This algorithm has been proposed by Hadi Eskander et al. and is based on the water cycle which takes place in nature. Water moving downwards forms streams, then goes to river and finally flows into sea. Water from the streams and rivers evaporates and forms clouds, then, it rains, hence the cycle continues.

Initial population: Like other meta heuristic algorithms, this also starts with an initial population. Here, population is taken that of raindrops. Then the cost of raindrop is evaluated as follows

$$C_i = Cost_i = f(x_1^i, x_2^i ....., x_{N_{\text{var}}}^i) \quad i = 1,..,N_{pop} \tag{3.47}$$

Where, 'N_{pop}' and 'N_{vars}' are number of raindrops and number of design variables respectively.

The raindrop having the minimum value is considered as the sea. Few of the minimum values are selected as number of rivers. Then 'N_{sr}' is given as follows:

N_{sr} = Number of rivers + 1 (3.48)

The above '1' signifies sea i.e. the minimum value and 'N_{sr}' is the raindrops with minimum values.

Rest of the population is calculated as

$$N_{raindrops} = N_{pop} - N_{sr} \tag{3.49}$$

Whether to assign a raindrop to a river or to a sea depends on the intensity of the flow and is given by:

$$NS_n = round\left\{\left|\frac{Cost_n}{\sum_{i=1}^{N_{sr}} Cost_i}\right| \times N_{raindrops}\right\}, \text{ n=1,…, } N_{sr} \tag{3.50}$$

'N_{sn}' is the number of streams which flow to the specific river or sea.

Stream flowing to river or sea: Raindrops forming streams or streams flowing to rivers are given as follows

$$X_{stream}^{i+1} = X_{stream}^i + rand \times C \times \left(X_{river}^i - X_{stream}^i\right) \tag{3.51}$$

$$X_{river}^{i+1} = X_{river}^{i} + rand \times C \times \left(X_{sea}^{i} - X_{river}^{i} \right) \quad (3.52)$$

Where, 'X_{stream}', 'X_{river}' and 'X_{sea}' represent positions of stream, river and sea respectively. 'rand' is a uniformly distributed random number between 'zero' and 'one'. 'C' has a value between 'one' and 'two'. Now, the positions of stream and river, or those of river and sea, are exchanged depending upon whichever has a better solution.

Evaporation: This is done to prevent the algorithm from rapidly converging. The distance between a river and a sea is checked if it is less than a given a small number 'd_{max}' (having value close to 'zero'). If it is found to be less then, it is assumed that the river has joined the sea. Then the evaporation process takes place. As in nature, raining (precipitation) follows evaporation. The value of 'd_{max}' decreases over the iterations as:

$$d_{\max}^{i+1} = d_{\max}^{i} + \frac{d_{\max}^{i}}{\max\_iteration} \quad (3.53)$$

Where, 'max_iteration' represents the total number of iterations.

Raining process: In this process, new raindrops form streams at new locations. And the whole algorithm repeats all over again. The best raindrop is considered the river which flows to the stream. Also the concept of variance in the form of 'μ' is used to enhance the searching process. Larger value of 'μ' increases the possibility to exit from feasible region, whereas, smaller value leads to searching in the region close to the optimum value.

3.7.2. Computational steps

In this case, the aim is to minimized the real power loss (P_L) and the objective function is according to (2.65). The decision vector is (P_i, Q_i) [ref. chapter 2, sec. 2.6].

Step 1. The initial parameters of WCA are chosen as N_{sr}, d_{max}, N_{pop} and max_iteration.

Step 2. Random initial population is generated. Here, population consists of the values the single DG unit which injects only P and five values of the VAR. Also the bus number at which these are placed is taken into account. That is the sizing and placement both accounted for. Initial streams (raindrops), rivers and seas are formed using (2.65) and (3.47).

Step 3. The cost of each raindrop is calculated. In this case, the cost function is the power loss for that particular set of values of DG and VAR which are placed at those specific buses.

Step 4. The intensity of flow of rivers and streams is calculated using (3.48).

Step 5. The streams flow to the rivers using (3.49), whereas river flows to the sea using (3.50).

Step 6. The position of a river with a stream as well as the position of a sea with a sea are exchanged depending on whichever has a better solution.

Step 7. The evaporation condition where the distance between river and sea is compared with 'd_{max}' (which has a value close to 'zero'). If the value is found to be less then, raining process begins.

Step 8. The value of 'd_{max}' gets reduced after each iteration as per (3.51).

Step 9. The stopping criteria is evaluated, which in this case, is the maximum number of iterations. If it is satisfied then the algorithm is stopped otherwise process gets repeated from '**step 5**'.

3.8. Social Spider Optimization (SSO) for Optimal power operation planning in a township

Social spider optimization is a newly advanced swarm categorized algorithmic technique by Eric Cuevas and Miguel Cienfuegos. In this technique, spider individuals (i.e. exploring representatives) perform interactive activity with each other depending on the cooperative colony's biological norms. The technique also incorporates gender consideration of the representatives. Communal web corresponding to these representatives is considered as the space for exploring. Each of the representatives' position indicates a solution within the exploration space.

3.8.1. Computational procedure applying SSO

For this optimization problem the objective function is according to (2.68) along with different constraints [ref. chapter 2, sec. 2.7]. It is represented hereafter as $(O_B(x))$. The decision vectors P_{FC} , P_{BM} $P_{BT}$and P_{SO} of eqn. (2.69) and (2.70) generate the Population (PO) of spiders' in eqn (3.54). Computational procedure for obtaining solution through this technique is as mentioned below:

Representatives' selection: Population (PO) of spiders' or exploring representatives' each having p-dimensions is selected. In the P, female representatives (PO_F) remain between 0.65-0.90 times (i.e. 65-90 %) of the PO in accordance to (3.54).

$$PO_F = floor \ \{(0.90 - rand.(0.25)).PO\} \tag{3.54}$$

Where, 'floor' keeps the integer part of a real valued population. '*rand*' is utilized for random number generation between 'zero' and 'one'. Male representatives (PO_M) are the complement of *PO* and PO_F in accordance to (3.55).

$$PO_M = \{PO - PO_F\} \tag{3.55}$$

Representatives' population initialization: The PO_F alongside PO_M gets initialized, and radius of mating (R_M) is calculated.

$$PO_{F_{q,r}}^{initl} = \{PO_r^{lowr} + rand\ (0,1).(PO_r^{uppr} - PO_r^{lowr})\} \text{ with } q = 1,2,3,4,...,PO_F \text{ , and } r = 1,2,3,4,...,DS \tag{3.56}$$

Where $PO_{F_{q,r}}^{initl}$ in (3.56) indicates an arbitrary beginning position of the q^{th} female representative in the PO_F considering the DS indices. PO_r^{lowr} indicates known lower beginning element limit. PO_r^{uppr} denotes known upper beginning element limit.

$$PO_{M_{s,r}}^{initl} = \{PO_r^{lowr} + rand\ (0,1).(PO_r^{uppr} - PO_r^{lowr})\}$$

$$\text{with } s = 1,2,3,4,...,PO_M \text{ , and } r = 1,2,3,4,...,DS \tag{3.57}$$

Where $PO_{M_{s,r}}^{initl}$ represents a randomized beginning position of the s^{th} male representative corresponding to the r^{th} DS index. Mating radius (R_M) is determined in accordance to (3.58).

$$R_M = \left\{ \frac{\sum_{r=1}^{DS} \left(PO_r^{uppr} - PO_r^{lowr} \right)}{(2.DS)} \right\} \tag{3.58}$$

Substituted function significance: A proper substituted function is utilized to attain global optimized solution in place of the objective function. The substituted function $(S_B(x))$ can be obtained by adding a penalty function $(F_N(x))$ to the objective function $(O_B(x))$ in accordance to (). A term is introduced in the penalty function for constraints' checking. This checking evaluates whether the constraints are in limits or not. Each of the representatives, involves in exploration, possesses a definite weight which determines its solution quality.

$$S_B(x) = \{O_B(x) + F_N(x)\} \text{with } F_N(x) = \left\{ J. \sum_{pr'=1}^{v} I_{pr'}^2(x) + J^{'}. \sum_{pr''=v+1}^{o'} I_{pr''}^2(x) \right\} \quad (3.59)$$

Where J and $J^{'}$ indicate the coefficients of penalty. A relative manner importance of each bounding is indicated by these coefficients. In order to decide their values, their importance with respect to each other is taken into consideration. $I_{pr'}(x)$ and $I_{pr''}(x)$ represent the inequality and equality constraints in the sequential manner. In some scenarios, $F_N(x)$ is not required depending on the problem and the constraints incorporated.

Solution quality determination: Every exploring personal carries a certain weight. This weighing amount indicates the quality of solution provided by it (i.e. personal performance capability). An expressional representation corresponding to exploring personal $pr^{'}s$ weight involves (3.60).

$$WE_{pr} = \left\{ \frac{WRS_{pr} - S_B(PS_{pr})}{WRS_{pr} - BS_{pr}} \right\} \quad (3.60)$$

with, $WRS_{pr} = \left\{ \underset{pr=1,2,3,4,...,PS}{MAXM} S_B(PS_{pr}) \right\}$, and

$BS_{pr} = \left\{ \underset{pr=1,2,3,4,...,PS}{MINM} S_B(PS_{pr}) \right\}$

Where, the WRS_{pr} indicates the maximum value of the $S_B(.)$ in terms of representative location. The $S_B(PS_{pr})$ denotes the fitness value of the position PS_{pr} for the personal pr. The BS_{pr} indicates the minimum $S_B(.)$ value in terms of a representative location. The WRS_{pr} and the BS_{pr} are defined in accordance to the objective goal.

Vibrational communication: In the communal exploring space, an information exchange among personnel happens via vibrations. The exchange depends on personal weight along with positional arrangement of personnel. The vibrational amount between the personnel locating nearer in the exploring space remains more in comparison to that of far locating personnel. Normally, three types of vibration are significant in the web (i.e. exploring space).

VB_{nm} : It corresponds to the one on representative 'm' by the 'n' having greater weight in comparison to the 'm', and sharing closest positional arrangement with it. Its expressional representation is in accordance to (3.61).

$$VB_{n\,m} = \left\{ WE_n . e^{-ed^2_{m,n}} \right\} \tag{3.61}$$

Where $ed^2_{m,n}$ indicates a Euclidian stretch between the personnel 'm' and 'n', and can be expressed as $\left\| PS_m - PS_n \right\|$.

$VB_{o\,m}$: It represents the one on representative 'm' due to 'o', the heaviest one in the exploring space. Its expressional view involves (3.62).

$$VB_{o\,m} = \left\{ WE_o . e^{-ed^2_{m,o}} \right\} \tag{3.62}$$

VB_{p_m}: The one representing the vibrational amount on 'm' due to 'c', the closest female personal to it in the exploring space. In expressional form:

$$VB_{c\,m} = \left\{ WE_c . e^{-ed^2_{m,c}} \right\} \tag{3.63}$$

Female representative cooperation: The PO_F shows either attracting or repelling behavior towards the remnant personnel without taking their gender into consideration. Vibrations impart driving for this behavior. An operator remains engaged with female cooperation to predict the cooperative behavior of the PO_F. For the prediction purpose, location changes are taken into consideration after the execution of each iteration. Modeling of this operator happens in accordance to (3.64).

$$PO_F^{iter+1} = \left\{ PO_F^{iter} + G.VB_{X_F} . \left(PO_X - PO_F^{iter} \right) + H.VB_{Y_F} . \left(PO_Y - PO_F^{iter} \right) + K. \left(rand - 0.50 \right) \right\} \tag{3.64}$$

Where PO_F^{iter+1} indicates the position of representative F during the $(iter+1)^{th}$ iteration. G, H, K along with *rand* represent randomized numbers between 'zero' and 'one'. PO_X indicates the positional arrangement of personal X having more weight than the F while PO_Y corresponds to the Y having the highest weight in the exploring space.

Male representatives and their cooperation behavior: The PO_M can be categorized as dominant ($PO_{M,D}$) and nondominant ($PO_{M,ND}$) by assigning one of the personnel as the median (MDN). The $PO_{M,D}$s possess greater weight than that of the MDN, and the $PO_{M,ND}$ s incorporate lesser weight than the MDN. An operator predicts the subsequent behavior of the PO_M personnel as mentioned next.

The $PO_{M,D}$ personnel show attractiveness towards the PO_F, and involve in mating. The $PO_{M,ND}$ personnel perform an approaching movement towards the PO_M's weighted manner averaging in the exploring space. Expressional representation of these personnel's movement involves (3.65).

$$PO_M^{iter+1} = \left\{PO_M^{iter} + G.VB_{C_M}.\left(PO_C - PO_M^{iter}\right) + H.(rand - 0.50)\right\}, \text{ in case } WE_{PO_F+M} > WE_{MDN}$$

$$= \left\{ PO_M^{iter} + G.\left(\frac{\sum_{q=1}^{PO_M} PO_q^{iter}.WE_{PO_F+q}}{\sum_{q=1}^{PO_M} WE_{PO_F+q}} - PO_M^{iter} \right) \right\}, \text{ in case } WE_{PO_F+M} \le WE_{MDN} \quad (3.65)$$

Where PO_M^{iter+1} indicates the position of representative M during execution of the iteration $iter+1$. PO_C tells about the position of the closest female personal in the space to be explored. The term $\left(\frac{\sum_{q=1}^{PO_M} PO_q^{iter}.WE_{PO_F+q}}{\sum_{q=1}^{PO_M} WE_{PO_F+q}} \right)$ in (3.65) represents the weighted manner averaging value of the PO_M.

Mating: This happens between PO_{M_e} male representatives $\left(e \in PO_{M,D}\right)$, and PO_{F_e} having positional arrangement inside the R_M. It assures about the seamless communal survival. The PO_{F_e} mentioned above represents a grouping of female searchers. Representative BD corresponding to the subsequent generation is the each searcher corresponding to the $PO_e = PO_{M_e} \bigcup PO_{F_e}$. In a scenario, when no PO_{F_e} exists in the R_M then, the mating remains absent. The affecting probabilistic value ($PRVA_a$) considering every searcher a is determined through Roulette method, and formulates the BD in accordance with (3.66).

$$PRVA_a = \{ WE_a \Big/ \sum_{a \in PO_e} WE_a \} \quad (3.66)$$

Where a indicates the $PO_{M,D}$ taking part in the mating phenomenon with the PO_{F_e}. Here, the BD gets compared with the $WRS_{WE_{pr}}$ in the exploring space. Then, the searcher with a smaller $F_N(x)$ value proceeds further after its selection. Considering the scenario, where each searcher is having the similar $F_N(x)$ value then, the preference is given to heavier

representative. In a scenario, where the BD gets prioritized, it acquires index as well as the gender of the $WRS_{WE_{pr}}$. Thus, desired proportion of the PO_F and the PO_M sustains.

Ending norm check: Moving towards the final activity, an evaluation of ending norm is made. In its successful bringing to fruition, the computation process ends. An unsuccessful bringing to fruition of the criterion, transfers control to searcher weighing computation step. Now, rerunning of the similar procedure takes place until the ending norm brings to fruition.

A schematic concerning sequential manner execution for the technique is in accordance to Fig. 3.5.

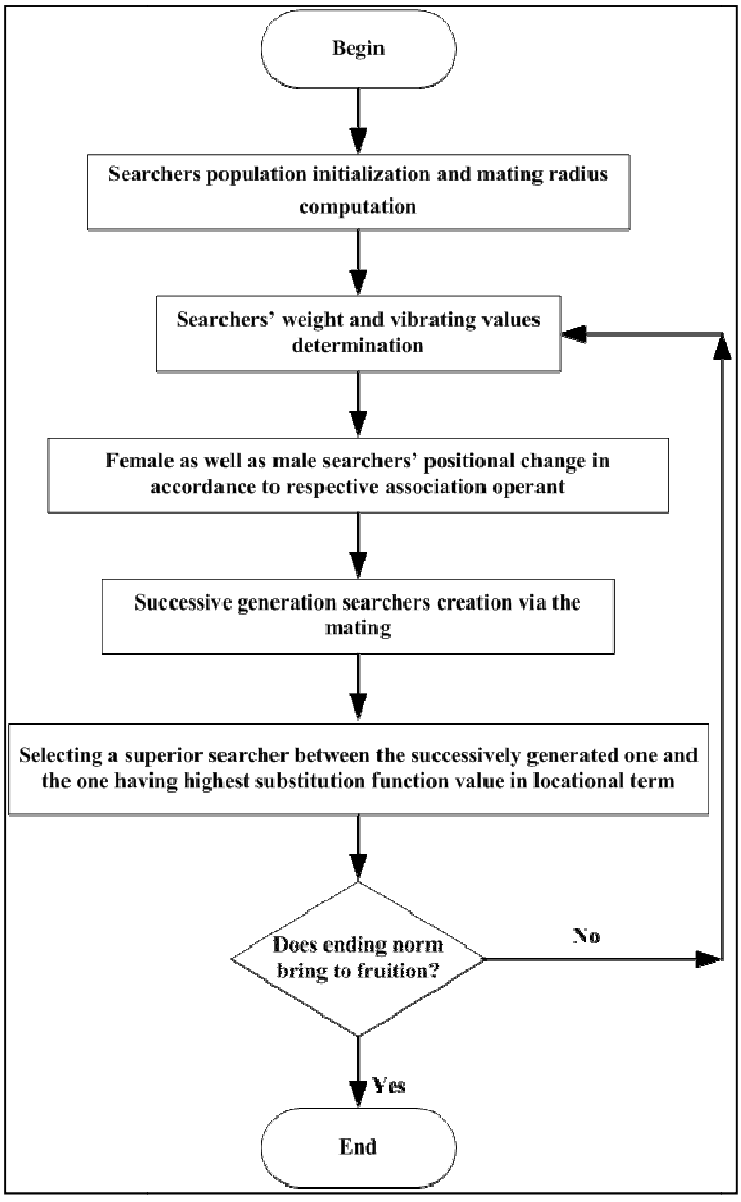

Figure 3.5. Computing steps for the social spider optimization

3.9. Gravitational search algorithm (GSA) for Optimal power operation planning in a rail-way rake maintenance depot

3.9.1 Implementation of GSA

This search algorithm (GSA) has been utilized to solve the optimization problem as stated in chapter 2, sec. 2.8. The implementation logic of this algorithm is described in following steps.

Step 1. Setting all the boundary values.

Step 2. Randomized initialization of all agents within limits (P_{bm}, P_{fc}, P_{bt}, P_{so}), with number of population equal to *N*. [ref. chapter 2, sec. 2.8].

Step3. Fitness evaluation of agents using the objective functions considering all constraints (**eqn**. 2.82-2.106, as appropriate for specific cases).

Step 4. Updating of *G(t), best(t), worst(t)* and *Mi(t)* for *i = 1,2,. . .,N*.

Step 5. Calculation of the total force in different directions.

Step 6. Calculation of acceleration and velocity.

Step 7. Updating the position of agents.

Step 8. Checking of space boundary, whether the agents have gone beyond the limits or have caused violation of the constraints.

Step 9. if **h** is true, set the relevant agent/s to limit values or reinitialize them/it.

Step 10. Repeat steps **c** to **i** until the stop criteria is reached.

Step 11. End.

3.9.2. Details of calculations in GSA

Let the decision vector (P_{bm}, P_{fc}, P_{bt}, P_{so}) be indicated as agent *X*. Then, considering a system with *N* agents the position of the i^{th} agent is defined by

$$X_i = \left(x_i^1, \ldots . x_i^d, \ldots . x_i^n\right) \text{ for } i \in (1, \ldots, N) \tag{3.67}$$

x_i^d is the position of i^{th} agent in the d^{th} dimension. At a specific time *t*, the force acting on mass of '*i*' from mass of '*j*' as following

$$F_{ij}^d(t) = G(t).\frac{M_{pi}(t).M_{aj}(t)}{\left(R_{ij}(t)+\varepsilon\right)^{Rpow}}.(x_j^d(t) - x_i^d(t)) \tag{3.68}$$

where M_{aj} is the active gravitational mass related to agent *j*, M_{pi} is the passive gravitational mass related to agent *i*, $G(t)$ is gravitational constant at time t, e is a small constant, and $R_{ij}(t)$ is the Euclidian distance between two agents *i* and *j*, and *Rpow* is a parameter. Which can be taken as (203) or (204).

$$R_{ij}(t) = \left\| X_i(t), X_j(t) \right\|_2 . \tag{3.69}$$

The gravitational constant *G*, is a function of the initial value G_0 and time *t*

$$G(t) = G_0 . \exp(-\alpha . \frac{t}{T}) \tag{3.70}$$

Here α is a tuning parameter which is set to be 20 and G_0 is initialized by 100.

Gravitational and inertia masses are simply calculated by the fitness evaluation. Assuming the equality of the gravitational and inertia mass, the following equations come.

$$M_{ai} = M_{pi} = M_{ai} = M_i \ , \ i \in (1,....,N) \tag{3.71}$$

$$m_i(t) = \frac{fit_i(t) - worst(t)}{best(t) - worst(t)} \tag{3.72}$$

$$M_i(t) = \frac{m_i(t)}{\sum_{j=1}^{N} m_j(t)} \tag{3.73}$$

Where $fit_i(t)$ represent the fitness value of the agent *i* at time *t*.

$$best(t) = \min_{j \in (1,...,N)} (fit_j(t)) \tag{3.74}$$

$$worst(t) = \max_{j \in (1,...,N)} (fit_j(t)) \tag{3.75}$$

A stochastic nature is introduced here assuming the total force acts on agent *i* in a dimension *d* be a randomly weighted sum of d^{th} components of the forces exerted from other agents.

$$F_i^d(t) = \sum_{j=1, j \neq i}^{N} rand_j . F_{ij}^d(t) \tag{3.76}$$

Or it can be taken as

$$F_i^d(t) = \sum_{j \in k_{best}, j \neq i} rand_j . F_{ij}^d(t) \tag{3.77}$$

Hence the acceleration of the agent *i* at time *t* and in d^{th} direction, $a_i^d(t)$ is given as follows

$$a_i^d(t) = \frac{F_i^d(t)}{M_{ii}(t)} \tag{3.78}$$

Where M_{ii} is the inertial mass of i^{th} agent. Its position and velocity are calculated as follows.

$$v_i^d(t+1) = rand_i.v_i^d(t) + a_i^d(t) \tag{3.79}$$

$$x_i^d(t+1) = x_i^d(t) + v_i^d(t+1) \tag{3.80}$$

3.10. Improved real coded genetic algorithm (IRCGA) for optimal power operation of PV aided nano-grid

Goals concerning continuous large sized exploring space are transacted with real coded genetic algorithmic procedure (RCGA) considering the difficulties associated with their binary form representation. Simulated binary manner crossover (SIBICR) along with the multinomial type mutation has been introduced in this methodology.

For implementation of the IRCGA, personal level matching challenge has been introduced in the RCGA to give a boost to convergence speed as well as solution quality. A descendant member copes up with the corresponding ancestor member on personal level. Initialization, ancestor members' community selection, crossover, mutation, and selection between ancestor and descendant members formulate different computing steps of the IRCGA.

In this optimization problem, the objective is to minimize (R_{anu}) of eqn (2.107).[ref. chapter 2, sec. 2.9]. The decision vector $P_{batt}(t)$ and $P_{phv}(t)$ forms The early community $\left(\overset{0}{p}_{bc}\right)$ of control variables hereafter. A brief discussion of each of the computing steps is mentioned herein.

3.10.1. Computational details

Initialization: The early community $\left(\overset{0}{p}_{bc}\right)$ of control variables is formulated through an arbitrary fashion selection from a uniform grouping of these variables within the lower and upper limiting values and can be expressed as

$$\left(\overset{0}{p}_{bc}\right) \sim UNF\left(p_c^{mn}, p_c^{mx}\right), \forall b \in N_{ab}, c \in n_{devb} \tag{3.81}$$

where n_{devb} indicates the total number of personal decision variables. N_{ab} represents community dimensions. The $\left({}^{0}p_{bc} \right)$ indicates the starting c^{th} variable of the b^{th} community while p_c^{mn} and p_c^{mx} indicate the minimum and the paramount limiting values corresponding to c. $UNF\left(p_c^{mn}, p_c^{mx}\right)$ represents the uniform manner range of an arbitrary variable over $\left(p_c^{mn}, p_c^{mx}\right)$. The objective function value fn_i (that corresponds to the i^{th} community) corresponding to each community is computed.

Ancestor member community selection: The binary tournament selection methodology has been utilized to choose ancestor members for mating pool. A chromosome duo is haphazardly selected from the community. Afterwards, a comparative analysis is made corresponding to their objective function values. The one with lower fn_i i.e. the winner one is set aside in the pool. This process continues until the pool gets completely filled by the chromosomes.

Simulated binary manner crossover (SIBICR): Methodology to find descendants p'_{b1} and p'_{b2} from two ancestors p_{b1} and p_{b2} through utilization of the SIBICR operator has been discussed as herein.

1) Generation of a random numeral *an* between [0,1].

2) Attainment of a parameter z with the help of a multinomial type probability allocation in accordance to (3.82).

$$z = \begin{cases} (an \times \delta)^{1/(\eta_{al}+1)}, & an \le 1/\delta \\ \left(\dfrac{1}{(2 - an \times \delta)}\right)^{1/(\eta_{al}+1)}, & \text{otherwise} \end{cases} \tag{3.82}$$

where, $\delta = 2 - \frac{1}{B^{(\eta_{al}+1)}}$ and B can be represented in accordance to (3.83).

$$B = 1 + \frac{2}{(p_{b2} - p_{b1})} mn\left[\left(p_{b1} - p_b^{mn}\right), \left(p_b^{mx} - p_{b2}\right)\right] \tag{3.83}$$

The parameter η_{al} represents an allocation index corresponding to the SIBICR; any nonnegative value can be assigned to it. A descendant community is generated in accordance to the value assigned to the η_{al}.The generated descendants remains either very distant or at closed quarters from the ancestor society in accordance to a smaller or larger value of the η_{al}.

3) Intermediary communities' computation takes place in accordance to (3.84) as well as (3.85).

$$p_{ba1} = 2^{-1}\left[\left(p_{b1} + p_{b2}\right) - z\left(\left|p_{b2} - p_{b1}\right|\right)\right] \tag{3.84}$$

$$p_{ba2} = 2^{-1}\left[\left(p_{b1} + p_{b2}\right) + z\left(\left|p_{b2} - p_{b1}\right|\right)\right] \tag{3.85}$$

Multinomial mutation: The multinomial probability allocation is used to generate a descendant in the vicinity of ancestor community by using a mutation operator. Its stating herein

1) Production of an arbitrary numeral an' in the $[0,1]$ range.

2) Computation of the parameter χ in accordance to (3.86).

$$\chi = \begin{cases} \left[\begin{matrix} 2\times an' \\ +\left(1-2\times an'\right)\times\left(1-\varphi\right)^{\left(\eta_m+1\right)} \end{matrix}\right]^{\frac{1}{\left(\eta_m+1\right)}} - 1 & , an' \le 2^{-1} \\ 1 - \left[\begin{matrix} 2\times\left(1-an'\right) \\ +2\times\left(an'-2^{-1}\right)\times\left(1-\varphi\right)^{\left(\eta_m+1\right)} \end{matrix}\right]^{\frac{1}{\left(\eta_m+1\right)}} & \text{, otherwise} \end{cases} \tag{3.86}$$

where, the ϕ can be expressed as

$$\phi = \frac{mn\left[\left(p_{ba} - p_b^{mn}\right), \left(p_b^{mx} - p_{ba}\right)\right]}{\left(p_b^{mx} - p_b^{mn}\right)}$$

The parameter η_{al} in the (3.86) represents the mutation allocation index; any nonnegative value can be assigned to it.

3) Computation of the mutated descendants takes place in accordance to (3.87) and (3.88).

$$p'_{b1} = p_{ba1} + \chi\left(p_b^{mx} - p_b^{mn}\right) \tag{3.87}$$

$$p'_{b2} = p_{ba2} + \chi\left(p_b^{mx} - p_b^{mn}\right) \tag{3.88}$$

A change in the perturbation can be made through iterative variations in the η_{al} and pr_{mut} as expressed in (3.89) and (3.90).

$$\eta_{al} = \eta_{al,mn} + itrn \tag{3.89}$$

$$pr_{mut} = \frac{1}{\eta_{chvb}} + \frac{itrn}{itrn_{mx}}\left(1 - \frac{1}{\eta_{chvb}}\right) \tag{3.90}$$

where $\eta_{al,mn}$ indicates the minimum value of the η_{al} and n_{chvb} and pr_{mut} represent the total number of choice variables and mutation probabilistic value respectively.

The fn_i value corresponding to each descendant is computed.

Selection between an ancestor and a descendant: A comparison of fn_i values is made corresponding to each ancestor p_{bc} and its matching descendant p'_{bc}. Out of these two, the one with lower fn_i value gets priority to participate in the succeeding iteration in accordance to (3.91).

$$p_{bc} = \begin{cases} p'_{bc}, & f(p'_{bc}) \le f(p_{bc}) \\ p_{bc}, \text{ otherwise} \end{cases} \tag{3.91}$$

This procedure continues until the maximum value of iteration $itrn_{mx}$ is reached. Fig. 3.6 demonstrates execution sequence outline of the IMRCGA.

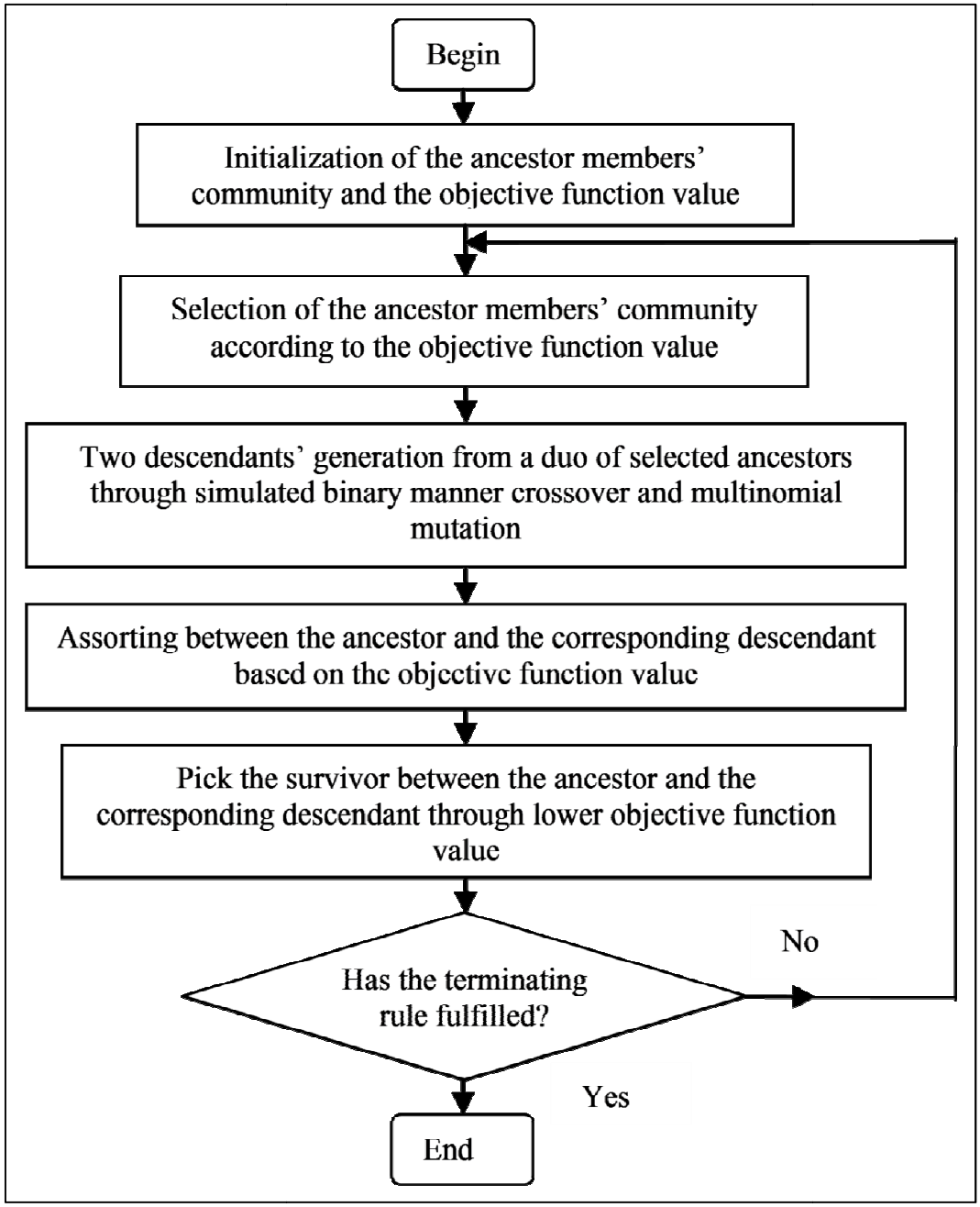

Figure 3.6. Computing execution flow of the IMRCGA

3.11. Grey wolf optimization for fault detection scheme in photovoltaic system

3.11.1. Grey Wolf Optimizer

GWO is a swarm intelligence based optimization technique inspired by grey wolves (Canis Lupus) [198]. It is based on the leadership hierarchy and the hunting mechanism of grey wolves in nature. The major three actions of this hunting mechanism are searching for prey, encompassing prey and attacking the prey. To enact these, four types of wolf, namely alpha, beta, delta and omega are employed.

The alpha wolves are the topmost member of the hierarchy and the most promising member. They are the best in terms of managing the group. Beta is the next in the hierarchy of grey wolves and they are superior to the others in the group. It enacts the character of an advisor to the alpha and discipliner for the pack of wolves. The beta strengthens the alpha's commands all through the pack and delivers feedback to the alpha. Those wolves that are not alpha, beta or omega are delta. They have to submit to alphas and betas, but dominate the omega.

The hunting behaviour is loosely modeled by the following two operators:

a) Encircling prey: Grey wolves encircle the prey during hunt. The mathematical modelling of encircling the prey is given as

$$\vec{D} = \left| \vec{C}.\vec{X}_p(t) - \vec{X}(t) \right| \tag{3.92}$$

$$\vec{X}(t+1) = \vec{X}_p(t) - \vec{A}.\vec{D} \tag{3.93}$$

Where t indicates the current iteration, $\vec{A}$ and $\vec{C}$ are coefficient vectors, $\vec{X}_p$ is the position vector of the prey, and $\vec{X}$ indicates the position vector of a grey wolf. The vectors $\vec{A}$ and $\vec{C}$ are calculated as follows

$$\vec{A} = 2\vec{a}.\vec{r}_1 - \vec{a} \tag{3.94}$$

$$\vec{C} = 2.\vec{r}_2 \tag{3.95}$$

Where components of $\vec{a}$ are linearly decreased from 2 to 0 over the course of iterations and r_1, r_2 are random vectors in [0, 1].

b) Hunting: For the mathematical representation of the hunting of the prey, it is supposed that the alpha ($\vec{x}_{\alpha}$) (best candidate solution) beta ($\vec{x}_{\beta}$), and delta ($\vec{x}_{\delta}$) have better knowledge about the potential location of prey. So the first three best solutions generated so far are saved and oblige the other search agents (including the omegas) to update their positions in accordance with the position of the best search agents. Then the position is calculated as given by the formulae in the previous section. The final updated position is given by (3.96).

$$\vec{x}(t+1) = \frac{\vec{x}_1 + \vec{x}_2 + \vec{x}_3}{3} \tag{3.96}$$

This optimization technique has great exportation and exploitation capability to search the optimum value in the search space as well as to avoid stagnation in local solutions. The values of $\vec{A}$ and $\vec{C}$ aid in the process. As $\vec{C}$ vector contains random values between [0,2] it favours exploration. On the other hand, the vector $\vec{A}$ helps in exploitation as the vector $\vec{a}$ is linearly decreased from 2 to 0.

3.11.2. Application of GWO in the fault diagnosis scheme

Here, the role of GWO, being applied as minimiser, is to minimize (2.134) [ref. chapter 2, sec. 2.9], that is, to find the exact OC and SC fault combination which can cause the same amount of current, that are flowing through the PV string. To implement the GWO, switching combinations (SWO, SWS) are distinguished as wolves. For this optimization problem, SWO and SWS are the decision vectors, where each has m number of elements. m is the total number of modules present in the string. The detailed encode scheme of computational flow of the fault diagnosis strategy following string current for PV string implementing GWO is as follows:

Step 1. Get $I_{meas}^{MPP}, P_{actual}$, module temperature (T) and irradiance (G) data from the physical PV string.

Step 2. Simulate $P_{simulated}$ for no fault condition at MPP and evaluate ε .

Step 3. If $P_{actual} < P_{simulated}$, go to Step 4, to start fault diagnosis algorithm using GWO.

Otherwise, display: "Healthy string connections" and go to Step 1.

Step 4. GWO Initialization:

a) Set N (number of Grey wolf position) & t (number of iterations).

---

b) Randomly initialize *N* number of switching combinations (SWO, SWS).

{This initialized switching combinations (SWO, SWS) resembles with $\vec{X}$ }

c) Initialize *a*, *A* and *C*

Step 5. Set Iteration count: *k=1*.

Step 6. Set Wolf count: *w*=1.

Step 7. Simulate $(I_{sim}^{MPP})_w$.

{Simulated string current at MPP for w^{th} wolf, i.e., switching combination $(SWO,SWS)_w$}

Step 8. Evaluate the fitness function $[FIT(SWO,SWS)]_w$

Step 9. If *w<N*, Set Wolf count: *w=w+1* and go to Step 7.

Otherwise, go to Step 10.

Step 10. Rank the Grey wolves based on the fitness:

$(SWO,SWS)_\alpha$ =The best search agent.

$(SWO\ ,SWS\ )_\beta$ =The second best search agent.

$(SWO,SWS)_\delta$ =The third best search agent.

Step 11. Update a, A, C and $(SWO,SWS)_j$

Step 12. If $|P_{simulated}-P_{actual}|<\varepsilon$, terminate GWO, return $(SWO,SWS)_\alpha$ and go to Step 14.

Otherwise, go to Step 13.

Step 13. If *k<t*, set Iteration count: *k=k+1* and go to Step 6.

Otherwise, terminate GWO, return $(SWO,SWS)_\alpha$ and go to Step 14.

Step 14. Display detected fault as: $(SWO,SWS)_\alpha$.

This page is left blank intentionally

Chapter 4

Results and discussion

==========

4.1. Numerical Study on ED problems

4.1.1. Solution Approach

To solve highly non-linear and specially multi-modal mathematical optimization problem like ED, a heuristic optimizer capable of wide exploration and in-depth fine searching in the wide search space is essential. The aforesaid stages of the algorithm determines the balance between exploration and exploitation in the search space. To prefer both the wide exploration and in-depth fine searching, each stage of the suggested algorithm is put into practice with equal probability during the whole search procedure. The search procedures of all three stages are computed in such a manner that during the first half each stage investigates search space while in the second half each stage utilizes the search space.

The proposed HTS algorithm is applied to three different power systems test cases. In each case 100 runs are conducted to compare the solution quality.

4.1.2. Parameter Selection

Test results have been built up to compare the recital of the suggested HTS with that of other stated evolutionary techniques. For all three cases, the tuning parameters of the proposed HTS algorithm (i.e. conduction, convection and radiation factors) have been set as 2, 2 and 10 respectively. The values of N_P and N_{max} have been selected based on the problem dimension for different test cases. Number of elite solutions (N_E) has been taken as top 10% of the population.

4.1.3. Test System 1

This is a 15-unit system with POZ and transmission losses [1]. Here, the system dimension is 15. N_P, N_E and N_{max} have been selected as 50, 5 and 100 respectively for this test system under consideration. The unit wise generation level and transmission loss acquired from HTS are as in table 4.1. Comparative results of particle swarm optimization (PSO) and improved particle swarm optimization (IPSO) are provided in table 4.2 [1,14]. Fig 4.1 indicates the convergence characteristic of HTS in this case.

Table 4.1

Unit generation (MW) and power loss (MW) for Test System 1.

Unit	Gen	Unit	Gen
1	562.7951	9	25.0000
2	455.0000	10	25.0000
3	130.0000	11	58.8098
4	130.0000	12	80.0000
5	150.0000	13	25.0000
6	460.0000	14	15.0000
7	465.0000	15	15.000
8	60.0000	**Ploss**	**26.6129**

Table 4.2

Comparison of performance for Test System 1

Techniques	Best cost($)	Average cost($)	Worst cost($)
HTS	32532.17	32533.04	32537.53
IPSO[12]	32704.45	32704.45	32704.45
PSO[8]	32858.00	33039.00	33331.00

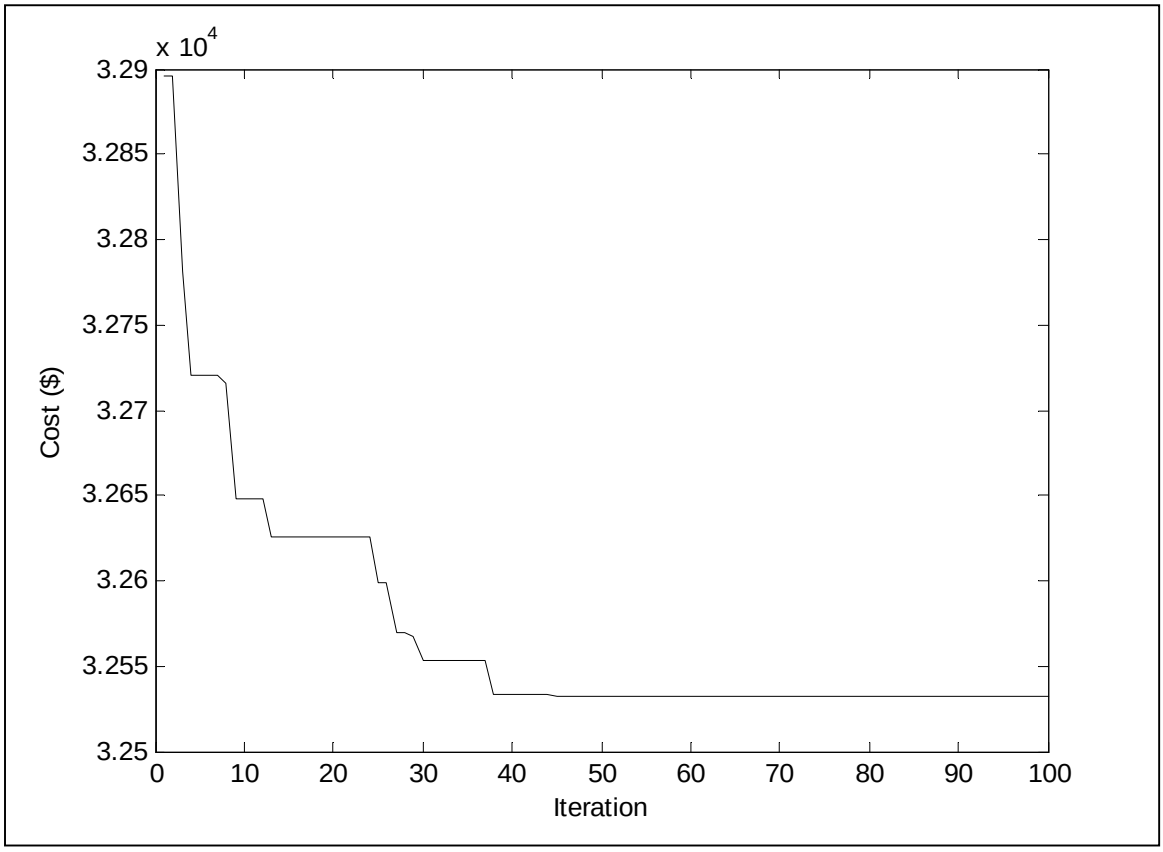

Figure 4.1. Convergence characteristic for Test System 1.

4.1.4. Test System 2

This system comprises of 40-unit system with valve-point effects [10]. Here, N_P, N_E and N_{max} have been selected as 100, 10 and 200 respectively for this 40-dimensional optimization problem. The solved generation level are as in table 4.3. The problem has also been solved by improved particle swarm optimization (IPSO), new particle swarm optimization with local random search (NPSO-LRS), continuous quick group search optimizer (CQGSO) and biogeography-based optimization (BBO) [10,12,13,14] The comparative results and convergence pattern of HTS are provided in table 4.4. and Fig 4.2 respectively.

Table 4.3

Unit generation (MW) for Test System 2.

Unit	Gen	Unit	Gen	Unit	Gen	Unit	Gen
1	110.803	11	94.000	21	523.279	31	190.000
2	110.800	12	94.000	22	523.279	32	190.000
3	97.3987	13	214.759	23	523.279	33	190.000
4	179.733	14	394.279	24	523.279	34	164.799
5	87.9996	15	394.279	25	523.279	35	194.394
6	140.000	16	394.279	26	523.279	36	199.802
7	259.599	17	489.279	27	10.000	37	110.000
8	284.599	18	489.279	28	10.000	38	110.000
9	284.599	19	511.279	29	10.000	39	110.000
10	130.000	20	511.279	30	87.799	40	511.278

Table 4.4

Comparison of performance for Test System 2

Techniques	Best cost($)	Average cost($)	Worst cost($)
HTS	121370	121374	121380
IPSO[12]	121403	121445	121525
NPSO-LRS[10]	121664	122209	122981
BBO[13]	121426	121503	121688
CQGSO[14]	121412	121423	121438

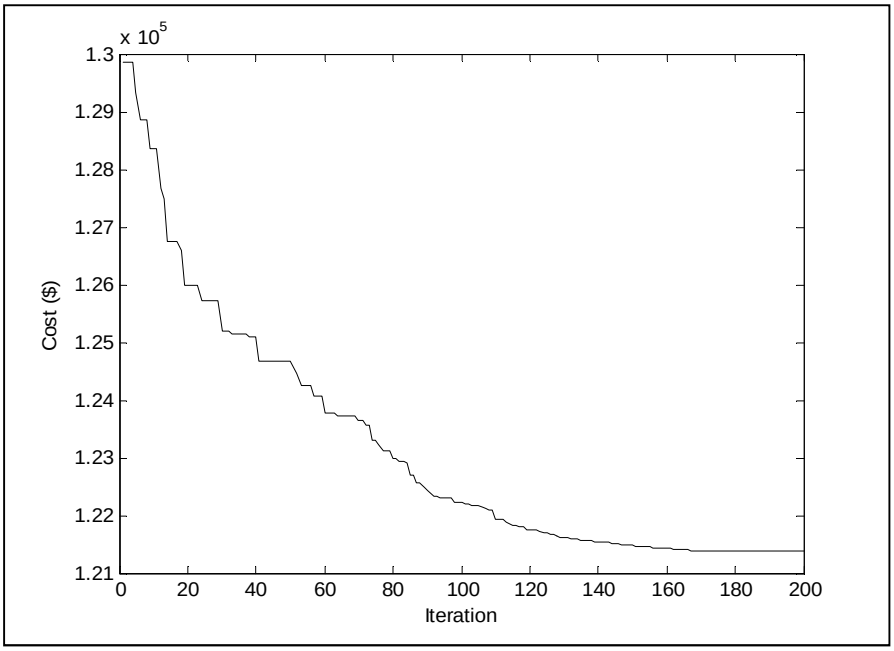

Figure 4.2. Convergence characteristic for Test System 2.

4.1.5. Test System 3

10-unit system considering multiple fuels with valve-point effects [4]. For this 10-dimensional problem, NP, NE and Nmax have been selected as 50, 5 and 100 respectively. The generation results from HTS are as in Table 4.5. The comparative results among improved particle swarm optimization (IPSO), continuous quick group search optimizer (CQGSO), new particle swarm optimization with local random search (NPSO-LRS) and improved genetic algorithm with multiplier updating (IGA_MU) are in Table 4.6 with convergence curve of HTS as in Fig.4.3 [4,10,12,14].

Table 4.5

Unit Generation (MW) for Test System 3

Unit	Gen	F	Unit	Gen	F
1	229.5981	2	6	242.3580	3
2	215.8744	1	7	306.2386	1
3	296.6904	1	8	244.2562	3
4	137.9270	1	9	440.0000	3
5	294.4132	1	10	292.6441	1

Table 4.6

Comparison of performance for Test System 3

Techniques	Best cost($)	Average cost($)	Worst cost($)
HTS	608.156	608.195	608.253
IPSO[12]	623.826	623.827	623.829
NPSO-LRS[10]	624.127	-	-
CQGSO[14]	623.827	623.834	623.850
IGA_MU[4]	624.517	-	-

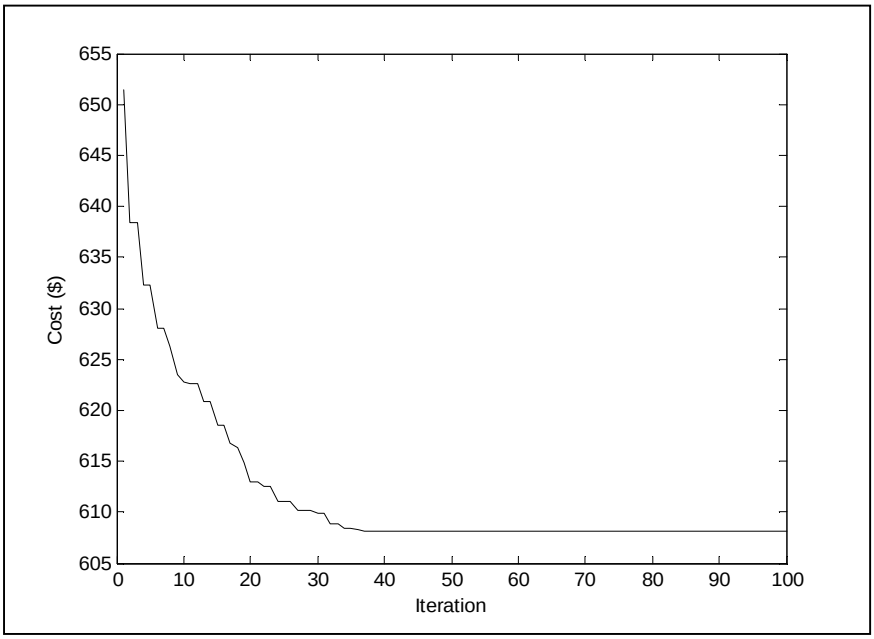

Figure 4.3. Convergence characteristic for Test System 3

4.1.6. Analysys

The considered test cases are of different dimensions with various constraints, which provide unique mathematical character for each of the models. In terms of best average and worst results for all the cases, the algorithm are found to be better than the other available solutions in the literature. These findings indicate adaptability and robustness of the proposed algorithm.

4.1.7. Conclusion

The proposed HTS algorithm has been successfully applied to three non-convex economic dispatch problems considering valve-point effects, prohibited operating zones with transmission losses and multiple fuels with valve-point effects. The results have been compared with those obtained by other evolutionary algorithms in the literature. It is seen from the comparisons that the proposed HTS algorithm performs better than other evolutionary algorithms in the literature.

4.2. Numerical Study on MAED problems

The proposed AIS algorithm has been applied to solve MAED problems in three different test systems for verify-ing its feasibility. The software has been written in MATLAB 7 on a PC (Pentium – IV, 80 GB, 3.0 GHZ).

4.2.1. Test system 1

This system consists of two areas. Each area consists of three generators with prohibited operating zones. Transmission loss is considered here. The generator data have modified from [235]. The generator data and B-coeffi-cients are given in the Appendix 4.2.1. The percentage of the total load demand in area 1 is 60% and 40% in area 2. The total load demand is 1,263 MW and power flow limit of the system is 100 MW.

The problem is solved by using AIS algorithm. Here, scaling factor of real power generation (mulG), scaling factor of tie line power transfer (mulT), population size (NP), number of clones (Nc) and maximum iteration num-ber (Nmax) are taken as 1, 0.5, … 50, 10 and 100, respec-tively for this test system under consideration.

To validate the proposed AIS-based approach, the same test system is solved using differential evolution (DE), evolutionary programming (EP) and real-coded genetic algorithm (RCGA). The population size, scaling factor and crossover constant have been selected as 200, 1.0 and 1.0, respectively, in case of DE. In case of EP, the population size and scaling factor have been selected 100 and 0.1, respectively. In RCGA, the popu-lation size, crossover and mutation probabilities have been selected as 100, 0.9 and 0.2, respectively. Maximum number of generations has been selected 100 for DE, EP and RCGA.

Results obtained from proposed AIS, DE, EP and RCGA have been summarized in Table 4.7. The cost con-vergence characteristic of this test system obtained from AIS, DE, EP and RCGA is shown in Fig 4.4.

Table 4.7

Simulation results for test system 1

	AIS	DE	EP	RCGA
P1,1 (MW)	500.0000	500.0000	500.0000	500.0000
P1,2 (MW)	200.0000	200.0000	200.0000	200.0000
P1,3 (MW)	149.9994	150.0000	149.9919	149.6328
P2,1 (MW)	204.1371	204.3341	206.4493	205.9398
P2,2 (MW)	154.8707	154.7048	154.8892	155.8322
P2,3 (MW)	67.6140	67.5770	65.2717	65.2209
T12 (MW)	82.7726	82.7731	82.7652	82.4135
PL1 (MW)	9.4268	9.4269	9.4267	9.4193
PL2 (MW)	4.1944	4.1890	4.1754	4.2064
Cost ($/h)	12,255.39	12,255.42	12,255.43	12,256.23

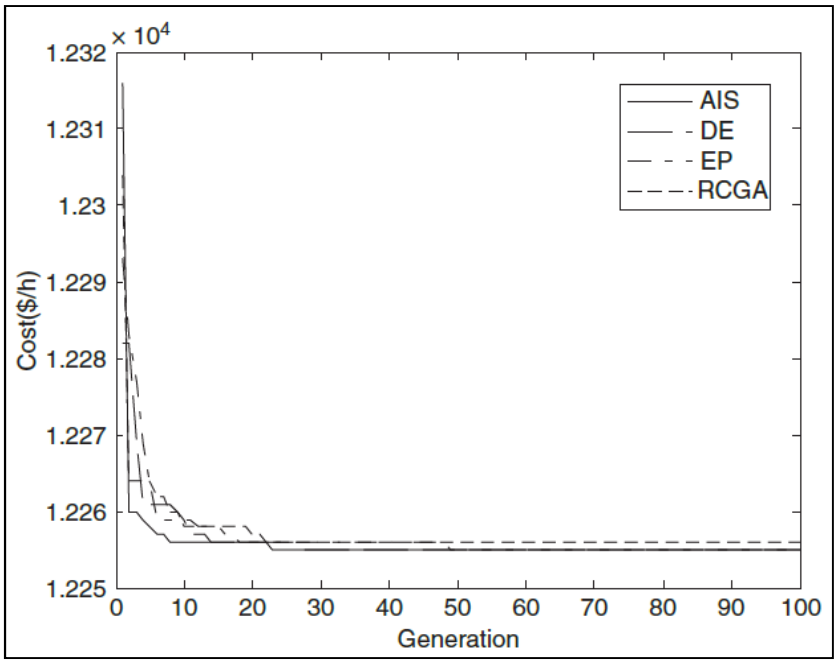

Figure 4.4. Cost convergence characteristic of test system 1

Appendix 4.2.1

Generator data for two area system

Generator ij	aij $/h	bij $/MWh	cij ($/MW)2h	P_{ij}^{min} MW	P_{ij}^{max} MW	Prohibited zones MW
G1,1	550	8.10	0.00028	100	500	[210 240] [350 380]
G1,2	350	7.50	0.00056	50	200	[90 110] [140 160]
G1,3	310	8.10	0.00056	50	150	[80 90] [110 120]
G2,1	240	7.74	0.00324	80	300	[150 170] [210 240]
G2,2	200	8.00	0.00254	50	200	[90 110] [140 150]
G2,3	126	8.60	0.00284	50	120	[75 85] [100 105]

The transmission loss formula coefficients of two-area system

$$\boldsymbol{B_1} = \begin{bmatrix} \mathbf{17} & \mathbf{12} & \mathbf{7} \\ \mathbf{12} & \mathbf{14} & \mathbf{9} \\ \mathbf{7} & \mathbf{9} & \mathbf{31} \end{bmatrix} \times \mathbf{10^{-6}}$$

$$\boldsymbol{B_{01}} = [\mathbf{-0.3908} \quad \mathbf{-0.1297} \quad \mathbf{0.7047}] \times \mathbf{10^{-3}}$$

$$\boldsymbol{B_{001}} = [\mathbf{0.045}]$$

$$\boldsymbol{B_{02}} = \begin{bmatrix} \mathbf{24} & \mathbf{-6} & \mathbf{-8} \\ \mathbf{-6} & \mathbf{129} & \mathbf{-2} \\ \mathbf{-8} & \mathbf{-2} & \mathbf{150} \end{bmatrix} \times \mathbf{10^{-6}}$$

$$\boldsymbol{B_{002}} = [\mathbf{0.056}]$$

4.2.2. Test system 2

This system comprises 10 generators with valve-point loading and multi-fuel sources having three fuel options. Transmission loss is considered here. The gen-erator data have been taken from [202]. The total load demand is 2,700 MW. The 10 generators are divided into three areas. Area 1 consists of the first four units; area 2 includes the next three units and area 3 includes the last three units. The load demand in area 1 is assumed as 50% of the total demand. The load demand in area 2 is assumed as 25% and in area 3 is taken as 25% of the total demand. The power flow limit from area 1 to area 2 or from area 2 to area 1 is 100 MW. The power flow limit from area 1 to area 3 or from area 3 to area 1 is 100 MW. Also the power flow limit from area 2 to area 3 or from area 3 to area 2 is 100 MW. The B-coefficients are given in the Appendix 4.2.2.

AIS algorithm is used to solve the problem. Here, scaling factor of real power generation (mulG), scaling factor of tie line power transfer (mulT), population size (NP), number of clones (Nc) and maximum itera-tion number (Nmax) are taken as 1, 0.5, 50, 10 and 300, respectively, for this test system under consideration.

In order to validate the proposed AIS-based approach, the same test system is solved using DE, EP and RCGA. In DE, the population size, scaling factor and crossover constant have been selected as 200, 1.0 and 1.0, respectively. The population size and scaling factor have been selected 100 and 0.1, respectively, in case of EP. In RCGA, the population size, crossover and mutation probabilities have been selected as 100, 0.9 and 0.2, respectively. Maximum number of generations has been selected 300 for DE, EP and RCGA.

Results obtained from proposed AIS, DE, EP and RCGA have been presented in Table 4.8. The cost convergence characteristic of this test system obtained from AIS, DE, EP and RCGA is shown in Fig 4.5.

Table 4.8

Simulation results for test system 2

	AIS		DE		EP		RCGA	
		Fuel		Fuel		Fuel		Fuel
P1,1 (MW)	249.9932	2	250.0000	2	250.0000	2	241.1238	2
P1,2 (MW)	230.0000	1	230.0000	1	230.0000	1	217.9371	1
P1,3 (MW)	425.7459	2	421.7415	2	421.7450	2	474.3300	2
P1,4 (MW)	259.3045	3	263.2026	3	263.1955	3	248.4239	3
P2,1 (MW)	235.9642	1	239.3128	1	244.3361	1	250.5749	1
P2,2 (MW)	233.4799	3	230.9321	3	233.2185	3	222.5926	3
P2,3 (MW)	254.4325	1	252.4330	1	243.3656	1	234.9363	1
P3,1 (MW)	232.8335	3	234.2974	3	240.1423	3	228.5379	3
P3,2 (MW)	370.6897	3	370.4444	3	371.5352	3	384.3050	3
P3,3 (MW)	241.0603	1	241.0873	1	235.8444	1	232.5959	1
T21 (MW)	100.0000		100		100		92.0603	
T31 (MW)	100.0000		99.9964		100		92.7851	
T32 (MW)	60.0060		61.2609		63.0646		67.8913	
PL1 (MW)	15.0000		14.9000		14.9000		16.7000	
PL2 (MW)	8.8826		8.9388		8.9848		8.9348	
PL3 (MW)	9.5775		9.5718		9.4573		9.7624	
Cost ($/h)	674.5502		674.8207		675.3977		687.4220	

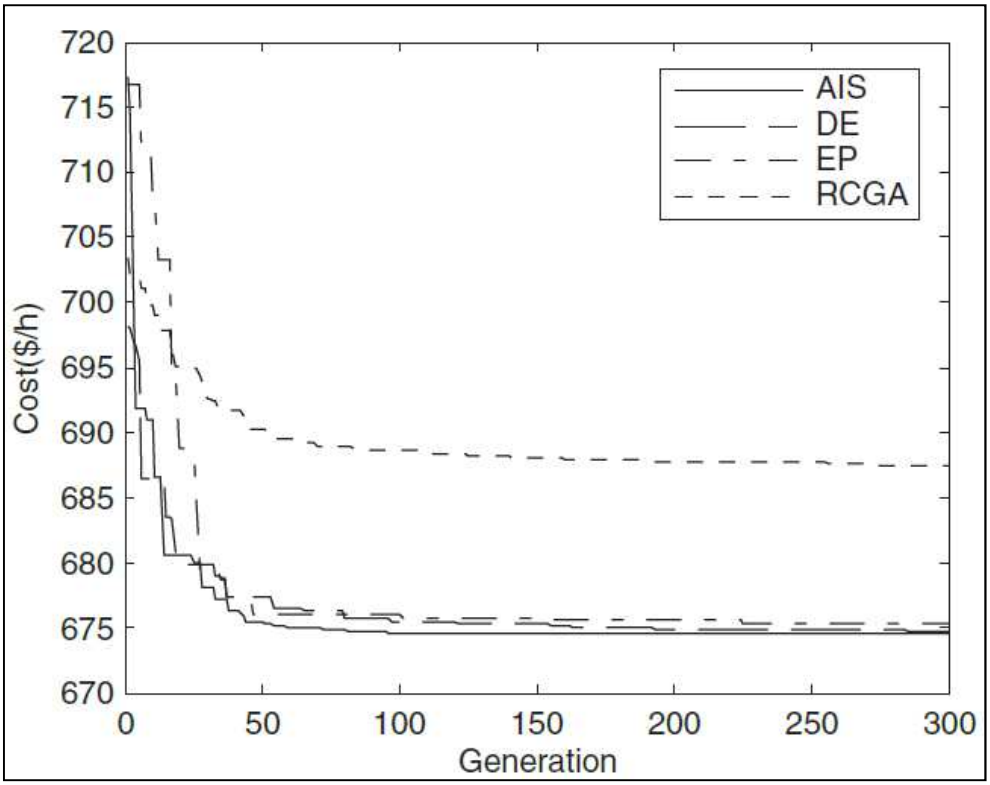

Figure 4.5. Cost convergence characteristic of test system 2

Appendix 4.2.2

The transmission loss formula coefficients of two-area system

$$\boldsymbol{B_1} = \begin{bmatrix} \mathbf{8.70} & \mathbf{0.43} & \mathbf{-4.16} & \mathbf{0.36} \\ \mathbf{0.43} & \mathbf{8.30} & \mathbf{-0.97} & \mathbf{0.22} \\ \mathbf{-4.61} & \mathbf{-0.97} & \mathbf{9.00} & \mathbf{-2.00} \\ \mathbf{0.36} & \mathbf{0.22} & \mathbf{-2.00} & \mathbf{5.30} \end{bmatrix} \times \mathbf{10^{-5}}$$

$$\boldsymbol{B_{01}} = [\mathbf{-0.3908} \quad \mathbf{-0.1297} \quad \mathbf{0.7047} \quad \mathbf{0.0591}] \times \mathbf{10^{-3}}$$

$$\boldsymbol{B_{001}} = [\mathbf{0.056}]$$

$$\boldsymbol{B_2} = \begin{bmatrix} \mathbf{8.60} & \mathbf{-80} & \mathbf{-37} \\ \mathbf{-0.80} & \mathbf{9.08} & \mathbf{-4.90} \\ \mathbf{0.37} & \mathbf{-4.90} & \mathbf{8.24} \end{bmatrix} \times \mathbf{10^{-6}}$$

$$\boldsymbol{B_{02}} = [\mathbf{0.2161} \quad \mathbf{-0.6635} \quad \mathbf{0.5034}] \times \mathbf{10^{-3}}$$

$$\boldsymbol{B_{002}} = [\mathbf{0.056}]$$

$$\boldsymbol{B_3} = \begin{bmatrix} \mathbf{1.20} & \mathbf{-0.96} & \mathbf{0.56} \\ \mathbf{-0.80} & \mathbf{9.08} & \mathbf{-0.30} \\ \mathbf{-0.56} & \mathbf{-0.30} & \mathbf{5.99} \end{bmatrix} \times \mathbf{10^{-6}}$$

$$\boldsymbol{B_{02}} = [\mathbf{-0.3216} \quad \mathbf{0.4635} \quad \mathbf{0.3503}] \times \mathbf{10^{-3}}$$

$$\boldsymbol{B_{002}} = [\mathbf{0.055}]$$

4.2.3. Test system 3

This system comprises 40 generators with valve-point loading. The generator data have been taken from [236]. The total load demand is 10,500 MW. The 40 generators are divided into four areas. Area 1 includes first 10 units and 15% of the total load demand. Area 2 has second 10 generators and 40% of the total load demand. Area 3 consists of third 10 generators and 30% of the total load demand. Area four includes last 10 generators and 15% of the total load demand. The power flow limit from area 1 to area 2 or from area 2 to area 1 is 200 MW. The power flow limit from area 1 to area 3 or from area 3 to area 1 is 200 MW. The power flow limit from area 2 to area 3 or from area 3 to area 2 is 200 MW. The power flow limit from area 4 to area 1 or from area 1 to area 4 is 100 MW. The power flow limit from area 4 to area 2 or from area 2 to area 4 is 100 MW. The power flow limit from area 4 to area 3 or from area 3 to area 4 is 100 MW. Transmission loss is neglected here.

The problem is solved by using AIS algorithm. Here, scaling factor of real power generation (mulG), scaling factor of tie line power transfer (mulT), population size (NP), number of clones (Nc) and maximum iteration num-ber (Nmax) are taken as 1, 0.05, … 100, 20 and 500, respectively, for the test system under consideration.

To validate the proposed AIS-based approach, the same test system is solved using DE, EP and RCGA. The population size, scaling factor and crossover constant have been selected as 400, 1.0 and 1.0, respectively, in case of DE. In EP, the population size and scaling factor have been selected 200 and 0.1, respectively. In case of RCGA, the population size, crossover and mutation prob-abilities have been selected as 200, 0.9 and 0.2, respec-tively. Maximum number of generations has been selected 500 for DE, EP and RCGA.

Results obtained from proposed AIS, DE, EP and RCGA have been depicted in Table 4.9. The cost conver-gence characteristic of this test system obtained from AIS, DE, EP and RCGA is shown in Figure 4.6.

Table 4.9

Simulation results for test system 3

Power (MW)	AIS	DE	EP	RCGA	Power (MW)	AIS	DE	EP	RCGA
$P_{1,1}$	113.7914	93.0826	114.0000	94.0855	$P_{3,4}$	525.4970	545.9437	531.7377	524.9246
$P_{1,2}$	113.9998	109.0592	114.0000	47.7313	$P_{3,5}$	527.2531	523.6608	526.7530	495.4096
$P_{1,3}$	64.7248	89.7493	63.7726	85.4353	$P_{3,6}$	550.0000	527.3677	550.0000	442.8850
$P_{1,4}$	80.1469	116.9489	138.8847	131.2807	$P_{3,7}$	10.0000	10.0000	10.0000	51.7060
$P_{1,5}$	97.0000	97.0000	75.3245	79.1771	$P_{3,8}$	10.0006	15.7851	10.0000	42.4448
$P_{1,6}$	109.0492	140.0000	106.4216	131.4026	$P_{3,9}$	10.0009	10.0000	10.0000	47.9812
$P_{1,7}$	260.3904	283.7266	300.0000	176.5484	$P_{3,10}$	97.0000	93.0253	89.7589	95.5812
$P_{1,8}$	300.0000	286.2646	300.0000	232.6707	$P_{4,1}$	160.1255	190.0000	173.5365	149.1883
$P_{1,9}$	285.9479	284.9088	284.9513	292.1746	$P_{4,2}$	190.0000	157.8968	190.0000	159.4065
$P_{1,10}$	130.0000	131.6349	136.7335	130.1531	$P_{4,3}$	162.0924	190.0000	116.4310	161.6999
$P_{2,1}$	159.9752	169.8738	175.3639	340.9307	$P_{4,4}$	169.7535	200.0000	180.6554	167.5135
$P_{2,2}$	160.0619	110.9708	94.0000	185.7976	$P_{4,5}$	167.6944	90.0000	162.0916	172.4220
$P_{2,3}$	393.4413	229.8845	263.8126	462.1471	$P_{4,6}$	169.8139	149.4540	173.0920	179.2210
$P_{2,4}$	394.2748	387.4742	331.0545	391.6765	$P_{4,7}$	59.6628	110.0000	109.4254	91.9333
$P_{2,5}$	394.2794	427.7543	394.2191	376.9261	$P_{4,8}$	110.0000	88.1630	74.3342	92.5453
$P_{2,6}$	394.2794	478.2780	413.0955	484.3564	$P_{4,9}$	91.5097	25.0000	99.6914	89.0354
$P_{2,7}$	489.2794	490.1819	499.6763	481.2045	$P_{4,10}$	458.7990	538.4695	541.9711	458.8239
$P_{2,8}$	489.2794	490.9476	500.0000	421.9451	T_{12}	113.8184	200	200	−118.7357
$P_{2,9}$	511.2794	511.9152	533.8328	469.0019	T_{31}	55.4544	91.5412	94.6831	−25.9549
$P_{2,10}$	511.2794	511.8241	508.9305	511.2801	T_{32}	152.4622	147.8992	186.0147	174.0405
$P_{3,1}$	530.0810	547.6323	520.6865	513.0630	T_{41}	78.3136	51.0838	46.2286	81.5599
$P_{3,2}$	523.4983	523.4937	531.7618	513.8375	T_{42}	36.2899	42.9964	100	19.4290
$P_{3,3}$	524.7380	522.6286	550.0000	524.4524	T_{43}	49.8478	69.9032	100	45.8003
Total cost ($/h)						123,246.1	124,544.1	124,574.5	129,911.8

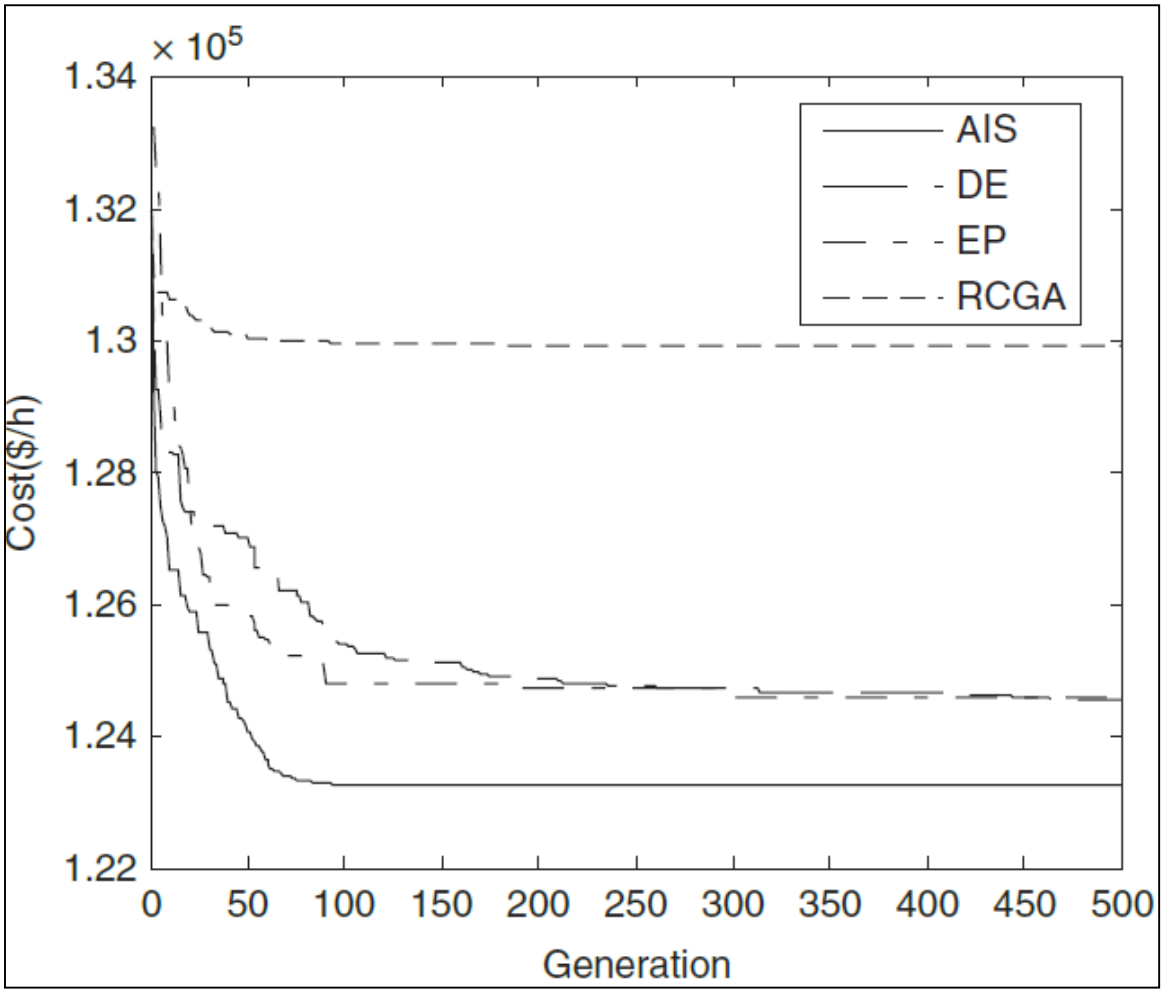

Figure 4.6. Cost convergence characteristic of test system 3

4.2.4. Discussion

Results show that the minimum production cost for three test systems as obtained by AIS is less compared to those obtained by DE, EP, and RCGA. This clearly shows that AIS has the ability to reach to the minimum solution consistently. It establishes the improved robustness of the algorithm. Convergence characteristics for test systems 1, 2, 3 obtained by AIS, as presented in Figures 4.4, 4.5 and 4.6 clearly reflects that AIS reaches to the minimum solutions within very few numbers of iterations. These establish the superior computational efficiency of AIS. Therefore, the above results prove the enhanced ability of AIS to solve complex, non-smooth, non-convex MAED problem in order to achieve superior quality solutions, in a computationally efficient and robust manner.

4.2.5. Conclusion

In this article, AIS has been successfully implemented to solve MAED problems. The effectiveness of the proposed method is illustrated by using three different test systems and the test results are compared with the results obtained from DE, EP and RCGA. It is seen from the comparison that the proposed AIS has the ability to con-verge to a better quality solution than DE, EP and RCGA.

4.3. Numerical Study on MAEED problems

4.3.1. Simulation results

A four area test system consisting of four generators in each area with nonsmooth fuel cost as well as functions related to pollutants' level has been implemented in the work for demonstrating the productivity of the MODE method. The generation data and tie line exchanging limits for the considered system are mentioned in the *Appendix 4.3.* Load demands corresponding to area 1, 2, 3, and 4 are 30 MW, 50 MW, 40 MW, and 60 MW respectively. The calculations have been done by an in-house developed code in the MATLAB R2013a.Total fuel cost as well as emission objectives have been minimized separately with real coded genetic algorithmic technique (RCGA) for finding the trade-off surface's extreme points. Comprehensive area wise system characteristics related to generation levels, corresponding operating costs and their emissions are depicted in Fig 4.7, Fig. 4.8, Fig 4.9 and Fig. 4.10 respectively for all four power system areas.

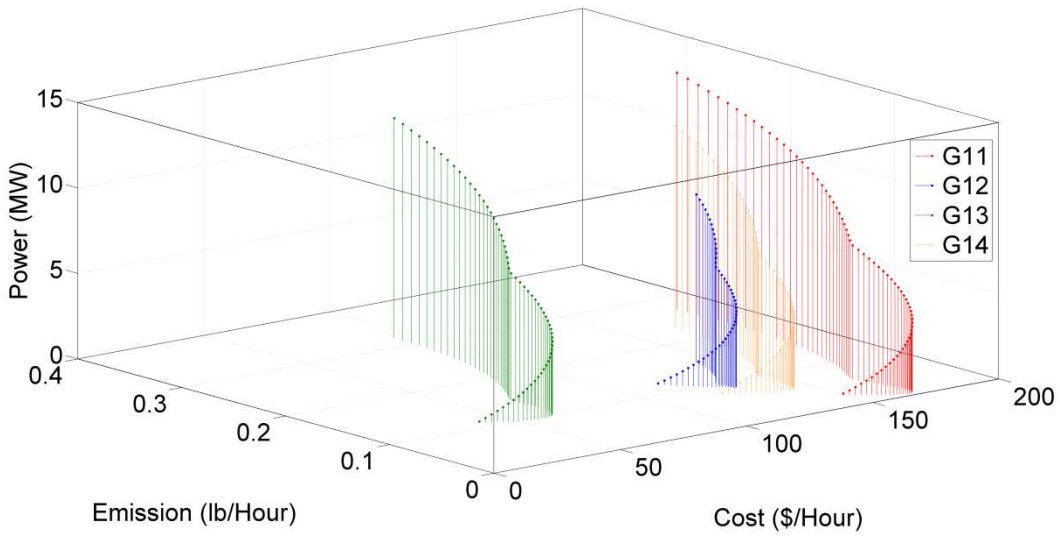

Figure 4.7. Power-cost-emission characteristics for Area 1.

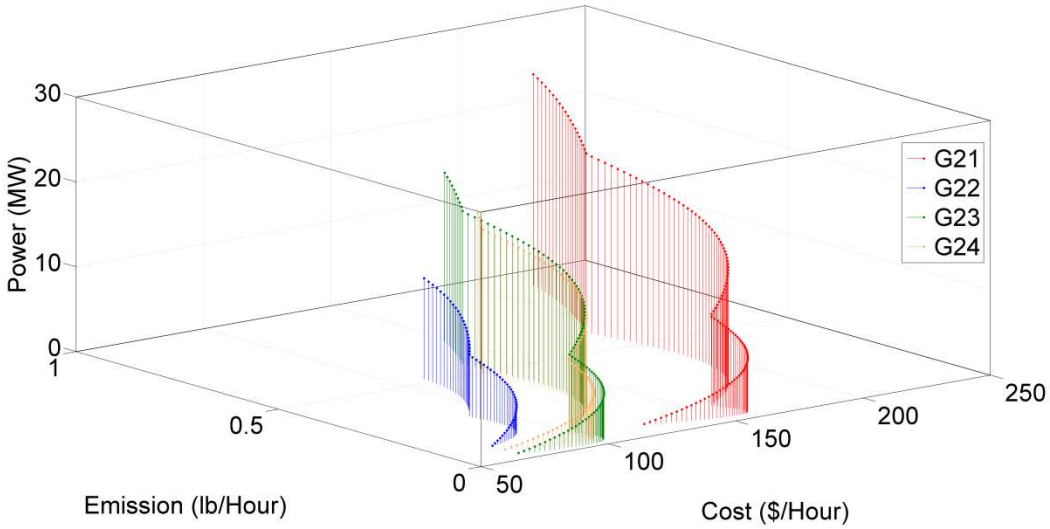

Figure 4.8. Power-cost-emission characteristics for Area 2.

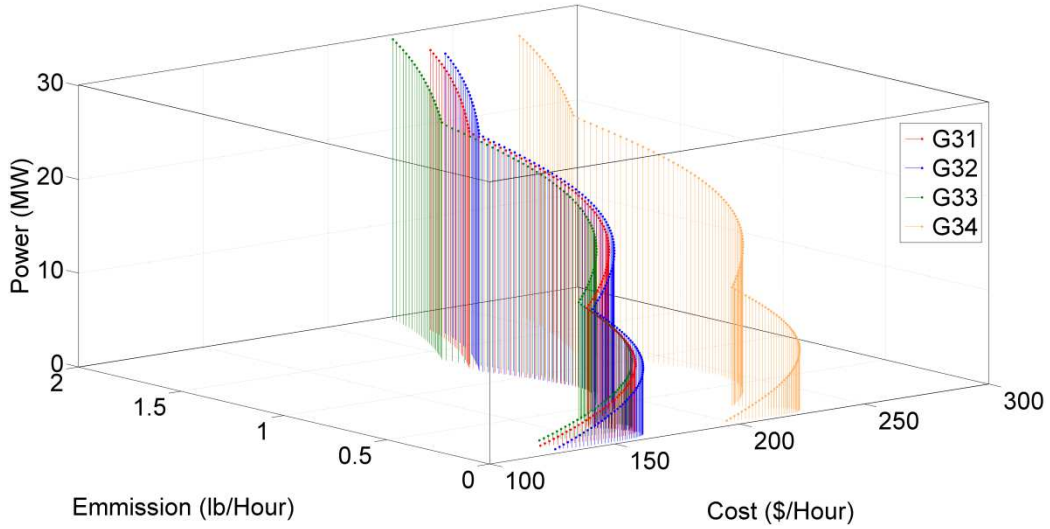

Figure 4.9. Power-cost-emission characteristics for Area 3.

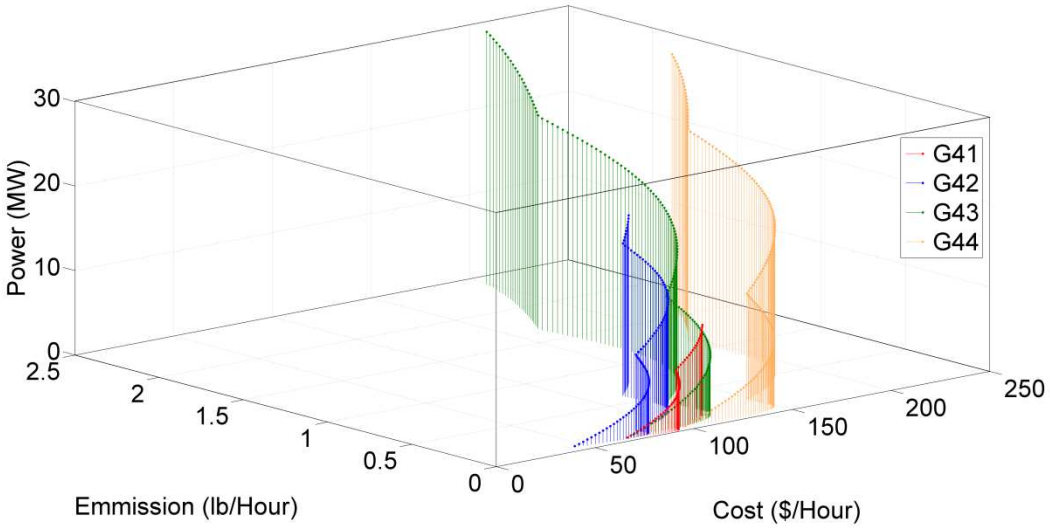

Figure 4.10 Power-cost-emission characteristics for Area 4.

Total members or population, maximum generation number, mutation probability, and crossover probability are taken as 100, 500, 0.2, and 0.9sequentially for aforementioned test system. It has been observed that for cost minimizing objective, fuel cost remains 1521.92 $/hr and emission level at 279.1049 lb/hr. An increment in the cost up to 2858.45 $/hr and emission decrement up to 250.6567 lb/hr was noticed with respect to emission minimization. Curves of convergence concerning cost and pollutants level have been presented in Fig. 4.11 and Fig. 4.12 sequentially. The generation amount in these Figures is in MW. In order to optimize cost as well as emission at the same time, the MODE was implemented.

For aforementioned purpose, parameters were selected as mentioned next. Total members or population, maximum generation number, mutation and crossover probabilities are 20, 50, 0.2 and 0.9sequentially for the considered system. It is seen that cost is 2306.15 $/hr which is more than 1521.92 $/hr and less than 2858.45 $/hr and emission is 263.0229 lb/hr which is less than 279.1049 lb/hr and more than 250.6567 lb/hr. For demonstrating the NDSGA II productivity, the SPEA II is selected for solving the MAEED objective. Parameters corresponding to the SPEA II have been mentioned next. Total members or population, mutation and crossover probabilities, and maximum generation number were chosen to be 20, 0.2and 0.9, and 50 sequentially.

Table 4.10 indicatesabout the best optimized solution corresponding to the final generation as achieved through the MODE as well as the SPEA II. Data corresponding to the least price value along with the least pollution level has also been presented in the same table. For aforementioned least values, the RCGA technique has also been implemented. Fig. 4.13 deals with the 20 nondominated solutions attained corresponding to the last generation of the MODE as well as the SPEA II.

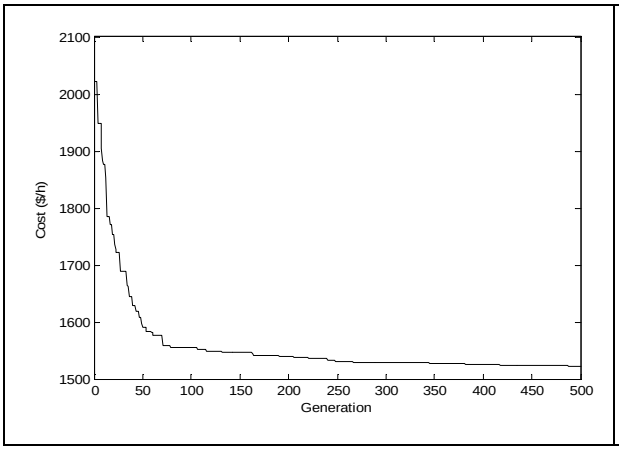

Figure 4.11. Cost convergence

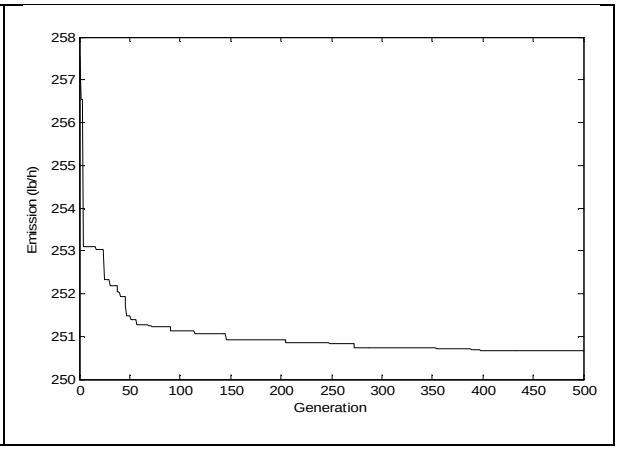

Figure 4.12. Emission convergence

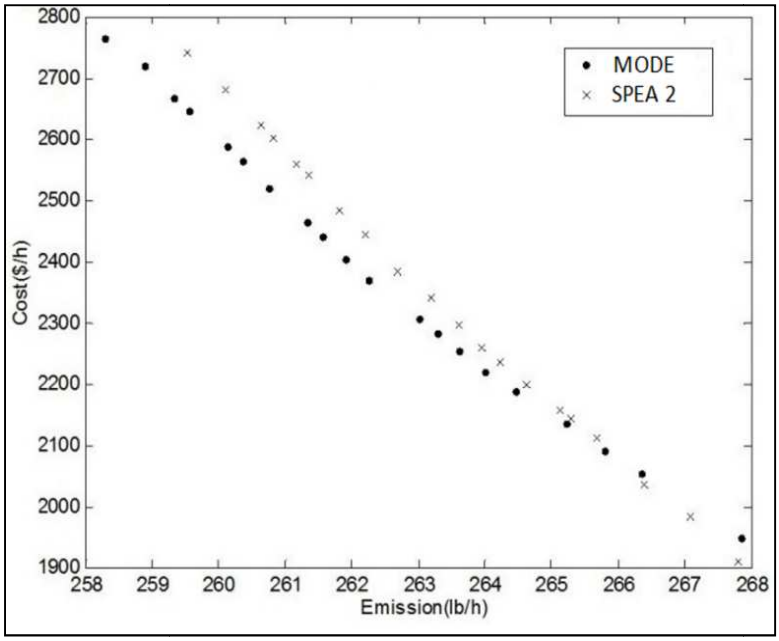

Figure 4.13. Pareto-optimal front as per the MODE and the SPEA II (with respect to the final generation)

Table 4.10

Simulation solutions corresponding to the system under consideration

	Minimum fuel cost	**Minimum emission level**	**MODE**	**SPEA II**
P11 (MWt)	6.2199	0.0582	4.2767	3.7801
P12 (MWt)	0.0500	0.0500	2.4432	1.9565
P13 (MWt)	0.0675	13.0000	5.0288	9.0004
P14 (MWt)	11.6650	11.9647	10.2873	9.0604
P21 (MWt)	8.6814	25.0000	15.6294	13.9816
P22 (MWt)	0.3559	12.0000	9.1385	8.0030
P23 (MWt)	20.0000	9.3437	12.1516	17.5303
P24 (MWt)	17.9797	9.9112	16.1274	15.6876
P31 (MWt)	0.0500	9.3729	11.1128	14.2898
P32 (MWt)	30.0000	9.1430	11.5027	6.8935
P33 (MWt)	8.0818	11.9394	9.2512	3.3478
P34 (MWt)	10.0555	12.8634	11.5776	18.2130
P41 (MWt)	1.4822	11.0000	7.8041	7.1157
P42 (MWt)	14.0633	16.8607	14.1608	13.0403
P43 (MWt)	30.0000	14.3553	21.1647	18.8948
P44 (MWt)	21.2478	13.1374	18.3432	19.2051

T21 (MWt)	6.0000	6.0000	4.4186	4.3529
T13 (MWt)	-3.9976	-0.7187	-2.5100	-1.5756
T41 (MWt)	2.0000	-1.7917	1.0355	0.2741
T32 (MWt)	3.5000	3.5000	1.4146	1.0910
T24 (MWt)	-5.4830	3.7549	0.0429	1.9407
T34 (MWt)	0.6898	-0.9000	-0.4802	0.0775
Cost ($/hr)	1521.92	2858.45	2306.15	2294.82
Emission (lb/hr)	279.1049	250.6567	263.0229	263.5606

4.3.2. Conclusion

In the presented brief, the multi-objective differential evolution (MODE) has been chosen to deal with the multiple objectives and constrained incorporating optimizing MAEEDS task. A comparison has been made between the results achieved through the NDSGA II and that achieved through the SPEA II. The MODE showed slightly better optimal front corresponding to this task. It has been observed from the comparison that the MODE gives novel optimized results.

Appendix 4.3

Generator characteristics (Generation limits)

Generator (GN_{gh})	P_{gh}^{min} **(MWt)**	P_{gh}^{max} **(MWt)**
GN11	0.05	14
GN12	0.05	10
GN13	0.05	13
GN14	0.05	12
GN21	0.05	25
GN22	0.05	12
GN23	0.05	20
GN24	0.05	18
GN31	0.05	30
GN32	0.05	30
GN33	0.05	30
GN34	0.05	30
GN41	0.05	11

GN42	0.05	20
GN43	0.05	30
GN44	0.05	30

Generator characteristics (Cost coefficients)

Generator (GN_{gh})	a_{gh} **($/hr)**	b_{gh} **($/MWthr)**	c_{gh} **($/MWt2 hr)**	d_{gh} **($/hr)**	e_{gh} **(rad/MWt)**
GN11	0	38.53900	0.15247	100	0.084
GN12	0	46.15916	0.10587	150	0.063
GN13	0	40.39655	0.02803	120	0.077
GN14	0	38.30553	0.03546	200	0.042
GN21	0	36.32782	0.02111	300	0.035
GN22	0	38.27041	0.01799	150	0.063
GN23	0	2.000000	0.00375	18.0	0.037
GN24	0	1.750000	0.01750	16.0	0.038
GN31	0	3.000000	0.02500	13.5	0.041
GN32	0	2.000000	0.00375	18.0	0.037
GN33	0	1.000000	0.06250	14.0	0.040
GN34	0	1.750000	0.01950	15.0	0.039
GN41	0	3.250000	0.06250	12.0	0.045
GN42	0	3.250000	0.00834	12.0	0.045
GN43	0	1.750000	0.01950	15.0	0.039
GN44	0	1.000000	0.00834	14.0	0.040

Generator characteristics (Emission coefficients)

Generator (GN_{gh})	α_{gh} (^{lb}/hr)	β_{gh} (^{lb}/MWthr)	γ_{gh} (^{lb}/MWt2hr)	η_{gh} (^{lb}/hr)	δ_{gh} (MWt-1)
GN11	13.85932	0.32767	0.00419	1.310000	0.05690
GN12	13.85932	0.32767	0.00419	0.914200	0.04540
GN13	40.26690	-0.54551	0.00683	0.993600	0.04060
GN14	40.26690	-0.54551	0.00683	0.655000	0.02846
GN21	42.89553	-0.51116	0.00461	0.503500	0.02075
GN22	42.89553	-0.51116	0.00461	0.914200	0.04540
GN23	40.91000	-0.05554	0.00649	0.000200	0.00285
GN24	2.54300	-0.06047	0.00563	0.000500	0.00333
GN31	6.13100	-0.05555	0.00515	0.000010	0.00666
GN32	3.49100	-0.05754	0.00639	0.000300	0.00265
GN33	4.25800	-0.05094	0.00458	0.000001	0.00800
GN34	2.75400	-0.05847	0.00523	0.000400	0.00287
GN41	5.32600	-0.03550	0.00338	0.002000	0.00200
GN42	5.32600	-0.03550	0.00338	0.002000	0.00200
GN43	2.75400	-0.05847	0.00523	0.000400	0.00287
GN44	4.25800	-0.05094	0.00458	0.000001	0.00800

Tie line power transfer limits

Tie line (T_{go})	$-T_{go}^{max}$ (MWt)	T_{go}^{max} (MWt)
T_{12}	-6.0	6.0
T_{13}	-4.0	4.0
T_{14}	-2.0	2.0
T_{23}	-3.5	3.5
T_{24}	-5.5	5.5
T_{34}	-0.9	0.9

4.4. Numerical Study on WMAEED problems

4.4.1. Simulation results

To examine the proficiency of the proposed power dispatch methodology, a standard wind integrated four area test system is considered as depicted in Figure 4.14. Along with the tie-line constraints, area-wise spinning reserve constraints, area-wise power balance, valve point loading and POZ; nonlinear constraints related to WUs are also considered for this WMAEED problem. A comparative analysis of the solutions obtained by NSGA-II and SPEA-II has been accomplished.

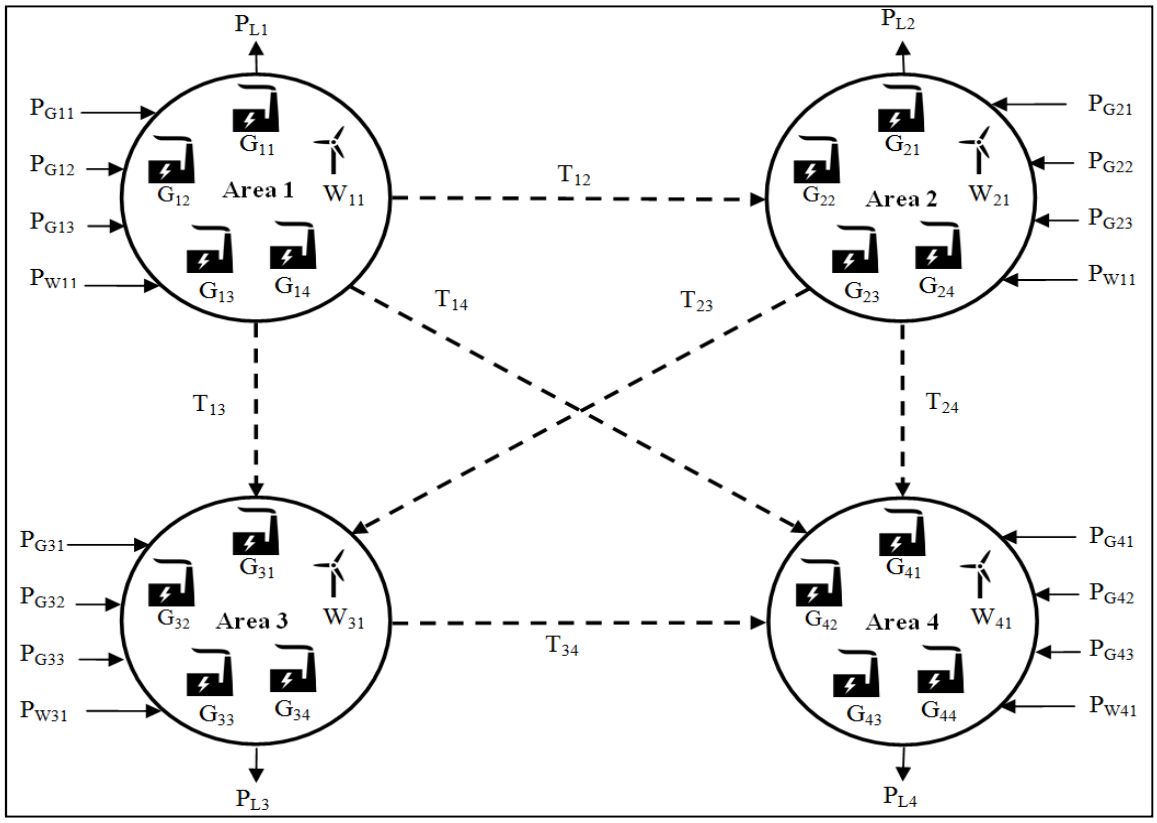

Figure 4.14. Representation of 4 area test system.

For this numeric study, a wind integrated four area test power system has been modeled mathematically. Each power system area contains 4 TUs and 1 WU. The total load of 180 MW is distributed over the 4 areas as 30 MW, 50 MW, 40 MW and 60 MW respectively. The transmission losses are considered to be negligible. Per area spinning reserve (SR_1, SR_2, SR_3 and SR_4) requirements are considered to be 12 MW, 18 MW, 15 MW and 21MW respectively. The power ratings of WUs of each area are 4 MW. The cut in, cut out and rated wind speeds are $5ms^{-1}$, $30ms^{-1}$ and $10ms^{-1}$ respectively. The cost coefficients, emission

coefficients, real power generation capacity constraints and POZ of TUs are tabulated in Table 4.11. The cost coefficients and real power generation capacity constraints of WUs are given in Table 4.12 and area-wise Weibull parameters are given in Table 4.13. Tie line capacities are given in Table 4.14. The data in Table 4.11, 4.12, and 4.14 are given in p.u. considering the system base as 100 MVA.

Table 4.11

Data of TUs (p.u.)

TU	Cost coefficient data					Emission coefficient data					Real power generation capacity constraints		POZ
	a_{Gij}	b_{Gij}	c_{Gij}	d_{Gij}	e_{Gij}	α_{Gij}	β_{Gij}	γ_{Gij}	η_{Gij}	δ_{Gij}	P_{Gij}^{min}	P_{Gij}^{max}	
G_{11}	**150**	**189**	**0.50**	**11**	**40**	**0.016**	**-1.50**	**23.333**	**0.1310**	**0.5690**	**0.0005**	**0.14**	**-**
G_{12}	**115**	**200**	**0.55**	8	**46**	**0.031**	**-1.82**	**21.022**	**0.0914**	**0.4540**	0.0005	**0.10**	**-**
G_{13}	**40**	**350**	**0.60**	10	**42**	**0.013**	**-1.25**	**22.050**	**0.0993**	**0.4060**	0.0005	**0.13**	**-**
G_{14}	**122**	**315**	**0.50**	9	**44**	**0.012**	**-1.36**	**22.313**	**0.0655**	**0.2846**	0.0005	**0.12**	**-**
G_{21}	**125**	**305**	**0.50**	17	**30**	**0.020**	**-1.90**	**21.313**	**0.0503**	**0.2075**	0.0005	**0.25**	**-**
G_{22}	**70**	**275**	**0.70**	9	**44**	**0.007**	**0.805**	**23.001**	**0.0914**	**0.4540**	0.0005	**0.12**	**-**
G_{23}	**70**	**345**	**0.70**	15	**35**	**0.015**	**-1.40**	**24.003**	**0.0200**	**0.0285**	0.0005	**0.20**	**-**
G_{24}	**70**	**345**	**0.70**	14	**37**	**0.018**	**-1.80**	**25.121**	**0.0500**	**0.0333**	0.0005	**0.18**	**-**
G_{31}	**130**	**245**	**0.50**	20	**25**	**0.019**	**-2.00**	**25.121**	**0.1012**	**0.0667**	0.0005	**0.30**	**0.20-0.25**
G_{32}	**130**	**245**	**0.50**	20	**25**	**0.012**	**-1.36**	**22.990**	**0.0358**	**0.0266**	0.0005	**0.30**	0.20-0.25
G_{33}	**135**	**235**	**0.55**	20	**25**	**0.033**	**-2.10**	**27.010**	**0.1533**	**0.0897**	0.0005	**0.30**	0.20-0.25
G_{34}	**200**	**130**	**0.45**	20	**25**	**0.018**	**-1.80**	**25.101**	**0.0443**	**0.0287**	0.0005	**0.30**	0.20-0.25
G_{41}	**70**	**345**	**0.70**	8.5	**45**	**0.018**	**-1.81**	**24.313**	**0.0273**	**0.0289**	0.0005	**0.11**	**-**
G_{42}	**45**	**389**	**0.60**	15	**35**	**0.030**	**-1.92**	**27.119**	**0.0347**	**0.0215**	0.0005	**0.20**	**-**
G_{43}	**75**	**355**	**0.60**	20	**25**	**0.020**	**-1.20**	**30.110**	**0.0469**	**0.0282**	0.0005	**0.30**	0.20-0.25
G_{44}	**100**	**370**	**0.80**	20	**25**	**0.040**	**-1.40**	**22.500**	**0.0114**	**0.0805**	0.0005	**0.30**	0.20-0.25

Table 4.12

Data of WUs (p.u)

WU	Cost coefficient data			Real power generation capacity constraints	
	d_{Wik}	p_{Wik}	r_{Wik}	$P_{Wik}^{\min}$	$P_{Wik}^{\max}$
W_{11}	25	12	2	0.0005	0.04
W_{21}	18	12	2	0.0005	0.04
W_{31}	22	12	2	0.0005	0.04
W_{41}	10	12	2	0.0005	0.04

Table 4.13

Area-wise wind parameters

	θ	λ (m s^{-1})
Area 1	1.6	6.5
Area 2	2	7
Area 3	1.8	7.5
Area 4	2.2	8

Table 4.14

Tie line capacities (p.u)

Tie line	$T_{il}^{\min}$	$T_{il}^{\max}$
T_{12}	0.001	0.060
T_{13}	0.001	0.040
T_{14}	0.001	0.200
T_{23}	0.001	0.035
T_{24}	0.001	0.055
T_{34}	0.001	0.009

The cost characteristics of TUs of four areas are given in Figure. 4.14.1, 4.14.2, 4.14.3 and 4.14.4. Likewise, the emission characteristics of TUs of four areas are depicted in Figure. 4.15.1, 4.15.2, 4.15.3 and 4.15.4. The cost characteristics of WUs of each area are given in Figure. 4.16. The Weibull probability density curves of each area are represented in Figure 4.17.

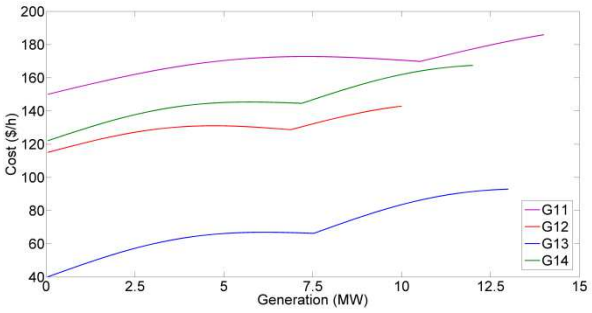

Figure 4.14.1. Cost characteristics of TUs of area 1.

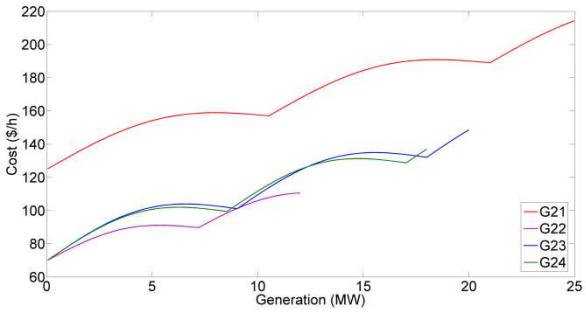

Figure 4.14.2. Cost characteristics of TUs of area 2.

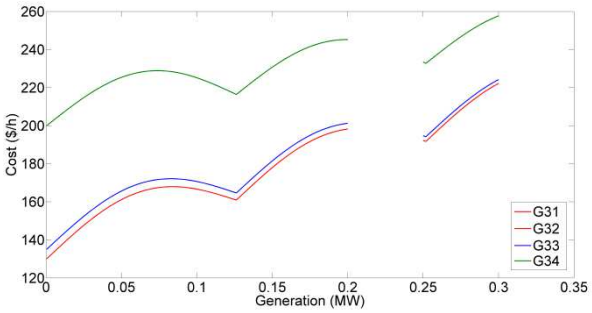

Figure 4.14.3. Cost characteristics of TUs of area 3.

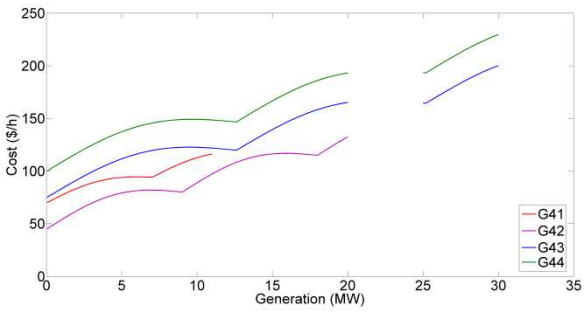

Figure 4.14.4. Cost characteristics of TUs of area 4.

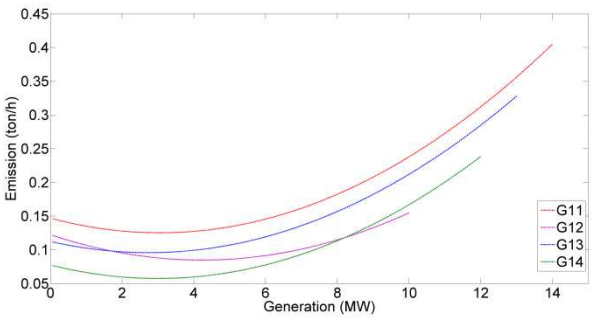

Figure 4.15.1. Emission characteristics of TUs of area 1.

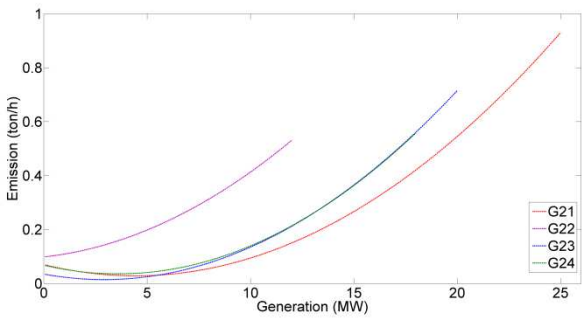

Figure 4.15.2. Emission characteristics of TUs of area 2.

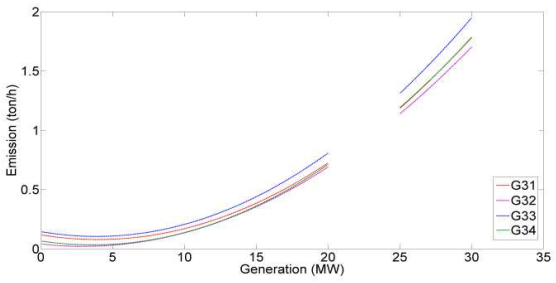

Figure 4.15.3. Emission characteristics of TUs of area 3.

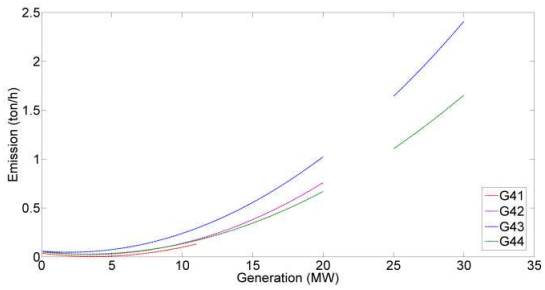

Figure 4.15.3. Emission characteristics of TUs of area 4.

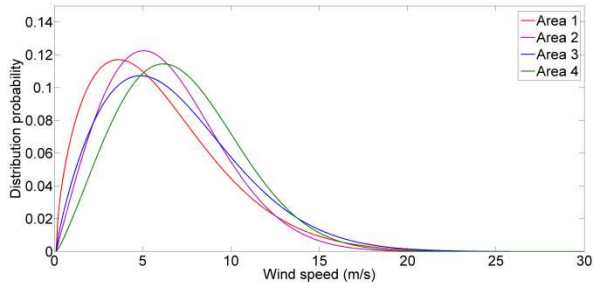

Figure 4.16. Area-wise Weibull probability density curves.

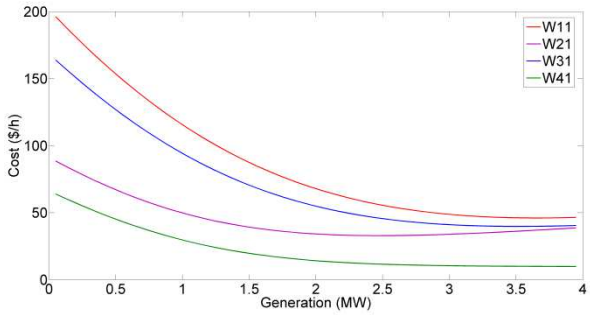

Figure 4.17. Cost characteristics of WUs.

Before solving the proposed multi-objective WMAEED problem, the effects of different parameters are analyzed using two single objective optimizations, i.e., cost minimization and emission minimization. These are solved using classical GA. The convergence characteristics up to 200 iterations are plotted in Figure 4.18 and Figure 4.19 respectively. The minimum cost obtained in the work is 2088.56 $/h and the minimum emission is 2.2710 ton/h.

The Pareto fonts obtained by the potential solutions from NSGA II and SPEA II have been depicted in Figure 4.20. From these Pareto fonts, the best compromised solutions have been chosen employing fuzzy selection method.

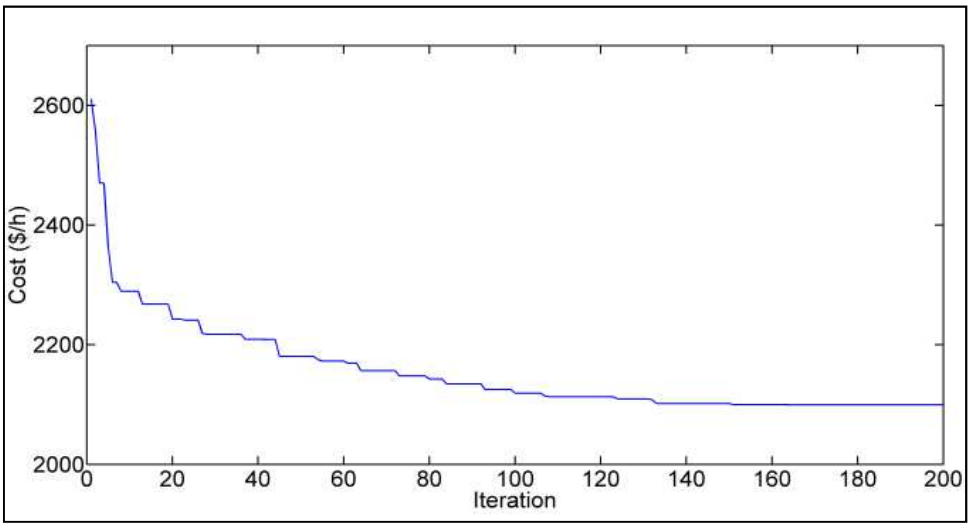

Figure 4.18. Cost convergence characteristics.

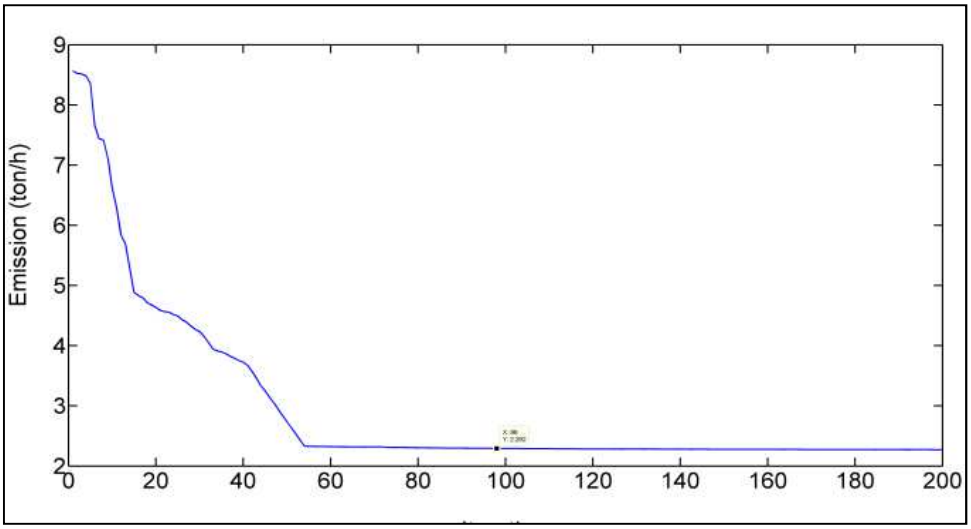

Figure 4.19. Emission convergence characteristics.

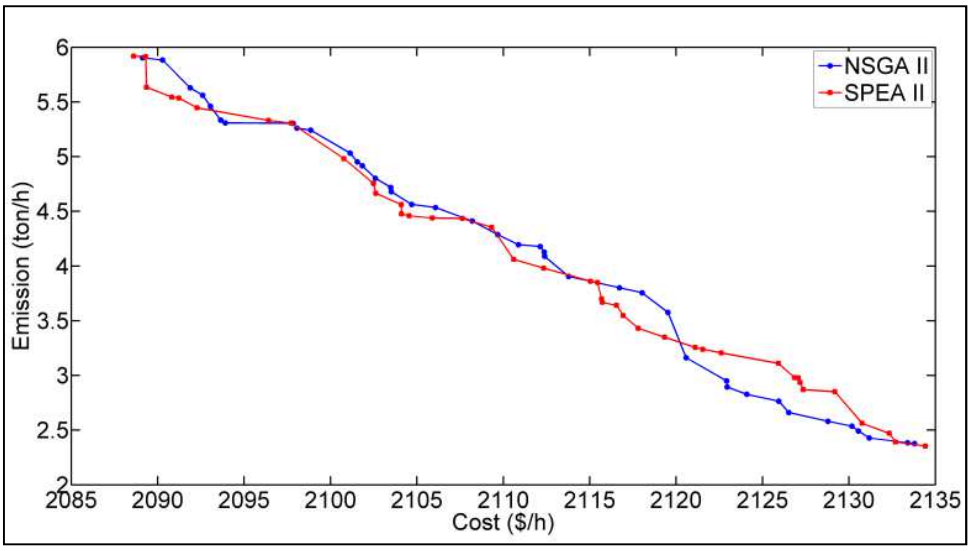

Figure 4.20. Cost-emission Pareto-front for NSGA II, SPEA II and MODE.

NSGA II has been applied to optimize both cost and emission objectives simultaneously. In this case the population size, maximum number of iterations, crossover and mutation probabilities have been selected as 20, 50, 0.9 and 0.2, respectively for this test system. It is seen that trade-off generation cost is 2126.52 $/h (1.82% higher than minimum cost, but 0.4% lesser than the cost corresponding to minimum emission) and trade-off emission level is 2.6612 ton/h (17.18% higher than minimum emission, but 55.52% lesser than the emission corresponding to minimum cost).

SPEA II has also been applied to solve WMAEED problem. In case of SPEA 2, the population size, crossover and mutation probabilities and the maximum number of iterations

have been selected as 20, 0.9, 0.2 and 50 respectively. As per the solution obtained from SPEA II, the trade-off cost is 2130.75 $/h (2.02% higher than minimum cost, but 0.21% lesser than the cost corresponding to minimum emission) and the trade-off emission is 2.5631ton/h (12.86% higher than minimum emission, but 57.16% lesser than the emission corresponding to minimum cost).

All of these obtained solutions may be considered as fair trade-offs. The particulars of these dispatch solution are tabulated in Table 4.15.

Table 4.15

Dispatch results

Dispatch particulars	Economic dispatch	Emission dispatch	NSGA II	SPEA II
P_{G11} (MW)	11.3557	10.6223	10.7582	10.2914
P_{G12} (MW)	9.8406	10	9.9705	9.985
P_{G13} (MW)	5.2021	8.6325	7.997	8.0093
P_{G14} (MW)	9.6524	10.6056	11.2437	11.1216
P_{W21} (MW)	3.7213	3.9691	3.9232	3.9458
P_{G21} (MW)	23.9455	12.5104	14.6291	13.5877
P_{G22} (MW)	11.8449	6.8151	7.747	7.2889
P_{G23} (MW)	17.7118	11.2011	12.4074	11.8145
P_{G14} (MW)	0.6841	12.3452	10.1847	11.2466
P_{W21} (MW)	2.5425	4	3.73	3.8627
P_{G31} (MW)	0.05	10.3413	8.4346	9.3718
P_{G32} (MW)	0.05	11.6008	9.4607	10.5126
P_{G33} (MW)	16.2745	9.8612	11.0494	11.4654
P_{G34} (MW)	28.0052	9.4023	12.0343	10.2491
P_{W31} (MW)	3.5874	4	3.9236	3.9611
P_{G41} (MW)	10.6365	11	10.9327	10.9658
P_{G42} (MW)	0.05	10.5753	8.6252	9.5837
P_{G43} (MW)	18.7546	7.2128	9.3512	8.3001
P_{G44} (MW)	2.2713	11.3056	9.6318	10.4545
P_{W41} (MW)	3.8199	4	3.9666	3.983
T_{12} (MW)	4.2959	0	0	0
T_{13} (MW)	-4	-1.1774	-2.7006	-2.4604
T_{14} (MW)	18.068	15.0069	16.5925	15.8129
T_{23} (MW)	-3.0671	-3.1282	-1.3019	-2.1996
T_{24} (MW)	-5.5	0	0	0
T_{34} (MW)	0.9	0.9	0.9	0.9
SR_1 (MW)	12.9492	9.1396	9.0307	9.5927
SR_2 (MW)	20.8137	32.1282	30.0319	31.0623
SR_3 (MW)	75.6203	78.7944	79.0211	78.4012
SR_4 (MW)	59.2876	50.9063	52.4592	51.6959
F_C ($/h)	2088.56	2135.15	2126.52	2130.76
F_E (lb/h)	5.9828	2.2710	2.6612	2.5631

It is noted from the results, that the obtained solutions from the multi-objective optimizers satisfy all the constraints, like, tie line capacity limits, POZ, spinning reserve and constraints related to wind power availability etc., those have been considered in the power system model.

In the works [59], [60] and [62], MAEED problem for 180 MW 4-area 16 TUs without incorporating WU have been solved. The available results in these works have been compared with the outcome of the current work, where 4 WUs are incorporated in same power system, to realize the effect of wind incorporation on overall fuel cost and emission level improvement in multi-area power system with area-wise uncertainty. The comparative results for economic dispatch and emission dispatch are tabulated in Table 4.16. These dispatch problems without considering wind generations, have been solved using particle swarm optimization (PSO) [59], differential evolution (DE) [60] and Jaya algorithm (JA) [62] respectively.

Table 4.16

Comparative results for economic dispatch and emission dispatch.

Power system	Optimizers	Economic dispatch		Emission dispatch	
		Minimum generation cost ($/h)	Corresponding emission level (lb/h)	Minimum emission level (lb/h)	Corresponding generation cost ($/h)
180 MW 4-area 16 TUs	PSO [59]	2166.82	3.3152	3.2301	2178.20
	DE [60]	2136.95	6.5383	2.4725	2178.28
	JA [62]	2135.99	5.8157	2.4429	2177.55
180 MW 4-area 16 TUs and 4 WUs	GA	2088.56	5.9828	2.2710	2135.15

It is evident from Table 4.16 that incorporation of WUs in a multi-area power system efficiently reduces both the generation cost and emission level with proper dispatch planning and effective management of wind power and other uncertainty. After integration of 4 WUs in the same 180 MW 4-area 16 TUs system, the minimum generation cost reduces to 3.61% of [59], 2.26% of [60] and 2.22% of [62] and the minimum emission level reduces to 29.69% of [59], 8.15% of [60] and 7.04% of [62].

The comparative results for trade-off solutions are tabulated in Table 4.17. These dispatch problems, without considering wind generations, have been solved using differential evolution with fuzzy selection (DEFS) [60] and improved gradient-based JA (IGJA) would [62] respectively.

Table 4.17

Comparative results for trade-off solutions.

Power system	**Optimizers**	**Trade-off generation cost ($/h)**	**Average trade-off generation cost ($/h)**	**Trade-off emission level (lb/h)**	**Average trade-off emission level (lb/h)**
180 MW 4-area 16 TUs	DEFS [60]	2161.70	2156.70	3.0873	3.0585
	IGJA [62]	2151.69		3.0297	
180 MW 4-area 16 TUs and 4 WUs	NSGA II	2126.52	2128.64	2.6612	2.6122
	SPEA II	2130.76		2.5631	

From Table 4.17 it is noted that the average trade-off generation cost of WUs integrated system appears to be 1.3% lesser than that of the power system without WU integration and the average trade-off emission level of WUs integrated system is 14.59% lesser than that of the power system without WU integration.

4.4.2. Conclusion

This work proposes a wind power integrated multi-area economic environmental dispatch model. The non-convexity and discontinuity of cost minimization and emission minimization objectives due to valve point effects and prohibited operating zones for thermal power generating units have been considered. Different realistic constraints, like power balance, generation limitations and power transmission limitations through tie-lines between areas have been included in the model. Constraints related to area-wise uncertainty of wind power availability following Weibull probability density function and penalties for over-commitment or under-estimation of wind power production have also been incorporated in the system model. The penalty cost is introduced in the model to intensify the motivation of apposite utilization of wind power by the power operators. To find reasonable trade-offs between the power production cost and the emission level in multi-area power system in the

presence of emission less wind power plants, different recognized multi-objective optimizer, like, NSGA II and SPEA II have been employed. The potential trade-off solutions have been procured on the basis of best compromised selection guided by fuzzy logic. The numerical studies have portrayed, with optimal area-wise wind integration to the conventional multi-area power system, 2.7% of on average generation cost is reduced in respect of cost minimization and 14.96% of on average emission level is reduced in respect of emission minimization. In view of the high penetration of clean wind power in global energy sector, it can be concluded that this type of wind integrated large scale multi-area power dispatch modeling is going to be highly relevant power system operational strategy in near future.

4.5. Numerical Study on short term hydro-thermal scheduling

The hydrothermal generation planning using improved RCGA (i.e. IRCGA) and the RCGA has been realized through MATLAB R2013a on windows 7 environment having particulars: Intel core i7 processor, RAM of 80 GB, 1600 MHz clock speed and 3 GHz frequency value. In this work, four cases with different test systems have been selected. For first three cases, optimization parameters like maximum number of iteration, population size, crossover, and mutation probabilities have been considered as 300, 50, 0.9, and 0.2 respectively for both IRCGA and RCGA. For the fourth case, maximum number of iteration, population size, crossover, and mutation probabilities have been chosen 900, 50, 0.9, and 0.2 respectively for both IRCGA and RCGA.

4.5.1. Case I

For this case, a test system consisting of multi-chain cascade of four reservoir containing hydro plants and an equivalent thermal plant has been considered. Here, scheduling period has been planned for 24 hours (i.e. 1 day). The scheduling period has been divided into 24 equal intervals. Detailed parameters for this system have been referred from [109]. Optimal hourly hydro discharge rates and total hydrothermal power generation obtained through the developed IRCGA have been tabulated in Table 4.18 and Table 4.19 respectively. The reservoir storage volumes of four hydro plants as acquired through the IRCGA have been demonstrated in Fig. 4.21. The best, average and the worst costs, and average CPU time among 100 runs of solutions obtained from the IRCGA and the RCGA have been tabulated in Table 4.20. Data corresponding to the generation costs from MDE [237], IPSO [116], TLBO [122], IFEP [102], and GA [109] techniques have also been mentioned in the Table 4.20.

Fig. 4.22 shows hourly optimal hydro discharge of test system-1 and Fig. 4.23. is for hourly optimal hydrothermal generation (MW) of test system-1.

The cost convergence characteristics acquired from the developed IRCGA and the RCGA are in accordance to Fig. 4.24. It has been observed from the Table 4.20 that the cost found from the IRCGA is the lowest among all techniques.

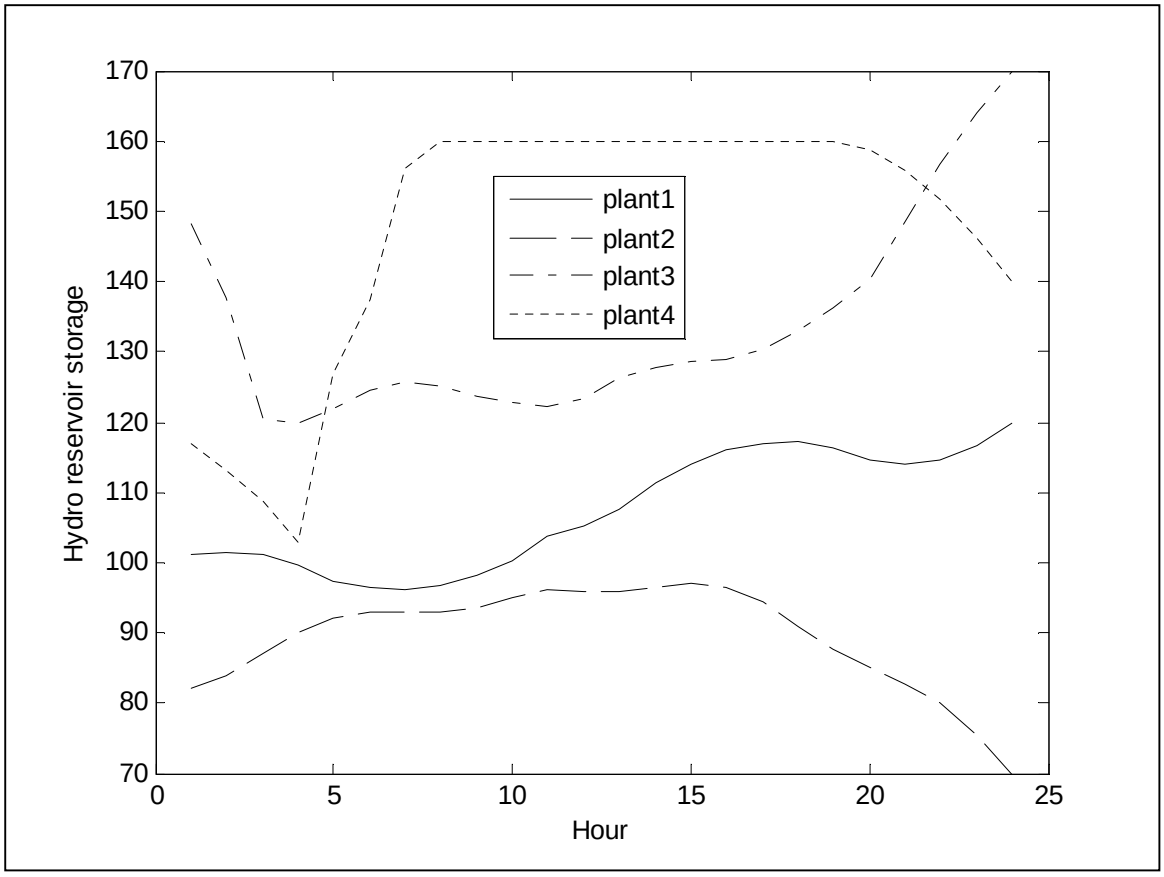

Figure 4.21. Reservoir storage volume for test system-1 incorporating head mobility.

Table 4.18

24 hours water discharge ($\times 10^4$ m^3) for test system-1 incorporating head mobility

Hour	$\mathbf{Q_{h1}}$	$\mathbf{Q_{h2}}$	$\mathbf{Q_{h3}}$	$\mathbf{Q_{h4}}$
1	8.7861	6.0009	30.0000	6.0000
2	8.6477	6.0001	18.5747	6.0000
3	8.5682	6.0000	29.9998	6.0000
4	8.3775	6.0006	17.3534	6.0008
5	8.1550	6.0000	15.4229	6.0005
6	8.0533	6.0030	15.9130	7.9993

7	8.1591	6.0910	15.9792	11.1179
8	8.4589	6.8847	16.5977	13.6690
9	8.6193	7.4527	16.4652	15.3635
10	8.7715	7.6903	16.5940	16.1257
11	8.5801	7.7683	17.1467	15.7670
12	8.6525	8.1049	16.8463	16.5977
13	8.5011	8.2039	17.4470	16.4653
14	8.3269	8.3350	17.8223	16.5934
15	8.2464	8.4235	18.7109	17.1544
16	8.0697	8.7110	18.4832	16.8390
17	8.0004	9.0106	16.9627	17.4464
18	7.8467	9.4610	15.9095	17.8224
19	7.8246	10.1045	14.5644	18.8539
20	7.7368	10.6701	13.8283	19.6055
21	7.5925	11.2530	11.0169	19.9997
22	7.3682	11.7971	11.5735	19.9999
23	6.9536	12.6091	12.0326	19.9999
24	6.7040	13.4245	12.5674	19.9998

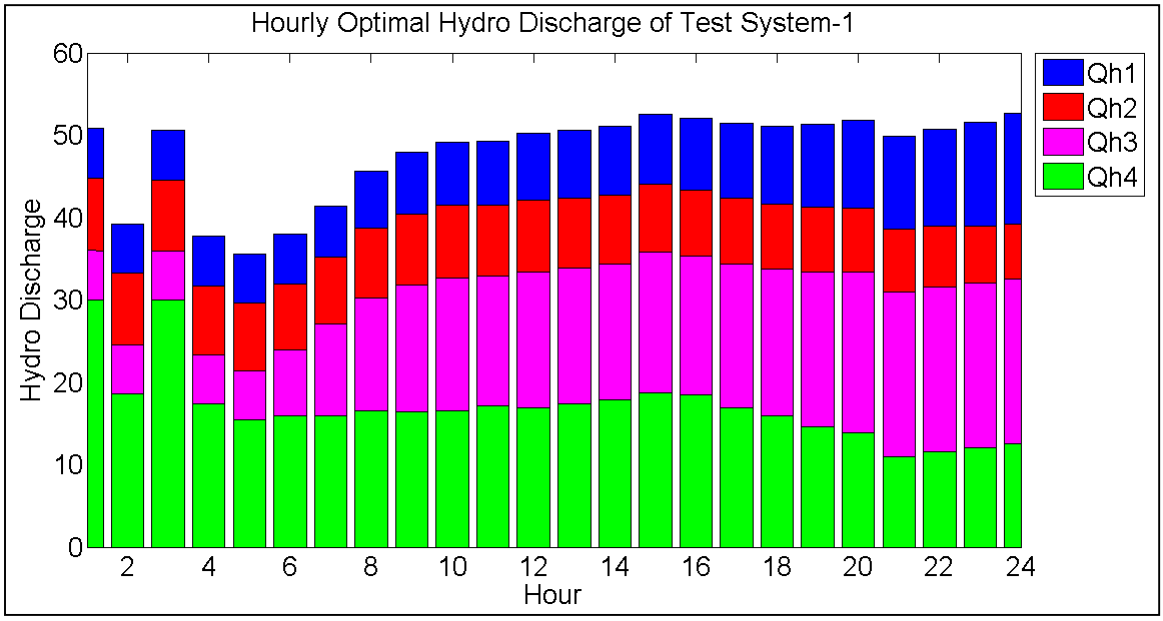

Figure 4.22. Hourly optimal hydro discharge of test system-1

Table 4.19

Optimal hydrothermal power generation (MW) schedule for test system-1 incorporating head mobility

Hour	P_{h1}	P_{h2}	P_{h3}	P_{h4}	P_s
1	79.7973	49.0061	0.0000	131.8801	1109.32
2	79.3927	50.1639	43.5292	129.0270	1087.89
3	79.0387	51.2957	0.0000	125.7437	1103.92
4	77.7373	52.9380	37.4242	121.6365	1000.26
5	75.9674	54.4995	42.2628	115.8283	1001.44
6	74.6619	55.5248	42.0011	163.8960	1073.92
7	74.9610	56.6535	42.7802	209.7731	1265.83
8	76.6787	62.1650	41.6644	252.8746	1566.62
9	77.7838	65.9683	41.8104	271.8340	1782.60
10	79.1114	67.7564	40.9661	278.4111	1853.75
11	78.7489	68.9033	38.9557	275.1930	1768.19
12	80.1994	71.5905	39.5975	282.2694	1836.34
13	79.6781	72.1369	38.3010	281.2003	1758.68
14	79.2573	72.8195	38.1722	282.2342	1727.52
15	79.5884	73.6734	35.5391	286.6439	1654.55
16	78.9796	75.6289	36.7765	284.1818	1594.43
17	78.8516	76.9618	41.8592	288.8606	1643.46
18	77.9593	78.3512	45.1334	291.6388	1646.92
19	77.8291	79.6915	48.4354	298.8079	1735.23
20	77.0919	80.4924	50.2710	303.4720	1768.67
21	75.8005	81.3147	51.4605	304.7025	1726.72
22	74.1001	81.9619	53.9109	301.5554	1608.47
23	71.1238	82.8437	56.0420	297.2275	1342.77
24	69.4655	81.8843	57.7491	291.3201	1089.58

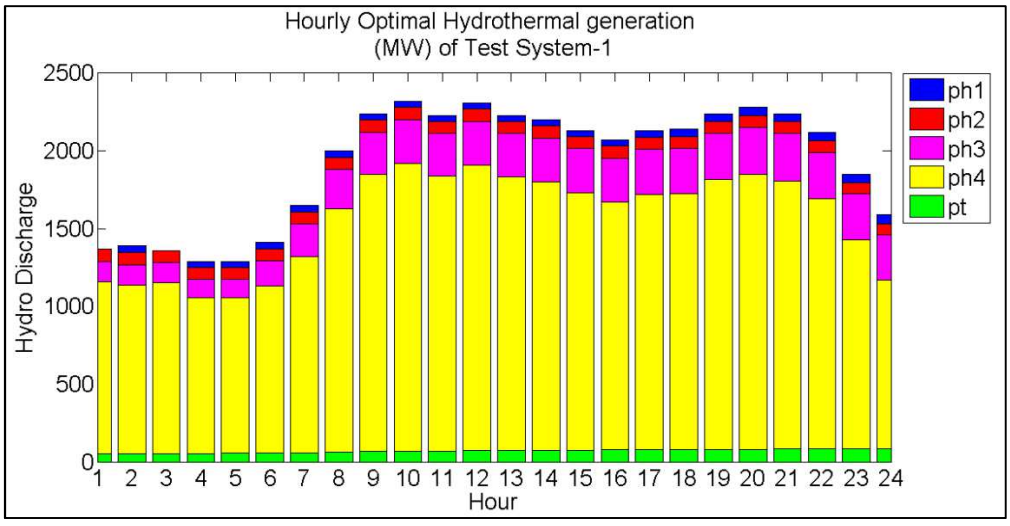

Figure 4.23. Hourly optimal hydrothermal generation (MW) of test system-1.

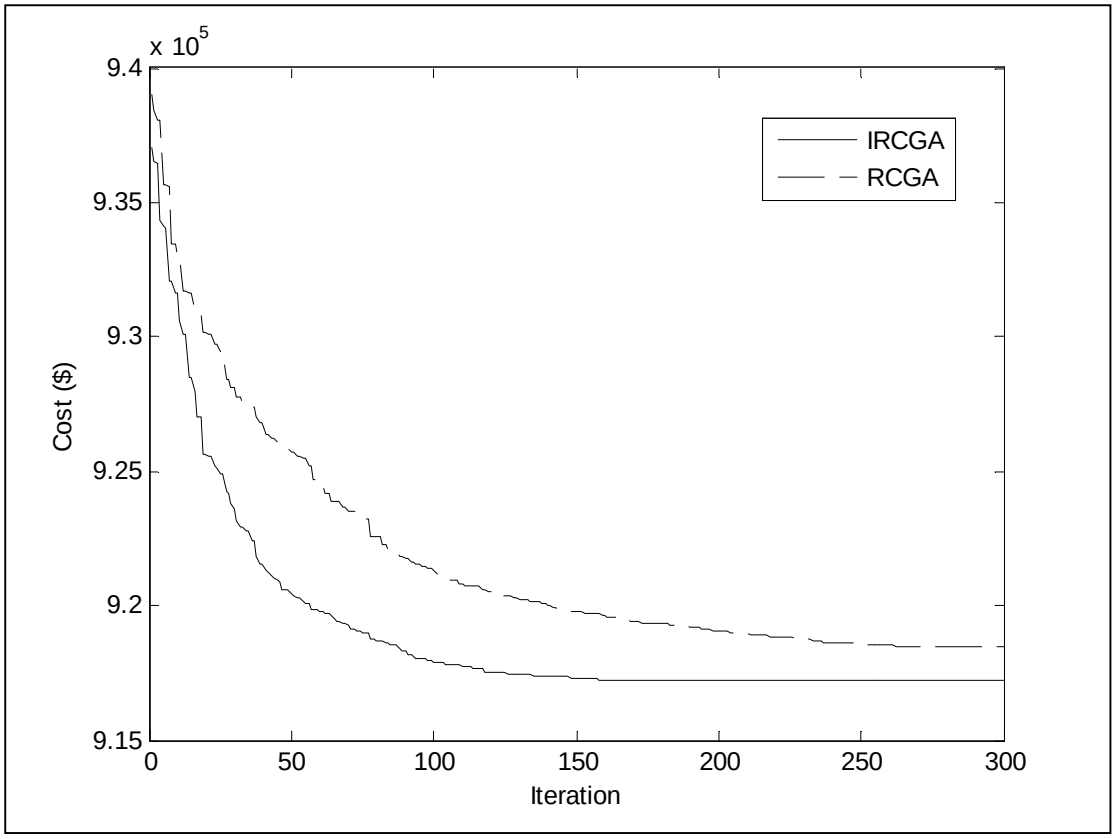

Figure 4.24. Cost convergence curve for test system-1 with head mobility.

Table 4.20
Comparative study of different techniques for test system-1incorporating head mobility.

Technique	Best cost ($)	Average cost ($)	Worst cost ($)	CPU time (s)
IRCGA	917199.44	917208.56	917221.37	257.03
RCGA	918480.03	918494.37	918504.47	256.75
TLBO [122]	922373.39	922462.24	922873.81	-
IPSO [116]	922553.49	-	-	-
MDE [237]	922556.44	-	-	-
IFEP [102]	930129.82	930290.13	930881.92	1033.2
GA [109]	926707	-	-	-

4.5.2. Case II

In this case, restricted operating section for hydro plant, and effect of valve point loading for thermal generator have been considered. Detailed parameters for this case have been taken from [102]. Table 4.21 and Table 4.22 show the optimal hourly discharge rates and

total hydrothermal generation acquired by the developed IRCGA respectively. Figure 4.25 shows the reservoir storage volume of four hydro plants acquired from the IRCGA. The best, average and the worst costs (in $) and average CPU time among 100 runs of solutions acquired from developed IRCGA and the RCGA have been summarized in Table 4.23.The cost values acquired from IFEP [102], IPSO [116] and TLBO [122] techniques have also been shown in Table 4.23. Fig. 4.26 shows hourly optimal hydro discharge of test system-2 and Fig. 4.28 is for hourly optimal hydrothermal generation (MW) of test system-2.

The cost convergence characteristics acquired from developed IRCGA and the RCGA have been demonstrated in Fig. 4.28. It can be seen from Table 4.23 that the cost found from the IRCGA is the lowest among all techniques.

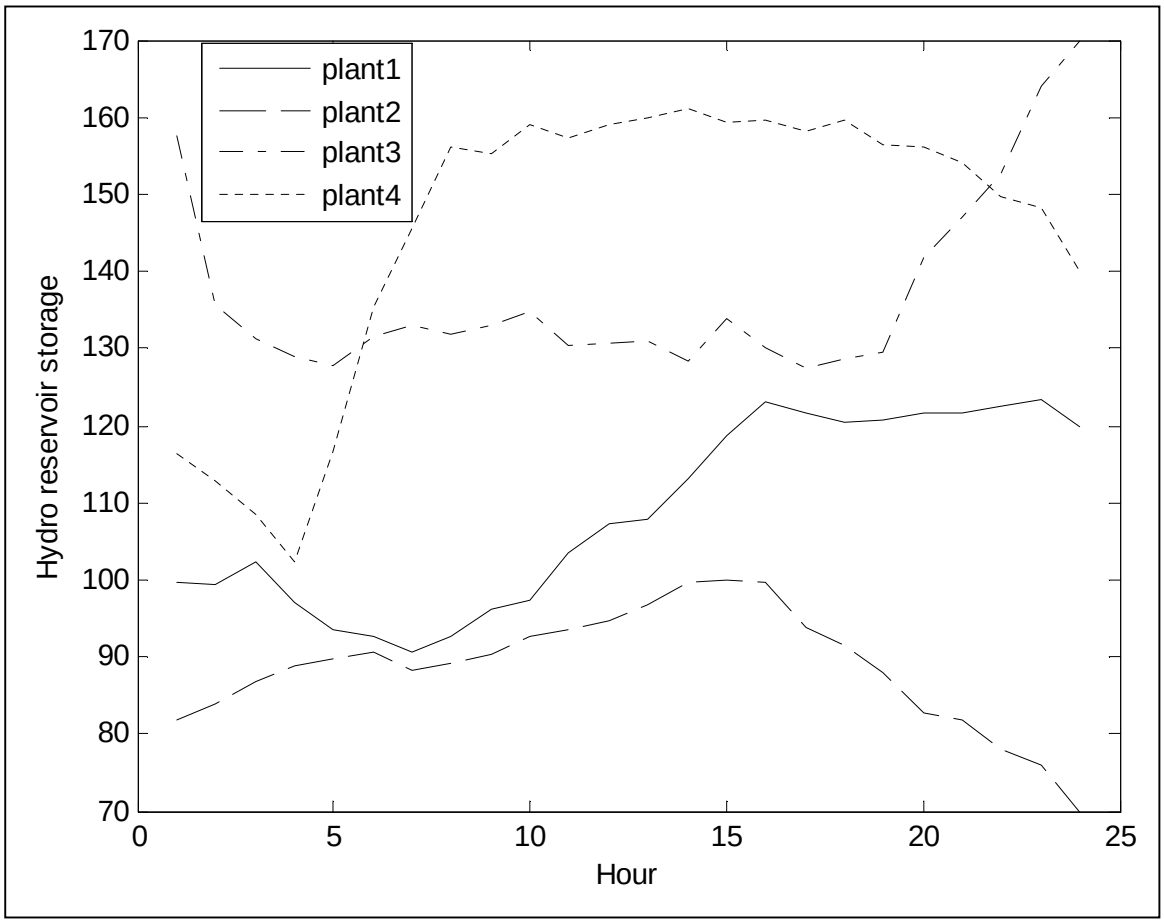

Figure 4.25. Reservoir storage volume for test system-2 incorporating head mobility.

Table 4.21

Water discharge ($\times 10^4$ m^3) in 24 hours for test system-2 incorporating head mobility.

Hour	Q_{h1}	Q_{h2}	Q_{h3}	Q_{h4}
1	10.1845	6.1121	20.5536	6.3438
2	9.3545	6.0000	29.9857	6.0059
3	5.0934	6.0672	18.8188	6.0081
4	12.3025	6.9922	19.7814	6.0011
5	9.4396	6.9832	15.2970	6.3376
6	7.8835	6.3622	18.4255	11.1545
7	10.2721	8.2105	18.0212	8.7499
8	6.7694	6.0283	17.9212	9.3215
9	6.6014	6.9949	16.6465	15.9994
10	9.8394	6.6298	14.1732	14.6373
11	5.8365	8.0881	17.9684	19.8695
12	6.2467	6.7252	18.3894	15.9965
13	10.4311	6.0065	16.4035	15.9976
14	6.7118	6.0342	19.8262	13.0358
15	5.2117	8.9019	14.7661	19.6512
16	5.8669	8.0785	18.5218	18.0045
17	10.3436	13.0473	15.8221	18.0241
18	9.0289	8.2601	15.6486	18.1861
19	6.8068	10.6257	18.4059	18.1376
20	5.0351	13.1212	10.7805	18.6221
21	7.2673	9.9088	11.9574	18.0174
22	7.0480	12.8178	11.9622	20.0000
23	7.9655	10.0050	10.1140	19.8378
24	13.2600	13.2228	11.6386	19.6248

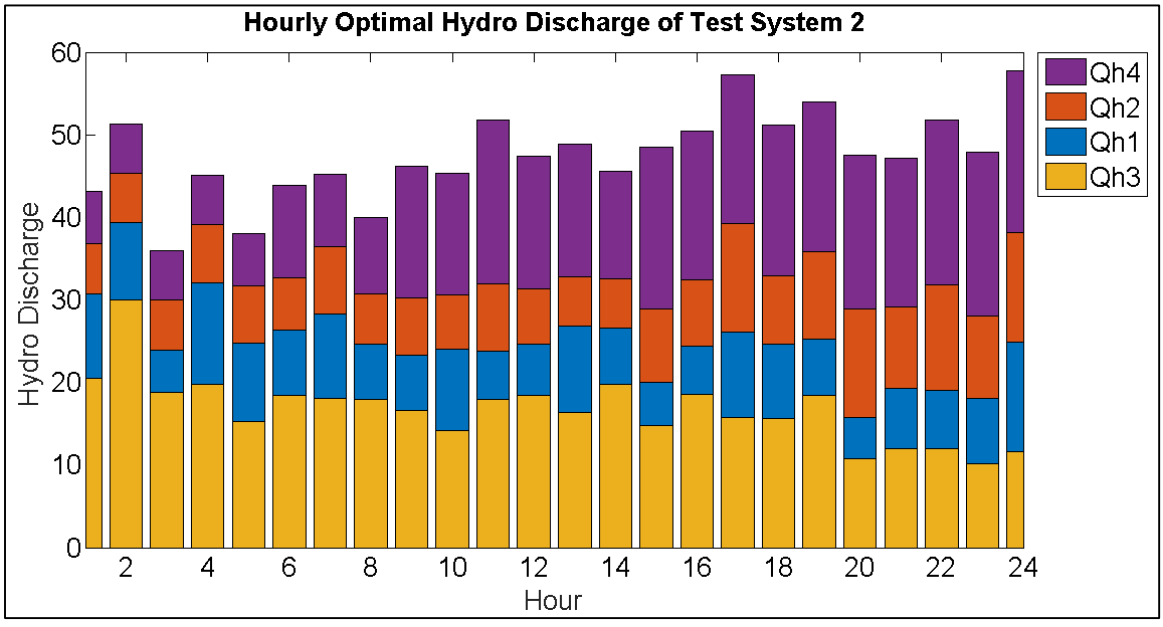

Figure 4.26. Hourly optimal hydro discharge for test system-2.

Table 4.22
Optimal hydrothermal power generation (MW) scheduling for test system-2 incorporating head mobility

Hour	P_{h1}	P_{h2}	P_{h3}	P_{h4}	P_s
1	86.8344	49.7921	42.4872	136.4915	1054.39
2	82.7927	50.0996	0.0000	128.7959	1128.31
3	53.2023	51.7131	38.206	125.5285	1091.35
4	95.3572	59.6889	32.3296	121.2998	981.32
5	82.2469	60.7180	45.8186	119.8371	981.38
6	72.3219	57.0068	36.5382	189.8853	1054.25
7	84.3272	69.3217	39.5418	180.8054	1276.01
8	63.8671	53.8113	40.4187	196.2406	1645.66
9	63.4079	61.0171	43.8752	273.675	1798.02
10	83.801	59.0764	48.8933	261.1712	1867.06
11	58.8915	69.7213	40.9075	304.3079	1756.17
12	63.6159	61.3895	37.7617	274.8044	1872.42
13	90.3650	56.9064	44.1043	276.5894	1762.03
14	68.1055	58.034	32.0219	249.5939	1792.24
15	56.4505	78.0365	46.5805	304.8704	1644.06
16	62.7673	73.2219	38.5827	292.2578	1603.17
17	93.8183	96.3354	45.1644	292.7708	1601.91
18	86.3257	71.3305	44.6121	292.334	1645.39
19	70.6874	82.4647	36.9713	293.5957	1756.28
20	55.3803	89.5719	48.3725	293.5926	1793.08
21	74.3523	73.9104	52.4342	289.3438	1749.96
22	72.6529	84.7098	53.7410	299.7932	1609.10
23	79.4951	71.3102	53.2242	294.2187	1351.75
24	104.9608	81.7733	57.2461	291.4408	1054.58

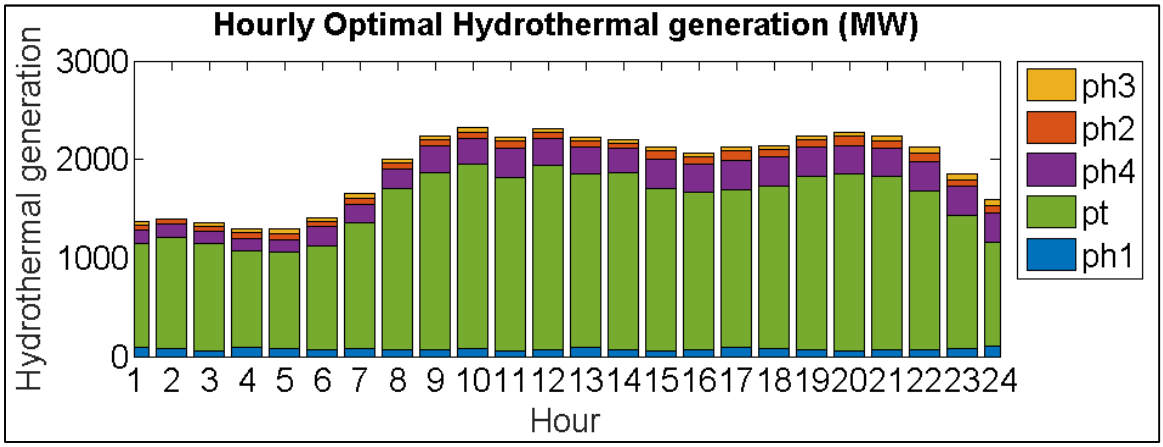

Figure 4.27. Hourly optimal hydrothermal generation (MW) for test system-2.

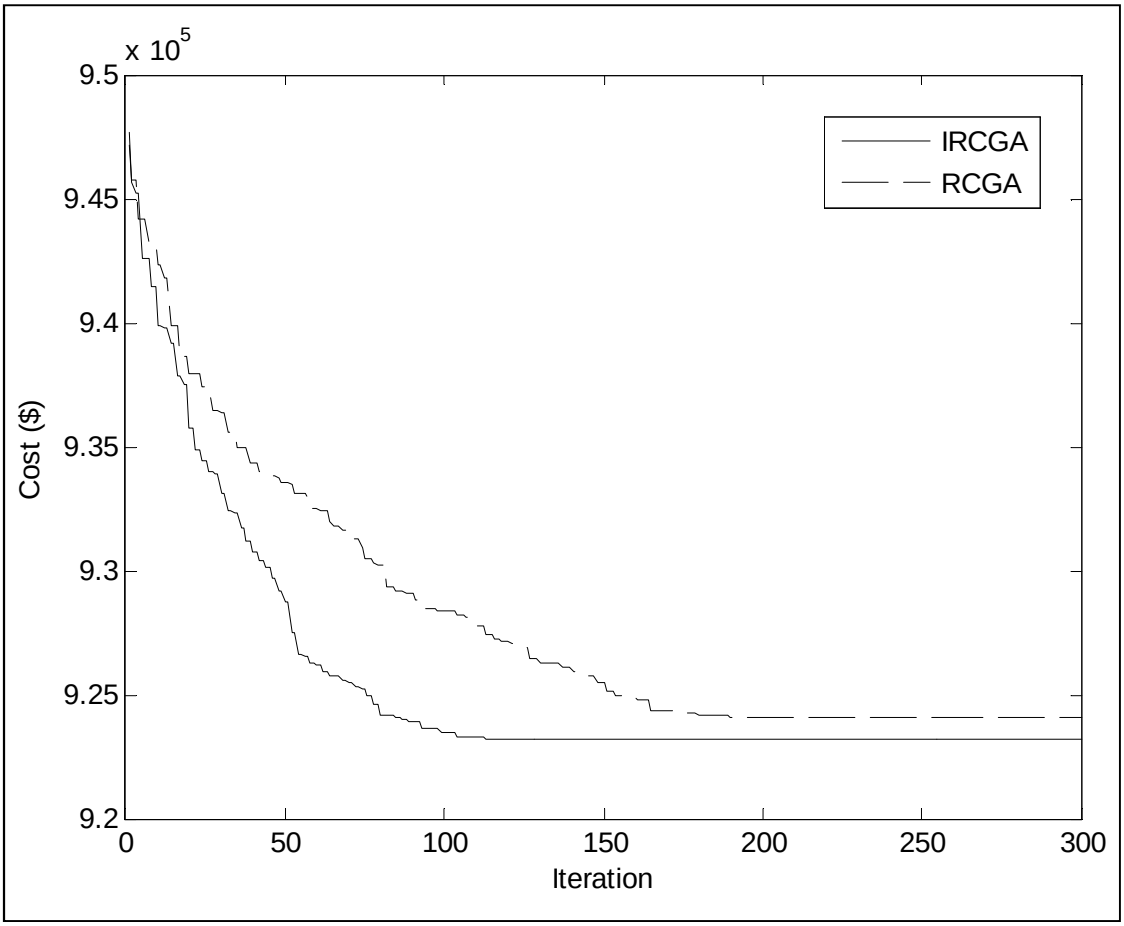

Figure 4.28. Cost convergence curves for test system-2 incorporating head mobility.

Table 4.23
Comparative study of different techniques for test system-2 incorporating head mobility

Technique	Best cost ($)	Average cost ($)	Worst cost ($)	CPU time (s)
IRCGA	923230.63	923242.45	923255.37	264.73
RCGA	924069.73	924083.56	924096.28	258.65
IFEP [102]	933949.25	938508.87	942593.02	1450.9
TLBO [122]	924550.78	924702.43	925149.06	-
IPSO [116]	925978.84	-	-	-

4.5.3. Case III

Here, a multi-chain cascaded four reservoir containing hydro plants and three thermal plants have been considered. The effect of valve point loading has also been taken into consideration. Transmission loss has also been incorporated. Detailed parameters for this case have been taken from [102]. Table 4.24 and Table 4.25 demonstrate optimal hourly discharge rates and hydrothermal generation acquired by the developed IRCGA respectively.

Figure 4.29 shows reservoir storage volume of each hydro plant as acquired from the IRCGA. The best, average and the worst costs (in $), and average CPU time (in s) among 100 runs of solutions as acquired from developed IRCGA and the RCGA have been summarized in Table 4.26. The cost acquired from MDE [237], CSA [120], and TLBO [122] is in accordance to Table 4.26. Fig. 4.30 shows hourly optimal hydro discharge of test system-3 and Fig. 4.31 is for hourly optimal hydrothermal generation (MW) of test system-3.

The cost convergence characteristics acquired from the developed IRCGA and the RCGA have been shown in Figure 4.31. It is observed from Table 4.26 that the cost found from the developed IRCGA is the lowest among all techniques.

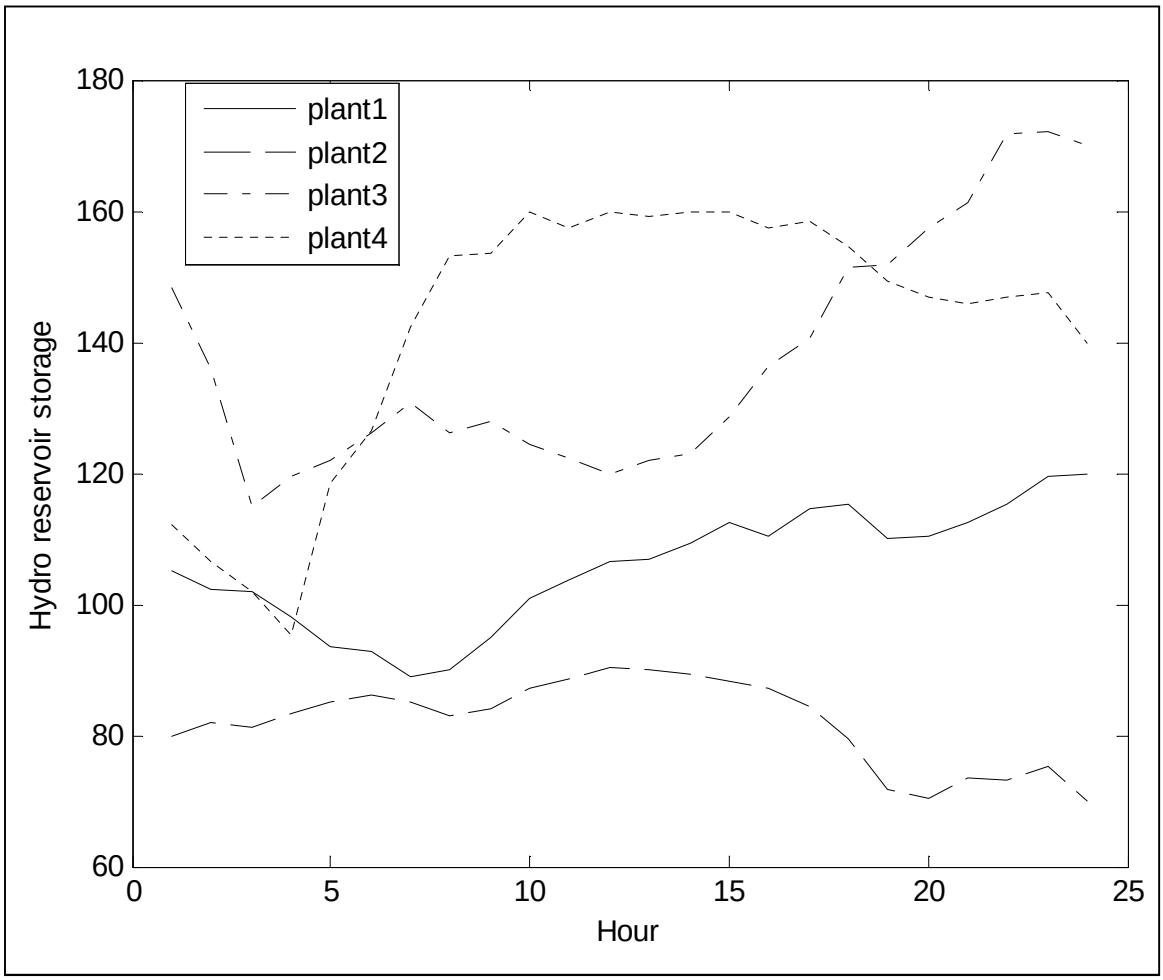

Figure 4.29. Reservoir storage volume for test system-3 incorporating head mobility.

Table 4.24
Water discharge ($\times 10^4$ m^3) in 24 hours for test system-3 incorporating head mobility

Hour	Q_{h1}	Q_{h2}	Q_{h3}	Q_{h4}
1	5.0000	8.1694	29.9825	10.6846
2	11.8249	6.0349	20.3834	8.1109
3	8.2756	9.3968	29.9993	6.0699
4	10.6764	7.1839	17.4356	6.5270
5	10.7913	6.1217	14.9166	7.0655
6	7.5122	6.0114	19.9168	12.2241
7	11.8929	7.1014	16.4236	14.2319
8	8.0364	8.9342	19.9639	6.3860
9	5.0000	7.0265	17.2913	14.8253
10	5.2012	6.0000	19.6801	13.3341
11	9.0382	7.4124	16.8647	18.8811
12	7.1895	6.083	16.7021	17.6400
13	10.756	8.4874	17.0601	18.0055
14	9.6444	9.6666	16.3546	18.8809
15	7.5333	10.1478	14.5476	16.8217
16	12.2331	9.0725	12.3182	19.4624
17	5.0001	9.8397	14.7639	16.0024
18	6.9996	10.8825	13.7793	20.0000
19	12.3816	14.8071	14.5850	20.0000
20	5.7002	9.2668	12.3534	14.4891
21	5.0013	6.0008	21.3704	15.8796
22	5.0078	9.1880	11.7756	12.9617
23	5.0002	6.0045	15.2021	13.6869
24	9.3038	13.1606	12.9722	19.9519

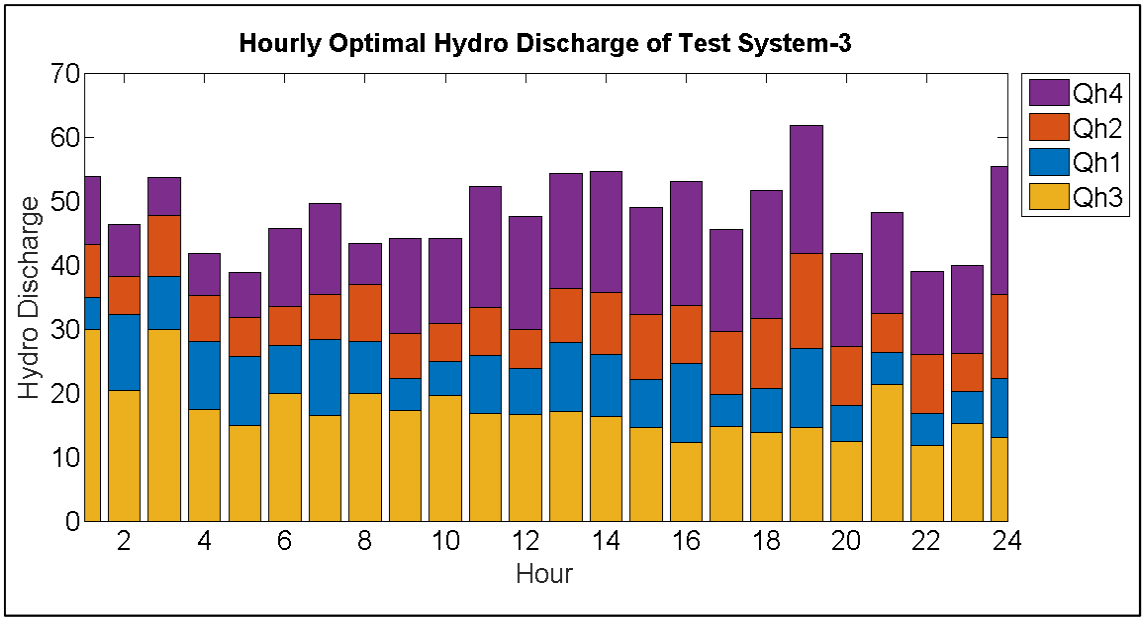

Figure 4.30. Hourly optimal hydro discharge for test system-3.

Table 4.25

Optimal hydrothermal power generation (MW) scheduling for test system-3 incorporating head mobility

Hour	P_{h1}	P_{h2}	P_{h3}	P_{h4}	P_{s1}	P_{s2}	P_{s3}
1	52.5001	62.9911	0.0000	188.4124	20.0000	40.0470	409.0353
2	94.9645	49.1472	36.0943	151.4483	20.0001	294.708	139.9935
3	77.4693	70.7940	0.0000	120.2516	174.9999	40.0626	229.7881
4	89.6264	57.8274	34.8294	121.7495	174.9999	40.0144	140.0427
5	88.6817	51.7208	43.1194	121.7213	20.0713	209.8746	139.7717
6	69.9013	51.9834	27.7926	202.2525	20.0027	294.7478	139.7384
7	90.041	59.9969	42.2954	229.2022	102.8131	294.9635	140.0704
8	71.5381	70.3084	31.274	155.4249	175.0000	294.7975	229.5029
9	49.9772	57.7790	39.9087	261.0326	174.9942	294.736	229.4873
10	53.0657	51.3073	31.4504	247.0815	102.6427	294.7893	319.319
11	81.4462	62.5231	40.4364	298.9633	20.0014	294.7375	319.3074
12	70.7288	54.3802	40.1454	287.9098	102.6722	294.7042	319.2878
13	91.5678	70.9632	38.1093	292.8062	20.0158	294.6822	319.319
14	86.4941	77.0705	40.8922	298.1207	102.6981	294.7381	139.8472
15	74.3655	79.0482	45.0727	283.9845	102.6488	294.7742	139.7885
16	98.9002	72.9424	48.6283	302.6975	20.0008	298.7904	229.5013
17	54.2296	76.2645	49.2103	274.8114	174.9981	294.7637	139.6912
18	71.4333	79.2985	51.6777	304.2234	102.6951	294.7382	229.7389
19	100.2199	87.8464	53.8828	300.4273	102.7774	294.7563	140.0848
20	60.3478	63.3576	55.0328	254.1731	20.0000	294.7757	319.3300
21	54.2311	42.9424	34.5069	264.0216	175.0000	40.0042	319.0230
22	54.5201	64.1698	56.8181	236.6617	20.0000	294.7116	139.6709
23	54.7321	44.8122	58.1308	244.4422	20.0024	294.6434	139.7895
24	87.5753	80.9892	59.3598	292.6200	20.0004	125.0043	139.8794

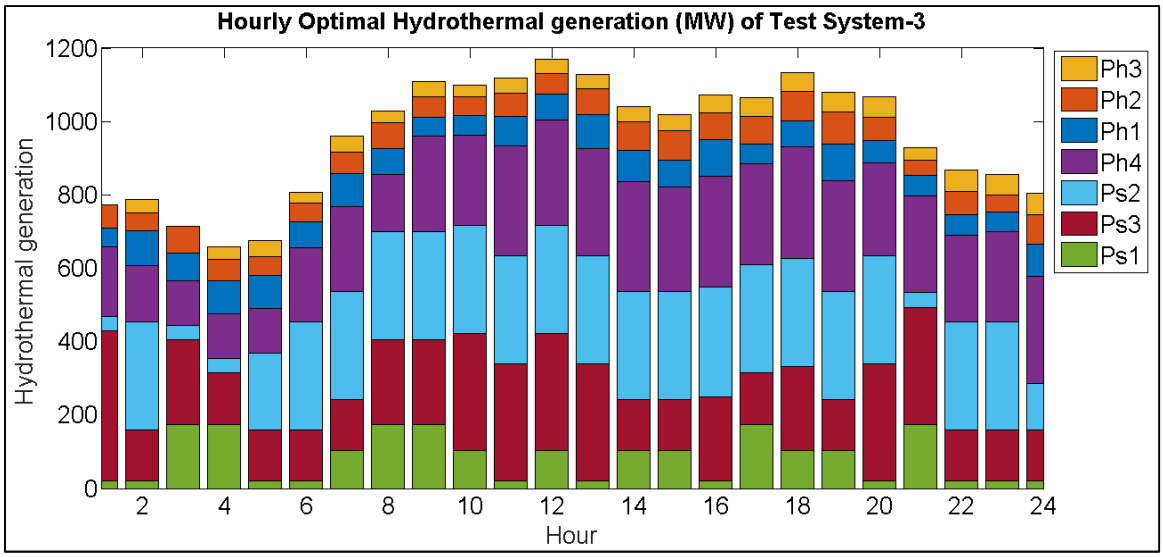

Figure 4.31. Hourly optimal hydrothermal generation (MW) for test system-3.

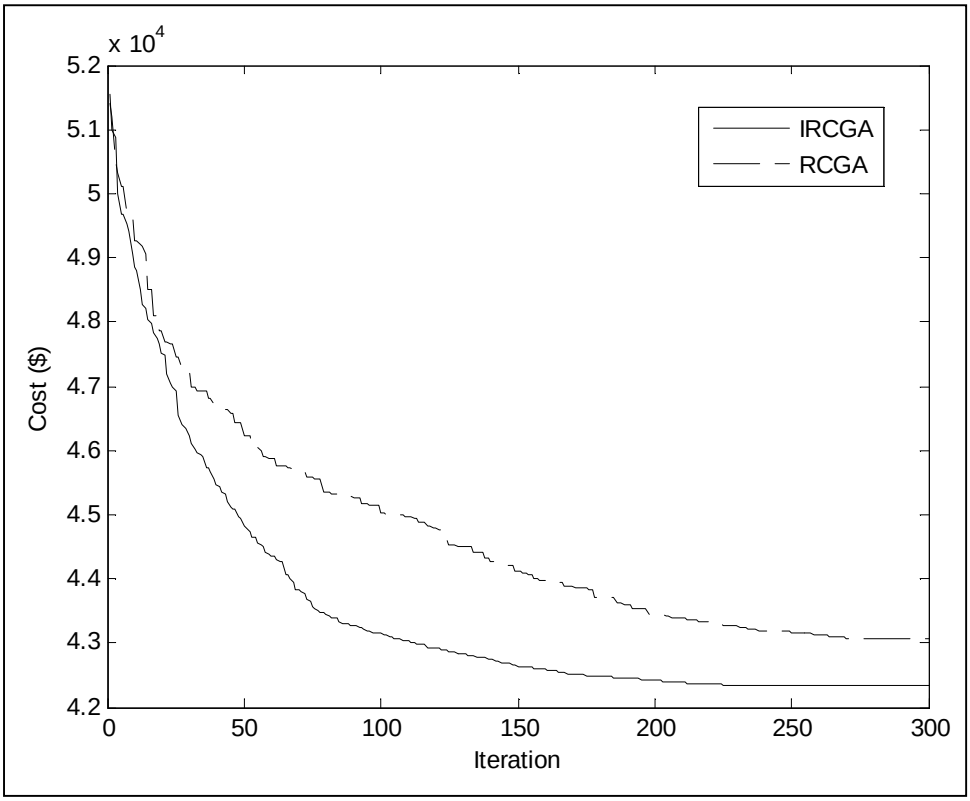

Figure 4.32. Cost convergence curves for test system-3 incorporating head mobility.

Table 4.26
Comparative study of different techniques for test system-3 incorporating head mobility

Technique	Best cost ($)	Average cost ($)	Worst cost ($)	CPU time (s)
IRCGA	42322.23	42330.53	42339.36	304.05
RCGA	43068.01	43079.52	43083.05	298.72
MDE [237]	43435.41	-	-	-
TLBO [122]	42385.88	42407.23	42441.36	-
CSA [120]	42440.574	-	-	-

4.5.4. Case IV

This system considers a multi-chain cascade of four reservoir containing hydro plants and ten thermal plants. The effect of valve point loading has also been taken into account. Here, transmission losses have not been considered. Detailed data for this system is taken from [112]. Table 4.27 and Table 4.28 show the optimal hourly discharges and hydrothermal generation acquired by the developed IRCGA respectively. Figure 4.33 shows the reservoir storage volumes of four hydro plants acquired from IRCGA. The best, average and worst cost and average CPU time among 100 runs of solutions acquired from the developed IRCGA and RCGA are summarized in Table 4.29. The cost acquired from DE [112] technique is also shown in Table 4.29. The cost convergence characteristics obtained from the developed

IRCGA and the RCGA are in accordance to Fig. 4.36. It has been observed from Table 4.29 that the cost found from the IRCGA is the lowest among all techniques. Fig. 4.34 shows hourly optimal hydro discharge of test system-4 and Fig. 4.35 is for hourly optimal hydrothermal generation (MW) of test system-4.

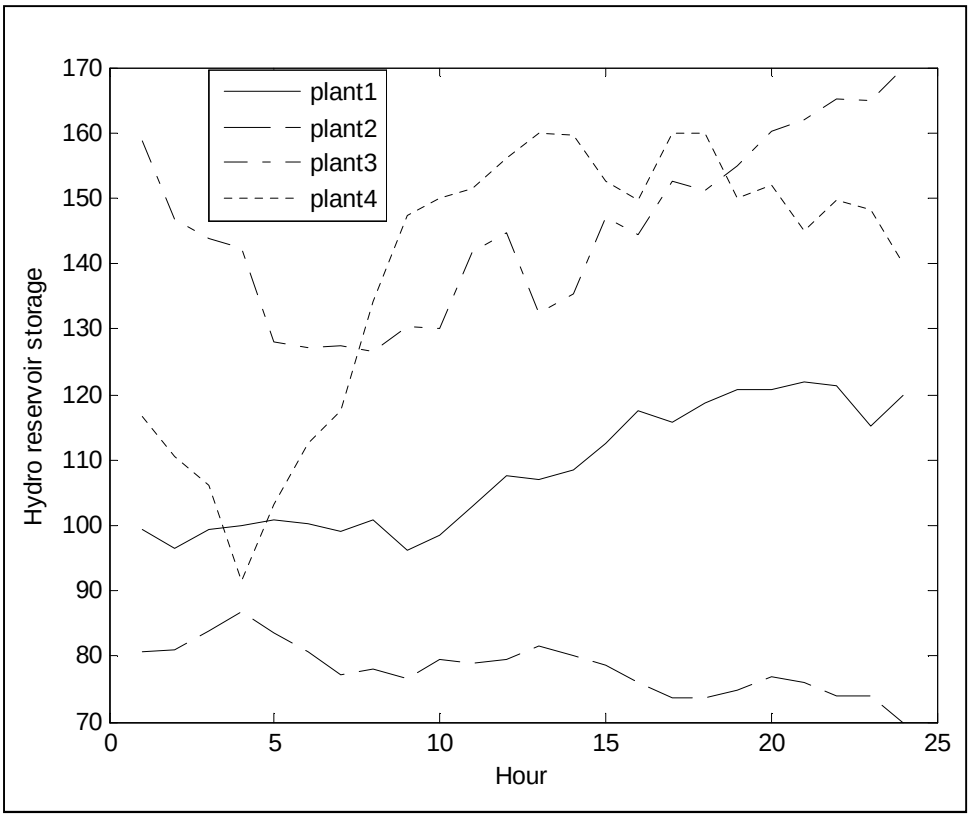

Figure 4.33. Reservoir storage volume for test system-4 incorporating head mobility.

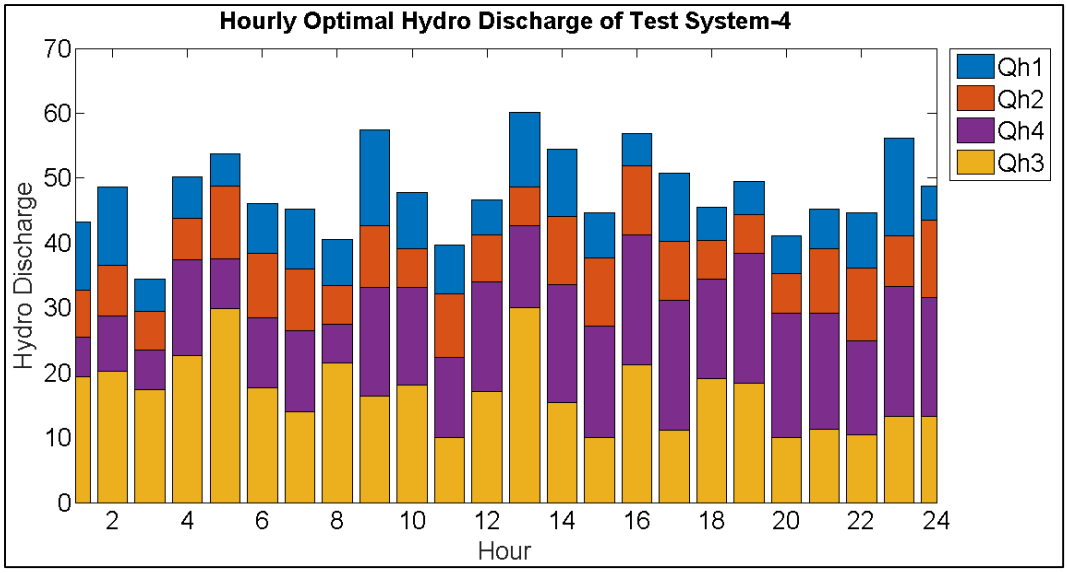

Figure 4.34. Hourly optimal hydro discharge of test system-4.

Table 4.27
Water discharge ($\times 10^4$ m^3) in 24 hours for test system-4 incorporating head mobility.

Hour	Q_{h1}	Q_{h2}	Q_{h3}	Q_{h4}
1	10.59	7.2207	19.437	6.0254
2	12.0523	7.7304	20.2455	8.5457
3	5.0001	6.0184	17.4557	6
4	6.4478	6.3207	22.6585	14.8061
5	5	11.135	29.9287	7.6698
6	7.6269	9.9408	17.607	10.8973
7	9.2146	9.5815	13.9492	12.4732
8	7.1216	6	21.4589	6.0044
9	14.722	9.4742	16.3758	16.8335
10	8.7003	6.0001	18.0804	15.0361
11	7.6528	9.7120	10.0203	12.3636
12	5.4338	7.2947	17.1649	16.8305
13	11.5460	6.0053	30.0000	12.6269
14	10.5001	10.4945	15.3613	18.1704
15	6.9555	10.5776	10.0003	17.1377
16	5.0000	10.6310	21.2541	19.9868
17	10.5398	9.0909	11.1185	19.9873
18	5.1753	6.0028	19.1245	15.2733
19	5.0000	6.0000	18.4536	19.9871
20	5.8448	6.0003	10.0100	19.2115
21	6.0854	9.8456	11.2876	17.9333
22	8.5236	11.1071	10.4763	14.4865
23	14.9775	7.8296	13.2974	19.9983
24	5.2899	11.9870	13.3435	18.2195

Table 4.28
Optimal hydrothermal power generation (MW) schedule for test system-4 incorporating head mobility.

Hour	P_{h1}	P_{h2}	P_{h3}	P_{h4}	P_{s1}	P_{s2}	P_{s3}	P_{s4}	P_{s5}	P_{s6}	P_{s7}	P_{s8}	P_{s9}	P_{s10}
1	88.57	57.22	47.08	132.22	139.75	199.58	94.96	119.95	274.69	139.73	45.00	134.50	98.19	178.56
2	93.42	60.86	40.34	161.19	50.00	350.60	20.43	20.00	224.39	239.41	281.91	85.18	25.02	127.25
3	51.68	49.75	46.67	123.35	229.28	124.06	20.00	119.83	274.36	89.80	163.14	134.30	97.08	176.69
4	64.20	53.58	22.20	210.91	229.23	124.65	20.05	119.57	224.58	139.82	104.17	134.65	25.00	177.39
5	52.48	81.84	0.00	124.65	140.14	199.97	95.32	120.03	175.65	40.20	222.70	135.15	103.36	178.50
6	72.98	74.59	39.64	172.76	228.43	199.60	20.14	69.36	174.63	289.50	222.84	134.78	25.00	75.75
7	82.22	70.99	47.20	198.36	318.93	199.57	94.69	119.92	174.64	139.77	45.00	234.60	97.79	126.33
8	69.02	47.23	22.25	129.73	229.43	422.79	95.50	119.60	273.98	189.46	102.88	84.92	97.35	125.86
9	98.83	68.78	42.67	258.01	319.36	423.92	20.31	69.80	25.01	139.90	163.48	184.45	98.09	177.38
10	78.04	46.93	38.92	257.21	319.82	274.80	95.29	69.95	224.61	189.18	163.61	35.05	159.97	126.61
11	72.45	70.95	47.72	234.14	319.29	124.73	94.81	120.22	224.58	139.52	341.31	35.01	98.20	177.07
12	56.84	56.99	45.91	275.89	230.03	50.75	20.17	119.53	379.12	289.12	104.27	184.79	160.00	176.59
13	94.90	48.78	0.00	242.21	139.83	274.44	95.14	69.84	469.99	89.68	163.39	84.89	160.00	176.89
14	90.58	75.87	46.97	293.94	229.40	274.45	94.60	20.01	273.23	139.83	281.79	35.00	98.48	75.84
15	70.06	75.26	49.06	286.25	50.00	424.09	94.71	130.00	174.56	40.00	45.06	284.12	160.00	126.83
16	54.46	74.44	31.43	298.21	229.35	199.34	129.99	70.04	25.00	189.00	400.01	134.43	97.61	126.69
17	93.64	65.38	52.59	295.18	50.01	273.98	94.47	69.89	74.80	289.24	281.74	184.31	98.39	126.38
18	56.39	45.19	43.01	270.90	229.48	423.84	94.65	69.88	174.65	189.67	163.65	184.46	98.20	76.03
19	54.96	45.17	44.96	305.80	454.33	274.42	20.30	69.57	74.39	239.45	104.26	184.79	159.99	37.62
20	62.71	45.81	53.50	290.73	50.00	274.67	94.94	119.53	324.17	90.09	222.82	134.43	159.97	126.63
21	64.79	69.73	56.20	284.47	229.45	349.33	20.00	20.00	273.79	139.52	45.00	184.71	97.36	75.65
22	83.18	74.65	55.53	250.31	319.55	349.28	20.00	119.75	75.51	40.06	163.35	84.74	98.45	125.66
23	107.42	57.02	58.04	295.22	229.34	199.76	95.15	119.70	75.18	140.39	163.42	84.81	98.20	126.35
24	57.38	76.52	57.98	282.60	319.28	274.03	94.48	69.68	25.00	139.51	45.00	134.71	98.00	125.83

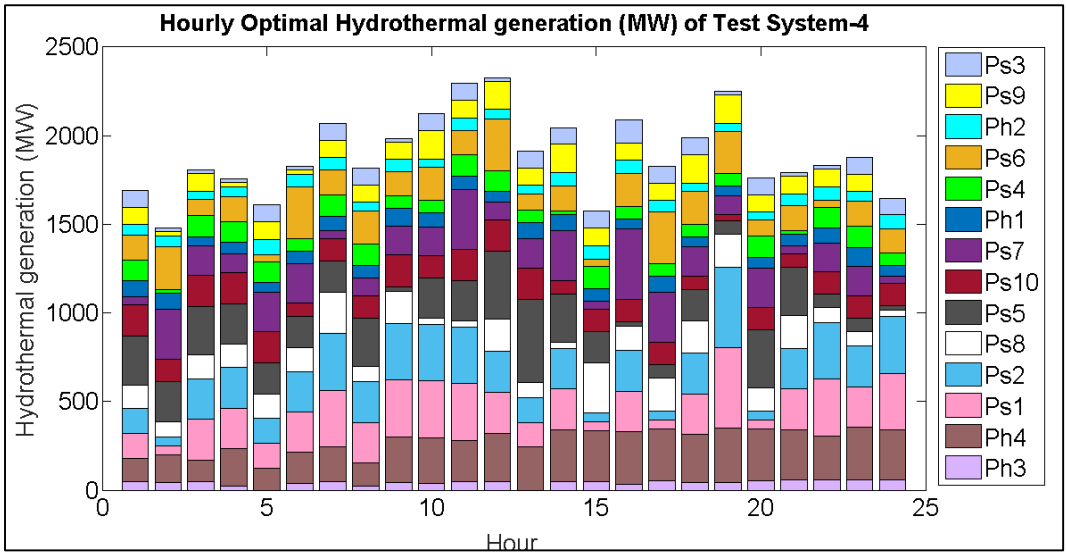

Figure 4.35. Hourly optimal hydrothermal generation (MW) for test system-4.

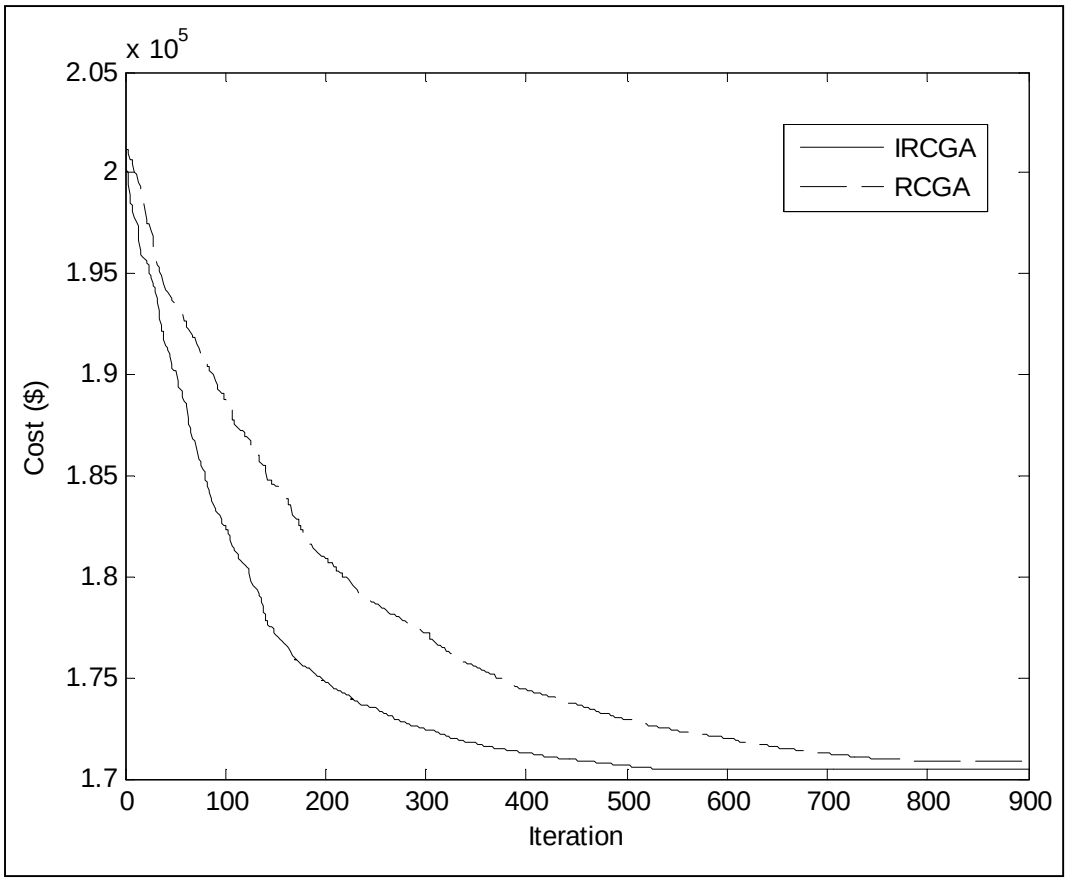

Figure 4.36. Cost convergence curves for test system-4 incorporating head mobility.

Table 4.29
Comparative study of different techniques for test system-4 incorporating head mobility.

Technique	Best cost ($)	Average cost ($)	Worst cost ($)	CPU time (s)
IRCGA	170452.35	170459.78	170468.52	472.51
RCGA	170915.57	170924.41	170935.28	459.92
DE [112]	170964.15	-	-	-

It has been observed from Table 4.19, Table 4.22, Table 4.25 and Table 4.28, and Fig. 4.23, Fig. 4.27, Fig.4.31 and Fig.4.35 that the third hydro unit has no output during some time interval. This is because of the fact that output from a particular hydro unit during a specified time interval depends on the availability of water, reservoir storage volume limit, water transport delay between cascaded reservoirs and on the system configuration as a whole. Depending on the system configuration and constraints for the present problem, this has happened in case of the third hydro unit. In this concise, four numerical experiments have been performed. Fig. 4.21, Fig. 4.25, Fig. 4.29, and Fig. 4.33 show reservoir storage volume at every hour in a day. The graph obtained from data of Table 4.18, Table 4.21, Table 4.24 and Table 4.27, and Fig. 4.22, Fig. 4.26, Fig. 4.30 and Fig. 4.34, show water discharge at every hour in a day. The optimal hydrothermal power generation scheduling of four test systems has been obtained in accordance to Table 4.19, Table 4.22, Table 4.25 and Table 4.28 respectively.

All four schedules give information about the power generation by different hydro and thermal units at every interval in a day to make economic operation. The cost convergence characteristics of four test systems are in accordance to Fig. 4.24, Fig. 4.28, Fig. 4.32, and Fig. 4.36 respectively. The solid line demonstrates IRCGA, and dotted line indicates RCGA. From these characteristic curves, it is clear that IRCGA curves fall sharply compared to that of the RCGA and thus, IRCGA proves to be more economic. The IRCGA has been modified by incorporating one-to-one challenge in conventional RCGA to boost the convergence speed and solution quality. Table 4.20, Table 4.23, Table 4.26, and Table 4.29 show the comparative studies along with the reference results. These comparative studies have proven that the IRCGA gives least price in least time.

4.5.5. Conclusion

In this paper, real coded genetic algorithm (RCGA) and improved real coded genetic algorithm (IRCGA) have been successfully implemented to solve short-term hydrothermal scheduling problem. To evaluate the performance of the IRCGA, it has been applied on four sample test systems comprising of multi-chain cascaded hydro and thermal units for a 24 hour time horizon (i.e. small horizon). In this concise, nonlinear and nonconvex relationships for power generation characteristics and the water transport delay time, have also taken into consideration. The results obtained for various test systems have been compared with modified differential evolution (MDE), teaching learning based optimization (TLBO), clonal selection algorithm (CSA), improved fast evolutionary programming (IFEP), improved particle swarm optimization (IPSO), and genetic algorithm (GA).

Test systems' results indicate that the total production cost obtained by proposed IRCGA method is less than other existing techniques over the scheduled time horizon. Moreover, since the encoding and decoding schemes entailed by GA are not needed in the proposed method, a lot of computer memory and computing time can be saved. Hence, the IRCGA confirms its superiority.

4.6. Numerical Study on optimal DG allocation problem

In this work, IEEE 33 bus radial distribution system has been selected to solve the DG placement problem applying meta heuristics. The SLD for the system is shown in Fig. 2.1 [ref chapter 2, sec 2.6]. Total active and reactive loads for this system are 3.715 MW and 2.3 MVAR respectively.

The calculations of active and reactive power losses without implementing DG are given in Table 4.30.

Table 4.30
Power loss without DG

Real Power Loss (kW)	Reactive Power Loss (kVAR)
210.9	143.0

Initially, the DG, which is proposed to be placed in the power system, is meant to inject both real and reactive power into the bus. To plump for the maximum amount of DG that should be considered to be installed for solving this DG sizing and allocation problem,

different trials with different maximum amount of installable DG have been considered. The maximum levels of total injected distributed generations have been taken as firstly 1000 kW and 750 kVAR (condition 1) and then 2000 kW and 1500 kVAR (condition 2) and finally 4000 kW and 3000 kVAR (condition 3).

This optimization problem has been solved by two well recognized optimizers like Real Coded Genetic algorithm (RCGA) and Classical Particle Swarm Optimization (CPSO) and a recently developed optimization technique, named Water cycle algorithm (WCA). In all of the cases, the total number of population for this technique has been taken as 50 and the maximum number of iterations 500.

Table 4.31 indicates comparative results obtained by these optimizers. It is evident from Table 4.31 that condition 3 (i.e. maximum DG injection level as 4000 kW and 3000 kVAR) exhibits less active and reactive power losses. It has been noted that increased level of DG injection reduces active and reactive power losses as obvious. Taking into account of the total active and reactive power demand of the system as 3.715 MW and 2.3 MVAR, increment of DG injection level beyond 'condition 3' seems not to be feasible.

One of the major purposes of this study is to examine the applicability of WCA for this type of optimization problem and this technique shows proficiency in the same by finding moderately better solutions of this problem, as noted in Table 4.31.

Table 4.31
Power loss with DG

Optimizer	Condition	Real power loss (kW)	Reactive power loss (kVAR)	Apparent power loss (kVA)
RCGA	1	138.362	126.985	187.801
	2	112.634	98.329	149.516
	3	63.261	52.151	81.986
CPSO	1	140.026	128.154	189.818
	2	111.974	97.968	148.781
	3	62.462	51.384	80.881
WCA	1	138.664	126.072	187.408
	2	111.544	97.328	148.036
	3	61.529	50.863	79.830

Table 4.32 indicates the optimal size and the locations (i.e. the bus numbers at which DGs are to be placed) for the case of condition 3, as solved by WCA. It has been seen that, DGs are placed in bus number 3, 6 and 2. Total amount of injected active and reactive powers are 2.774 MW and 1.734 MVAR respectively.

Table 4.32
Optimal allocation & sizing of DG as obtained from WCA

Size of DG		Location of DG (Bus No)
Active power inj. (MW)	***Reactive power inj. (MVAR)***	
0.325	0.254	3
1.873	1.154	6
0.576	0.326	2

Furthermore, WCA is applied in IEEE 33 bus radial distribution system for optimal placement of two extra capacitor banks as VAR compensators at two different buses, along with these three DGs at bus 2, 3 and 6. Here, the total number of iterations is taken as 1000 and the number of search agents is taken as 100. The number of rivers is taken to be 20. The maximum injections of total active and reactive power have been supposed to be 3000 kW and 2500 kVAR respectively.

The real power loss, reactive power loss and total power loss as obtained using WCA are shown in Table 4.33. The optimal location that is the bus number as well as the optimal size of the DG and five VAR compensators are also shown. According to the results, total amount of injected active and reactive powers are 2.743 MW and 1.937 MVAR respectively.

Table 4.33
Optimal Size, Location & Losses

Bus No.	**Optimal size**		**Total power loss (kVA)**	**Active power loss (kW)**	**Reactive power loss (kVAR)**
	kW	***kVAR***			
2	658	533			
3	513	594			
6	1572	457	73.827	55.865	48.266
13	-	182			
29	-	171			

From the results, it can be noted that further distribution of VAR generators in different busses causes less power loss in the system. At the same time the result indicate slightly lesser total active power injection than the previous solution.

The above results are for base loading. The power flow calculations were also done for different load steps from 50% to 150%. In Fig. 4.37, voltage angle at each bus is plotted. This is done for load variations of 50% to 150% of the base loading. Since five reactive power injectors are placed at five different buses, it has effects on the bus voltage angle and hence

the system stability. It can be inferred from the Fig. 4.38 that the voltage angle has considerably improved thus aiding voltage stability.The voltage profile for each bus at every load step is shown in Fig. 4.38. As it can be seen from the figure minimum voltage level occurs at bus number 18. As seen in Fig. 2.1, bus number 18 is the end bus for the longest branch. Hence, the power loss, here, is the minimum at each step of load variation. In Fig. 4.39, the total power loss, real power loss and reactive power loss with load variation are shown. With increasing load, as expected, losses increase.

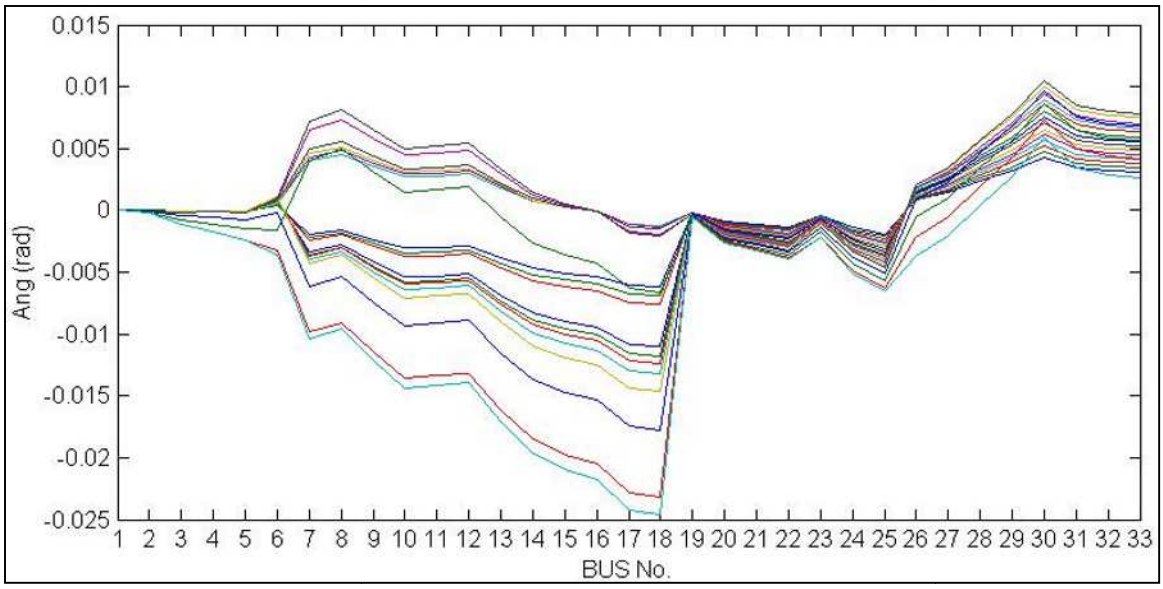

Figure 4.37. Variation of voltage angle with bus number at every load change

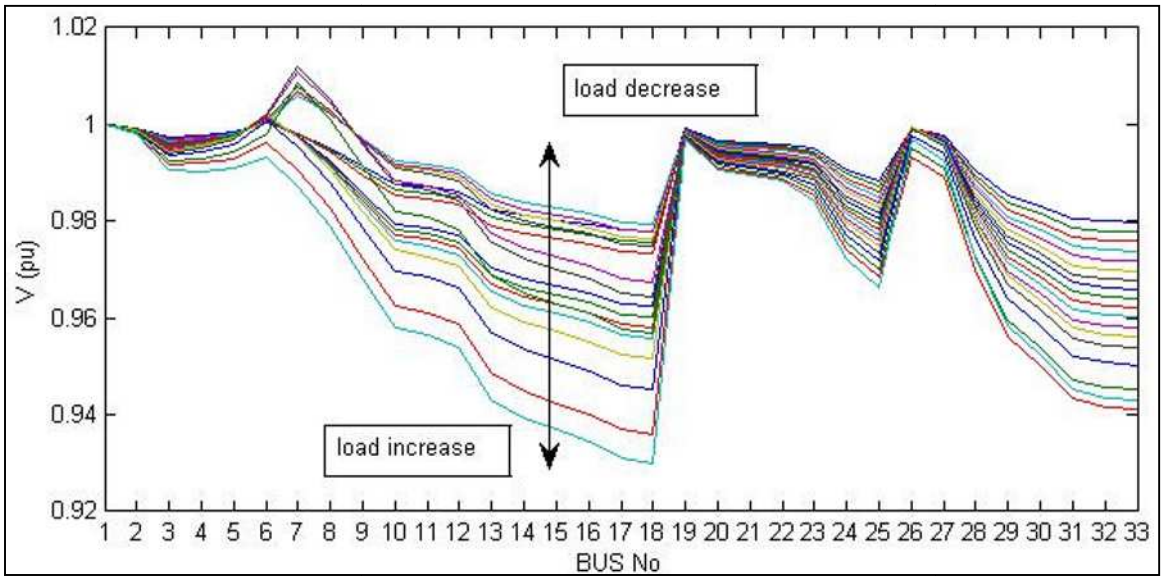

Figure 4.38. Variation of voltage magnitude with bus number at every load change

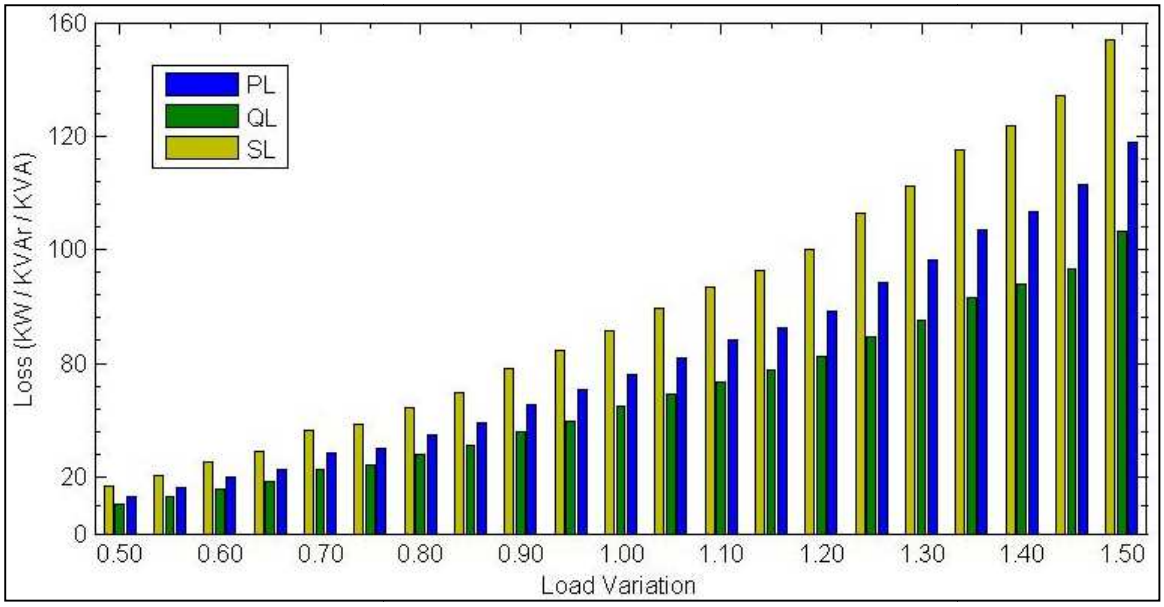

Figure 4.39. Variation of power losses at different loading levels

In this work, a problem of optimal allocation and sizing of DG with capacitor bank placement has been studied. The problem has been solved for IEEE 33 bus radial distribution test system. WCA has been used as optimizer to solve this optimization problem and the applicability of WCA for this type of optimization problem has been noted. Here, multiple DGs along with five capacitor banks at different busses have been proposed to be placed. By this method, it has been seen that total active, reactive and apparent power losses are reduced by 73.51%, 66.25% and 71.03% respectively for the system.

4.7. Numerical Study on Optimal power operation planning in a township

Average power demands of the whole micro-grid at a particular hour on a single day during summer and winter season are shown in the Fig. 4.40. The initial and operating costs of DERs are as mentioned in Table 4.34 and Table 4.35 respectively. Cost and lifetime of different equipments forming the micro-grid for each case are as mentioned in Table 4.36. Installable capacity of different energy resources for optimal operation in each case are given in Table 4.37.

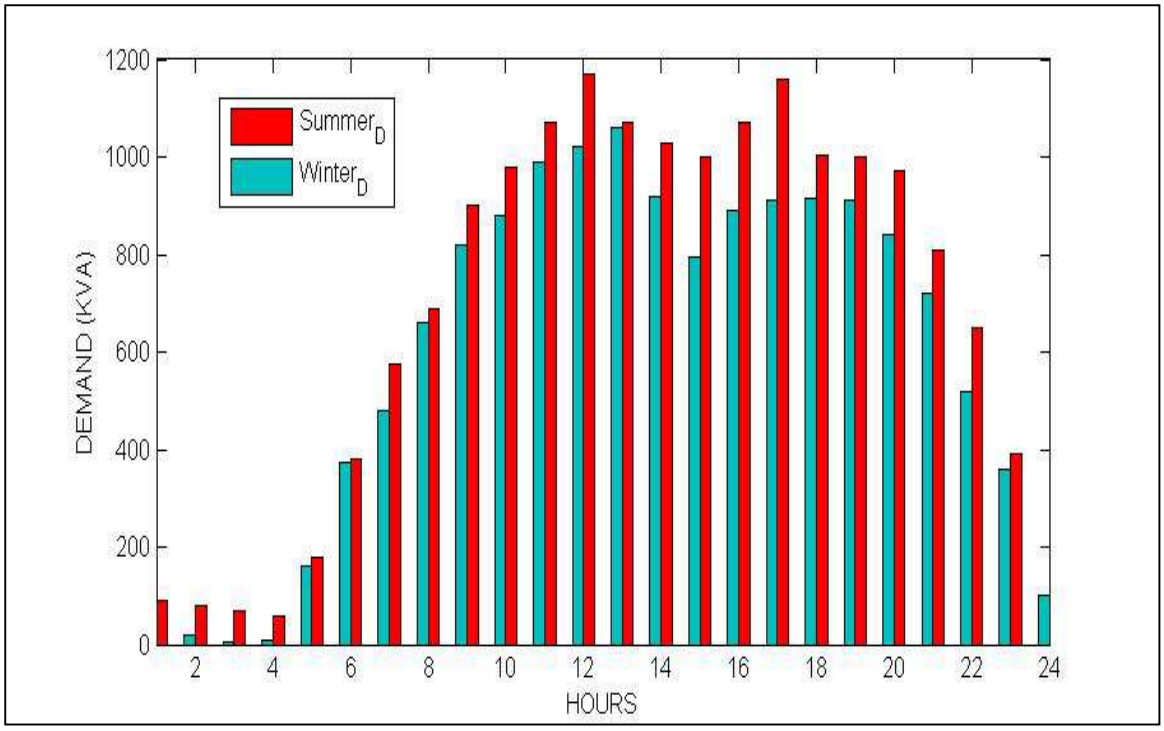

Figure 4.40. Power demands of micro-grid on a particular day during summer and winter seasons

Table 4.34
Initial cost of DERs

DER	**Micro-grid system (Case 1) (Rs $\times_{10^8}$)**	**Micro-grid system (Case 2) (Rs $\times_{10^8}$)**
BMGU	1.9935	-
BESS	4.3355	4.3355
SPS	7.1736	7.1736
PAFC	-	0.9450

Table 4.35
Operating cost of DERs

DER	**Micro-grid system (Case 1) (Rs/kWh)**	**Micro-grid system (Case 2) (Rs/kWh)**
BMGU	2.5	-
BESS	6	6
SPS	0	0
PAFC	-	10

Table 4.36
Cost and lifetime of micro-grid equipments

Equipment forming micro-grid	**Case 1**		**Case 2**	
	Cost (Rs$\times_{10}^{8}$)	Lifetime (in years)	Cost (Rs$\times_{10}^{8}$)	Lifetime (in years)
Switching equipment	0.00437000	6	0.00437000	6
Transformers (step up and step down)	0.03350000	15	0.03350000	15
Controller	0.00020000	30	0.00020000	30
Cables(underground and overhead)	0.10900000	20	0.05000000	20

Table 4.37
Installable capacity of DERs

Optimal operation	**Micro-grid system(Case 1) (kW)**	**Micro-grid system (Case 2) (kW)**
BMGU	850	-
BESS	110	140
SPS	350	350
PAFC	-	650
PP	20	20

In this work, the economic feasibility of hybrid DERs for the micro-grid and its optimal operation has been found with the help of SSO algorithm using an in-house developed code in MATLAB R2013a. The equated annual cost of each hybrid DER for optimal operation and micro-grid formation is shown in the Table 4.38 given below.

Table 4.38
Equated annual cost of each hybrid DER

Micro-grid operation	**Equated annual cost (Rs)**
Case 1	$1.2984 \times_{10}^{8}$
Case 2	$1.3217 \times_{10}^{8}$

The optimal operation by different DERs and corresponding load demand, during summer and winter seasons for case 1, is shown in Fig. 4.41. Here, hourly basis power generation from each DER, during summer and winter seasons is depicted.

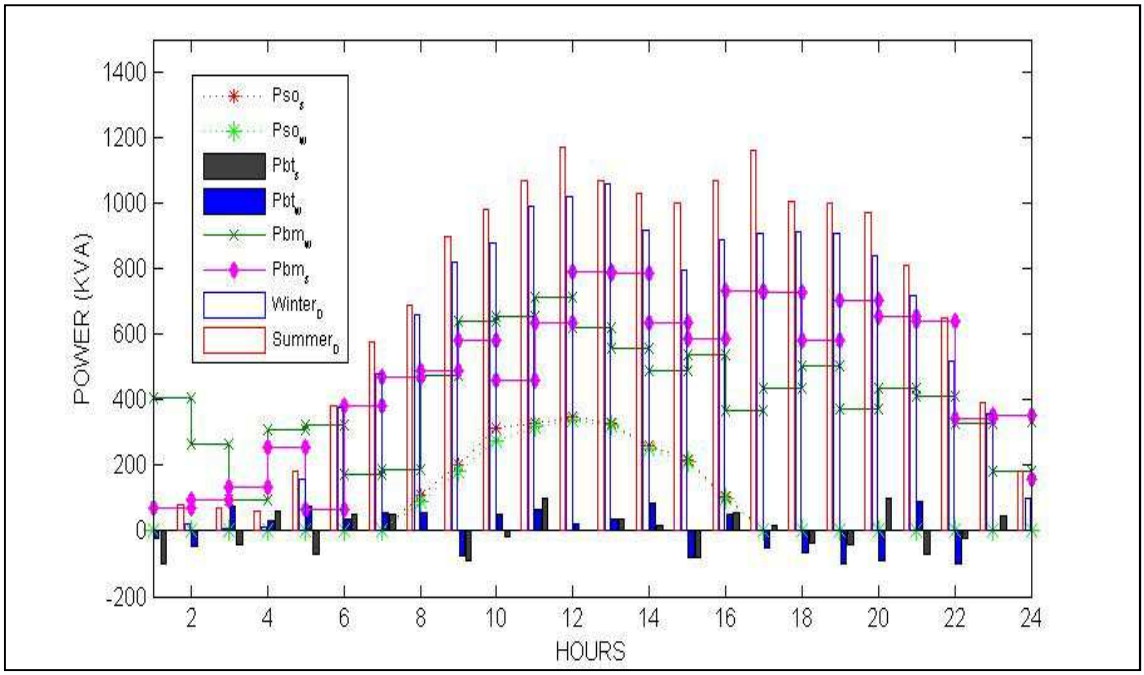

Figure 4.41. Optimal operation and corresponding load demand for case 1 of hybrid DER

It has been observed, that, the combination of SPS and BMGU with BESS (i.e. case 1) is 1.76 percent cheaper than that of SPS and PAFC with BESS (i.e. case 2), for the same load demands.

SSO is a newly appeared technique. For the sake of its reliability, the case 1 of hybrid DER has also been analyzed by another well established, common meta heuristic, population based optimization technique, named Genetic algorithm (GA). Since the case 1 of hybrid DER is more economical, the convergence comparison has been made for this case as shown in Fig. 4.40. Here, it is evident, that, in early iterations, GA converges faster than SSO, but as the iterations go on, SSO converges more than GA and finally gives better result.

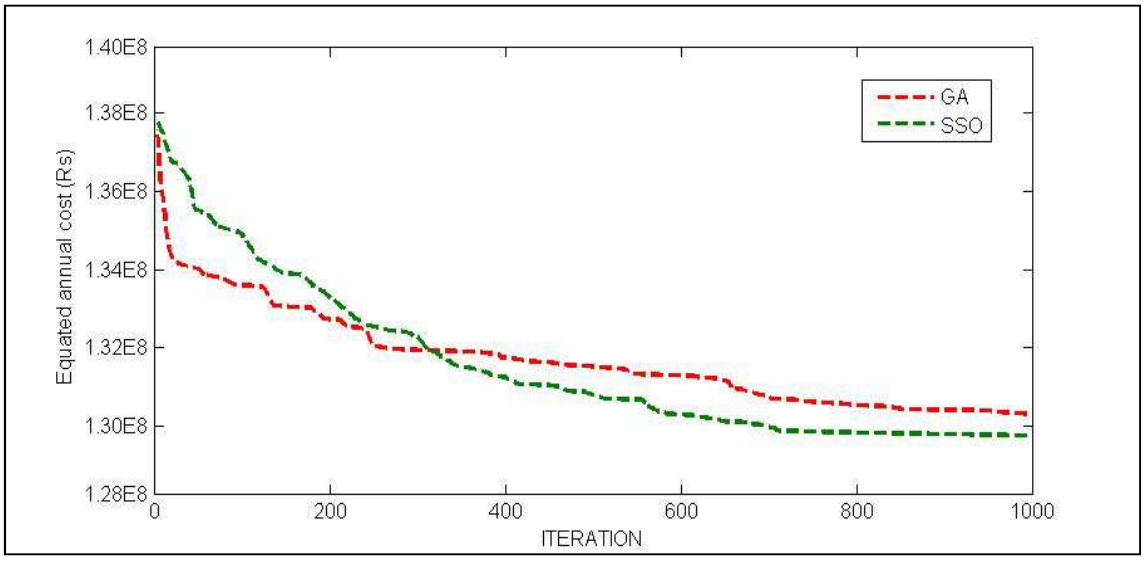

Figure 4.42. Convergence comparison curves of cost for case 1 of hybrid DER

The cost evaluation of different hybrid DERs for micro-grid has been made with the help of SSO algorithm. It shows some advantages over other evolutionary algorithms, like avoidance of premature convergence, improved balance between exploration and exploitation for obtaining the global optimal solution etc. Thus, it is evident, that, SSO is compatible to solve this type of optimization problem. Hybrid DER, as distributed generator, is found to be good approach to mitigate power demands of small and remotely situated localities. Hence, a lot of research is going on renewable energy resources. The operating and installation costs of these resources are likely to be decreased more in near future. Then, this scheme of distributed power generation with hybrid DERs will be more attractive.

4.8. Numerical Study on Optimal power operation planning in a rail-way rake maintenance depot

4.8.1. Input Parameters

Variation in power demand of the consumer throughout the day is depicted below in Fig. 4.43.

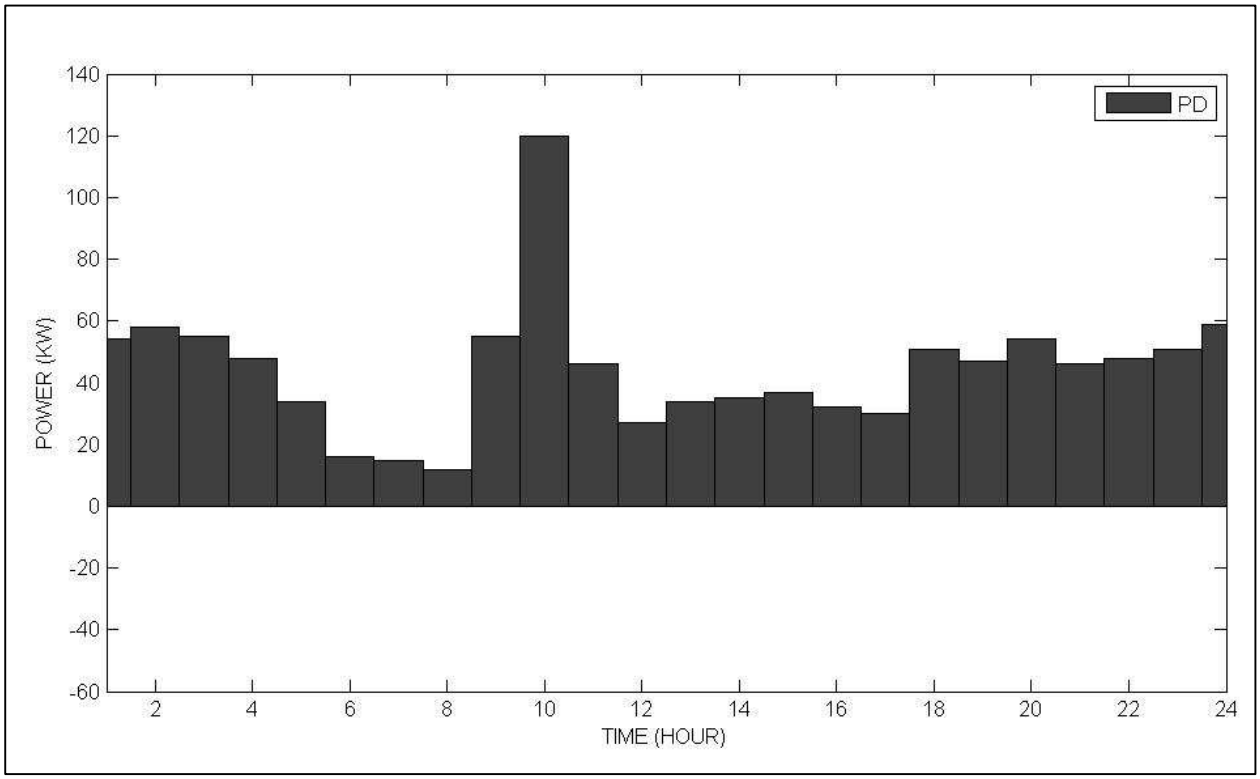

Figure 4.43. Power demand

The installation and running costs [238-242] of different DERs and their maximum installable capacities[243] are tabulated in Table 4.39.

Table 4.39
Cost of DERs

DERs	Installation Cost (Rs./KW)	Operating Cost (Rs./KWH)	Life time (Years)	Maximum installable capacity (KW)
BMGU	11	2	10	20
PAFC	35000	10	5	1000
BESS	725	5	5	100
SPS	328000	-	10	150

Inputs associated to formation of micro-grid [244] are tabulated in table 4.40.

Table 4.40
Details of micro-grid cost.

Equipments		Cost (Rs.)	Life time (Years)
Switching Equipments		47400	8
Transformers	100 KVA	256000	20
	315 KVA	465000	20
	630 KVA	713000	20
Controller		20000	30
UG Cable (4 core,11 KV grade)		78100	20

Individual tariff for different DERs [244] are given below in Table 4.41.

Table 4.41
Tariff for DERs

DERs	BMGU	PAFC	SPS
Rate (Rs./KWH)	4	11	11

Existing Tariff [244] to purchase power from grid is as in Table 4.42**.**

Table 4.42
Energy Tariff

Time slab	Normal	Peak	OFF-peak	Demand Charge (Rs./KVA/month)
Rate (Rs./KWH)	6.12	8.57	4.04	317

4.8.2. Results and Analysis

In this work, Economic analysis to implement distributed generation using DERs, with optimal power operation planning, in the aforesaid Rail-Way car-shed has been done. To get the best result as well as test the performance of GSA, 16 consecutive runs of the in-house developed programs have done in Matlab R2013a, for different cases with different combinations of tuning parameters and randomizing equations. Let, Rpow is a parameter, which is suggested to be 2 or 1 and Type (a or b) is the indication of the selection of randomizing equation. The simulation results are tabulated below in Table 4.43.

Table 4.43
Obtained results

Case	Sl No	Type	R-pow	Pop. Size (N)	No. of Iteration (I)	Optimum installation Capacity				Equated Annual Cost (RS)	Energy Cost (Rs./KWH)
						BMGU	PAFC	BESS	SPS		
I	1	a	1	50	1000	12	-	47	65	4.7897 e6	12.33
	2	a	2	50	1000	18	-	31	97	5.1073 e6	13.15
	3	b	1	50	1000	12	-	41	60	4.4987 e6	11.58
	4	b	2	50	1000	19	-	46	125	4.7478 e6	12.22
II	5	a	1	50	1000	-	572	35	66	9.4018 e5	2.42
	6	a	2	50	1000	-	996	47	126	3.7755 e6	9.72
	7	b	1	50	1000	-	583	42	60	9.7941 e5	2.53
	8	b	2	50	1000	-	933	47	94	3.6589 e6	9.42
III	9	a	1	50	1000	12	620	41	73	1.2451 e6	2.83
	10	a	2	50	1000	20	946	47	102	4.0101 e6	10.33
	11	b	1	50	1000	11	583	43	62	8.5629 e5	2.20
	12	b	2	50	1000	18	945	39	71	3.2973 e6	8.49
	13	a	1	80	1000	11	581	40	64	8.4839 e5	2.18
	14	b	1	50	1500	12	616	43	70	1.0867 e6	2.79
II	15	a	1	80	1000	-	580	30	64	9.3278 e5	2.40
	16	b	1	50	1500	-	588	41	64	9.7532 e5	2.51

Analyzing the obtained results, it is clear that Case I is not economically faceable. Case II is optimum to some extent, but Case III is the most optimum economically. From the view

point of performance of GSA, it can be noted that, the type of randomizing equation, population size and no. of iteration do no significantly affect the results. But, in case of Rpow, value of 2 performs more efficiently than 1 for this optimization problem. Possibly, in case of Rpow = 2, the discontinuity caused by transformer price when amount of surplus power exceeds 700 KW, cannot be arrested. However, among the results, the most economic solution comes out from thy 13th run, which belongs to case III.

This optimization problem was also solved by PSO technique. The best value arrived by this is also goes for case III with Equated Annual Cost of Rs 8.8547 e5, which means energy cost of Rs 2.26/KWH.

The convergence curve of Equated Annual Cost for both GSA and PSO are shown in Fig. 44. For GSA, it shows drastic convergence in early iterations and in latter iterations the value improved slightly. Whereas, in case of PSO, the convergence is comparatively gradual.

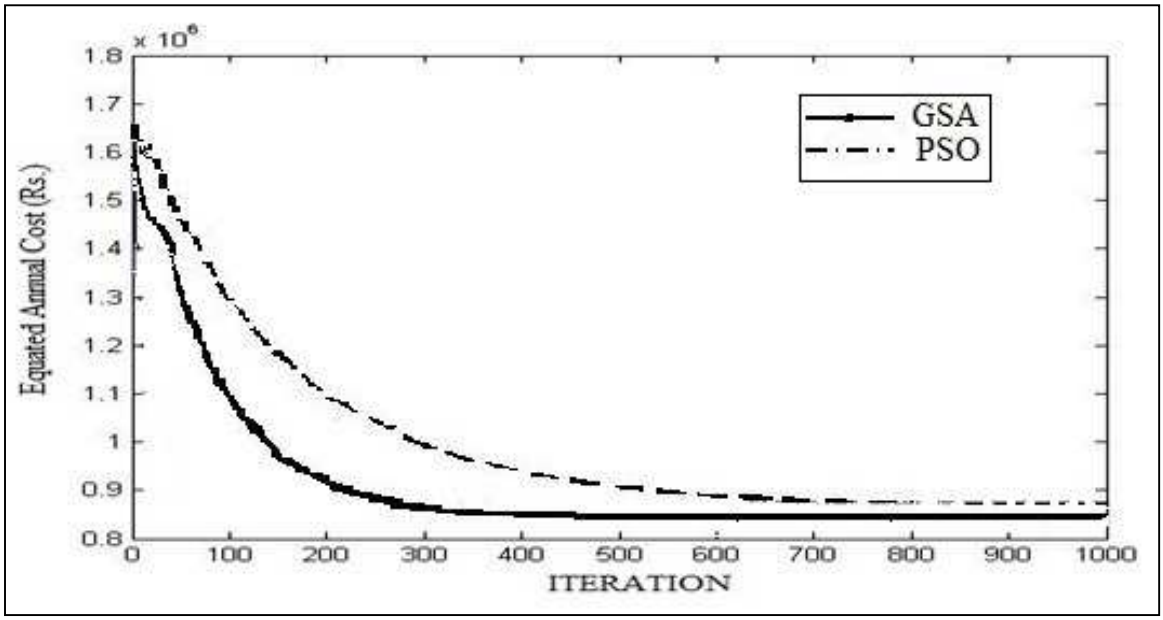

Figure 4.44. Convergence curve

The optimal power operation considering this result is graphically depicted below in figure 4.45.

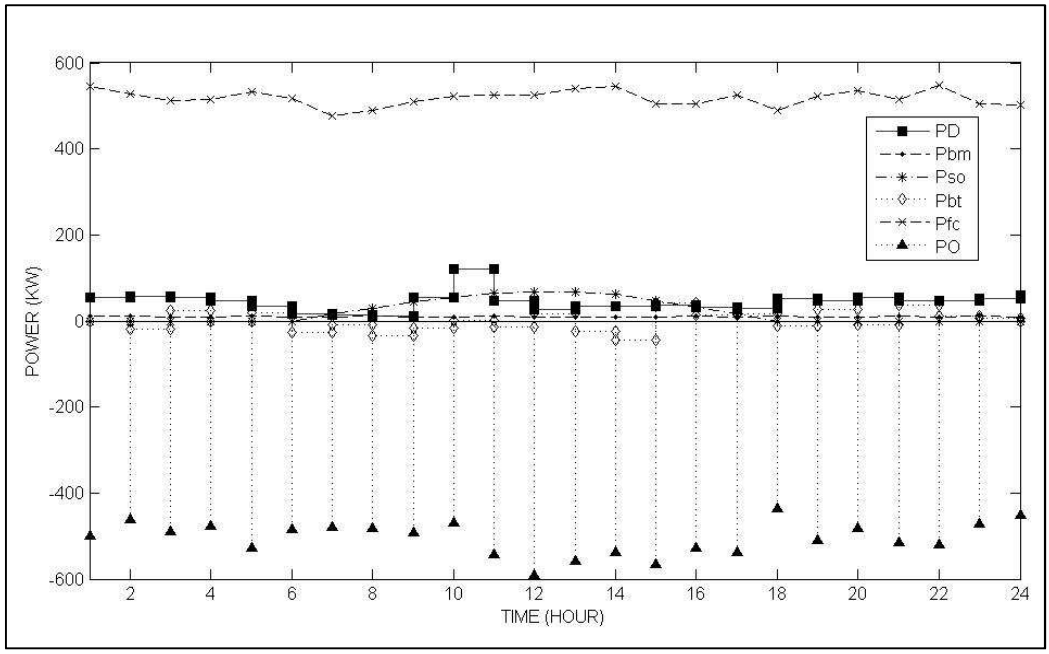

Figure 4.45. Optimal Power Operation

Here, 'Pfc', 'Pso' and 'Pbm', which indicate the hourly power generation by PAFC, SPS and BMGU, are represented in figure 4.28. The BESS operation is also present there as 'Pbt'. The positive side indicates battery discharging and the negative side indicates charging. There also exists the hourly basis demand curb, 'PD'. Lastly, in the negative power axis, the amount of surplus energy fed to the grid is represented as 'PO'. Anyways, in this figure, power operation of BMGU, SPS and BESS, and the demand curb are not prominent, to get clear view of these, omitting power operation of PAFC and power fed to the grid, Figure 4.46 is presented below.

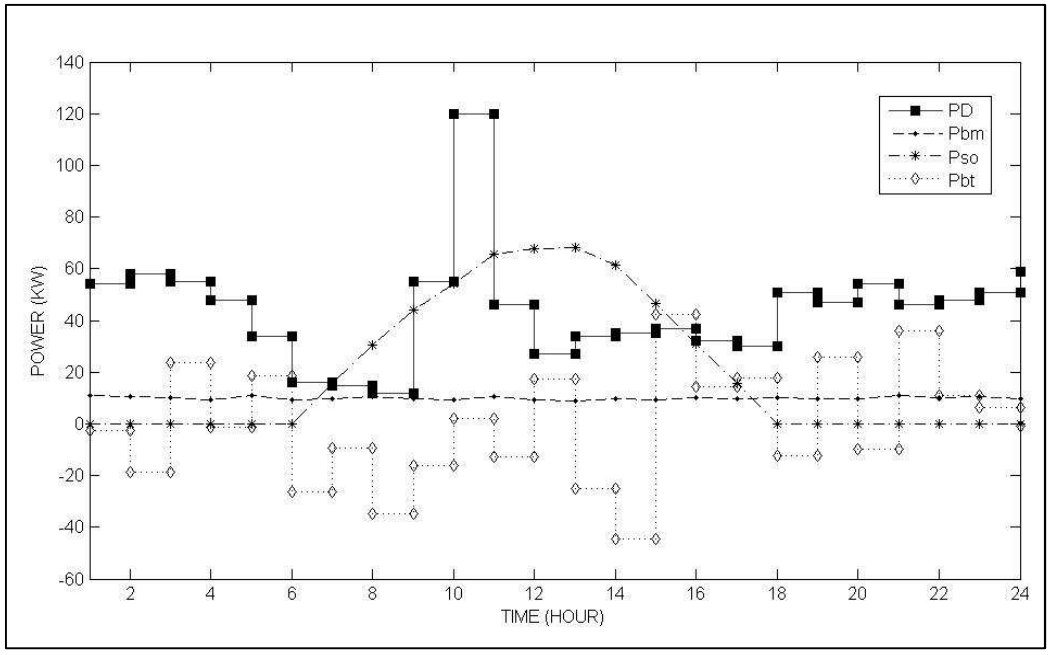

Figure 4.46. Optimal Power Operation

4.8.3. Conclusion

Giving priority to the economy, a theoretic analysis to implement DG with optimal power operation has been made. GSA is used to solve this optimization problem. It performed slightly better than normal PSO method for this case. So it seems that GSA can be successfully and reliably implemented in these types of optimization problems.

As per the proposal, the energy cost should effectively be Rs. 2.18 per KWH and it will be possible to feed renewable energy of 4.3513 GWH per year. Effectively it results savings of 4.7397 GWH energy, mostly generated from conventional thermal power plants. It will be beneficial to the environment. In spite of that, there may arise some conflicts. As per the obtained results, for case II (when BMGU is discarded), the minimal energy cost will be Rs. 2.40 per KWH, which may be comparable to case III. As it is definite that, BMGU has very low power density, omitting BMGU may spare a large amount of land area of the consumer, which will attract them (the authority of the railway car-shed). As lots of researches are going on DERs technology, it can be assumed that the installation and operating costs of different DERs will definitely be reduced in near future and they will come with greater efficiency and power density. At that time, implementation of DG using DERs will be more attractive for the most consumers.

4.9. Numerical Study on optimal power operation of PV aided nano-grid in a hopital campus

4.9.1. Simulation and results

Total power consumption in the hospital campus throughout a day is presented below as in Fig. 4.47**.** Here, the power demand has been recorded at every quarter hour interval throughout a day for a set of randomly chosen 36 days of different months throughout a whole year and the power demand has been averaged to realize the 24 hrs demand profile.

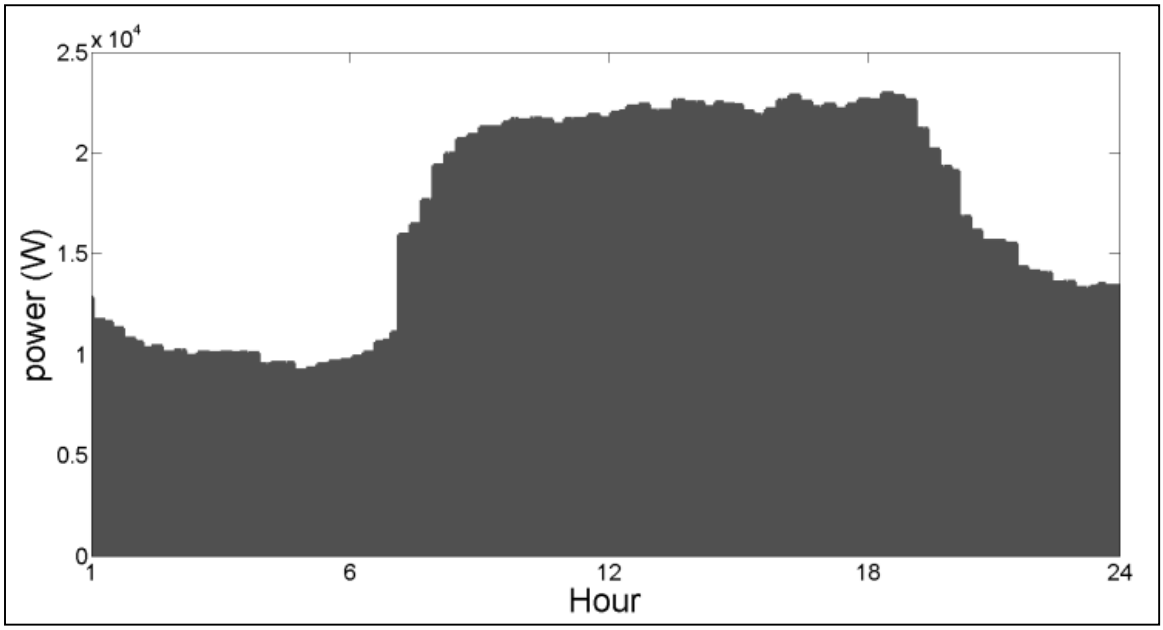

Figure 4.47. 24 hours power demand of the hospital campus

The running cost of different renewable energy resources and their installed capacity are tabulated in Table 4.44.

Table 4.44
Running costs and installed capacities

Renewable energy resource	**Running cost (INR/kWh)**	**Installed capacity (KW)**
Battery energy storage system	5	5
Solar photovoltaic system	-	10

Existing time dependent tariff to purchase power from grid is as in table 4.45 [245]**.**

Table 4.45
Energy tariff of the utility grid

Time period	4:00 am - 10:00 am	10:00 am - 10:00 pm	10:00 pm - 4:00 am	**Base charge (Rs./KVA/month)**
Rs./kWh	6.88	7.57	6.40	317

The parameters for the optimizer have been tuned as follows. The community dimension N_{ab}, the allocation index corresponding to the SIBICR η_{al}, and the maximum iteration $itrn_{mx}$, have been set as 100, 0.5 and 1000 respectively.

To ensure the performance of the proposed methodology solved by the IMRCGA, 10 simultaneous runs of an in-house developed code have been done in MATLAB R2013a

environment, by a computing system based on a standard Intel i7 micro-processor with 16 GB 1600 MHz RAM and with 64 bit Windows 7 professional operating system. The problem has also been solved by RLCGA to compare the result with the proposed methodology. To assure a justified comparison, The community dimension N_{ab}, and the maximum iteration $itrn_{mx}$ have been set as the same of the case of IMRCGA. The averaged simulation results are given below in Table 4.46. The average computing time taken to get the solutions are 15.82 and 16.21 seconds for RLCGA and IMRCGA respectively.

Table 4.46
Annual operating cost

Annual operating cost (INR)		
Without active DSM	***With DERs (solved by RLCGA)***	***With DERs (solved by IMRCGA)***
7.4286e+05	5.9381e+05	5.4021e+05

It is evident from the results that the proposed IMRCGA technique performs better in respect of producing a more economic solution. The optimal economic power operations of nano-grid as per the obtained solution of the proposed IMRCGA have been depicted in Fig. 4.48.

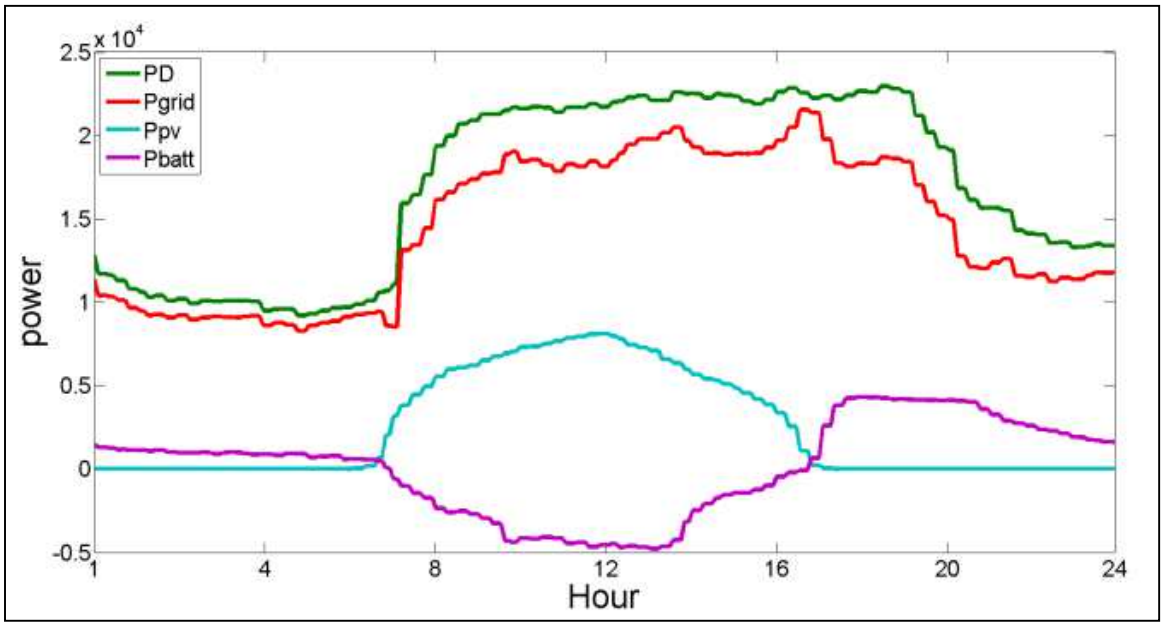

Figure 4.48. 24 hours optimal power operation

Here, the PD denotes the power consumption and P_{grid} represents power purchased from the utility grid. The area between these two curves summarizes the net energy saving throughout the day. The P_{pv} and P_{batt} curves denotes power contribution of the PV and The BESS units respectively. Negative portion of the P_{batt} line represents charging of the BESS and the positive portion represents the discharging mode of the BESS.

Two separate tracking controllers have been designed to operate the PV and BESS following the power operational references. These are represented as

$$G_{c1}(s) = 50.046 + \frac{10.028}{s} \tag{3.97}$$

$$G_{c2}(s) = 1.523 + \frac{1.216}{s} + \frac{0.514s}{s+1e8} \tag{3.98}$$

The PI controller, $G_{c1}(s)$, is used to control the PV system described by (21)-(29) The PID controller, $G_{c2}(s)$, is used to control the BES system described by (30)-(32). The corresponding closed-loop system frequency response is shown in Fig. 4.49a and Fig. 4.49b respectively.

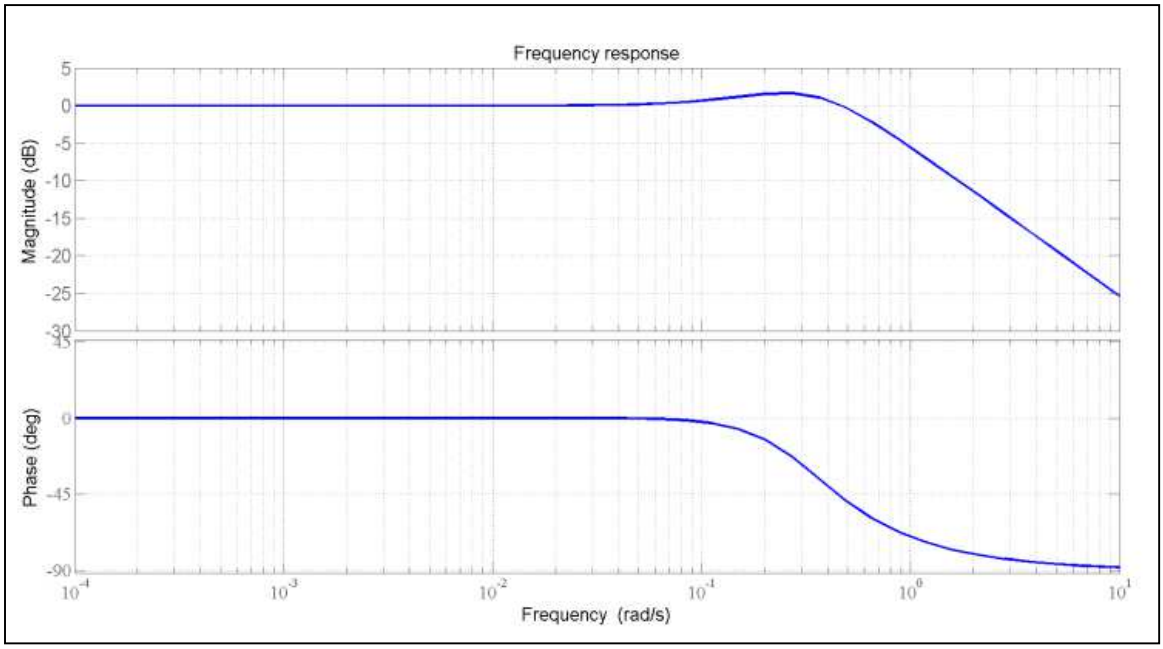

Figure 4.49a. Closed loop frequency response of the PV system.

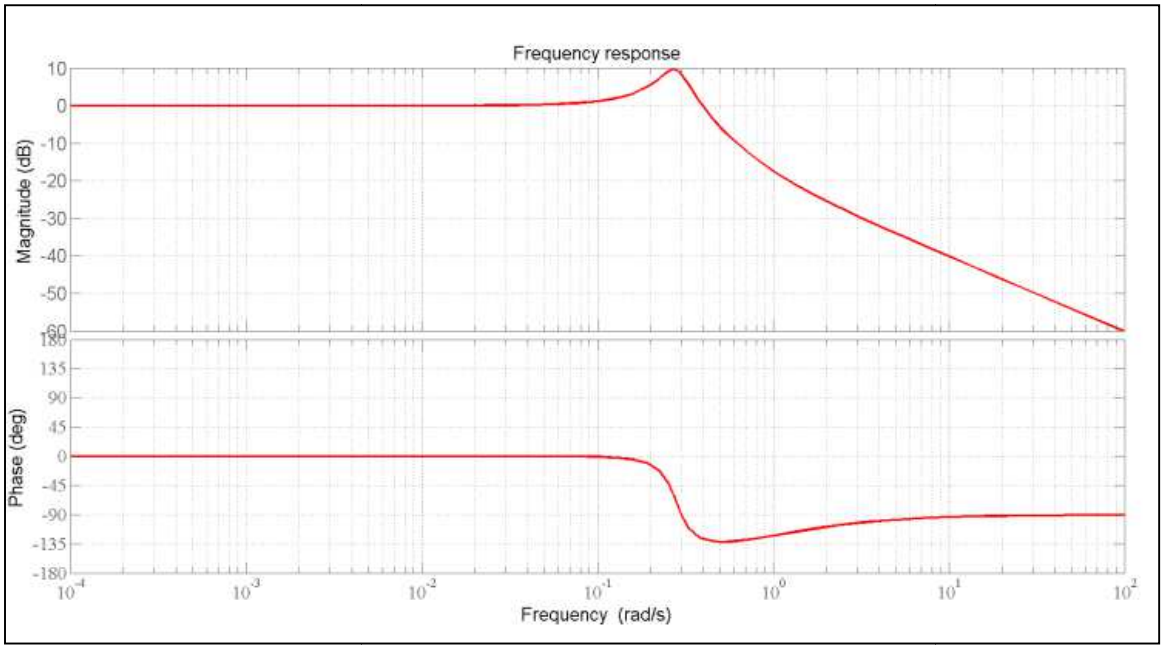

Figure 4.49b. Closed loop frequency response of the BES system.

The closed loop frequency responses in Fig. 4.49a and Fig. 4.49b show stability at low frequency steady state and higher frequency noise rejection.

The transient behaviors of the PV and BES system have been examined with real-time Hardware-in-Loop (HiL) simulations on a real-time platform viz. Opal RT OP4500 and MATLAB Real-Time Windows Target (RTWT). The scheme of the HiL Simulation, as shown in Fig. 4.50, the analog outputs from the Opal-RT OP4500 module, which is in loop with the controller hardware Advantech PCI 171, are fed directly to a storage oscilloscope.

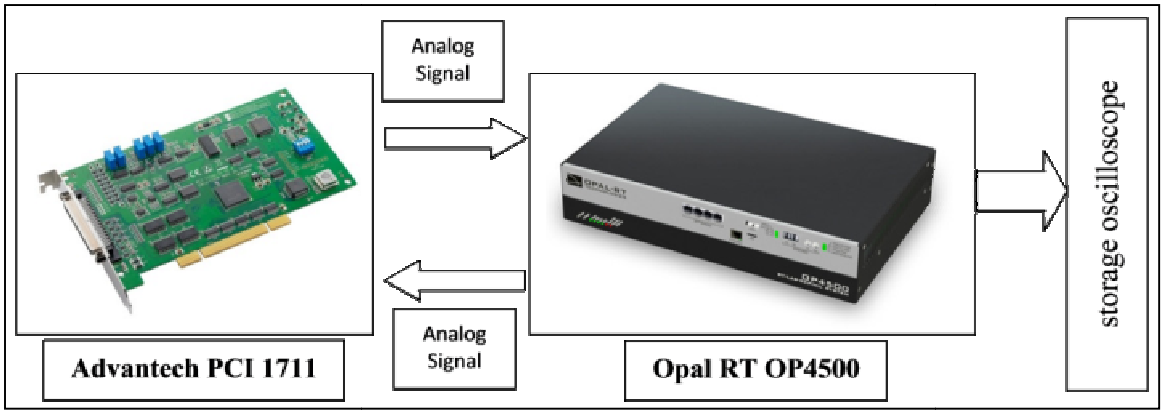

Figure 4.50. Hardware-in-Loop (HiL) scheme

The time responses of the PV and BES system have been captured for 120 seconds through this real-time HiL scheme. In this period of simulation, some realistic changes of references due to ambient uncertainty have been taken into account.

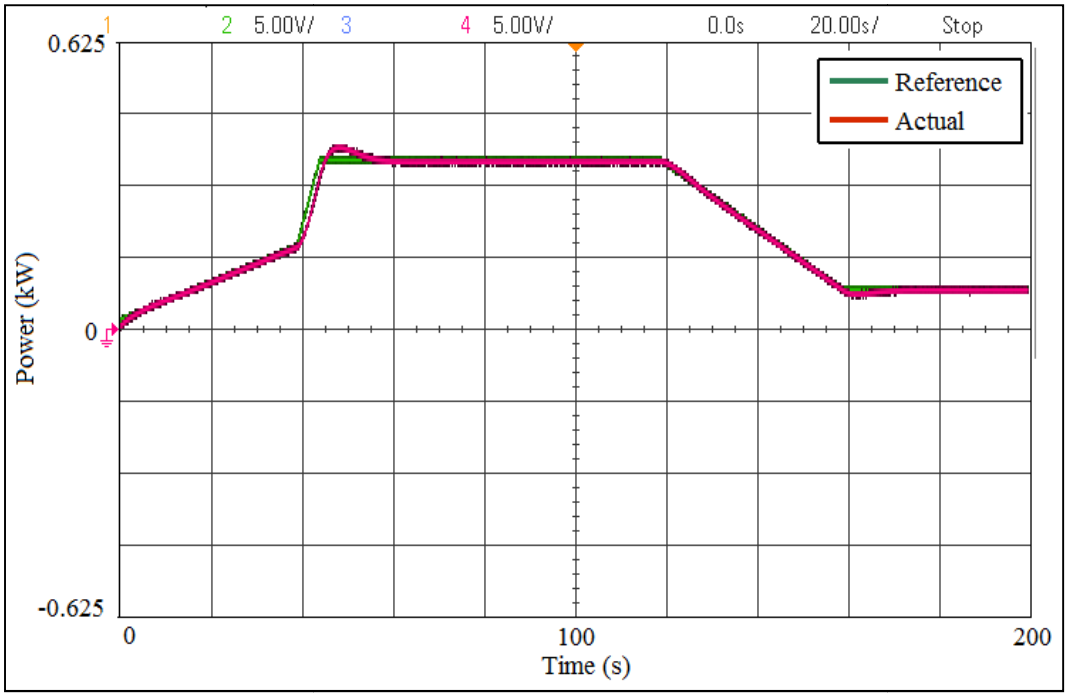

Figure 4.51. PV power

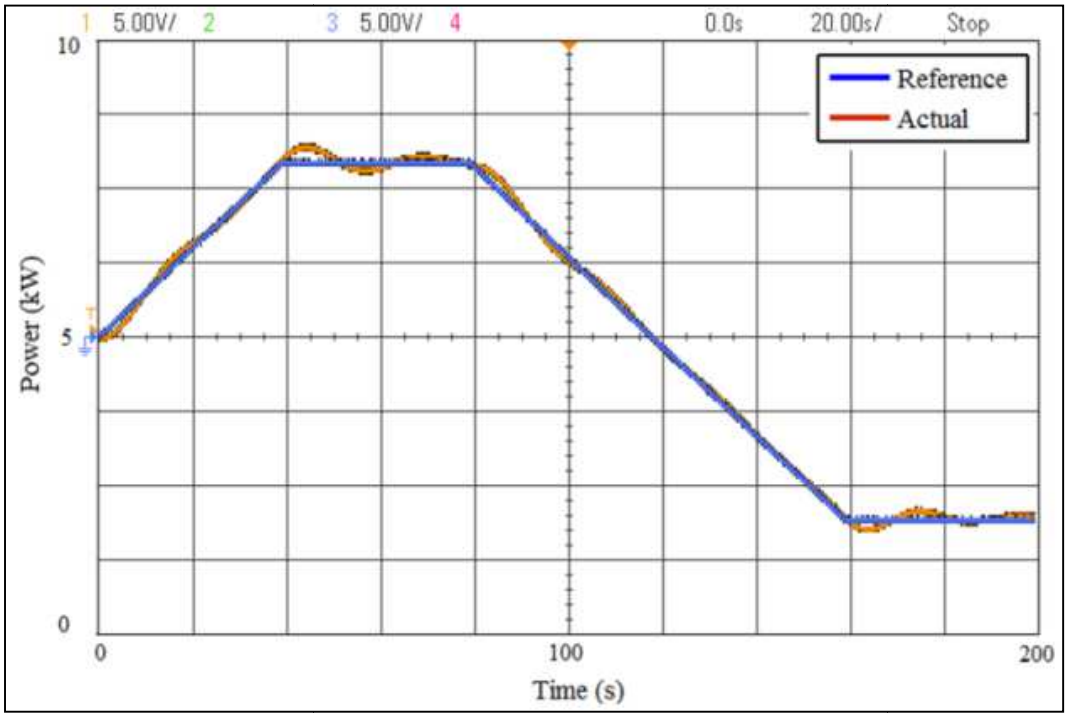

Figure 4.52. BESS power

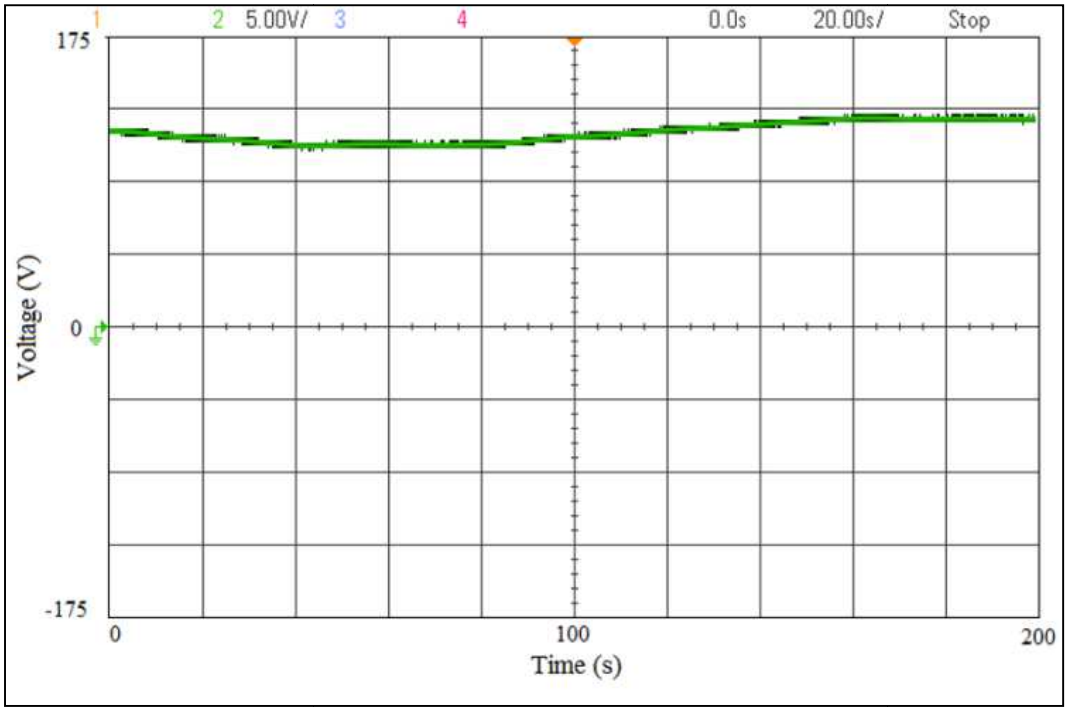

Figure 4.53a. BESS terminal voltage

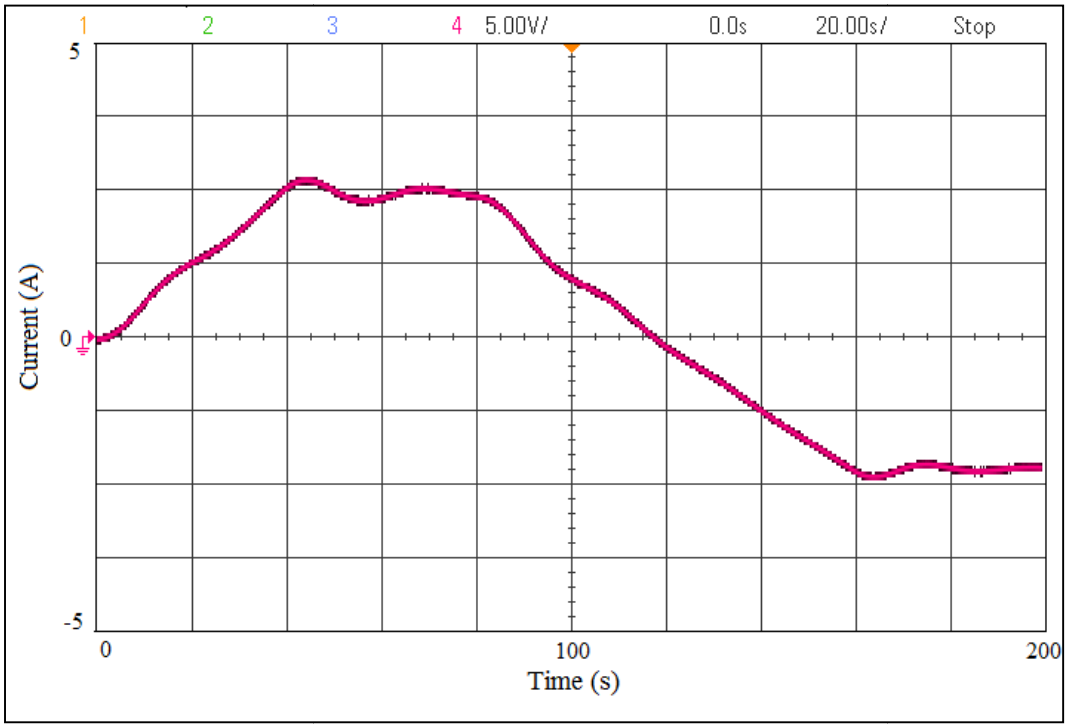

Figure 4.53b. BESS current

Generated traces from the simulator connected storage oscilloscope are presented in Fig. 4.51, Fig. 4.52, Fig. 4.53a and Fig. 4.53b. Figure 4.51 and Fig. 4.52 represent the real-time reference power tracking of the PV and BES system respectively. The associated BES

terminal voltage and current waveforms have been depicted in Fig. 4.53a and Fig. 4.53b respectively. Figure 4.51 and Fig. 4.52 show satisfactory power tracking performances for both the PV and BES systems.

4.9.2. Conclusion

With priority to economic demand side management forming a PV-BESS assisted nano-grid, a theoretic analysis to find optimal annual operating cost has been done. It can be concluded that evolutionary optimization techniques like real coded genetic algorithm (RLCGA) and improved real coded genetic algorithm (IMRCGA) can be successfully used as optimizer to solve this kind of optimization problem and IMRCGA suits better than RLCGA in this type of problem.

Electrically modeled power network of the hospital campus in the form of a nano-grid containing PV, inverter and BES systems along with designed controllers analytically show proficient performance in steady state and transient reference tracking.

As an obvious future, distributed generation would be preferred over conventional centralized power generation. In that situation, distribution networks, which are presently designed according to the conventional centralized power generation, would have to be changed according to the distributed generation requirements. For this particular case, it has been seen that by implementing active distribution system with renewable energy resources, the annual operating cost gets reduced by 27.28 percent approximately and in addition, it saves almost 21.9 MWh of electrical energy produced by conventional centralized power generation system per annum.

4.10. Experimentation and validation of the proposed optimization based fault detection scheme in photovoltaic system

4.10.1. Experimental setup

To test the performance of the proposed methodology, a physical test system has been created in the laboratory, which consists of 10 numbers of identical 36 multi-crystalline cells, 10 Watts PV modules. Here all the modules have been connected in series to construct a PV

string. The generated power has been fed to an electrical load through an MPPT controller and converter. The technical specifications of the PV modules are summarized in Table 4.47. All the technical data are collected at standard test condition (STC) (Irradiance- 1000 W/m^2, AM 1.5, 25°C Temperature). A Matlab-Simulink model, identical to this test system, has been constructed to perform the evaluations needed by the optimizer as the simulated PV system and the fault analyzer block in Fig. 2.12. [ref. to chapter 2, sec 2.10] Here, in this block, the optimizer subsystem contains the in house developed logical source code to implement GWO for fault detection. The sub-systems named PV string and MPPT controller and converter are depicted below in Fig. 4.54 and Fig.4.55 respectively.

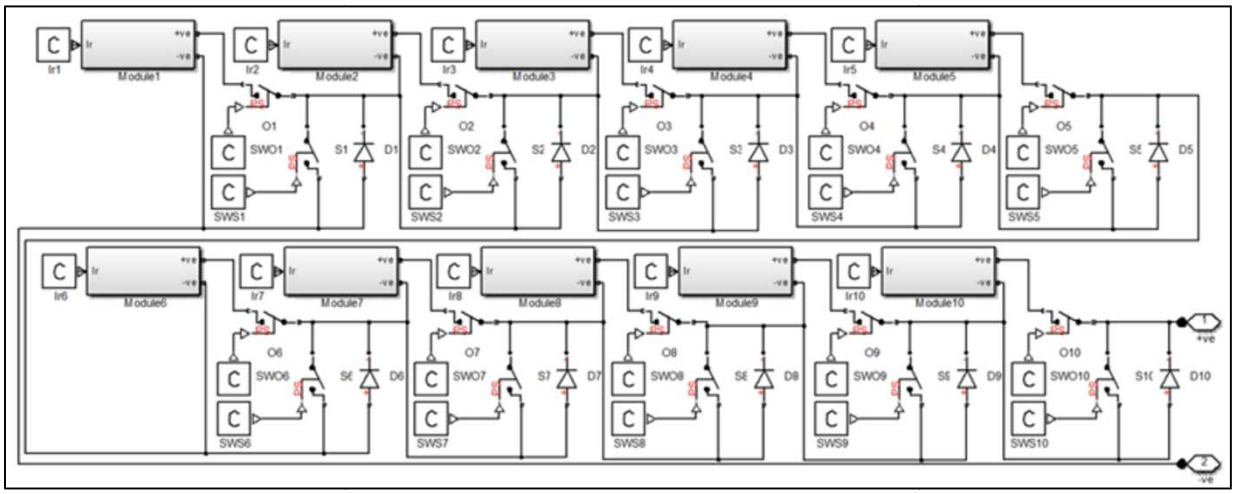

Figure 4.54. PV string sub-system.

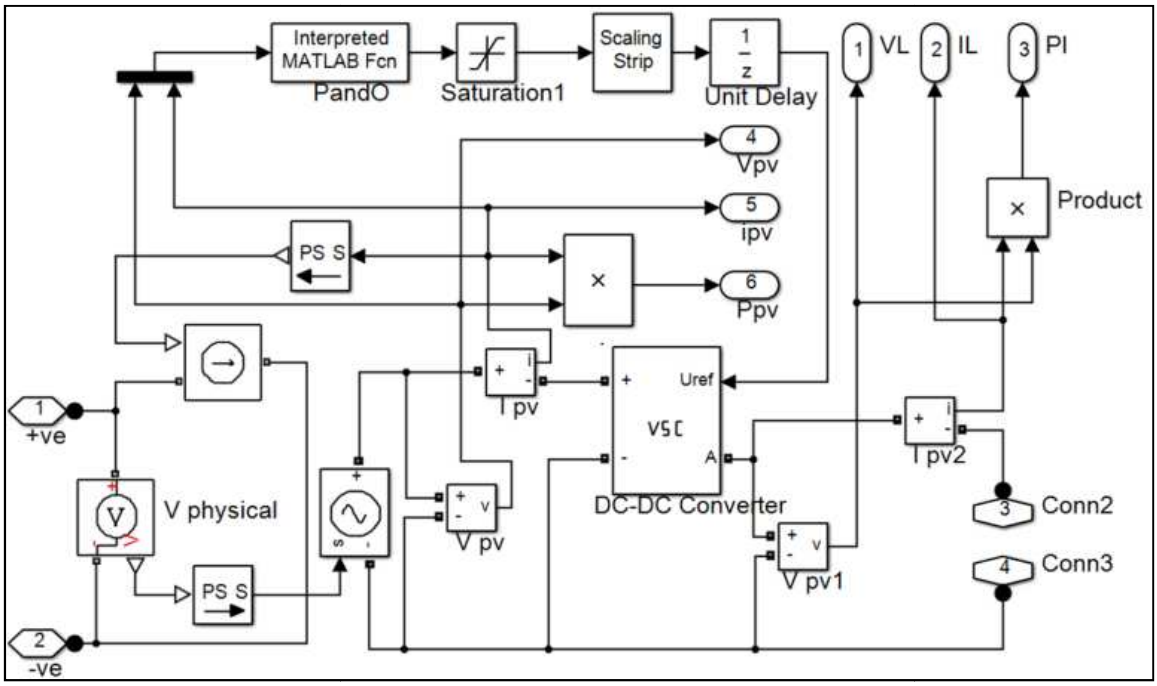

Figure 4.55. MPPT controller and converter Sub-system.

Table 4.47
Electrical characteristics of test modules.

Parameter	Value
Make	SOVA SOLAR
Maximum Power (Pmax)	10.51 W
Voltage at Pmax (Vpm)	18.18 V
Current at Pmax (Ipm)	0.58 A
Open-Circuit Voltage (Voc)	22.14 V
Short-Circuit Current (Isc)	0.64 A
Series Resistance (Rs)	1.73 Ω
Shunt Resistance (Rsh)	613.94 Ω
FF	0.75
Module efficiency (Eff,m)	13.29%
Cell efficiency (Eff,c)	16.41%

4.10.2. Results and discussions

Nonuniform irradiance throughout the PV string has a significant effect on the string current. As it causes deformation of power-voltage characteristics of the PV string, the operating point (MPP) of the string is changed by the MPPT controller and power converter, which affects the string current. Here, the proposed methodology follows this string current to detect OC and SC faults. So, a keen attention has been paid on performance evaluation of the methodology in case of MPPT controller and converter connected PV string in nonuniform irradiance with different module temperatures. To realize the performance in these different conditions, 4 sets of PV string system irradiance and temperature conditions (C1-C4) have been considered, as tabulated in Table 4.48. The irradiance values of modules for test conditions C1 and C2 ranges from 807-987 W/m^2 and 475-718 W/m^2 respectively, while for conditions C3 and C4, some irradiance values have been considered very low values, as ranges from 71-576 W/m^2 and 84-929 W/m^2 , to replicate heavily shaded conditions in some modules in the PV string. Such ranges of irradiance levels for different test conditions are selected to examine the effectiveness of the proposed methodology in cases of moderate and highly non-uniform irradiance conditions.

Table 4.48
Irradiance levels and corresponding temperatures

PV System Conditions		C1	C2	C3	C4
1st Module	$G_1(W/m^2)$	931	575	166	841
	$T_1(°C)$	62.91	49.56	34.22	59.53
2nd Module	$G_2(W/m^2)$	807	553	408	254
	$T_2(°C)$	58.26	48.73	43.30	37.52
3rd Module	$G_3(W/m^2)$	970	706	98	84
	$T_3(°C)$	64.37	54.47	31.67	31.15
4th Module	$G_4(W/m^2)$	987	718	71	344
	$T_4(°C)$	65.01	54.92	30.66	40.90
5th Module	$G_5(W/m^2)$	936	791	299	929
	$T_5(°C)$	63.10	56.66	39.21	62.83
6th Module	$G_6(W/m^2)$	952	475	576	750
	$T_6(°C)$	63.70	45.81	49.60	56.12
7th Module	$G_7(W/m^2)$	949	578	204	197
	$T_7(°C)$	63.58	49.67	35.65	35.38
8th Module	$G_8(W/m^2)$	878	659	351	551
	$T_8(°C)$	60.92	52.71	41.16	48.66
9th Module	$G_9(W/m^2)$	831	684	351	616
	$T_9(°C)$	59.16	53.65	41.16	51.10
10th Module	$G_{10}(W/m^2)$	834	702	134	473
	$T_{10}(°C)$	59.27	54.32	33.02	45.73

Under each condition, the fault diagnosis technique has been tested four times. One in each of them contains no fault, two consist of only OC or SC faults. Another case contains different combinations of OC and SC faults. Thus, sixteen (4x4) number of consecutive experiments (E1-E16) have been done to validate the proposed methodology with different test conditions. Different combinations of SC and OC faults have been created in the physical test system with different irradiance level as stated above. Corresponding module temperatures have also been considered.

GWO has been selected here as the optimizer to solve this optimization problem. Moreover, two other well-recognized optimization technique such as Genetic Algorithm (GA) and Tabu Search (TS) have also been adopted to solve these problems.

The simulation and algorithm have been run in MATLAB R2013a on Windows 7 environment, with Intel core i7 processor and RAM of 32 GB. The thorough results acquired from these experimentations have been tabulated as in Table 4.49.

Table 4.49

Fault diagnosis results

Experiment	Condition	Actual Fault		I^{MPP}_{meas} (A)	Optimality Condition (∈)	Algorithm	I^{MPP}_{sim} (A)	Fitness Value (*FIT*)	$\lvert P_{simulated} - P_{actual} \rvert$	Detected Fault	
		OC	SC							OC	SC
E1	C1	Nil†	Nil†	0.505690	0.04849	GWO	0.505692	0.000002	0.0019	Nil†	Nil†
						GA	0.505692	0.000002	0.0019	Nil†	Nil†
						TS	0.505692	0.000002	0.0019	Nil†	Nil†
E2		6,10	Nil†	0.505270	0.04935	GWO	0.505273	0.000003	0.0021	6,10	Nil†
						GA	0.505273	0.000003	0.0021	6,10	Nil†
						TS	0.505273	0.000003	0.0021	6,10	Nil†
E3		Nil†	2-4*,8	0.512000	0.06530	GWO	0.511994	0.000006	0.0033	Nil†	2-4*,8
						GA	0.511994	0.000006	0.0033	Nil†	2-4*,8
						TS	0.511994	0.000006	0.0033	Nil†	2-4*,8
E4		1,7,9	4,10	0.502760	0.04454	GWO	0.502764	0.000004	0.0027	1,7,9	4,10
						GA	0.502764	0.000004	0.0027	1,7,9	4,10
						TSΩ	0.502799	0.000039	0.0483	1,7,10	4,9
E5	C2	Nil†	Nil†	0.300940	0.01199	GWO	0.300939	0.000001	0.0004	Nil†	Nil†
						GA	0.300939	0.000001	0.0004	Nil†	Nil†
						TS	0.300939	0.000001	0.0004	Nil†	Nil†
E6		2,4,7	Nil†	0.299880	0.01182	GWO	0.299877	0.000003	0.0002	2,4,7	Nil†
						GA	0.299877	0.000003	0.0002	2,4,7	Nil†
						TS	0.299877	0.000003	0.0002	2,4,7	Nil†
E7		Nil†	1,3,5	0.346420	0.04114	GWO	0.346421	0.000001	0.0006	Nil†	1,3,5
						GA	0.346421	0.000001	0.0006	Nil†	1,3,5
						TS	0.346421	0.000001	0.0006	Nil†	1,3,5
E8		4,9	6-7	0.298840	0.01151	GWOΩ	0.298971	0.000131	0.1951	1,4,9	6
						GAΩ	0.298892	0.000052	0.0127	4,9	1,6
						TS	0.298838	0.000002	0.0011	4,9	6-7
E9	C3	Nil†	Nil†	0.187560	0.03647	GWO	0.187563	0.000003	0.0018	Nil†	Nil†
						GA	0.187563	0.000003	0.0018	Nil†	Nil†
						TS	0.187563	0.000003	0.0018	Nil†	Nil†
E10		1,8,9	Nil†	0.186780	0.03645	GWO	0.186784	0.000004	0.0026	1,8,9	Nil†
						GA	0.186784	0.000004	0.0026	1,8,9	Nil†
						TS	0.186784	0.000004	0.0026	1,8,9	Nil†
E11		Nil†	3,7	0.184294	0.00929	GWOΩ	0.184293	0.000001	0.2794	Nil†	2,7
						GAΩ	0.184092	0.000202	0.0752	2	7
						TSΩ	0.184452	0.000158	0.3661	3	7
E12		3	6-8*	0.21200	0.06366	GWO	0.211972	0.000018	0.0054	3	6-8*
						GA	0.211972	0.000018	0.0054	3	6-8*
						TSΩ	0.211033	0.000967	0.0683	Nil†	2,6-8*
E13	C4	Nil†	Nil†	0.298060	0.2820	GWO	0.298065	0.000005	0.0039	Nil†	Nil†
						GA	0.298065	0.000005	0.0039	Nil†	Nil†
						TS	0.298065	0.000005	0.0039	Nil†	Nil†
E14		4,8,9	Nil†	0.459330	0.2136	GWO	0.459321	0.000009	0.0062	4,8,9	Nil†
						GA	0.459321	0.000009	0.0062	4,8,9	Nil†
						TS	0.459321	0.000009	0.0062	4,8,9	Nil†
E15		Nil†	7-10*	0.460980	0.2342	GWO	0.460978	0.000002	0.0008	Nil†	7-10*
						GA	0.460978	0.000002	0.0008	Nil†	7-10*
						TS	0.460978	0.000002	0.0008	Nil†	7-10*
E16		2,6	8	0.295900	0.17754	GWO	0.295912	0.000012	0.0055	2,6	8
						GA	0.295912	0.000012	0.0055	2,6	8
						TS	0.295912	0.000012	0.0055	2,6	8

† Nil represents no occurrences of those faults. * SC fault among these modules in between. Ω Wrong fault detection

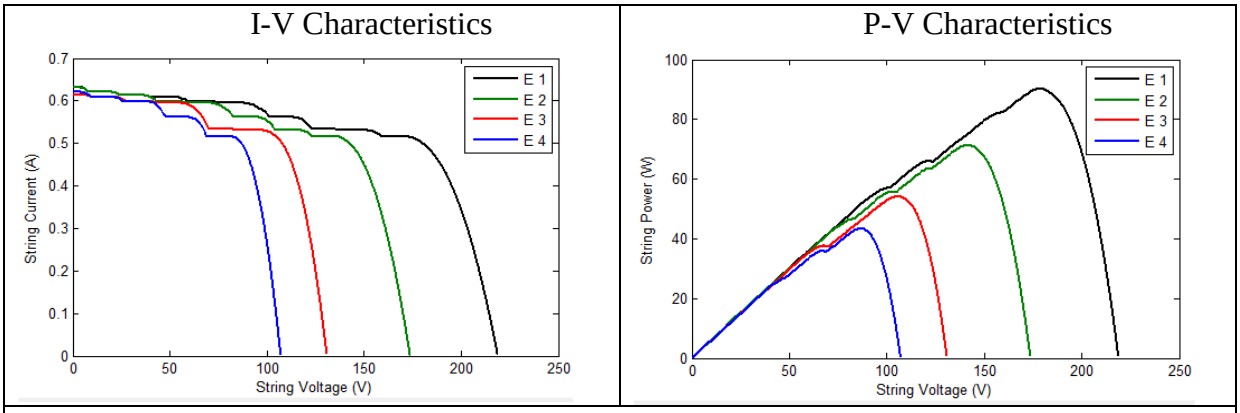

Fig. 4.56(a). Condition: C1, Experiment: E 1, E 2, E 3, E 4.

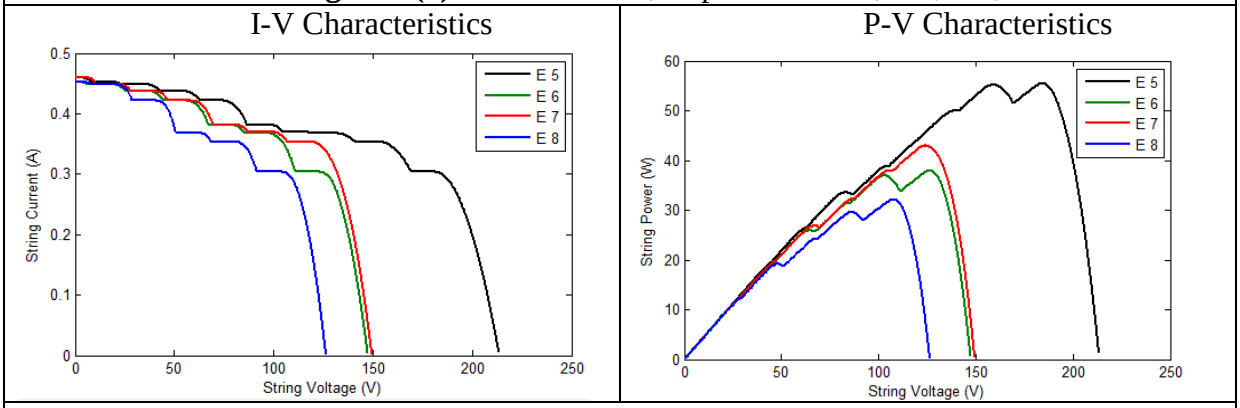

Fig. 4.56(b). Condition: C2, Experiment: E 5, E 6, E 7, E 8.

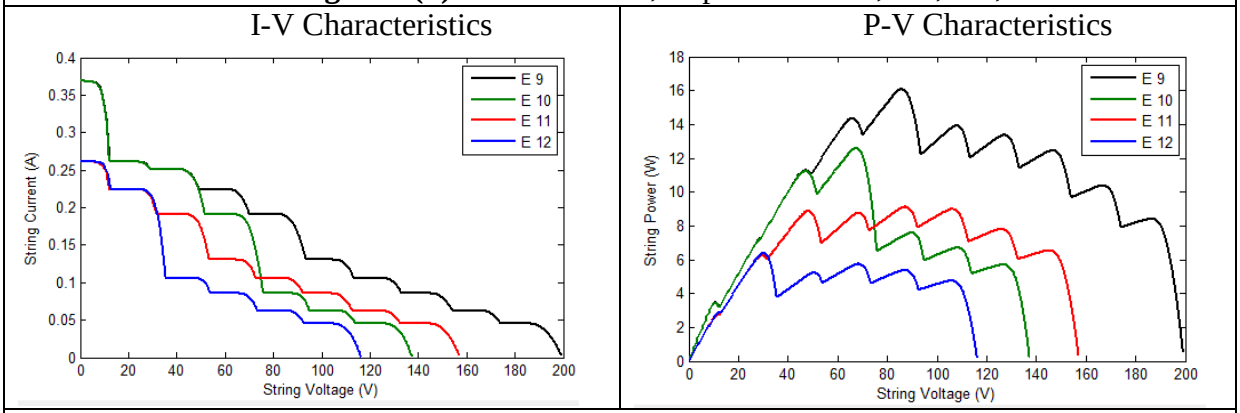

Fig. 4.56(c). Condition: C3, Experiment: E 9, E 10, E 11, E 12.

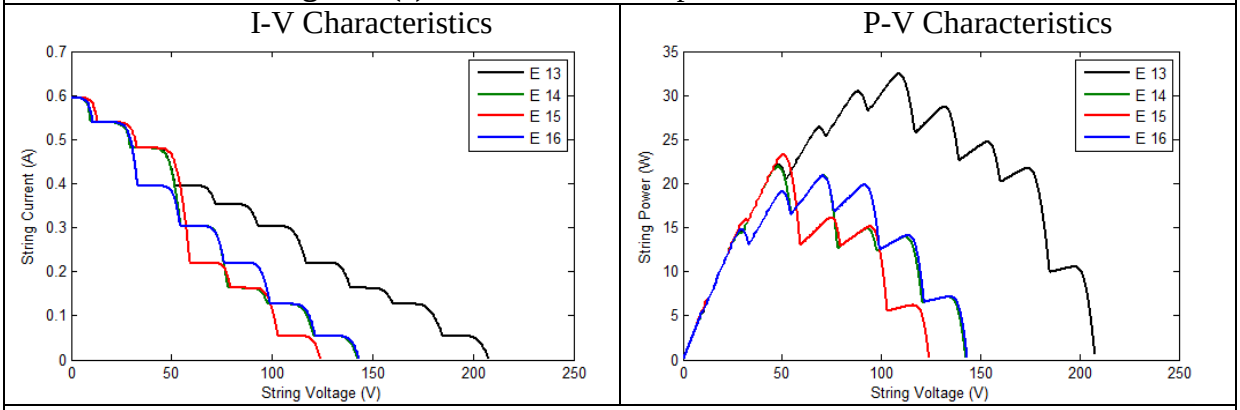

Fig. 4.56(d). Condition: C4, Experiment: E 13, E 14, E 15, E 16.

Fig. 4.56. P-V and I-V curves of the experimental test systems.

Here, in E1, E5, E9 and E13 no fault has been formed. In E2, E6, E10, and E14, there are only OC faults and in E3, E7, E11 and E15, there are only SC faults. Experiments E4, E8, E12 and E16 have a combination of both OC and SC faults.

Power-voltage (P-V) and current-voltage (I-V) characteristics for all of the experimental conditions are shown in Fig. 4.56. Here, all black, continuous curves represent the character of a healthy PV string (no fault). Whereas, green and red lines show P-V and I-V characteristics of the PV string with only OC and only SC faults, respectively. Blue lines represent both OC and SC faults together.

Motivation to perform the tests for healthy PV string is to confirm the capability of the proposed methodology to distinguish between faulty and healthy PV string in non-uniform irradiance. It has been noted in Table 4.49, that the proposed methodology qualifies for all these no-fault cases.

In E4, 1^{st}, 7^{th} and 9^{th} modules were open circuited, and 4^{th}, 10^{th} modules were short circuited. GWO and GA detect the fault correctly. But TS detects 1^{st}, 7^{th} and 10^{th} module as open circuited, and 4th and 9th modules as short circuited. Similarly, in case of E8, GWO and GA fail to detect the exact fault, but TS detects that. Again in E12, GWO and GA is able to detect faults correctly, but TS fails. In E11, all the techniques GWO, GA and TS fail to detect fault correctly. In all other experiments, except these four out of sixteen, all the three techniques are successful. It has been noted, it is able to distinguish between faulty and healthy conditions of a PV string under non-uniform irradiance with some moderately shaded and highly shaded PV modules.

Significantly, it has also been noted that, in all the cases where the optimizers have failed to detect faults, low fitness values have been achieved, but the optimality conditions for respective cases have not been fulfilled. In other successful cases, low fitness values have been achieved as well as the respective optimality conditions have been satisfied. Mathematically, this heuristic based fault diagnosis technique is a minimization problem with minimum possible value of zero. Though, the optimal solutions corresponding to the actual fault combinations are the unique solution to the proposed model, there are small gaps between the measured string current and the calculated fault current. In these cases, it may be counted as a success achieving a tiny number tending towards zero (sub-optimal point), if the fault combination causing the result matches exactly with the actual occurred faults. Hence, to validate the effectiveness of the obtained results, some facts have to be taken account. The test system is equipped with small 10 W modules. The generated current is small. There are limitations in accurate measurement of this physical string current. Thus, it can be assumed

that, if the optimizer reaches a sub-optimal point, but satisfies the optimality condition, the optimizer has performed successfully arresting the actual fault combination and the sub-optimality is caused by the limitations of sensors employed in physical parameter measurements. On the other hand, if the optimizer reaches a sub-optimal point, but does not satisfy the optimality condition, it is a failure of the optimizer and the detected fault combination is wrong. In those cases, the optimizer may be successful, if the iteration count is increased further than that has been set for this fault diagnosis method. But, it may not be feasible because it will consume large computational time, which is not suitable for real time fault detection scheme.

Analyzing the obtained results for different optimizers, it may be concluded that all these optimizers as solver are suitable in most of the cases. As discussed in the introduction, all the existing single fault diagnosis method alone is unable to completely diagnose the OC and SC faults and their locations in the faulty string. Some of them can detect SC faults only, some are only for OC faults, some can differentiate between the faulty or healthy string, some only find the number of OC and SC faults, and some can only distinguish the OC and SC fault type and so on. Here, the proposed methodology succeeds to detect and distinguish OC and SC faults and their locations in the PV string. It is also able to distinctly identify faulty string and healthy string under non-uniform irradiance.

4.10.3. Conclusion

In this work a new method of fault diagnosis in PV systems following string current has been presented. Grey Wolf Optimizer as well as Genetic Algorithm and Tabu Search Algorithm have been used here as a search technique. This method has been applied to a physical PV string consisting of 10 numbers of 12V, 10W 36 cell PV modules which detects faults correctly in most of the cases. Thus the effectiveness of the proposed methodology and the applicability of meta-heuristic optimization techniques as a solver have been confirmed.

The proposed method is able to explicitly identify the number and location of short circuit and open circuit faults in a PV string operating at MPP or whether it is in healthy condition in non-uniform irradiance regardless of the number of PV modules in a PV string. This fault detection algorithm follows the string current. So the number of monitoring parameter needed is less.

Here, only SC and OC type of faults have been considered. There are chances of occurrences of other related faults which can affect the PV string characteristics, including

string current, which can cause a placebo OC and SC faults. That may lead the proposed methodology to false detection of OC and SC faults.

Some preventive measures have been taken to minimize the chance to be incurred in false detection. The PV panels taken here to construct the test system were almost free from other deformities and well calibrated. The simulated PV system has also been minutely tuned with the physical test system. These help to cancel the effects on PV string currents caused by other faults and deformities and detect faults accurately in test cases performed in the laboratory.

Being a calculation based soft computing method; this proposed fault detection methodology is directly applicable to practical large scale PV systems. In this work, the PV panels of the physical test system are only of 10 watts. So, the change of string current caused by OC, SC faults is here in few mA ranges. There are limitations in measuring these small amounts of currents with high accuracy. In this downscaled laboratory environment, the global optimizer may often have a chance of failure to search the best answer. However, in practical large PV systems, OC, SC faults causes a large difference in string current. In those cases, the optimizers may likely to be more efficient to find faults.

Considering these studies and analysis, it can be concluded that the proposed methodology may be employed as a proficient fault detection method for PV systems.

This page is left blank intentionally

Chapter 5

Conclusion & Future-scope

==========

In this thesis optimization of power systems by application and development of soft computing techniques have been performed. The power system optimization problems have been proposed here to be categorized in two segments, namely, Large-scale power system optimization problems and Micro-scale power system optimization problems.

In class of Large-scale power system optimization problems, several studies have been done about optimal strategies and operation planning for economic dispatch and economic-environmental dispatch of single area and multi area large power systems, Wind power integrated multi area economic-environmental dispatch and short term hourly basis hydro-thermal generation scheduling of different power systems considering several technical constraints. Mathematical modeling in form of objective functions and constraints have been formulated. A novel energy policy that encourages proper estimation and maximization of wind energy generation has been proposed. Applicability of different heuristic and meta-heuristic optimization algorithms for different cases have been studied. Comparative studies of the obtained solutions by different techniques have also been done. Soft computing techniques to employ HTS algorithm for ED problems, AIS algorithm for MAED problems, MODE algorithm for MAEED problems, NSGA II algorithm for WMAED problems and IRCGA algorithm for short term hydro-thermal scheduling problems have been developed and solved throughout this thesis.

In class of Micro-scale power system optimization problems, several studies have been done on optimal placement and sizing of Distributed generation systems in power distribution networks. Transmission loss minimization along with voltage profile maintenance and have been focused. Studies with variation of load have been done. These optimization problems have been successfully solved applying WCA algorithm. Optimal integration and operation of distributed renewable energy recourses focusing on economic aspect have been studied for several realistic cases with different demand profile like a whole township (where overall power demand prominently varies with the weather), a typical railway rake maintenance depot (contains very unique load profile) and a typical hospital campus. In those cases, economic power operations increasing the share of renewable energy recourses have been proposed. Optimal power operation planning in a township has been done applying SSO

algorithm. For the case of optimal power operation planning in a rail-way rake maintenance depot, GSA algorithm has been employed. These techniques showed proficiency.

Active distribution systems have been thoroughly designed forming mocro-grid and even nano-grids. Focusing on the control prospect; comprehensive electrical modeling and then mathematical modeling have been done to optimally design these type of micro/nano scale power networks. Optimum economic power operation for a PV aided battery storage connected nano-grid for a typical hospital campus have been proposed. Robust tracking controllers for automatic power operation have been designed. IRCGA algorithm has been successfully used to perform these tasks. Focusing on the fault analysis aspect; faults of photovoltaic system, which takes a large share in renewable energy sector, have been considered for studying. Detailed mathematical model of photovoltaic string along with other accessories like maximum power point tracking converter etc, have been constructed. A novel optimization technique based fault detection scheme with methodology has been proposed that can proficiently detect and locate open and short circuit faults of modules in a photovoltaic string. Application of GWO algorithm has been done to validate this proposed fault detection scheme in this thesis.

There are endless scopes to perform research in power system optimization problems in near future. Share of renewable energy in global energy sector is gaining drastically. Need of more optimum unit commitment and generation planning with complex power networks, with different renewable energy resources with different characteristics, is evident. Optimum policies on economic bidding of renewable power producers in competitive electricity market ensuring reliable and environment friendly operation is going to be a vital matter of optimization. There are scopes of optimization in various power system protection problems like over frequency error caused by adequacy of wind generation in some countries, harmonics reduction and power quality improvement of the supplied power from the renewable energy generators associated with number of power electronic devices, and so on. A large share of global energy demand is for transportion sector. In near future almost all transportation will be done utilizing electrical energy. That will affect the power demand scenario of complex power systems. Optimal placement of electric vehicle charging stations is going to be a crucial power system optimization problem. Nano-scale power systems of smart buildings will need instance operation planning and optimization. Fault analysis and minimization of different renewable energy generators is tending to be a vital research goal. Researches on these power system optimization problems (along with many others) may be performed extending the basis of the works in this thesis.

This page is left blank intentionally

References

[1] Walters, David C., and Gerald B. Sheble. "Genetic algorithm solution of economic dispatch with valve point loading." *IEEE transactions on Power Systems* 8.3 (1993): 1325-1332.

[2] Orero, S. O., and M. R. Irving. "Economic dispatch of generators with prohibited operating zones: a genetic algorithm approach." *IEE Proceedings-Generation, Transmission and Distribution* 143.6 (1996): 529-534.

[3] Lin, Whei-Min, Fu-Sheng Cheng, and Ming-Tong Tsay. "An improved tabu search for economic dispatch with multiple minima." *IEEE Transactions on power systems* 17.1 (2002): 108-112.

[4] Chiang, Chao-Lung. "Improved genetic algorithm for power economic dispatch of units with valve-point effects and multiple fuels." *IEEE transactions on power systems* 20.4 (2005): 1690-1699.

[5] Pereira-Neto, A., C. Unsihuay, and O. R. Saavedra. "Efficient evolutionary strategy optimisation procedure to solve the nonconvex economic dispatch problem with generator constraints." *IEE Proceedings-Generation, Transmission and Distribution* 152.5 (2005): 653-660.

[6] Yang, Hong-Tzer, Pai-Chuan Yang, and Ching-Lien Huang. "Evolutionary programming based economic dispatch for units with non-smooth fuel cost functions." *IEEE transactions on Power Systems* 11.1 (1996): 112-118.

[7] Sinha, Nidul, R. Chakrabarti, and P. K. Chattopadhyay. "Evolutionary programming techniques for economic load dispatch." *IEEE Transactions on evolutionary computation* 7.1 (2003): 83-94.

[8] Gaing, Zwe-Lee. "Particle swarm optimization to solving the economic dispatch considering the generator constraints." *IEEE transactions on power systems* 18.3 (2003): 1187-1195.

[9] Park, Jong-Bae, et al. "A particle swarm optimization for economic dispatch with nonsmooth cost functions." *IEEE Transactions on Power systems* 20.1 (2005): 34-42.

[10] Selvakumar, A. Immanuel, and K. Thanushkodi. "A new particle swarm optimization solution to nonconvex economic dispatch problems." *IEEE transactions on power systems* 22.1 (2007): 42-51.

[11] Chaturvedi, Krishna Teerth, Manjaree Pandit, and Laxmi Srivastava. "Self-organizing hierarchical particle swarm optimization for nonconvex economic dispatch." *IEEE transactions on power systems* 23.3 (2008): 1079-1087.

[12] Park, Jong-Bae, et al. "An improved particle swarm optimization for nonconvex economic dispatch problems." *IEEE Transactions on Power Systems* 25.1 (2010): 156-166.

[13] Bhattacharya, Aniruddha, and Pranab Kumar Chattopadhyay. "Biogeography-based optimization for different economic load dispatch problems." *IEEE transactions on power systems* 25.2 (2010): 1064-1077.

[14] Moradi-Dalvand, Mohammad, et al. "Continuous quick group search optimizer for solving non-convex economic dispatch problems." *Electric Power Systems Research* 93 (2012): 93-105.

[15] Noman, Nasimul, and Hitoshi Iba. "Differential evolution for economic load dispatch problems." *Electric Power Systems Research* 78.8 (2008): 1322-1331.

[16] dos Santos Coelho, Leandro, Teodoro Cardoso Bora, and Viviana Cocco Mariani. "Differential evolution based on truncated Levy-type flights and population diversity measure to solve economic load dispatch problems." *International Journal of Electrical Power & Energy Systems* 57 (2014): 178-188.

[17] Zhao, Jian, Shixin Liu, and Yifan Wang. "Cuckoo search algorithm with interactive learning for economic dispatch." *Control Conference (CCC), 2017 36th Chinese*. IEEE, 2017.

[18] Zhao, Jian, Shixin Liu, and Yifan Wang. "Cuckoo search algorithm with interactive learning for economic dispatch." *Control Conference (CCC), 2017 36th Chinese*. IEEE, 2017.

[19] Patel, Vivek K., and Vimal J. Savsani. "Heat transfer search (HTS): a novel optimization algorithm." *Information Sciences* 324 (2015): 217-246.

[20] Chowdhury, Badrul H., and Saifur Rahman. "A review of recent advances in economic dispatch." *IEEE Transactions on Power Systems* 5.4 (1990): 1248-1259.

[21] Shoults, Raymond R., et al. "A practical approach to unit commitment, economic dispatch and savings allocation for multiple-area pool operation with import/export constraints." *IEEE Transactions on Power Apparatus and Systems* 2 (1980): 625-635.

[22] Quintana, V. H., et al. "Constrained economic dispatch of multi-area systems using the Dantzig-Wolfe decomposition principle." *IEEE Transactions on Power Apparatus and Systems* 4 (1981): 2127-2137.

[23] Doty, K. W., and P. L. McEntire. "An analysis of electric power brokerage systems." *IEEE Transactions on Power Apparatus and Systems* 2 (1982): 389-396.

[24] Desell, A. L., et al. "Transmission constrained production cost analysis in power system planning." *IEEE transactions on power apparatus and systems* 8 (1984): 2192-2198.

[25] Helmick, S. D., and R. R. Shoults. "A practical approach to an interim multi-area economic dispatch using limited computer resources." *IEEE transactions on power apparatus and systems* 6 (1985): 1400-1404.

[26] Ouyang, Z., and S. M. Shahidehpour. "Heuristic multi-area unit commitment with economic dispatch." *IEE Proceedings C (Generation, Transmission and Distribution)*. Vol. 138. No. 3. IET Digital Library, 1991.

[27] Wang, Chunyan, and S. M. Shahidehpour. "A decomposition approach to nonlinear multi-area generation scheduling with tie-line constraints using expert systems." *IEEE Transactions on power systems* 7.4 (1992): 1409-1418.

[28] Streiffert, Dan. "Multi-area economic dispatch with tie line constraints." *IEEE Transactions on Power Systems* 10.4 (1995): 1946-1951.

[29] Wernerus, J., and L. Söder. *Area price based multi-area economic dispatch with transmission losses and constraints*. No. NEI-SE--206. 1995.

[30] Yalcinoz, T., and M. J. Short. "Neural networks approach for solving economic dispatch problem with transmission capacity constraints." *IEEE Transactions on Power Systems* 13.2 (1998): 307-313.

[31] Jayabarathi, G. Sadasivam, V. Ramachandran, T. "Evolutionary programming-based multiarea economic dispatch with tie line constraints." *Electric Machines &Power Systems* 28.12 (2000): 1165-1176.

[32] Chen, Chun-Lung, and Nanming Chen. "Direct search method for solving economic dispatch problem considering transmission capacity constraints." *IEEE transactions on power systems* 16.4 (2001): 764-769.

[33] De Castro, Leandro Nunes, and Fernando José Von Zuben. "Artificial immune systems: Part I–basic theory and applications." *Universidade Estadual de Campinas, Dezembro de, Tech. Rep* 210.1 (1999).

[34] De Castro, Leandro N., and Fernando J. Von Zuben. "Learning and optimization using the clonal selection principle." *IEEE transactions on evolutionary computation* 6.3 (2002): 239-251.
[35] Nicosia, Giuseppe. *Artificial Immune Systems: Third International Conference: Proceedings*. Springer, 2004.
[36] Cutello, Vincenzo, et al. "Immune algorithms with aging operators for the string folding problem and the protein folding problem." *European Conference on Evolutionary Computation in Combinatorial Optimization*. Springer, Berlin, Heidelberg, 2005.
[37] Cutello, V., et al. "Real coded clonal selection algorithm for global numerical optimization using a new inversely proportional hypermutation operator." *21st ACM SAC*. 2006.
[38] Cutello, Vincenzo, et al. "On the convergence of immune algorithms." *Foundations of Computational Intelligence, 2007. FOCI 2007. IEEE Symposium on*. IEEE, 2007.
[39] Rahman, Titik Khawa Abdul, Saiful Izwan Suliman, and Ismail Musirin. "Artificial immune-based optimization technique for solving economic dispatch in power system." *Neural Nets*. Springer, Berlin, Heidelberg, 2006. 338-345.
[40] Liao, Gwo-Ching. "Short-term thermal generation scheduling using improved immune algorithm." *Electric Power Systems Research* 76.5 (2006): 360-373.
[41] Hanneschlager, R. E.: Clean Air Act Amendments of 1990, 1990.
[42] J.L. Golden, C.J. Stansbeny, R.L. Vice, J.T. Wood, J. Ballance, G. Brown et al., "Potential impacts of clean air regulations on system operations," IEEE Trans. Power Syst., vol. 10, no. 2, pp. 647-656, May 1995.
[43] J. Nanda, D.P. Kothari, and K.S. Lingamurthy, "Economic emission load dispatch through goal programming techniques," IEEE Trans.Energy Convers., vol. 3, no. 1, pp. 26–32, Mar 1988.
[44] J.S. Dhillon, S.C. Parti, and D.P. Kothari, "Stochastic economic emission load dispatch," Electr. Power Syst. Res., vol. 26, no. 3, pp. 179-186, Apr 1993.
[45] D. Srinivasan, C.S. Chang, and A.C. Liew, "Multiobjective generation scheduling using fuzzy optimal search technique," in Proc. IEE Gener. Transm. Distrib., vol. 141, no. 3, pp. 233-242, May 1994.
[46] A. Farag, S. Al-Baiyat, and T.C. Cheng, "Economic load dispatch multiobjective optimization procedures using linear programming techniques," IEEE Trans. Power Syst., vol. 10, no. 2, pp. 731-738, May 1995.
[47] C.M. Huang, H.T. Yang, and C.L. Huang, "Bi-objective power dispatch using fuzzy satisfaction-maximizing decision approach," IEEE Trans. Power Syst., vol. 12, no. 4, pp. 1715-1721, Nov 1997.
[48] D.B. Das, and C. Patvardhan, "New multi-objective stochastic search technique for economic load dispatch," in Proc. IEE Gener. Transm. Distrib., vol. 145, no. 6, pp. 747-752, Nov 1998.
[49] M.A. Abido, "Environmental/economic power dispatch using multiobjective evolutionary algorithms," IEEE Trans. Power Syst., vol. 18, no. 4, pp. 1529-1537, Nov 2003.
[50] R.T.F.A. King, H.C.S. Rughooputh and K. Deb, "Evolutionary multi-objective environmental/economic dispatch: stochastic versus deterministic approaches," in Proc. Evol. Multi-Criterion Optim. Int. Conf., Lect. Notes Compu. Sci., vol. 3410, C.A.C. Coello, A. H. Aguirre and E. Zitzler, Eds. Berlin, Heidelberg: Springer, 2005, pp. 677-691.
[51] M.A. Abido, "Multiobjective evolutionary algorithms for power dispatch problem," IEEE Trans. Evol. Comput., vol. 10, no. 3, pp. 315-329, Jun 2006.
[52] L. Wang, and C. Singh, "Stochastic economic emission load dispatch through a modified particle swarm optimization algorithm," Electr. Power Syst. Res., vol. 78, no. 8, pp. 1466–1476, Aug 2008.

[53] S. Agrawal, B.K. Panigrahi, and M.K. Tiwari, "Multiobjective particle swarm algorithm with fuzzy clustering for electrical power dispatch," IEEE Trans. Evol. Comput., vol. 12, no. 5, pp. 529–541, Oct 2008.
[54] N. Srinivas, and K. Deb, "Multiobjective optimization using nondominated sorting in genetic algorithms," Evol. Comput., vol. 2, no. 3, pp. 221-248, Sep 1994.
[55] C.A.C. Coello, "A comprehensive survey of evolutionary-based multiobjective optimization techniques," Knowledge and Information Syst., vol. 1, no. 3, pp. 269-308, Aug 1999.
[56] E. Zitzler, M. Laumanns and L. Thiele, "SPEA2: improving the strength pareto evolutionary algorithm," TIK Report, no. 103. Zurich, Switzerland: Swiss Federal Institute of Technology (ETH),2001, pp. 1-21.
[57] K. Deb, A. Pratap, S. Agarwal, and T. Meyarivan, "A fast and elitist multiobjective genetic algorithm: NSGA-II," IEEE Trans. Evol. Comput., vol. 6, no. 2, pp. 182-197, Apr 2002.
[58] Wang, L., Singh, C.: 'Reserve-constrained multiarea environmental/economic dispatch using enhanced particle swarm optimization'. Proc. Symp. System and Information Engineering Design, Charlottesville, VA, USA,April2006,pp. 96–100
[59] Wang, L., Singh, C.: 'Reserve-constrained multiarea environmental/economic dispatch based on particle swarm optimization with local search', Eng. Appl. Artif. Intell., 2009, 22, (2), pp. 298–307
[60] Pandit, M., Srivastava, L., Sharma, M.: 'Environmental economic dispatch in multi-area power system employing improved differential evolution with fuzzy selection', Appl. Soft Comput., 2015, 28, pp. 498–510
[61] Secui, D. C.: 'The chaotic global best artificial bee colony algorithm for the multi-area economic/emission dispatch', Energy, 2015, 93, (2), pp. 2518–2545
[62] Azizipanah-Abarghooee, R., Dehghanian, P., Terzija, V.: 'Practical multi-area bi-objective environmental economic dispatch equipped with a hybrid gradient search method and improved Jaya algorithm', IET Gener., Transm. Distrib., 2016, 10, (14), pp. 3580–3596
[63] Basu, M.: 'Teaching–learning-based optimization algorithm for multi-area economic dispatch', Energy, 2014, 68, pp. 21–28
[64] 'Global wind energy outlook', http://gwec.net/publications/global-wind-energy-outlook/, accessed 22 September 2017
[65] Kuo, C. C.: 'Generation dispatch under large penetration of wind energy considering emission and economy', Energy Convers. Manage., 2010, 51, (1), pp. 89–97
[66] Kuo, C. C., Taso, T. F.: 'Generation dispatch under large penetration of wind power considering emission and economy'. Proc. Int. Conf. Energy Environment Technology, Guilin, Guangxi, China, October 2009, 1, pp. 679–682
[67] Kuo, C. C.: 'Wind energy dispatch considering environmental and economic factors', Renew. Energy, 2010, 35, (10), pp. 2217–2227
[68] Liao, G. C.: 'Solve environmental economic dispatch of smart microgrid containing distributed generation system–Using chaotic quantum genetic algorithm', Int. J. Elect. Power Energy Syst., 2012, 43, (1), pp. 779–787
[69] Kherfane, N., Kherfane, R. L., Younes, M., et al.: 'Economic and emission dispatch with renewable energy using HAS', Energy Procedia, 2014, 50, pp. 970–979
[70] Zhao, X., Wu, L., Zhang, S.: 'Joint environmental and economic power dispatch considering wind power integration: Empirical analysis from Liaoning Province of China', Renew. Energy, 2013, 52, pp. 260–265
[71] Lianjun, S., Ming, Z., Fan, Y., et al.: 'Economic dispatch model considering randomness and environmental benefits of wind power'. Proc. Int. Conf. Electrical and Control Engineering, Wuhan, China, June 2010, pp. 3676–3679

[72] Nguyen, N., Johnson, V., Mitra, J.: 'Environmental-economic dispatch of power system in the presence of wind generation'. Proc. North American Power Symposium, Charlotte, NC, USA,October2015, pp. 1–6
[73] Jia-qing, Z.: 'Research on environmental economic dispatch of power system including wind farm', Phys. Procedia, 2012, 24, pp. 107–113
[74] Lu, Z., He, S., Feng, T., et al.: 'Robust economic/emission dispatch considering wind power uncertainties and flexible operation of carbon capture and storage', Int. J. Elect. Power Energy Syst., 2014, 63, pp. 285–292
[75] Wei, W., Liu, F., Wang, J., et al.: 'Robust environmental-economic dispatch incorporating wind power generation and carbon capture plants', Appl. Energy, 2016, 183, pp. 674–684
[76] Liao, H. L., Wu, Q. H., Li, Y. Z., et al.: 'Economic emission dispatching with variations of wind power and loads using multi-objective optimization by learning automata', Energy Convers. Manage., 2014, 87, pp. 990–999
[77] Wais, P.: Two and three-parameter Weibull distribution in available wind power analysis. Renew. Energy, 2017, 103, pp. 15–29
[78] Jin, J., Zhou, D., Zhou, P., et al. 'Environmental/economic power dispatch with wind power', Renew. Energy, 2014, 71, pp. 234–242
[79] Azizipanah-Abarghooee, R., Niknam, T., Roosta, A., et al.: 'Probabilistic multiobjective wind-thermal economic emission dispatch based on point estimated method', Energy, 2012, 37, (1), pp. 322–335
[80] Jadhav, H. T., Roy, R.: 'Gbest guided artificial bee colony algorithm for environmental/economic dispatch considering wind power', Expert Syst. Appl., 2013, 40, (16), pp. 6385–6399
[81] Mondal, S., Bhattacharya, A., nee Dey, S. H.: 'Multi-objective economic emission load dispatch solution using gravitational search algorithm and considering wind power penetration', Int. J. Elect. Power Energy Syst., 2013, 44, (1), pp. 282–292
[82] Lu, Z., He, S., Feng, T., et al. 'Robust economic/emission dispatch considering wind power uncertainties and flexible operation of carbon capture and storage', Int. J. Elect. Power Energy Syst., 2014, 63, pp. 285–292
[83] Zhu, Y., Wang, J., Qu, B.: 'Multi-objective economic emission dispatch considering wind power using evolutionary algorithm based on decomposition', Int. J. Elect. Power Energy Syst., 2014, 63, pp. 434–445
[84] Bilil, H., Aniba, G., Maaroufi, M.: 'Probabilistic economic/environmental power dispatch of power system integrating renewable energy sources', Sustain. Energy Technol. Assessments, 2014, 8, pp. 181–190
[85] Ghasemi, A., Gheydi, M., Golkar, M. J., et al.: 'Modeling of wind/environment/economic dispatch in power system and solving via an online learning meta-heuristic method', Appl. Soft Comput., 2016, 43, pp. 454–468
[86] Jin, J., Zhou, D., Zhou, P., et al.: 'Dispatching strategies for coordinating environmental awareness and risk perception in wind power integrated system', Energy, 2016, 106, pp. 453–463
[87] Lin, J.: 'Multiple-objective problems: 'Pareto-optimal solutions by method of proper equality constraints', IEEE Trans. Autom. Control, 1976, 21, (5), pp. 641–650
[88] Zitzler, E., Thiele, L.: 'Multiobjective evolutionary algorithms: A comparative case study and the strength pareto approach', IEEE Trans. Evol. Comput., 1999, 3, (4), pp. 257–271
[89] Xue, F., Sanderson, A. C., Graves, R. J.: 'Pareto-based multi-objective differential evolution'. Proc. Congress Evolutionary Computation, Canberra, ACT, Australia, Australia,December2003, 2, pp. 862–869

[90] Wood, A. J., & Wollenberg, B. F. (2012). Power generation, operation, and control. John Wiley & Sons.
[91] Carvalho, M. F., &Soares, S. (1987). An efficient hydrothermal scheduling algorithm. IEEE Transactions on Power Systems, 2(3), 537-542.
[92] Pereira, M. V. F., & Pinto, L. M. V. G. (1983). Application of decomposition techniques to the mid-and short-term scheduling of hydrothermal systems. IEEE Transactions on power apparatus and systems, (11), 3611-3618.
[93] Xi, E., Guan, X., & Li, R. (1999). Scheduling hydrothermal power systems with cascaded and head-dependent reservoirs. IEEE Transactions on power systems, 14(3), 1127-1132.
[94] Tufegdzic, N., Frowd, R. J., &Stadlin, W. O. (1996). A coordinated approach for real-time short term hydro scheduling. IEEE Transactions on Power Systems, 11(4), 1698-1704.
[95] Engles, L., Larson, R. E., Peschon, J., & Stanton, K. N. (1976). Dynamic programming applied to hydro and thermal generation scheduling. In IEEE tutorial course text. IEEE New York.
[96] Jin-Shyr, Y., &Nanming, C. (1989). Short term hydrothermal coordination using multi-pass dynamic programming. IEEE Transactions on Power Systems, 4(3), 1050-1056.
[97] Chang, S. C., Chen, C. H., Fong, I. K., & Luh, P. B. (1990). Hydroelectric generation scheduling with an effective differential dynamic programming algorithm. IEEE transactions on power systems, 5(3), 737-743.
[98] Sjelvgren, D., Andersson, S., Andersson, T., Nyberg, U., & Dillon, T. S. (1983). Optimal operations planning in a large hydro-thermal power system. IEEE Transactions on Power Apparatus and Systems, (11), 3644-3651.
[99] Nilsson, O., & Sjelvgren, D. (1996). Mixed-integer programming applied to short-term planning of a hydro-thermal system. IEEE Transactions on Power Systems, 11(1), 281-286.
[100] Jia, J. (2013). Mixed-integer linear programming formulation for short-term scheduling of cascaded hydroelectric plants with pumped-storage units. Electric Power Components and Systems, 41(15), 1456-1468.
[101] Wong, K. P., & Wong, Y. W. (1994).Short-term hydrothermal scheduling part. I. Simulated annealing approach. IEE Proceedings-Generation, Transmission and Distribution, 141(5), 497-501.
[102] Sinha, N., Chakrabarti, R., & Chattopadhyay, P. K. (2003).Fast evolutionary programming techniques for short-term hydrothermal scheduling. Electric Power Systems Research, 66(2), 97-103.
[103] Yang, P. C., Yang, H. T., & Huang, C. L. (1996).Scheduling short-term hydrothermal generation using evolutionary programming techniques. IEE Proceedings-Generation, Transmission and Distribution, 143(4), 371-376.
[104] Hota, P. K., Chakrabarti, R., & Chattopadhyay, P. K. (1999).Short-term hydrothermal scheduling through evolutionary programming technique. Electric Power Systems Research, 52(2), 189-196.
[105] Werner, T. G., & Verstege, J. F. (1999).An evolution strategy for short-term operation planning of hydrothermal power systems. IEEE Transactions on power systems, 14(4), 1362-1368.
[106] Basu, M. (2004). An interactive fuzzy satisfying method based on evolutionary programming technique for multiobjective short-term hydrothermal scheduling. Electric Power Systems Research, 69(2-3), 277-285.
[107] Gil, E., Bustos, J., & Rudnick, H. (2003).Short-term hydrothermal generation scheduling model using a genetic algorithm. IEEE Transactions on power systems, 18(4), 1256-1264.

[108] Goldberg, D. E. (2014).Genetic algorithms in search, optimization, and machine learning, addison-wesley, reading, ma, 1989. Google Scholar.
[109] Orero, S. O., & Irving, M. R. (1998).A genetic algorithm modelling framework and solution technique for short term optimal hydrothermal scheduling. IEEE Transactions on Power Systems, 13(2), 501-518.
[110] Kumar, V. S., & Mohan, M. R. (2011).A genetic algorithm solution to the optimal short-term hydrothermal scheduling. International Journal of Electrical Power & Energy Systems, 33(4), 827-835.
[111] Gjorgiev, B., Kančev, D., & Čepin, M. (2013).A new model for optimal generation scheduling of power system considering generation units availability. International Journal of Electrical Power & Energy Systems, 47, 129-139.
[112] Mandal, K. K., & Chakraborty, N. (2008).Differential evolution technique-based short-term economic generation scheduling of hydrothermal systems. Electric Power Systems Research, 78(11), 1972-1979.
[113] Eberhart, R. C., & Kennedy, J. (1995).Particle swarm optimization. In IEEE International Conference on Neural Networks, Perth, Australia.
[114] Shi, Y., & Eberhart, R. (1998, May). A modified particle swarm optimizer. In Evolutionary Computation Proceedings, 1998. IEEE World Congress on Computational Intelligence., The 1998 IEEE International Conference on (pp. 69-73). IEEE.
[115] Eberhart, R. C., & Shi, Y. (1998, March).Comparison between genetic algorithms and particle swarm optimization. In International conference on evolutionary programming (pp. 611-616).Springer, Berlin, Heidelberg.
[116] Hota, P. K., Barisal, A. K., & Chakrabarti, R. (2009).An improved PSO technique for short-term optimal hydrothermal scheduling. Electric Power Systems Research, 79(7), 1047-1053.
[117] Yu, B., Yuan, X., & Wang, J. (2007). Short-term hydro-thermal scheduling using particle swarm optimization method. Energy Conversion and Management, 48(7), 1902-1908.
[118] Amjady, N., & Soleymanpour, H. R. (2010).Daily hydrothermal generation scheduling by a new modified adaptive particle swarm optimization technique. Electric power systems research, 80(6), 723-732.
[119] Mahor, A., &Rangnekar, S. (2012). Short term generation scheduling of cascaded hydro electric system using novel self adaptive inertia weight PSO. International Journal of Electrical Power & Energy Systems, 34(1), 1-9.
[120] Swain, R. K., Barisal, A. K., Hota, P. K., & Chakrabarti, R. (2011).Short-term hydrothermal scheduling using clonal selection algorithm. International Journal of Electrical Power & Energy Systems, 33(3), 647-656.
[121] Rao, R. V., Savsani, V. J., & Vakharia, D. P. (2012). Teaching–learning-based optimization: an optimization method for continuous non-linear large scale problems. Information Sciences, 183(1), 1-15.
[122] Roy, P. K. (2013). Teaching learning based optimization for short-term hydrothermal scheduling problem considering valve point effect and prohibited discharge constraint. International Journal of Electrical Power & Energy Systems, 53, 10-19.
[123] Bai, X., & Shahidehpour, S. M. (1996).Hydro-thermal, scheduling by tabu search and decomposition method. IEEE Transactions on Power Systems, 11(2), 968-974.
[124] Huang, S. J. (2001). Enhancement of hydroelectric generation scheduling using ant colony system based optimization approaches. IEEE Transactions on Energy Conversion, 16(3), 296-301.

[125] Liao, X., Zhou, J., Zhang, R., & Zhang, Y. (2012).An adaptive artificial bee colony algorithm for long-term economic dispatch in cascaded hydropower systems. International Journal of Electrical Power & Energy Systems, 43(1), 1340-1345.
[126] Holland, J. H. (1992). Adaptation in natural and artificial systems: an introductory analysis with applications to biology, control, and artificial intelligence. MIT press.
[127] Deb, K., & Agrawal, R. B. (1995). Simulated binary crossover for continuous search space. Complex systems, 9(2), 115-148.
[128] Herrera, F., Lozano, M., & Verdegay, J. L. (1998).Tackling real-coded genetic algorithms: Operators and tools for behavioural analysis. Artificial intelligence review, 12(4), 265-319.
[129] Kari Alanne, and ArtoSaari, "Distributed energy generation and sustainable development," Elsevier, ScienceDirect, Renewable and Sustainable Energy Reviews, vol. 10, iss. 6,pp. 539–558, December 2006.
[130] Hassan Nikkhajoei, and Robert H. Lasseter, "Distributed generation interface to the CERTS microgrid," IEEE Trans. Power Delivery, vol. 24, no. 3, July 2009.
[131] Michiel Houwing, Petra Heijnen, and Ivo Bouwmans, "Socio-technical complexity in energy infrastructures," Conceptual framework to study the impact of domestic level energy generation, storage and exchange; in Proc.2006 IEEE Systems, Man, and Cybernetics International Conf., Taipei, Taiwan, pp. 906-911, 8-11 October, 2006.
[132] Thomas Ackermann, Göran Andersson, and Lennart Söder, "Distributed generation: a definition," Elsevier, ScienceDirect, Electric Power Systems Research, vol. 57, iss. 3, pp. 195–204, April 2001.
[133] Satish Kumar Injeti, and N. Prema Kumar,"A novel approach to identify optimal access point and capacity of multiple DGs in a small, medium and large scale radial distribution systems," Elsevier, ScienceDirect, Int J Electrical Power &Energy Systems, vol. 45,pp.142–151, 2013.
[134] Tuba Gözel, and M. Hakan Hocaoglu,"An analytical method for the sizing and siting of distributed generators in radial systems," Electric Power Systems Research, vol. 79, iss. 6, pp. 912–918, June 2009.
[135] Duong Quoc Hung, and Nadarajah Mithulananthan, "Multiple distributed generator placement in primary distribution networks for loss reduction," IEEE Trans. Industrial Electronics, vol. 60, no. 4, pp. 1700–1708, April 2013.
[136] M.M. Aman, G.B. Jasmon, H. Mokhlis, and A.H.A. Bakar, "Optimal placement and sizing of a DG based on a new power stability index and line losses," Elsevier, ScienceDirect, Int J Electrical Power &Energy Systems, vol. 43, iss. 1, pp. 1296–1304, December 2012.
[137] M.A. Kashem, An D.T. Le, M. Negnevitsky, and G. Ledwich,"Distributed generation for minimization of power losses in distribution systems," IEEE PES General Meeting, pp. 1-8, 2006.
[138] Fahad S. Abu-Mouti, and M. E.El-Hawary, "Optimal distributed generation allocation and sizing in distribution systems via Artificial Bee Colony algorithm," IEEE Trans. Power Delivery, vol. 26, iss. 4, pp. 2090–2101, October 2011.
[139] Carmen L.T. Borges, and Djalma M. Falcão, "Optimal distributed generation allocation for reliability, losses, and voltage improvement," Elsevier, ScienceDirect, Int J Electrical Power and Energy Systems, vol. 28, iss. 6, pp. 413–420, July 2006.
[140] Sh. Abdi, and K. Afshar,"Application of IPSO-Monte Carlo for optimal distributed generation allocation and sizing," Elsevier, ScienceDirect, Int J Electrical Power & Energy Systems, vol. 44, iss. 1, pp. 786–797, January 2013.
[141] Juan Andrés, Martín García, and Antonio José Gil Mena, "Optimal distributed generation location and size using a modified teaching– learning based optimization algorithm,"

Elsevier, ScienceDirect, Int J Electrical Power &Energy Systems, vol. 50, pp.65–75, September 2013.

[142] Y. M. Atwa, E. F. El-Saadany, M. M. A. Salama, and R.Seethapathy, "Optimal renewable resources mix for distribution system energy loss minimization," IEEE Trans. Power Systems, vol. 25, no. 1, pp. 360–370, February 2010.

[143] FerryA. Viawan, and Daniel Karlsson, "Voltage and reactive power control in systems with synchronous machine-based distributed generation," IEEE Trans. Power Delivery, vol. 23, no. 2, pp. 1079–1087, April 2008.

[144] Naresh Acharya, Pukar Mahat, and N. Mithulananthan, "An analytical approach for DG allocation in primary distribution network," Int J Electrical Power& Energy Systems, vol.28, iss. 10, pp. 669–678, December 2006.

[145] Hadi Eskandar, Ali Sadollah, Ardeshir Bahreininejad, and Mohd Hamdi, "Water cycle algorithm –A novel metaheuristic optimization method for solving constrained engineering optimization problems," Elsevier, ScienceDirect, Computers & Structures vols. 110-111, pp. 151-166, November 2012.

[146] R. Lasserter, A. Akhil, C. Marnay, H. Stephens, J. Dagle, R. Guttromsonet al., "The CERTS microgrid concept," in Proc. CERTS, 2002.

[147] C. A. Hernandez-Aramburo, T. C. Green, N. Mugniot, "Fuel consumption minimization of a microgrid," IEEE Trans. Ind. Appl., vol.41, no. 3, pp. 673–681, May–Jun. 2005.

[148] C. Marnay, G. Venkataramanan, M. Stadler, A. S. Siddiqui, R. Firestone, B. Chandran, "Optimal technology selection and operation of commercial-building microgrids," IEEE Trans. Power Syst., vol. 23,no. 3, p. 975, Aug. 2008.

[149] IEA, "Distributed generation in liberalized energy markets," [Online].Available: http://iea.org/textbase/nppdf/free/2000/distributed2002.pdf

[150] M. Maribua, K. Firestone, M. Ryan, C. Marnay, and A. S. Siddiquica,"Distributed energy resources market diffusion model," Elsevier Energy Policy, pp. 4471–4484, 2007.

[151] W. D. Patterson, J. W. Whitham, " The Virtual Power Plant, Standard & Poor's Utilities & Perspectives Special Technology," New York, USA: McGraw-Hill, 1998.

[152] S. Watson, R. Fredericksen, T. Lorencz, "Chicago PowerPark Project Monthly Status Rep.," 2001. [Online]. Available:http://www.nemw.org

[153] F. Marin, A.B. Rey, A. Guerrero, A. F. deRuz, "A future microgrid implementation based on renewable distributed resources for a clean green energy production," in Proc. IEEE PES Winter Meeting, CERTS Int. Conf., pp. 305–308,2002.

[154] T. Som, N. Chakraborty, " Studies on economic feasibility of an autonomous power delivery system utilizing alternative hybrid distributed energy resources," IEEE Trans. on power systems, vol.29, no. 1, pp 172-181, Jan. 2014

[155] Sachin Jain, Vivek Agarwal, "An integrated hybrid power supply for distributed generation applications fed by nonconventional energy sources," IEEE Trans. on Energy Conversion, vol.23, no. 2, pp. 622-631, June 2008.

[156] Erik Cuevas, Miguel Cienfuegos, "A new algorithm inspired in the behavior of the social-spider for constrained optimization," Expert Systems with Applications,vol. 41, pp. 412–425, 2014 .

[157] James J.Q. Yu, Victor O.K. Li, "A social spider algorithm for global optimization," Technical Report No. TR-2003-004,Dept. of Electrical & Electronic Engineering,The University of Hong Kong, pp. 1-16, Oct 2013.

[158] James J.Q. Yu, Victor O.K. Li, "Base station switching problem for green cellular networks with social spider algorithm," 2014 IEEE Congress on Evolutionary Computation (CEC), Beijing, China, pp. 2338-2344, July 6-11, 2014.

[159] Esmat Rashedi, Hossein Nezamabadi-pour, Saeid Saryazdi. "GSA: A Gravitational Search Algorithm". Information Sciences, Elsevier, vol.179, pp. 2232–2248, 2009.
[160] A. R. Hosseinabadi, M. yazdanpanah and A. S. Rostami, “A new search algorithm for solving symmetric traveling salesman problem based on gravity”, World Applied Sciences Journal, vol.16 (10), pp 1387-1392, 2012.
[161] Gu W X, Li X T, Zhu L, “A gravitational search algorithm for flow shop scheduling”, CAAI Transactions on Intelligent Systems.vol. 5(5), pp. 411-418, 2010.
[162] J. Xiao, Z. Cheng, “Theories and Applications DNA Sequences Optimization Based on Gravitational Search Algorithm for Reliable DNA computing", Sixth International Conference on Bio-Inspired Computing. IEEE Computer Society, 2011.
[163] J. Sachs, and O. Sawodny, “A two-stage model predictive control strategy for economic diesel-PV-battery island microgrid operation in rural areas,” IEEE Trans. Sustain. Energy, vol. 7, no. 3, pp. 903-911, Jul. 2016.
[164] K. P. Detroja, “Optimal autonomous microgrid operation: A holistic view,” Appl. Energy, vol. 173, pp. 320-330, Jul. 2016.
[165] S. Upadhyay, and M. P. Sharma, “A review on configurations, control and sizing methodologies of hybrid energy systems,” Renew. Sustain. Energy Rev., vol. 8, pp. 47-63, Oct. 2014.
[166] B.-R. Ke, T.-T.Ku, Y.-L. Ke, C.-Y. Chung, and H.-Z. Chen, “Sizing the battery energy storage system on a university campus with prediction of load and photovoltaic generation,” IEEE Trans. Ind. Appl., vol. 52, no. 2, pp. 1136-1147, Mar./Apr. 2016.
[167] A. Hazra, and M. Basu, "Economic analysis to implement distributed generation system in a rail-way rake maintenance depot," Renewable Energy, Elsevier, 78, pp. 157-164, 2015.
[168] M. J. E. Alam, K. M. Muttaqi, and D. Sutanto, “Effective utilization of available PEV battery capacity for mitigation of solar PV impact and grid support with integrated V2G functionality,” IEEE Trans. Smart Grid, vol. 7, no. 3, pp. 1562-1571, May 2016.
[169] D. Tenfen, and E. C. Finardi, “A mixed integer linear programming model for the energy management problem of microgrids,” Elect. Power Syst. Res., vol. 122, pp. 19-28, May 2015.
[170] B. Zhao, X. Zhang, P. Li, K. Wang, M. Xue, and C. Wang, “Optimal sizing, operating strategy and operational experience of a stand-alone microgrid on Dongfushan island,” Appl. Energy, vol. 113, pp. 1656-1666, Jan. 2014.
[171] M. Marzband, M. Ghadimi, A. Sumper, and J. L. Domínguez-García, “Experimental validation of a real-time energy management system using multi-period gravitational search algorithm for microgrids in islanded mode,” Appl. Energy, vol. 128, pp. 164-174, Sep. 2014.
[172] A. Khodaei, “Microgrid optimal scheduling with multi-period islanding constraints,” IEEE Trans. Power Syst., vol. 29, no. 3, pp. 1383-1392, May 2014.
[173] Frei, Christoph, et al. World energy scenarios: Composing energy futures to 2050. No. INIS-FR--14-0059. ConseilFrancais de l'energie, 2013.
[174] I. E. Agency and Organization for Economic Cooperation and Development. Technology Roadmap: Solar Photovoltaic Energy. France: Org. for Economic Co-operation and Development (OECD), 2014.
[175] Herrerias, A. T., &Klinge, T. (2015). Photovoltaic growth slows despite new opportunities in emerging markets. Renewable Energy Focus, 16(5), 167-170.
[176] European Photovoltaic Industry Association. (2014). Global market outlook for photovoltaics 2014–
2018.[Online]Available:http://www.epia.org/fileadmin/user_upload. Publications/44_epia_gmo_report_ver_ 17_mr. pdf.

[177] Kazmerski, L. L. (1997). Photovoltaics: A review of cell and module technologies. Renewable and sustainable energy reviews, 1(1-2), 71-170.
[178] Hasan, M. A., &Sumathy, K. (2010). Photovoltaic thermal module concepts and their performance analysis: a review. Renewable and Sustainable Energy Reviews, 14(7), 1845-1859.
[179] Tao, J., & Yu, S. (2015). Review on feasible recycling pathways and technologies of solar photovoltaic modules. Solar Energy Materials and Solar Cells, 141, 108-124.
[180] Efficiency, E. (2006). Solar Energy Technologies Program. Updated on October, 24, 2006.
[181] NFPA70, 2014 National Electrical Code, , Published by the National Fire Protection Association, Quincy, MA, approved Aug 21, 2013.
[182] Zhao, Y., Ball, R., Mosesian, J., de Palma, J. F., & Lehman, B. (2015). Graph-based semi-supervised learning for fault detection and classification in solar photovoltaic arrays. IEEE Transactions on Power Electronics, 30(5), 2848-2858.
[183] Kuo, C. L., Chen, J. L., Chen, S. J., Kao, C. C., Yau, H. T., & Lin, C. H. (2015). Photovoltaic energy conversion system fault detection using fractional-order color relation classifier in micro distribution systems. IEEE Transactions on Smart Grid.
[184] Jahn, U., &Nasse, W. (2004). Operational performance of grid-connected PV systems on buildings in Germany. Progress in Photovoltaics: Research and applications, 12(6), 441-448.
[185] Platon, R., Martel, J., Woodruff, N., &Chau, T. Y. (2015). Online fault detection in PV systems. IEEE Transactions on Sustainable Energy, 6(4), 1200-1207.
[186] Hare, J., Shi, X., Gupta, S., &Bazzi, A. (2016). Fault diagnostics in smart micro-grids: A survey. Renewable and Sustainable Energy Reviews, 60, 1114-1124.
[187] Quater, P. B., Grimaccia, F., Leva, S., Mussetta, M., &Aghaei, M. (2014). Light unmanned aerial vehicles (UAVs) for cooperative inspection of PV plants. IEEE Journal of Photovoltaics, 4(4), 1107-1113.
[188] Buerhop, C., Schlegel, D., Niess, M., Vodermayer, C., Weißmann, R., &Brabec, C. J. (2012). Reliability of IR-imaging of PV-plants under operating conditions. Solar Energy Materials and Solar Cells, 107, 154-164.
[189] Hu, Y., Cao, W., Ma, J., Finney, S. J., & Li, D. (2014). Identifying PV module mismatch faults by a thermography-based temperature distribution analysis. IEEE Transactions on Device and Materials Reliability, 14(4), 951-960.
[190] Silvestre, S., da Silva, M. A., Chouder, A., Guasch, D., & Karatepe, E. (2014). New procedure for fault detection in grid connected PV systems based on the evaluation of current and voltage indicators. Energy Conversion and Management, 86, 241-249.
[191] Chine, W., Mellit, A., Lughi, V., Malek, A., Sulligoi, G., & Pavan, A. M. (2016). A novel fault diagnosis technique for photovoltaic systems based on artificial neural networks. Renewable Energy, 90, 501-512.
[192] Akram, M. N., &Lotfifard, S. (2015). Modeling and health monitoring of DC side of photovoltaic array. IEEE Transactions on Sustainable Energy, 6(4), 1245-1253.
[193] Guerriero, P., Di Napoli, F., Vallone, G., d'Alessandro, V., & Daliento, S. (2016). Monitoring and diagnostics of PV plants by a wireless self-powered sensor for individual panels. IEEE Journal of Photovoltaics, 6(1), 286-294.
[194] Gokmen, N., Karatepe, E., Celik, B., & Silvestre, S. (2012). Simple diagnostic approach for determining of faulted PV modules in string based PV arrays. Solar Energy, 86(11), 3364-3377.
[195] Gokmen, N., Karatepe, E., Silvestre, S., Celik, B., & Ortega, P. (2013). An efficient fault diagnosis method for PV systems based on operating voltage-window. Energy conversion and management, 73, 350-360.

[196] Hu, Y., Zhang, J., Cao, W., Wu, J., Tian, G. Y., Finney, S. J., & Kirtley, J. L. (2015). Online two-section PV array fault diagnosis with optimized voltage sensor locations. IEEE Transactions on Industrial Electronics, 62(11), 7237-7246.
[197] Patel, H., & Agarwal, V. (2008). Maximum power point tracking scheme for PV systems operating under partially shaded conditions. IEEE transactions on industrial electronics, 55(4), 1689-1698.
[198] Mirjalili, S., Mirjalili, S. M., & Lewis, A. (2014). Grey wolf optimizer. Advances in Engineering Software, 69, 46-61.
[199] Goldberg, D. E., & Holland, J. H. (1988). Genetic algorithms and machine learning. Machine learning, 3(2), 95-99.
[200] Glover, F., & Laguna, M. (2013). Tabu Search∗ (pp. 3261-3362). Springer New York.
[201] Walter DC, Sheble GB. Genetic algorithm solution of economic dispatch with valve point loading. IEEE Trans Power Syst 1993; 8:1325–32.
[202] Chiang C-L. Improved genetic algorithm for power economic dispatch of units with valve-point effects and multiple fuels. IEEE Trans Power Syst 2005; 20:1690–9.
[203] D.C. Walters, and G.B. Sheble, "Genetic algorithm solution of economic dispatch with valve point loading," IEEE Trans. Power Syst., vol. 8, no. 3, pp. 1325-1332, Aug 1993.
[204] M.R. Gent, and J.W. Lamont, "Minimum Emission Dispatch," IEEE Trans. Power Apparatus Syst., vol. PAS-90, no. 6, pp. 2650-2660, Nov 1971.
[205] Wang, C., Shahidehpour, S. M.: 'Effects of ramp-rate limits on unit commitment and economic dispatch', IEEE Trans. Power Syst., 1993, 8, (3), pp. 1341–1350.
[206] Hetzer, J., David, C. Y., Bhattarai, K.: 'An economic dispatch model incorporating wind power', IEEE Trans. Energy Convers., 2008, 23, (2), pp. 603–611.
[207] Lee, F. N., Breipohl, A. M.: 'Reserve constrained economic dispatch with prohibited operating zones', IEEE Trans. Power Syst., 1993, 8, (1), pp. 246–254.
[208] [Online]. Available: https://maps.google.co.in/
[209] Marketing Summary: Energy Center of Wisconsin, "Fuel cells for distributed generations," Tech. Rep., Mar. 2000.
[210] J.M. Feret, J. L. Kelly, A. J. Pereira, M. K. Wright, A. K. Kush, "Westinghouse PAFC Program House," in Proc. 4th Annu. Fuel Cells Contractors Rev. Meeting, 1992.
[211] F. A. Farhat, M. G. Simoes, "Itegration of Alternative Sources of Energy," Hoboken, NJ, USA: Wiley, 2006.
[212] A. B. Bhattacharya, S. K. Kar, R. Bhattacharya, "Diffuse solar radiation and associated meteorological parameters in India," Annu. Geophys., vol. 14, pp. 1051–1059, 1996.
[213] A. C. Caputo, M. Palumbo, P. M. Pelagagge, F. Scacchia, "Economics of biomass energy utilization in combustion and gasification plants: Effects of logistic variables," Biomass Bio Energy, vol. 28, pp. 35–51, 2005.
[214] C. Z.Wu, H. Huang, S. P. Zhengh, X. L. Yin, "An economic analysis of biomass gasification and power generation in China," Bioresource Technol., vol. 83, pp. 65–70, 2002.
[215] A. Oudalov, R. Cherkaoui, A. Beguin, "Sizing and optimal operation of battery energy storage system for peak shaving application," presented at the IEEE Powertech. , Paper 561, unpublished, July 2007.
[216] N. H. Ravindranath, P. Balachandra, "Sustainable bioenergy for India: Technical economic and policy analyses," Int. J. Energy, vol. 34, pp. 1003–1013, 2009.
[217] R. Banerjee, "Comparison of options for distributed generation in India," Int. J. Energy Policy, vol. 34, pp. 101–111, 2006.

[218] González, D., Ramos Paja, C. A., Saavedra Montes, A. J., ArangoZuluaga, E. I., &Carrejo, C. E. (2012). Modeling and control of grid connected photovoltaic systems. RevistaFacultad de Ingeniería Universidad de Antioquia, (62), 145-156.

[219] Barth, N., Jovanovic, R., Ahzi, S., & Khaleel, M. A. (2016). PV panel single and double diode models: Optimization of the parameters and temperature dependence. Solar Energy Materials and Solar Cells, 148, 87-98.

[220] S. S. Rao, *Engineering Optimization Theory and Practice*, Hoboken, New Jersey; Canada: John Wiley & Sons Inc., 2009.

[221] Chen, Y. P., & Jiang, P. (2010). Analysis of particle interaction in particle swarm optimization. Theoretical Computer Science, 411(21), 2101-2115.

[222] Liu, C. A. (2008, October). New dynamic constrained optimization PSO algorithm. In Natural Computation, 2008. ICNC'08. Fourth International Conference on (Vol. 7, pp. 650-653). IEEE.

[223] Devi, S., Jadhav, D. G., & Pattnaik, S. S. (2011, December). PSO based memetic algorithm for unimodal and multimodal function optimization. In International Conference on Swarm, Evolutionary, and Memetic Computing (pp. 127-134). Springer, Berlin, Heidelberg.

[224] Kim, D. H., Abraham, A., & Cho, J. H. (2007). A hybrid genetic algorithm and bacterial foraging approach for global optimization. Information Sciences, 177(18), 3918-3937.

[225] Dorigo, M., Maniezzo, V., & Colorni, A. (1996). Ant system: optimization by a colony of cooperating agents. IEEE Transactions on Systems, Man, and Cybernetics, Part B (Cybernetics), 26(1), 29-41.

[226] Shi, Y. (2001). Particle swarm optimization: developments, applications and resources. In evolutionary computation, 2001. Proceedings of the 2001 Congress on (Vol. 1, pp. 81-86). IEEE.

[227] Eberhart, R. C., Shi, Y., & Kennedy, J. (2001). Swarm intelligence (The Morgan Kaufmann series in evolutionary computation).

[228] Farmer, J. D., Packard, N. H., & Perelson, A. S. (1986). The immune system, adaptation, and machine learning. Physica D: Nonlinear Phenomena, 22(1-3), 187-204.

[229] Formato, R. A. (2008). Central force optimization: A new nature inspired computational framework for multidimensional search and optimization. In Nature Inspired Cooperative Strategies for Optimization (NICSO 2007) (pp. 221-238). Springer, Berlin, Heidelberg.

[230] R. Storn and K. V. Price, Differential evolution- a simple and efficient heuristic for global optimization over continuous spaces, Journal of Global Optimization vol. 11, no. 4, pp. 341-359, 1997.

[231] K. V. Price, R. Storn and J. Lampinen. Differential Evolution: A Practical Approach to Global Optimization. Springer-Verlag, Berlin, 2005.

[232] J. Ronkkonen, S. Kukkonen and K. V. Price, Real-parameter optimization with differential evolution, in Proceeding IEEE Congress Evolutionary Computation, Edinburgh, Scotland, September 2005, pp. 506-513.

[233] Goldberg, D. E., & Deb, K. (1991). A comparative analysis of selection schemes used in genetic algorithms. In *Foundations of genetic algorithms* (Vol. 1, pp. 69-93).Elsevier.

[234] Baker, J. E. (1987, July). Reducing bias and inefficiency in the selection algorithm.In *Proceedings of the second international conference on genetic algorithms* (pp. 14-21).

[235] Gaing Z-L. Particle swarm optimization to solving the economic dispatch considering the generator constraints. IEEE Trans Power Syst 2003; 18:1187–95.

[236] Sinha N, Chakrabarti R, Chattopadhyay PK. Evolutionary programming techniques for economic load dispatch. IEEE Trans Evol. Comput 2003; 7:83–94.

[237] Lakshminarasimman, L., & Subramanian, S. (2006). Short-term scheduling of hydrothermal power system with cascaded reservoirs by using modified differential evolution. *IEE Proceedings-Generation, Transmission and Distribution*, *153*(6), 693-700.
[238] J. S. Derman, F. Pettersson, " Structural and operational optimisation of distributed energy systems," *Appl. Thermal Eng.*, vol. 26, pp. 1400–1408, 2006.
[239] J. D. Pandya, K. K. Ghosh, S. K. Rastogi, "A phosphoric acid fuel cell coupled with biogas," *Energy*, vol. 13, no. 4, pp. 383–388, 1988.
[240] E. Carlson, R. Zogg, P. E. Sriramulu, K. Roth, J. Brodrick, "Using phosphoric acid fuel cells for distributed generation," in *Proc. ASHRAE*, vol. 49, pp. 50–51, 2006.
[241] A. Oudalov, D. Chartouni, C. Ohler, G. Linhofer, " Value analysis of battery energy storage applications in power systems," in *Proc. 2nd IEEE PES Power Syst. Conf. Expo.*, pp. 2206–2211, 2006.
[242] L. Goldstein, B. Headman, "Gas-fired distributed energy resources technology characterization," *US DOE Office of Energy Efficiency and Renewable Energy, Tech. Rep.*.
[243] Office of the Sonarpur TRS / EMU Rail-Way Car-shed, E. Rly.: Private communication.
[244] "Vidyuth Bhavan", Head Office of WBSEDCL.: Private communication.
[245] "CESC Bhavan", Head office of Calcutta Electric Supply Corporation: Private communication.